# Investigation of Waterborne Epoxies for E-Glass Composites

Robert E. Jensen

Dissertation submitted to the Faculty of the
Virginia Polytechnic Institute and State University
in partial fulfillment of the requirements for the degree of

Doctor of Philosophy

in

Chemistry

Thomas C. Ward, Chair
Richey M. Davis
John G. Dillard
Judy S. Riffle
James P. Wightman

June 9, 1999
Blacksburg, Virginia

KEYWORDS: Waterborne epoxy, cooperativity, moisture uptake, interphase, interfacial shear strength

Investigation of Waterborne Epoxies for E-Glass Composites

Robert E. Jensen

Committee Chairman: Thomas C. Ward

Chemistry

(Abstract)

Research is presented which encompasses a study of epoxies based on diglycidyl ether of bisphenol A (DGEBA) cured with 2-ethyl-4-methylimidazole (EMI-24) in the presence of the nonionic surfactant Triton X-100. Interest in this epoxy system is due partially to the potential application as a waterborne replacement for solvent cast epoxies in E-glass laminated printed circuit boards. This research has revealed that the viscoelastic behavior of the cured epoxy is altered when serving as the matrix in a glass composite. The additional constraining and coupling of the E-glass fibers to the segmental motion of the epoxy matrix results in an increased level of viscoelastic cooperativity. Current research has determined that the cooperativity of an epoxy/E-glass composite is also sensitive to the surface chemistry of the glass fibers. Model single-ply epoxy/E-glass laminates were constructed in which the glass was pretreated with either 3-aminopropyltriethoxysilane (APS) or 3-glycidoxypropyltrimethoxysilane (GPS) coupling agents. Dynamic mechanical analysis (DMA) was then used to create master curves of the storage modulus (E ) in the frequency domain. The frequency range of the master curves and resulting cooperativity plots clearly varied depending on the surface treatment of the glass fibers. It was determined that the surfactant has surprisingly little effect in the observed trends in cooperativity of the composites. However, the changes in cooperativity due to the surface pretreatment of the glass were lessened by the aqueous phase of the waterborne resin. Moisture uptake experiments were also performed on epoxy samples that were filled with spherical glass beads as well as multi-ply laminated composites. No increases in the diffusion constant could be attributed to the surfactant. However, the surfactant did enhance the final equilibrium moisture uptake levels. These equilibrium moisture uptake levels were also sensitive to the surface pretreatment of the E-glass.

**Acknowledgements**

I would like to thank the following individuals who provided assistance and support during the course of my research. I would like to express my sincere thanks to my advisor, Dr. Thomas C. Ward, for allowing me the opportunity to study under his guidance at Virginia Tech. I feel that Dr. Ward has given me the correct type of knowledge and the skills required to succeed in all aspects during my professional career. I would also like to thank my committee, Dr. Richey Davis, Dr. John Dillard, Dr. Judy Riffle, and Dr. Wightman for their guidance during my graduate career.

I am especially grateful for the assistance provided from the staff of CASS –Linda, Katy, Kim, and Tammy Jo. These ladies personally bailed me out of many "red tape" administrative situations with the graduate school. The CASS sponsored trips to Adhesion Society and Adhesive and Sealant Council meetings were very enjoyable. I also would like to acknowledge the secretaries in the NSF center –Joyce, Esther, Mille, and Laurie. Without their help graduate school would have been more difficult.

I wish to express my thanks to the members of the PolyPkem group, past and present, for the good times and sharing the knowledge and skills. This list includes Mark Vrana, Dan Hahn, Tony Williams, Ming Chen, Saikat, Ojin Kwon, Mark Muggli, Kermit Kwan, Dave Porter, Jianli Wang, Jen Robertson, Amy Eichstadt, Emmett O'Brien, and Sandra Case. I would also like to thank the students and staff from other groups/departments that have helped out – Rachel Giunta, Slade Gardner, Fred Gibson, Dr. Rick Clark, Mitch Jackson, Owen Hewitt, Dan Brannegan, Nikhil Verghese, Steve McCartney, Frank Cromer, and Fred Blair. I also had the privilege of working with two excellent SURP students – LaShanda James and Chad Johnson. Dr. David Lewis also provided much guidance during my summer internship for IBM.

Finally, I would like to thank my family for their support during my academic career, especially my wife Michelle. Her love has made graduate school seem much less overwhelming and much more enjoyable.

## TABLE OF CONTENTS

## TABLE OF FIGURES

## List of Tables

# Chapter 1 Introduction

## 1.1 Problem Statement

The chemical, mechanical, and viscoelastic properties of the fiber-matrix interphase dominate the ultimate performance characteristics of fiber reinforced polymeric composites. These three fundamental properties are certainly related to each other. As an example of the importance of these basic concepts, the understanding of the interfacial properties in E-glass fiber reinforced composites is necessary in predicting the long-term reliability of such materials. This is particularly important for printed circuit board (PCB) manufacturers, because of the detrimental effects of interfacial moisture. Printed circuit boards are constructed from E-glass fibers bound with an epoxy matrix. If moisture is present at the epoxy-glass interface then delamination and other defects during component soldering can arise during the assembly of the PCB.[1] Moisture can also corrode the metal oxides in the E-glass, leading to defects in the fiber and decreased mechanical strength.[2] This interfacial corrosion can cause metal migration and electrical short circuits while the PCB is in use.[1] Printed circuit boards have traditionally used an organic solvent, such as methyl ethyl ketone, to cast the epoxy during the pre-pregging stages of construction. The low viscosity and environmentally friendly nature of waterborne epoxies is ideally suited as alternative matrix materials for PCB's. But, hydrophilic surfactants are needed to stabilize the dispersed phase of waterborne epoxies. Surfactant present at the epoxy-glass interface could have detrimental effects on the mechanical properties and lifetime of the PCB. Little prior research has been directed toward examination of these effects and their origins.

The epoxy resins are used to construct printed circuit boards are exposed to an extremely harsh environment during the manufacturing process. This process includes drilling, degreasing, drying, copper plating, rinsing, stripping, etching, immersing in molten tin, reflow, and cleaning.[3] The testing of a printed circuit board includes cyclic temperature and humidity exposure as well as boiling samples in pressure cookers. If the circuit board has absorbed any water at the fiber-epoxy interface then the circuit board will delaminate when dipped in molten solder. This is caused by the rapid expansion of

trapped water into steam. This could be a major problem near the plated through holes of the circuit board, as illustrated in Figure 1-1.

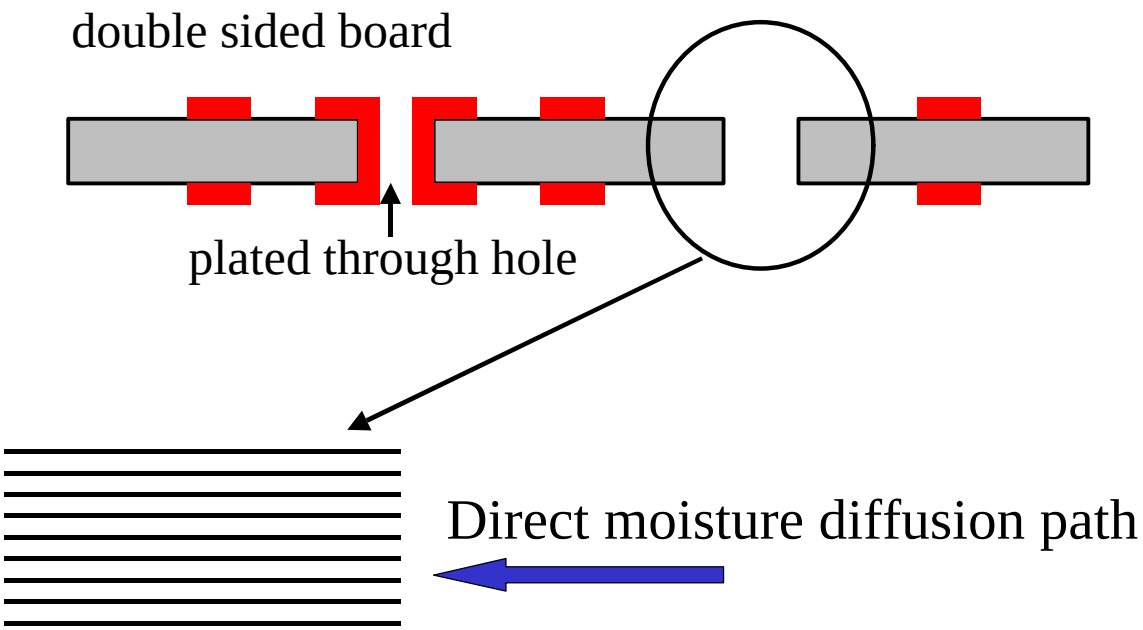


Figure 1-1. Schematic diagram of double sided laminated printed circuit board.[4]

The epoxy composite printed circuit board must meet stringent mechanical and electrical standards to meet the demands of the final product. Some of these properties that are desirable are a glass transition temperature ($T_g$) of 120 - 130°C, a thermal coefficient of expansion of 14-20 x $10^{-6}$ /K below $T_g$, and 50-70 x $10^{-6}$ /K above $T_g$, as well as a dielectric constant of 4.0 - 5.5 at 1 MHz.[4] The epoxy-glass composite must also absorb less than 3 percent by weight water when exposed to moisture or a humid atmosphere.[4] While there is a strong need for the electronics industry to use waterborne resins, it is not known what the effects of added surfactant are on the long term performance and durability of potential products. It has been estimated that water diffusion can occur up to 450 times faster through the polymer-substrate interface than through the polymer matrix in a solvent cast epoxy.[5] Because a surfactant is present, water diffusion has the potential to be a large problem when using waterborne epoxies to construct circuit boards. Knowing how the surfactant interacts with the epoxy as well as the location and distribution of surfactant in the cured system are key pieces of information that are needed to answer questions pertaining to bond durability.

## 1.2 Research Goals

The goal of this research project is to understand the effects of a surfactant additive in a waterborne epoxy on the fiber-matrix interfacial properties of a glass reinforced composite. The research will be done by characterizing the moisture uptake, viscoelastic, and mechanical properties of the fiber-matrix interphase. A model E-glass composite system consisting of the nonionic surfactant Triton X-100 and a diglycidyl ether of bisphenol A (DGEBA) epoxy resin, which has been cured with 2-ethyl-4-methylimidazole (EMI-24), will be used as the matrix phase. These reactants are illustrated in Figure 1-2.

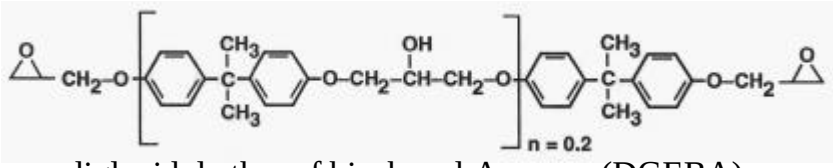


diglycidyl ether of bisphenol A epoxy (DGEBA)

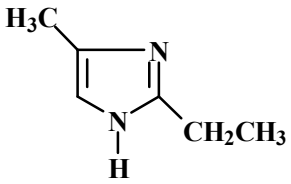


2-ethyl-4-methylimidazole (EMI-24)

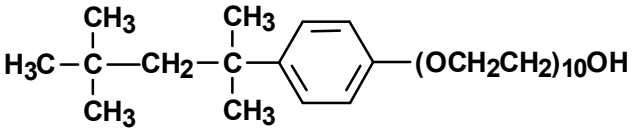


Triton X-100

Figure 1-2. DGEBA epoxy resin, 2-ethyl-4-methylimidazole, and Triton X-100.

# Chapter 2 Background

## 2.1 Reaction Mechanism

Farkas and Strohm[6] were the first to study the reaction mechanism between an imidazole and an epoxide ring. These authors used EMI-24 as the curing agent and phenylglycidyl ether (PGE) as the epoxide. Phenylglycidyl ether is illustrated in Figure 2-1. Farkas and Strohm postulated that the pyrrole-type nitrogen at the one position of EMI-24 reacts with the terminal carbon of PGE to form a 1:1 adduct. This 1:1 adduct can then further react with another molecule of PGE to form a 1:2 adduct. Farkas and Strohm believed that both nitrogens of EMI-24 form permanent covalent bonds with PGE and that the imidazole is not regenerated during the reaction.

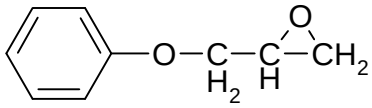

Figure 2-1. Phenyl Glycidyl Ether (PGE).

Barton and Shepherd[7] also studied the reaction between EMI-24 and PGE. These authors were able to show that the 1:1 adduct of EMI-24 and PGE has the same reaction rate with the epoxide as EMI-24 alone. Based on these findings, Barton and Shepherd concluded that the basic, pyridine type nitrogen was the reactive site of the imidazole. Barton and Shepherd also postulated that the imidazole became permanently incorporated into the polymer. This reaction mechanism is illustrated in Figure 2-2. [8]

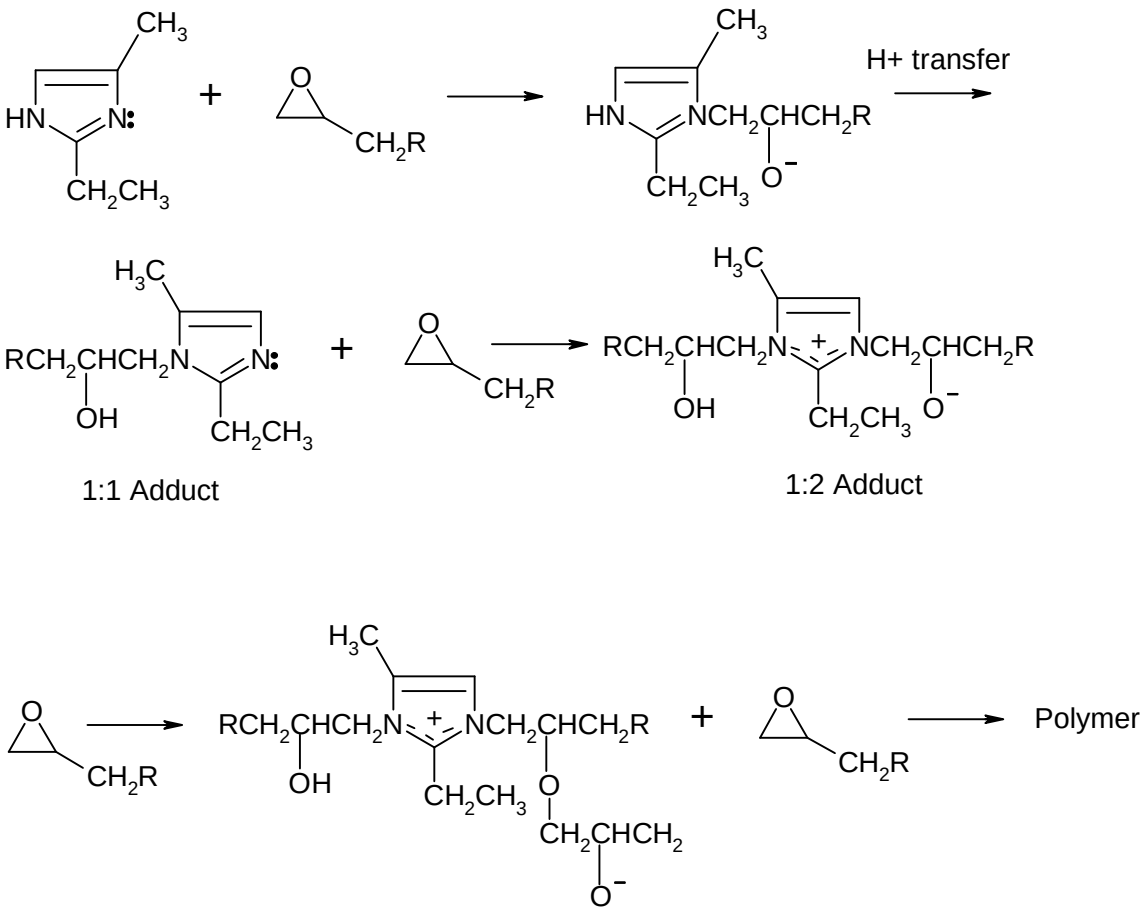


Figure 2-2. Adduct forming reaction mechanism.[8]

Ricciardi[8] and his co-workers studied the reaction mechanisms between PGE and a variety of imidazoles including 1-methylimidazole, 2-methylimidazole, and 1,2-dimethylimidazole. These authors disputed the reaction mechanisms that were proposed in earlier research.[6,7] When the products of the reaction were observed by Fourier transform infrared spectroscopy (FTIR), carbon-carbon double bond stretching bands were observed in the region of 1650-1770cm$^{-1}$. This cannot be explained by the adduct-forming reaction mechanism of Barton and Shepherd.[7] Ricciardi then proposed that the imidazole can be regenerated from an epoxy-imidazole adduct during the course of the reaction by N-dealkylation of the imidazole. Ricciardi states that if a 1:2 adduct were formed (Figure 2-2) then a Hofmann elimination could occur. This elimination is believed to lead to the formation of an enol, which can undergo keto-enol tautomerism. This is important because Ricciardi also observed ketones during the course of the

reaction. This reaction mechanism, as postulated by Ricciardi, are portrayed in Figure 2-3.

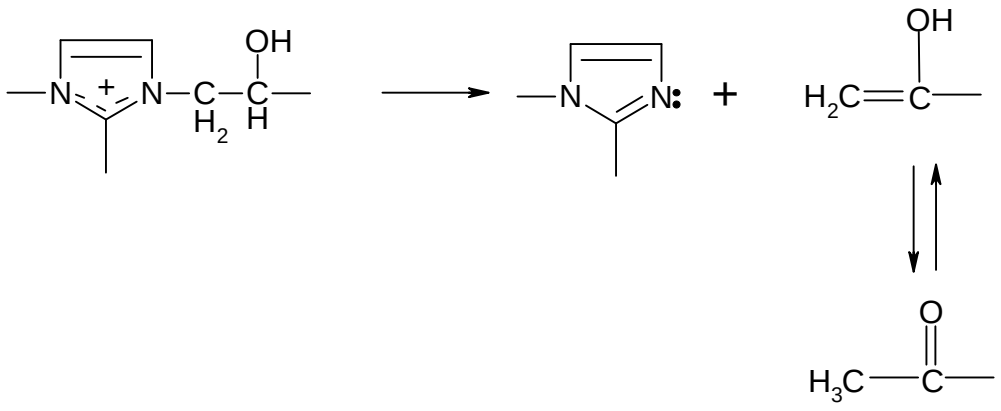

Figure 2-3. Regeneration of imidazoles.[8]

Jisova[9] also studied the reaction mechanisms between imidazoles with PGE as well as DGEBA. Jisova performed a comparative study between EMI-24, 1-n-butylimidazole, 2-phenylimidazole, imidazole, 1-vinylimidazole, and benzimidazole. Jisova was able to determine by FTIR and differential scanning calorimetry (DSC) that EMI-24 is the most effective imidazole catalyst for polymerizing epoxies. Jisova also agrees with Ricciardi that N-dealkylation of an N-substitutuent from either an adduct or a polymer formed by these adducts can lead to the regeneration of the imidazole catalyst during the reaction.

While these works[6,7,8,9] have afforded insight into the reaction mechanisms of imidazoles with epoxides, one must also consider that PGE is not capable of crosslinking. Jisova did study the reaction mechanism of DGEBA with imidazoles, but made no mention of the crosslinking ability or crosslinking mechanism of the imidazole. Chang[10] has studied the effect of thermal history on the crosslinking ability of EMI-24 with DGEBA. Chang used DSC to determine that hydroxyl group (-OH) propagation was more probable at higher temperatures, which can lead to an increase in the crosslink density of the epoxy. Chang was also able to show that the $T_g$ of a given imidazole/DGEBA system can be made to vary by as much as 70°C depending on the thermal history. While this is interesting, the curing conditions of this epoxy system selected for the current investigation will not vary and will remain fixed at 195°C for 2 hours.

Heise and Martin[11,12,13] have performed the research that is the most directly related to the thesis research of this project. These authors have performed extensive studies in the crosslinking ability of EMI-24 on DGEBA as well as determining a concentration dependence. Heise and Martin mainly used FTIR and DSC as their characterization techniques. In agreement with previous studies, Heise and Martin also proposed an epoxy-imidazole adduct as the initial step of the curing reaction. Once this adduct is formed, these authors then believe that crosslinking of the epoxy will occur through the alkoxide anions and hydroxyl groups that are formed when the imidazole opens up the epoxide rings of the DGEBA. Heise and Martin were also able to determine that the etherification reactions that lead to crosslinking do not commence until the adduct reactions are complete. They reported the highest $T_g$ epoxy using 7 mol % EMI-24 per 100 mols of DGEBA. The $T_g$ of the 7 mol % EMI-24 epoxy was approximately 100°C greater than a 100 mol % EMI-24 epoxy. The reasoning behind this is that the etherification, or crosslinking, reaction does not begin until the majority of the imidazole has been used in forming adducts. The adduct reaction consumes an epoxide group in a non-crosslinking bond. Therefore, using a low mol % of imidazole will result in more epoxide groups being available to form crosslinking ether bonds. The crosslinking mechanism between DGEBA and an imidazole is illustrated in Figure 2-4. It should also be noted that Heise and Martin do not discuss in any of their papers the regeneration of the imidazole during the course of the reaction.

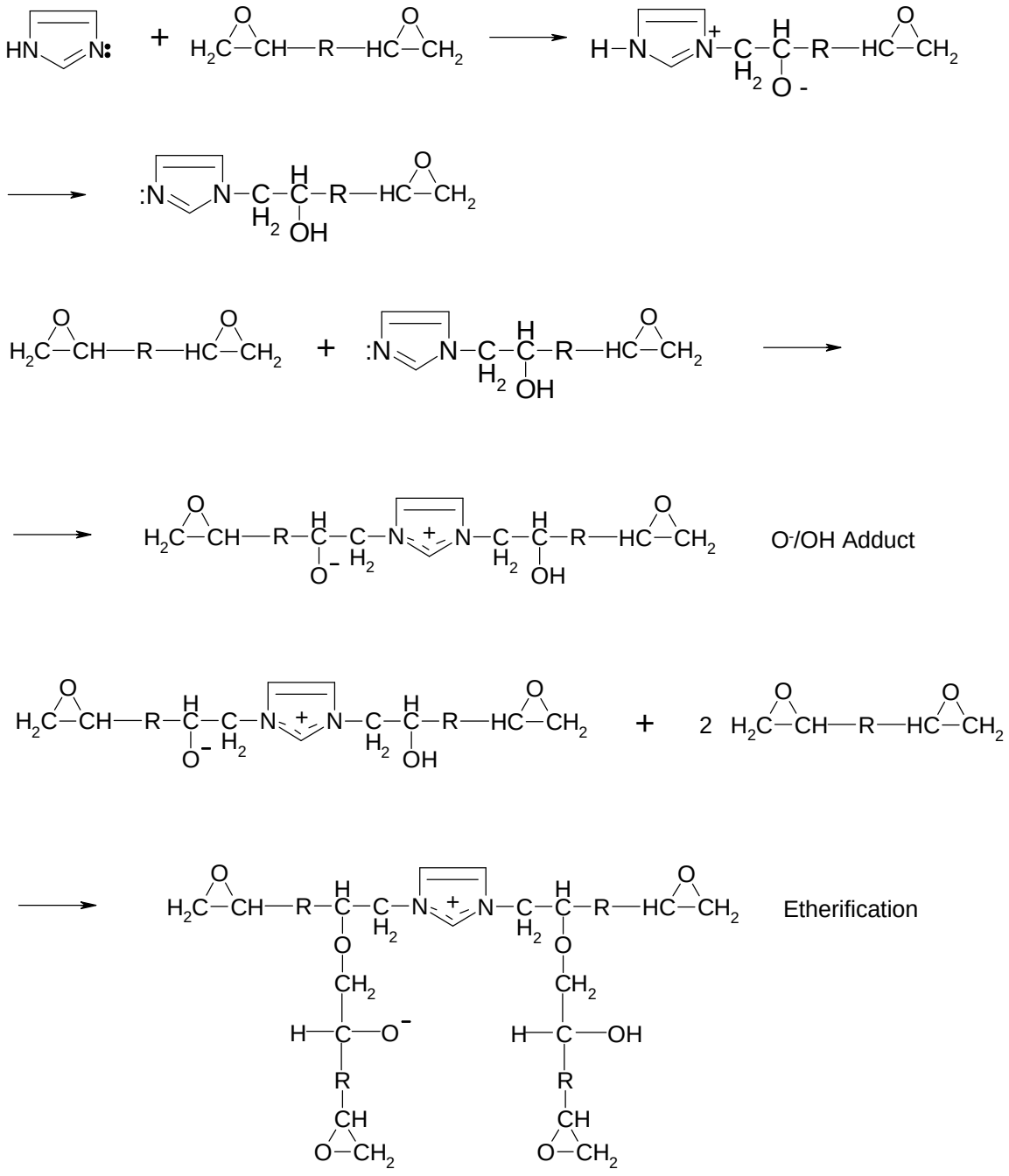


Figure 2-4. Crosslinking of an epoxy by an imidazole.[13]

Examination of the reaction mechanism proposed by Heise and Martin reveals the presence of an alkoxide anion. The location of these anions is not fixed during the reaction as proton exchanges with any available hydroxyl group are possible. Crosslinking will occur no matter where the alkoxide anion is located in the epoxy. The

alkoxide anion could possibly exchange protons with the terminal -OH of the X-100 surfactant molecule according to this reaction scheme.

## 2.2 Surfactants

### 2.2.1 Triton X-100

It is the very nature of a surfactant that makes their behavior in an adhesive system the subject of much study. Surfactants are molecules that contain both hydrophilic and hydrophobic regions. It is this dual nature that gives surfactants a high surface activity and a large affinity for interfaces.[14] The term surfactant is short for surface active agent. It is this high surface activity which enables a hydrophobic epoxy resin to be stabilized in a water phase as an emulsion. The surfactant accomplishes this by adsorbing to the hydrophobic regions of the epoxy resin particles. The hydrophilic regions of the surfactant then remain associated with the water phase.

Triton X-100 was chosen for this research because it is nonionic and is widely utilized in research and applications. A cationic or anionic surfactant could lead to electrical short-circuiting in a printed circuit board because of their inherent positive or negative charges. The Ortho Pharmaceutical Corporation originally synthesized Triton X-100, along with the nonionic surfactant nonyl phenol, in the 1940s as birth control contraceptives.[15] By 1952 Triton X-100 had already been used as an emulsifying agent for household and industrial detergents, degreasing agents, metal cleaners, insecticides, herbicides, fungicides, paints, wool scouring, asphalt, dispersion in paper manufacturing, de-inking agents, and as a dispersing agent for inks and dyes.[16] Triton X-100 is certainly one of the most widely used nonionic surfactants in existence.

Triton X-100 has an average molecular weight of 650g/mol. The polyethylene oxide tail contains an average of 9.9 repeat units as determined by nuclear magnetic resonance (NMR) spectroscopy.[17] The surface free energy of Triton X-100 is 29.1 $mJ/m^2$.[18] In an aqueous solution Triton X-100 has a critical micelle concentration of 0.16g/l or 0.00025mols/l.[18] Triton X-100 has a micellar molecular weight of about 90,000g/mol, which translates to approximately 140 molecules per micelle.[18] Some proposed micelle structures for Triton X-100 are shown in Figure 2-5.

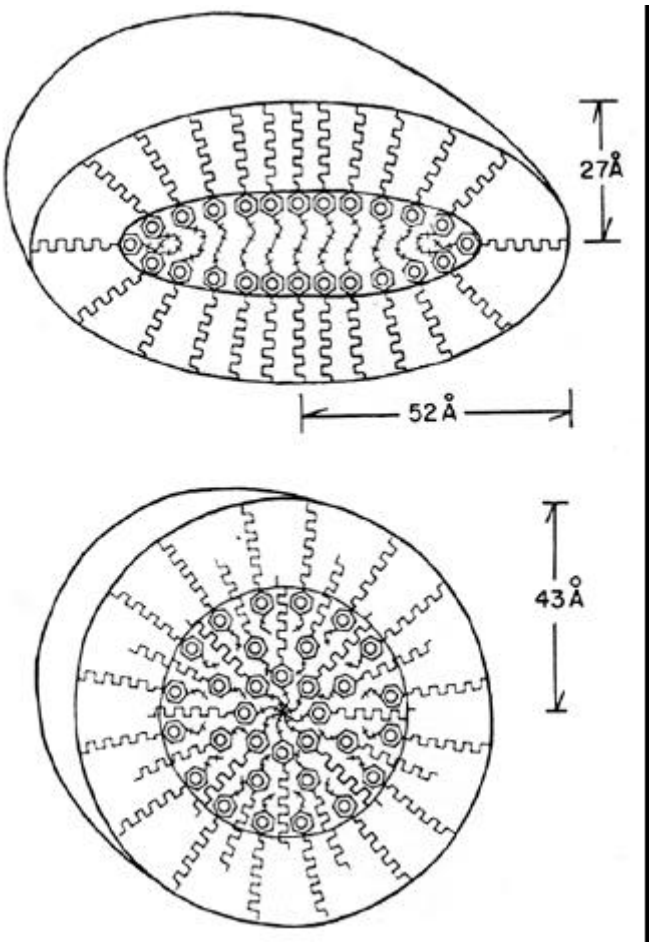


Figure 2-5. Proposed micelle structures for Triton X-100.[19]

### 2.2.2 Latex Film Formation

Waterborne emulsions, or latexes, form continuous films via a rather interesting path. Most researchers agree that the formation of a continuous film from a two phase emulsion involves several distinct steps.[20] The basic stages of film formation are illustrated in Figure 2-6.

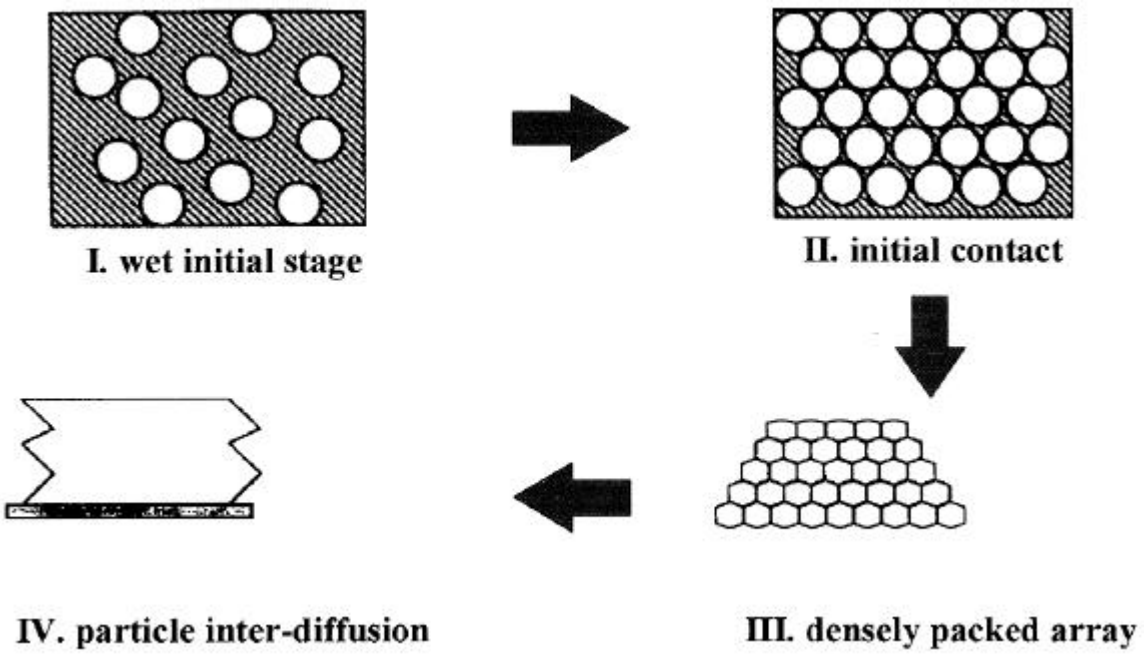


Figure 2-6. Basic stages of latex film formation.[21]

Stage I is the "wet initial stage". This is simply the surfactant-stabilized polymer suspended in the water phase. Once the emulsion is cast as a film on a substrate the water will begin to evaporate until stage II is reached. Stage II is where the particles come into initial contact. Interstitial water between the particles will eventually be lost and the particles will deform into the close packed array of stage III. And finally, if the polymer is above the glass transition temperature ($T_g$), diffusion can occur across the particle boundaries leading to the continuous film of stage IV. The progression from stage III to stage IV is commonly referred to as autohesion or further gradual coalescence.[22] However, the basic stages of film formation illustrated in Figure 2-6 do not describe the fate of the surfactant, which is very important for adhesive applications, and a critical issue for this thesis research.

## 2.3 Surfactant Location

Holl and Kientz[21,23] have studied the distribution and location of surfactant in latex films. These authors provided an extensive summary of some of the trajectories that are available to a surfactant in a polymer latex.[23] Among the options that Holl and Kientz cite are that the polymer and surfactant could be miscible with each other, or the

surfactant could phase separate from the polymer, or the surfactant could simply remain at the interfaces between the individual latex particles. Whether or not the surfactant is miscible or immiscible with the polymer, there is also the possibility that the surfactant could migrate towards the film-air (F-A) and or film-substrate (F-S) interfaces. Holl and Kientz also state that in real systems a combination of each of these possibilities is often encountered. Holl and Kientz believe that the major factors that will influence the distribution of surfactant in a latex film are the polymer-surfactant interactions, substrate surface chemistry, the age of the film, the total amount of surfactant in the latex, as well as the temperature and humidity conditions during the formation of the film. Holl and Kientz state that the polymer-surfactant interactions are the most basic and fundamental parameters that will influence the surfactant distribution.

The experimental work performed by Holl and Kientz[23] consisted of preparing latex films of poly(2-ethylhexyl methacrylate) (P2EHMA) that had been stabilized individually with a variety of surfactants including sodium dodecyl sulfate (SDS), hexadecyl trimethylammonium bromide (HTAB), hexadecylpyridinium chloride (HPCL), and the ethoxylated nonyl phenols NP10 and NP25. These films were then cast on soda lime glass (A-glass) slides and examined using attenuated total reflectance Fourier transform infrared spectroscopy (ATR-FTIR). The concentration of surfactant that was present at the F-A and F-S interfaces was studied as a function of total surfactant concentration in addition to the film formation conditions.

The literature review provided by Holl and Kientz is excellent[23], but several questions are raised by the experimental work that was performed. Holl and Kientz illustrate how the concentration of surfactant increases at both the F-A and F-S interfaces for each sample as the total concentration of surfactant is raised. The authors also calculated the sampling depth of the infrared beam to be 1.06μm at an incident angle of 45° using a germanium crystal. The sampling depth was 4.88 ± .32μm with a KRS-5 crystal at the same incident angle. If the thickness of the surfactant layer at either the F-S or F-A interfaces was much smaller than the sampling depth, then their reported increases in interfacial surfactant concentrations actually could have resulted from the infrared beam sampling some bulk material. In other words, how much of the depth that was sampled by the infrared beam actually composed the polymer-crystal interphase? Holl and Kientz

also encountered problems with the characteristic absorption peaks of the nonionic nonyl phenol surfactants overlapping with those of the P2EHMA. The absorption peaks due to these surfactants had to be subtracted from those of the polymer, which could be a large source of error. Holl and Kientz also did not calculate the surface free energies of the polymer, surfactants, or the glass substrate. The solubility parameters of the polymer and surfactants were also not obtained. It would be interesting to know if there was a driving force for surfactant migration due to possible differences in surface free energies between the polymer and the substrate as well as any polymer-surfactant incompatibility.

Holl, Kientz, and Charmeau later used the 180° peel test to study the same P2EHMA-surfactant latex systems.[21] The films were peeled from a glass substrate at varying rates. The peel energy was evaluated as a function of peel rate and total surfactant concentration. It was determined that for each of the surfactants, that the peel energy was independent of surfactant concentration when the peel rate was extrapolated to zero. The authors give no explanation for the peel energy being independent of surfactant concentration. One possible explanation is that once the surface of the glass is covered with a monolayer of surfactant, further addition of surfactant will simply no longer change the peel energy required to lift the film from the glass. If this is the case then the peel test does not confirm the authors' previous conclusion that adding more surfactant to the latex will increase the amount of surfactant present at the F-S interface. If the surfactant covers the surface of the glass as a monolayer then adding more surfactant could simply raise the bulk concentration. This would then have no effect on the amount of surfactant at the F-S interface and the peel energy would then be independent of surfactant concentration once monolayer surface coverage was obtained. Again, the sampling depth of ATR-FTIR was probably too great to detect this.

Holl[24,25] has recently performed peel testing of model latex films from glass substrates, which were stabilized with a variety of surfactants, that lend more insight as to the role of surfactants in adhesives. Holl has identified several possible effects of a surfactant on the adhesive peel strength of a latex film. The first effect is due to the presence of surfactant directly at the polymer-substrate interface. Surprising, Holl found this to result in an increase in the peel energy. If a hydrophobic polymer is placed on a hydrophilic substrate, such as glass, the peel energy will be low. But, because a

surfactant has both a hydrophilic and hydrophobic component, the surfactant can act as compatibilizer between the glass and polymer and increase the peel strength. This first type of interface effect is contained within a length scale of 1nm from the substrate surface.

The second effect identified by Holl[24] was concerned with surfactant concentrated within the interphase region (length scale of 1μm from the substrate surface). A large amount of surfactant in this region will change the energy dissipation near the fracture tip during a peel test. A high concentration of surfactant in the fracture tip will act as a weak boundary layer and decrease the peel strength of the adhesive.

Additional factors identified by Holl[24] are plasticizing-antiplasticizing effects in the bulk film (length scale of 10μm from the substrate surface). If the surfactant acts as a plasticizer then the peel strength will increase. The peel strength could decrease if the surfactant acts as an antiplasticizer, depending on the temperature and peel rate. Holl's research demonstrates the complicated nature of surfactants. If a surfactant is present at the polymer-substrate interface the peel strength may not necessarily decrease. The zero rate peel energies measured by Holl were still three to four times greater than the thermodynamic reversible work of adhesion.

Holl[25] also studied the migration of a series of ethoxylated nonionic surfactants in stryene/butyl acrylate latex films. Holl has concluded that the driving force for surfactant migration in latex films is the thermodynamic reduction of surface free energies. He determined that polymer-surfactant and surfactant-glass interactions are always favored over direct polymer-glass interactions. Holl used a nonyl phenol nonionic surfactant with a polar poly(ethylene oxide) tail. The tail group of this surfactant is similar in structure to Triton X-100. The peel strengths measured by Holl were invarient with respect to the length of the poly(ethylene oxide) tail, which ranged from 4 to 30 repeat units. Holl also observed that it is possible for the surfactant to migrate to an interface in a completely dried and coalesced latex film. XPS surface analysis detected no surfactant at the polymer-air interface of dry films. When water was added to this interface the films whitened after a short time as surfactant migrated towards the film-water interface. Again, Holl believes that there is a thermodynamic driving force for the surfactant to lower the surface free energy between the polymer and the water. The migration ability

of the surfactant would certainly depend on the molecular mobility of both the surfactant and the film. These results are very interesting because these changes in interfacial concentrations of surfactant could influence the durability of a waterborne epoxy printed circuit board after long periods of time.

Urban and Niu[26] stated that several factors will affect the distribution of surfactant in a latex film, including polymer-surfactant compatibility, the surface free energy of the substrate, temperature, and the rate of water evaporation during coalescence. To study these effects, Urban and Niu copolymerized a polystyrene/poly(n-butyl acrylate) (sty/BA) latex that was stabilized with sodium dioctyl sulfosuccinate (SDOSS) as the surfactant. These authors then cast thin films of this material on sheets of poly(tetrafluoroethylene) (PTFE) and examined the F-S and F-A interfaces using ATR-FTIR. The presence of SDOSS at either interface is easily detected by ATR-FTIR due to the unique absorption band at 1050$cm^{-1}$ due to S-O stretching modes. Urban and Niu found that when the styrene content of the copolymer was increased that more surfactant was detected at the F-S interface. This was attributed to a decrease in compatibility between the surfactant and the sty/BA copolymer as the amount of hydrophobic styrene was increased. Urban and Niu also state that the rate at which the water evaporates from the latex is also important because SDOSS is water soluble and will preferentially remain in the aqueous phase. The location of the surfactant will therefore be influenced by the water flux during coalescence of the film. These authors also believe that the surface free energy of the substrate is also important. Because the surface free energy of PTFE is so low (18$mJ/m^2$) there will be a driving force for the surfactant to migrate towards the F-S substrate to minimize the difference in surface free energies between the film and the substrate. The $T_g$ of the film was also stated as a factor that can influence the location of surfactant in a latex film. Urban and Niu state that if the $T_g$ of the film increases rapidly during the coalescence, then the surfactant may become trapped in the polymer and surfactant diffusion to either interface will become impeded. Although the rate of diffusion could be inhibited, there may still be enough free volume in the polymer to allow surfactant migration to the interface over an extended period of time.

Urban and Tebelius[27] completed a similar study using latexes of polystyrene and poly(n-butyl acrylate). However, in this study the latex was not a copolymer. Instead,

each component was polymerized independently and the mixed together with SDOSS to form the latex. Again, Urban and Tebelius list polymer-surfactant interactions, substrate surface free energy, and the water flux during coalescence as the major factors that will influence the location and distribution of surfactant in a latex film. These authors state that if the latex particles are allowed to flocculate before coalescence then the surfactant will be displaced into the aqueous phase. These displaced surfactant molecules will become more available for migration during the coalescence process. This effect could then also have an influence on the location and distribution of surfactant in a waterborne coating.

The research of Urban[26,27] indicates that the surfactant location and distribution in a latex film is a complicated process that is influenced by a high number of variables. Urban's characterization techniques are unfortunately difficult to apply to the specific epoxy-surfactant-substrate system to be used in this research. Urban cast latex films on a PTFE substrate and then peeled the film from the substrate to examine the interface using ATR-FTIR. Urban's choice of SDOSS as the surfactant provides a unique $SO_3^-$ group that is easily distinguished from the polymer using FTIR. The chemical groups that compose DGEBA and X-100 are similar in nature and it is doubtful that FTIR would be as sensitive. Urban also cast his films on PTFE. This substrate has an extremely low surface free energy, so it is not surprising that the surfactant migrated towards this interface. When studying an adhesive system one must also consider the substrate to which the adhesive is being bonded. Examining surfactant migration of latex films that have been cast on PTFE is insightful, but is not that relevant for adhesive research.

Several other techniques have been employed in studying the adsorption behavior of surfactants at various interfaces. Somasundaran *et al.*[28] used Zeta potential measurements in studying the adsorption behavior of the cationic surfactant, tetradecyl trimethyl ammonium chloride, and a nonionic surfactant, pentadecylethoxylated nonyl phenol, at the interface between water and alumina. Somasundaran[29] also examined the adsorption behavior of sodium dodecyl sulfate (SDS) on alumina using fluorescence, electron spin resonance, and Raman spectroscopy. Veggeland and Nilsson[30] examined polymer-surfactant interactions between poly(ethylene oxide) and several alkylethoxysulfonate surfactants using nuclear magnetic resonance spectroscopy (NMR)

and gel permeation chromatography (GPC). Rutland and Senden[31] studied the adsorption of a poly(oxyethylene) nonionic surfactant to the surface of silica using atomic force microscopy (AFM). Gentle *et al.*[32] used neutron reflectivity and ellipsometry measurements to study the structure of a hydroxyl terminated 1,4-polyisoprene surfactant at the air-water interface.

The previous paragraph suggests that a wide variety in characterization techniques exists for studying the adsorption behavior of surfactants at specific interfaces. This may be true, but when attempting to determine the effects of a surfactant on adhesive properties, the number of characterization techniques becomes limited. The literature cited in this section focuses on polymer-surfactant-substrate systems that would have little applicability as adhesive systems. One of the objectives of this present thesis is to examine fundamentally an epoxy-surfactant system that could potentially be used in manufacturing laminated circuit boards. This immediately eliminates the an ionic surfactant. Ionic surfactants typically contain functional groups, such as $SO_3^-$, that can be easily isolated from a polymer using spectroscopic techniques like FTIR. Most nonionic surfactants do not present such a possibility. One must also consider the substrate to be an integral part of the adhesive system. Therefore, casting films on PTFE and examining the F-S interface would not provide any useful information pertaining to some of the objectives of this research. Taking these facts into account, the characterization methods to be used for determining the effects of the surfactant on the adhesive properties of the epoxy have been targeted to those relevant to the actual epoxy/E-glass composites.

## 2.4 The Fiber-Matrix Interphase

Composite materials are composed of a material with high strength properties, but are difficult for direct production methods. Typically they consist of, e.g. glass fibers, and some sort of matrix material to hold the high tensile strength component together, e.g. epoxy resin.[33] In an epoxy-glass fiber composite the epoxy matrix also serves to aid in the handling and processing of the glass fiber. In addition to holding the glass fibers together the epoxy matrix serves to transfer and distribute the external stresses applied to the composite to the high strength glass fibers. However, the overall mechanical

properties of the composite are not simply governed by the properties of the matrix and reinforcing phases. The mechanical properties of the composite do not abruptly change from those of the bulk fiber to those of the bulk matrix at the interface, or sharp boundary, between the two phases. Instead, the properties in the region near the fiber surface and matrix phase will gradually change from the fiber phase to those of the matrix phase. This small region or phase of material of differing physical properties between the fiber and matrix phases is defined as the interphase. The interphase may only compose as little as one percent of the total volume of material in the composite, but plays a large role in the overall durability and mechanical performance of the composite.[34] The level of stiffness in the interphase region can mean the difference between the composite failing in a rapid catastrophic manner or with a more progressive compliant failure mechanism.[34] The interphase region may differ in chemical concentration, extent of chemical reaction, impurity and voiding level, as well as fiber morphology and surface treatment. A schematic representation of the interphase is illustrated in Figure 2-7.

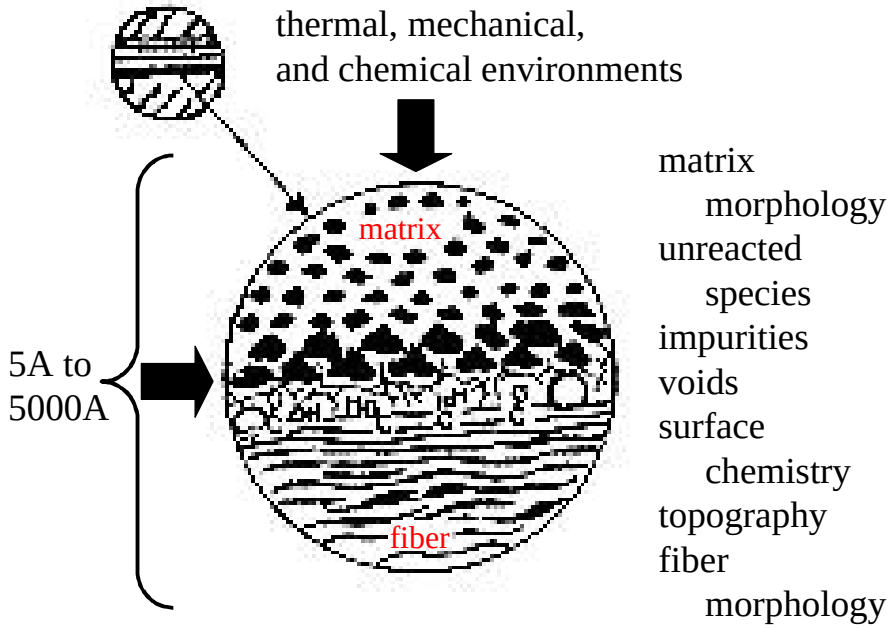


Figure 2-7. Schematic of the fiber-matrix interphase.[33]

### 2.4.1 Preferential Adsorption in Interphase Formation

One possible model for the formation of an interphase region is the preferential adsorption of some component of the matrix phase onto the surface of the fiber. Williams *et al*.[35] believe that this preferential adsorption of an active species could arise due to entropic effects. Due to the two dimensional nature of the fiber surface, a large polymer molecule will be more constrained due to adsorption than a small molecule. This is not entropically favored and thus provides a thermodynamic driving force for the preferential adsorption of small molecules at the fiber-matrix interface. For a crosslinked epoxy matrix the effect of this entropic driving force would be to increase the concentration of chain ends and network defects at the fiber glass interface. Williams *et al.* believe that this would increase the free volume and decrease the $T_g$ of the polymer in the interphase.

Mahy *et al*.[36] used X-ray photoelectron spectroscopy (XPS) and secondary ion mass spectrometry (SIMS) to investigate the interphase of a carbon fiber/epoxy composite. These researchers synthesized a range of epoxy resin monomers with varying degrees of polar functionality. It was determined that ether linkages and hydroxyl groups may adsorb to the surface of the fiber because of polar interactions. These researchers also used a fluorine- labeled difunctional amine to cure the matrix epoxy. The fluorine was used to map a cross section of the matrix-fiber interphase using SIMS. The results of these experiments verified that the stoichiometry of the epoxy-amine reaction differed from the bulk at distances of up to 10μm from the fiber surface.

Delong *et al*.[37] have suggested that the amine curing agent of the matrix phase can migrate into the sizing of the fiber surfaces. This migration of the amine hardener can change the $T_g$ of the interphase in relation to the bulk matrix. Maps of the interphase were created using Auger electron spectroscopy (AES) and Fourier transform infrared spectroscopy. Brominated epoxy resins were used construct model bilayer interphases. The results of these experiments indicated that FTIR does not possess the spacial resolution for spectroscopically probing the fiber-matrix interphase. AES has a sharper spacial resolution, but electrical charge build up could pose a problem of interpretation with this technique.

Marshall *et al.*[38] also determined that the interphase stoichiometry between an amine curing agent and epoxy resin differs from the bulk ratios. The micro-debond test was used to measure the interfacial shear strength between an epoxy resin matrix and sized carbon fibers. The amine to epoxy ratio of bulk samples was then varied to achieve an identical matrix shear strength. It was found that the amine to epoxy ratio of the bulk samples needed to be decreased to match the matrix and interfacial properties of the composite. These results suggested that the interphase region was deficient in amine curing agent.

Dirand *et al.*[39] studied the interphases of crosslinked vinyl ester/glass composites using FTIR and $^{13}C$ nuclear magnetic resonance spectroscopy. It was concluded that a concentration gradient of polystyrene existed at the vinyl ester-glass interface. This interphase was found to measure between 100 and 300μm thick. The interphase region also had a different elastic modulus than the bulk matrix material. These researchers proposed that the interphase region could be very important in the transfer of stress in a composite material.

### 2.4.2 Thermodynamics of Interphase Formation

Palmese and McCoullough[40], as well as Larson and Drzal[41], indicate that preferential adsorption at the interphase could be the result of the surface free energies (γ) and chemical interactions between the substrate and the matrix phase. These chemical interactions can result from dipole-dipole interactions, Van der Waals dispersive forces, hydrogen bonding, or chemical bonding. Surface free energy can be defined by the following equation.

$$\gamma = \left( \frac{dG}{dA} \right)_{T,P} \tag{1}$$

In this expression, A is the surface area and G is the Gibbs free energy. Young's equation can then be used to provide the equilibrium thermodynamic relationship between the contact angle, liquid surface free energy, and the solid surface free energy:[42]

$$\gamma_{SV} = \gamma_{SL} + \gamma_{LV} \cos\theta \tag{2}$$

$\gamma_{sv}$ = surface free energy of the solid in equilibrium with the saturated vapor of the liquid

$\gamma_{sl}$ = interfacial surface energy between the solid and liquid

$\gamma_{lv}$ = surface free energy of the liquid in equilibrium with the vapor

$\theta$ = liquid-solid contact angle

A vector representation of this equation is illustrated in Figure 2-8.

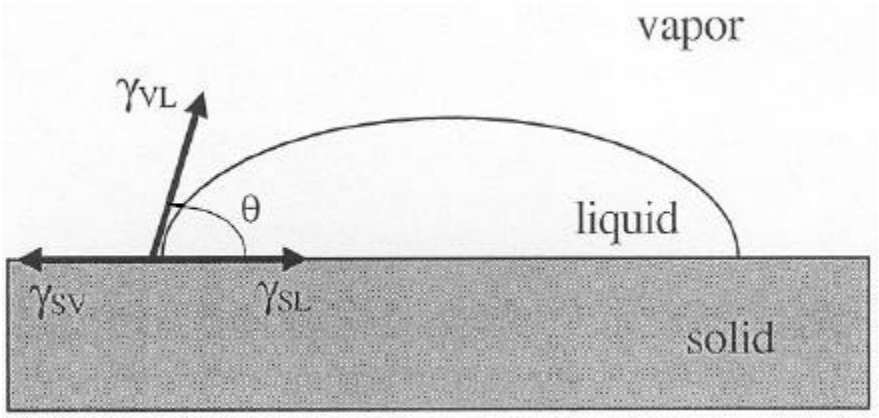


Figure 2-8. Physics of Young's equation.[43]

If the contact angle the liquid makes with the solid is equal to 0°, then the liquid will spread on the substrate. If the contact angle is less than 90° then the liquid is capable of wetting the surface. If the contact angle is greater than 90° then the liquid is non-wetting. For a composite to have good processability, the surface free energy of the matrix phase must be lower than the surface free energy of the fiber surface.[41]

The spreading pressure ($\pi_{sv}$) must also be considered when examining Young's equation.

$$g_S - g_{SV} = p_{SV} \tag{3}$$

In Equation 3 $\gamma_S$ is the surface free energy of the solid in equilibrium with its own vapor. Equation 3 can then be substituted into Young's equation to give the following expression.

$$g_{SL} - g_S + g_{LV}\cos q + p_{SV} = 0 \tag{4}$$

The spreading pressure represents the decrease in the surface free energy of the solid due to vapor adsorption. The spreading pressure can generally be neglected at moderate values of $\theta$.[43]

Referring to Young's equation it can be seen that the spreading of the liquid over the surface of the solid will only occur if the Gibbs free energy is decreased. Dupre defined

the work of adhesion ($W_a$) as $-\Delta G/A$, which is equal to $\gamma_{sv} + \gamma_{lv} - \gamma_{sl}$.[42] Therefore, wetting will occur favorably when the difference in interfacial surface free energy between the solid and liquid is low, the surface free energy of the liquid is low, and the surface free energy of the solid substrate is high. The surface free energy of the substrate often is invariant and the matrix-vapor free energy will have no effect upon the interfacial adhesion between the fiber and the matrix phase. Therefore, the controllable thermodynamic driving force for the preferential adsorption of specific components of the liquid matrix phase involves a decrease in $\gamma_{sl}$, which will decrease the Gibbs free energy of the fiber-matrix interface.

Following is the argument given by Palmese and McCullough[40] for the migration of amine curing agent to the surface of carbon fiber in amine-epoxy systems. Palmese and McCullough[40] reported that the typical surface free energy of an epoxy resin can lie in a range of 45 to 52 $mJ/m^2$ and the typical surface free energy values for amine hardeners range between 23 and 26 $mJ/m^2$. Therefore, thermodynamically it is preferential for the amine component of the liquid matrix phase to adsorb on the surface of the fiber. These thermodynamic conclusions are based on the assumption that is kinetically possible for the migration to occur prior to the amine reacting with the epoxy or the formation of a crosslinked epoxy network, which would limit diffusion. This concept is shown schematically in Figure 2-9.

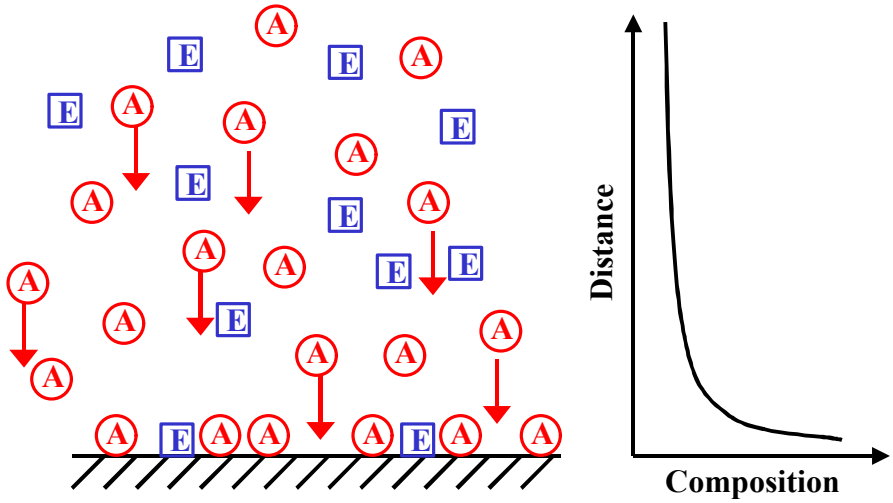


Figure 2-9. Palmese and McCullough model for interphase formation.[40]

Similar arguments have been presented as a possible explanation for surfactant migration in latex films. Urban has stated that if the surface free energy of the solid substrate is lower than the surface free energy of the latex to be spread across the substrate, there will be a driving force for the surfactant to migrate towards the film-substrate interface.[44,45] This will be true if the surfactant has a lower surface free energy than the latex polymer of the film. The result would be a decrease in the interfacial free energy and a lower overall free energy for the wetting process. Urban's results on cast latex films on PTFE substrates seemed to verify his hypothesis.

## 2.5 Silane Coupling Agents

The most common method of altering the surface chemistry of E-glass is with a silane coupling agent pretreatment. The purpose of the silane coupling agent is to provide a covalent chemical bond between the matrix phase and glass fibers of the composite. The generic molecular formula for a silane coupling agent is $R_nSiX_{(4-n)}$.[46] The X group is a hydrolyzable group, such as a methoxy or ethoxy group. Once this group is hydrolyzed in an aqueous solution a reactive silanol group is formed. This silanol group can then condense on the surface of the glass and chemically bond with the silanols present on the glass. The R group can have a wide range of funtionalities, but is usually chosen to react with the matrix phase in composite materials.[46] The reaction scheme between the silane coupling agent and the glass surface is illustrated in Figure 2-10.

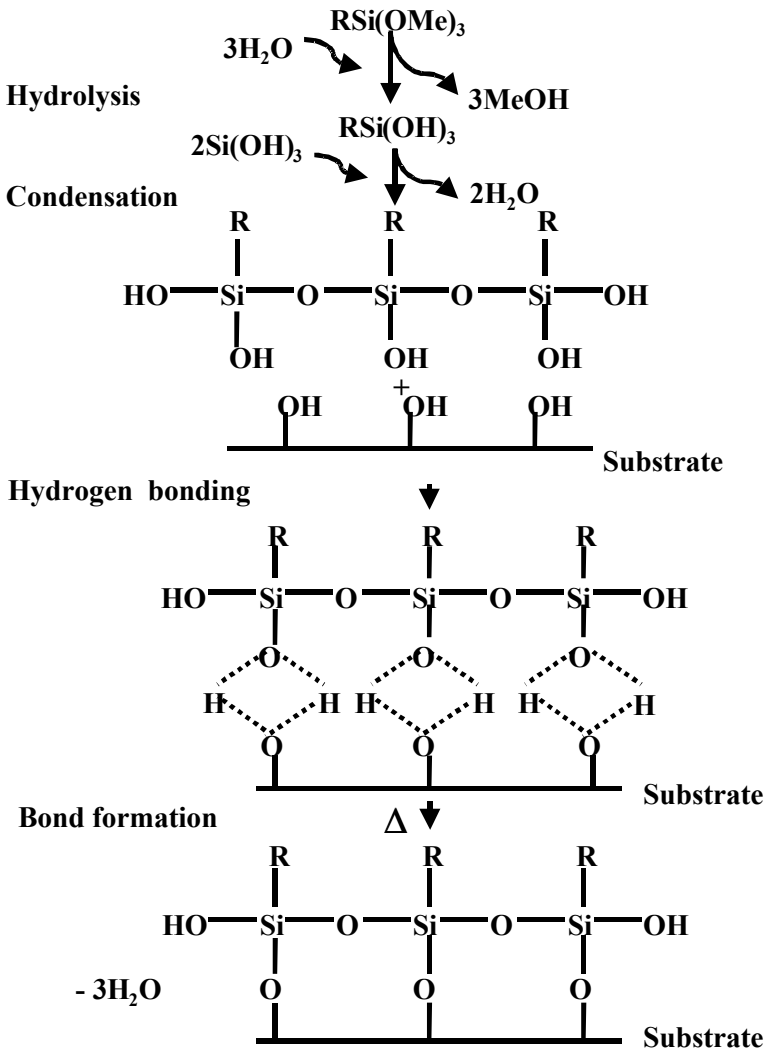


Figure 2-10. Deposition of a silane coupling agent onto the surface of glass.[46]

This reaction scheme between the silane coupling agent and the glass surface is highly idealized. The silane coupling agent is actually deposited onto the surface of the glass in multiple layers. Wang and Jones[47,48] have performed extensive studies of the surface of silane treated glass using time-of-flight secondary ion mass spectrometry (TOF-SIMS) and X-ray photoelectron spectroscopy. These researchers coated an E-glass slide from a 1.5 percent concentration of aqueous γ-aminopropyltriethoxysilane (APS) solution. It was determined that the silane coupling agent on the glass surface was approximately 60nm thick. This corresponds to about 10 monolayers of APS. XPS angular analysis also revealed that the amine groups of the APS were oriented away from the surface of the glass. The microstructure of the deposited silane also varied with depth. The outer

layers of silane are only physically adsorbed and are oligomeric in nature. The crosslink density of the silane increases as the surface of the glass is approached. These outer layers of silane can be extracted with organic solvents or water. The layer of silane in immediate proximity to the glass surface is chemically bonded to the surface silanols of the glass and cannot be removed through extraction. Wang and Jones also determined that this chemically bonded layer of silane also has a very high crosslink density. Chua *et al.*[49] have referred to the bonded and adsorbed layers of silane as chemisorbed and physisorbed, respectively. A schematic representation of this glass surface-silane interphase is illustrated in Figure 2-11.

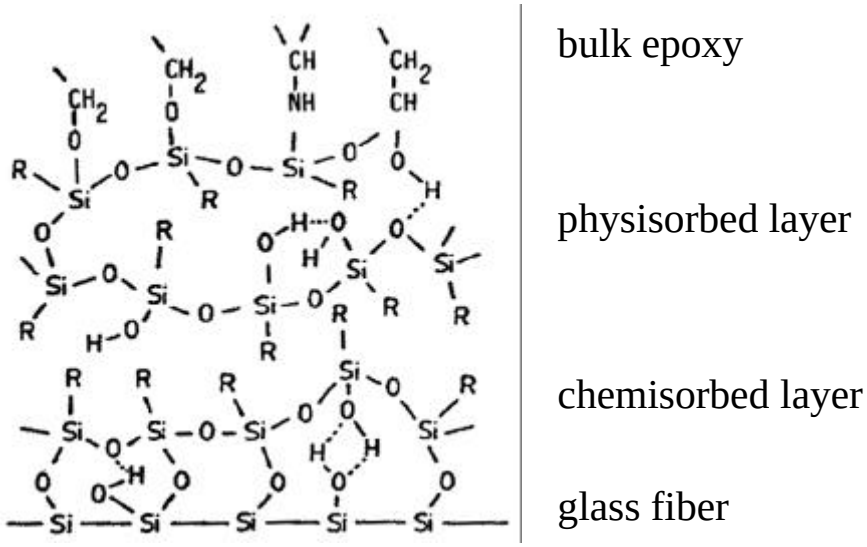


Figure 2-11. Schematic model of the glass-silane coupling agent interphase.[49]

The interactions of the physisorbed and chemisorbed layers of silane coupling agent with the matrix phase of the composite are complex. One obvious effect of the silane glass pretreatment is to alter the surface free energy and wetting ability of the matrix phase over the glass fibers. Mader[50] has measured the surface free energy of silane pretreated E-glass fibers with respect to an epoxy resin. Using a Wilhelmy method, Mader measured a surface free energy of a typical DGEBA based epoxy resin to be 44mJ/m$^2$. The surface free energies of an untreated E-glass fiber, APS pretreated E-glass fiber, and an amine-epoxy silane pretreated E-glass fiber were 58.3mJ/m$^2$, 31.6mJ/m$^2$, and 34.7mJ/m$^2$, respectively. Therefore, untreated glass fibers are favored for

thermodynamic wetting by an epoxy resin. But, the trade-off associated with the high surface free energy of an untreated glass fiber is poor moisture resistance.

Once the matrix phase has wetted the silane coated fibers further matrix-silane interactions can occur through inter-diffusion mechanisms. Depending on the level of silane-matrix miscibility the silane can plasticize the matrix phase.[51] Drzal *et al.*[51] have estimated the silane-matrix interphase region thickness to range between 100 to 500nm. These researchers have conducted studies of stiochiometric blends of various coupling agents, such as N-(2-aminoethyl)-3-aminopropyltrimethoxysilane and 3-glycidoxypropyltrimethoxysilane, with basic DGEBA epoxy resins. Their findings indicate that the interphase region can have a higher modulus and tensile strength, but lower $T_g$ and fracture toughness than the bulk epoxy matrix phase.

Koenig and Chang[52] have proposed that a silane coupling agent can induce changes in the extent of reaction of an epoxy resin, which will lead to the formation of a fiber-matrix interphase region. In their study FTIR was used to monitor the reaction between a DGEBA epoxy resin and nadic methyl anhydride as the matrix phase of an E-glass composite. The glass fibers were pretreated with N-methylaminopropyltrimethoxysilane. The degree of conversion of the epoxy resin increased by as much as 10 percent in the fiber matrix interphase due to the amine groups of the coupling agent. These authors propose that the crosslink density of the epoxy is greater in the interphase than the bulk matrix phase. Chang and Koenig also state that it is possible for a low molecular weight epoxy resin to penetrate and diffuse into the silane coupling agent layer. These results also have implications with respect to the moisture uptake properties of a composite. If the crosslink density of the interphase region is increased then the moisture diffusion rate of the interphase should decrease. Although the moisture diffusion rate could possibly be reduced in the fiber-matrix interphase, Chang and Koenig believe that silane coupling agents increase the moisture durability of glass composites by protecting the actual glass surface from moisture.

Cossins *et al.*[53] monitored the curing reaction of a DGEBA epoxy resin with poly(oxypropylenediamine) using silica optical fibers and near infrared spectroscopy. The silica optical fibers were pretreated with trimethoxysilylpropyldiethylenetriamine. The results of this study indicated that the silane coupling agent had no effect on the

degree of conversion of epoxy resin at the fiber-matrix interphase. These authors suggest that because the coupling agent and curing agent both have active amine hydrogen atoms that the curing mechanism is similar in both the bulk matrix phase and interphase region.

## 2.6 The Interphase and Mechanical Properties

Yumitori *et al.*[54] identified the importance of the fiber-matrix interphase region with respect to the ultimate mechanical properties of composite materials. These researchers performed the single fiber fragmentation test for carbon fibers embedded in either a thermoplastic poly(ethersulfone) (PES) matrix or thermoset epoxy matrix. The surface preparation for the carbon fibers varied from 1) untreated and unsized, 2) oxidized and unsized, and 3) sized with a brominated epoxy resin. The interfacial shear strength ($\tau$) between the PES and embedded carbon fibers was approximately 38 MPa for the brominated epoxy resin sizing, 27 MPa for the oxidative treatment, and 20 MPa for the untreated fibers. The interfacial shear strength between the epoxy matrix and carbon fibers was approximately 35 MPa for the oxidized fibers, 25 MPa for the brominated epoxy resin sizing, and 18 MPa for the untreated fibers.

Yumitori *et al.*[54] proposed that the differences in the trends of $\tau$ between the carbon fibers and PES or epoxy matrices are due to differences in the interphase structures. Because of the bromine atom in the epoxy resin sizing, the penetration of the sizing into the matrix phase could be measured using time-of-flight secondary ion mass spectrometry. The results of the TOF-SIMS experiments indicated that the brominated epoxy resin sizing had achieved a greater degree of penetration into the PES matrix than the epoxy matrix. These researchers then concluded that the intermixing between the PES and sizing promoted strong dipolar interactions, which increase the interfacial bond strength. However, the brominated epoxy resin sizing simply acts as an interlayer when an epoxy matrix is used, which decreased the interfacial bond strength relative to the PES matrix. A schematic representation of Yumitori's interphase region is shown in Figure 2-12.

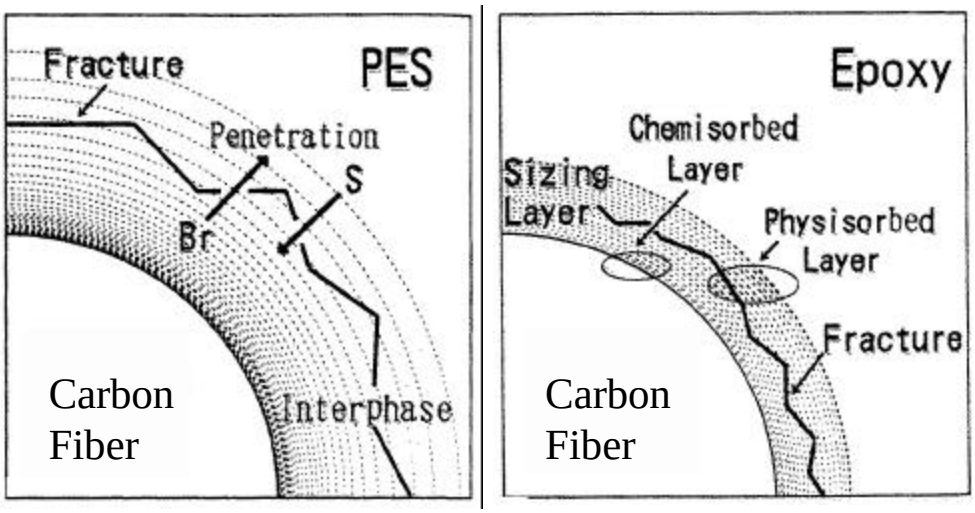


Figure 2-12. Schematic of sizing-matrix interphase region surrounding carbon fiber.[54]

Sottos and Li[55] studied the effects of temperature on the interfacial shear strength of epoxy-carbon fiber composites. These researchers proposed that the glass transition temperature of the interphase region should highly influence the interfacial shear strength of a composite material. The matrix material transfers the applied load to the high modulus fibers of the composite. The modulus and $T_g$ of the matrix-fiber interphase will influence the efficiency of this load transfer. In this study carbon fibers were pretreated with either a low modulus/low $T_g$ sizing, high modulus/high $T_g$ sizing, or were left uncoated. The interfacial shear strength was then determined by a fiber fragmentation technique. The uncoated and low modulus/low $T_g$ sized fiber composites had the highest room temperature interfacial shear strengths (≈ 45 MPa), but showed a 26 % reduction in $\tau$ as the temperature was increased to 100°C. The high modulus/high $T_g$ sized fiber composite resulted in a room temperature $\tau$ of 40 MPa, but only showed a 10 % reduction in interfacial shear strength as the temperature was increased to 100°C. Sottos and Li believe that the interphase $T_g$ of the untreated carbon fiber composite was depressed due to a non-stoichiometric curing reaction between the epoxy resin and hardener near the fiber. The glass transition and modulus of the interphase region are yet additional factors that must be taken into consideration when predicting the mechanical properties of a composite.

Cheng *et al.*[56] also showed that an unsized oxidized pretreated carbon fiber-epoxy composite could achieve higher levels of $\tau$ than sized epoxy-carbon fiber composites. A

fiber fragmentation test was used to determine values of $\tau$ equal to 18 MPa for untreated and unsized carbon fibers, 33 MPa for unsized and oxidized fibers, and 26 MPa for aqueous emulsion epoxy resin sized fibers. An oxidized carbon fiber surface can interact strongly with the epoxy resin matrix, leading to a high interfacial shear strength. Cheng *et al*. also state that the epoxy sizing used to pretreat the carbon fibers has a favorable affinity for the fiber surface. If the sizing interacts too well with the fiber surface and not so well with the matrix phase, then little inter-diffusion between the matrix phase and the sizing will occur. This could potentially result in a weakened interphase between the carbon fiber and epoxy matrix. Cheng *et al.* also observed a sizing molecular weight dependence with respect to the interfacial shear strength of the composite. As the molecular weight of the sizing was decreased, $\tau$ increased. This again supports the hypothesis that some amount of inter-diffusion between the fiber sizing and matrix phase is required to attain strong interfacial adhesion.

The quantity of literature that states the importance of the matrix-fiber interphase to the overall mechanical performance and durability of composite materials is vast and extensive. Piggott[57,58] has theorized that the ideal interphase for shear strength and toughness would have a modulus intermediate between that of the fiber and matrix. Palmese and McCullough[59] stated that as the modulus of the interphase region is increased that the residual thermal stress in the matrix phase will decrease. A high level of residual stress in the matrix phase can lessen the ultimate mechanical strength of a composite material. In contrast, Tryson and Kardos[60] determined that a ductile elastomeric interphase improves the mechanical properties of E-glass composites by providing buffer zones around the fibers. Madhukar and Drzal[61,62] have performed extensive research in correlating the level of fiber-matrix adhesion and interfacial properties with the failure modes of composite materials. The literature available pertaining to the fiber-matrix interphase is often contradictory, but most of the researchers agree that the properties of the fiber-matrix interphase are very important and further study is needed.

## 2.7 Mechanical Testing

### 2.7.1 Single Fiber Pull-Out Test

There have been many mechanical test methods used in characterizing the adhesive strength between a fiber and the matrix polymer of composite materials. This reflects the importance of the physical properties of the interphase region. The fiber and the matrix have a substantial influence on the ultimate mechanical properties of the composite, as presented above. If a composite with high strength is required then "good" adhesion is required between the fiber and the matrix.[63] If the adhesive strength of the matrix-fiber interphase is too "good" then the composite may become very brittle which will result in decreased fracture toughness. The moisture adsorption properties of composite materials have are also dependent on the quality of bonding between the matrix phase and fiber reinforcement.[64]

There are two basic mechanical tests to characterize the adhesive properties and average interfacial shear stresses ($\tau_{avg}$) between the matrix and fiber of composite materials. One class of tests is performed on single-fiber composites while the other class of tests is performed on multi-ply laminate composite samples.[65] Mechanical tests performed on single-fiber composites include the fiber pull-out or debond test, microbond pull-out test, and the fiber fragmentation test. Real composites can be examined by indentation tests, short beam shear tests, Iosipescu shear tests, as well as off-axis tensile tests.

Extensive research has been performed using all three of the previously mentioned single-fiber composite tests. [63,66,67,68] These mechanical tests are portrayed in Figure 2-13. This will be followed by a brief analysis of the fiber debond test as used by DiFrancia *et al.*[67,68], which will be used in the research presented in this thesis.

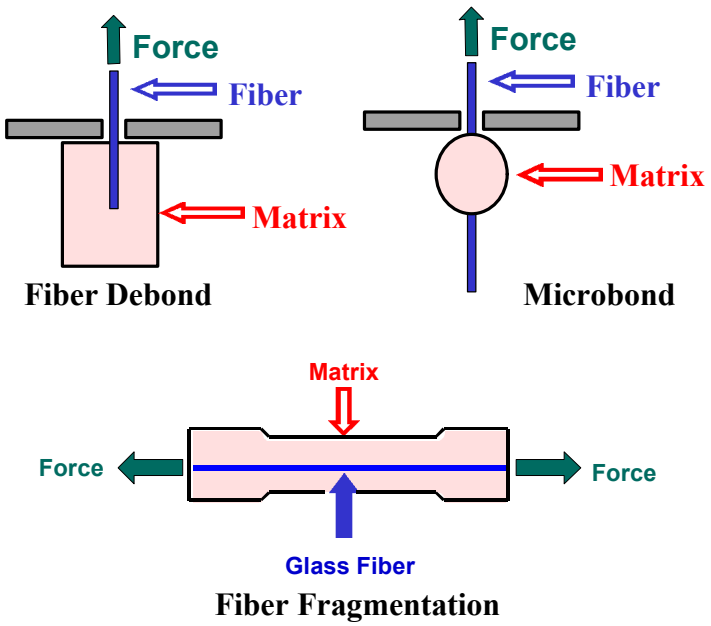


Figure 2-13. Single fiber composite tests used to determine $\tau_{avg}$.[63]

#### 2.7.1.1 Fiber Debond Test

DiFrancia et al.[66,68] were able to use a modified version of the single fiber fragmentation test to determine the interfacial shear stresses caused by crack initiation, debond propagation, and the frictional sliding of a single fiber from a dogbone sample. In this work a polyimide coated optical fiber was placed in a dogbone sample that was composed of tetraglycidyl-4,4'-diaminodiphenylmethane cured with 4,4'-diaminodiphenylsulfone. Rather than fragmenting the embedded fiber, the dogbone was first cracked perpendicular to the fiber direction prior to stretching. When this sample was strained in a Minimat® tensile tester the fiber simply pulled out of the dogbone. A schematic representation of this testing configuration is shown in Figure 2-14.

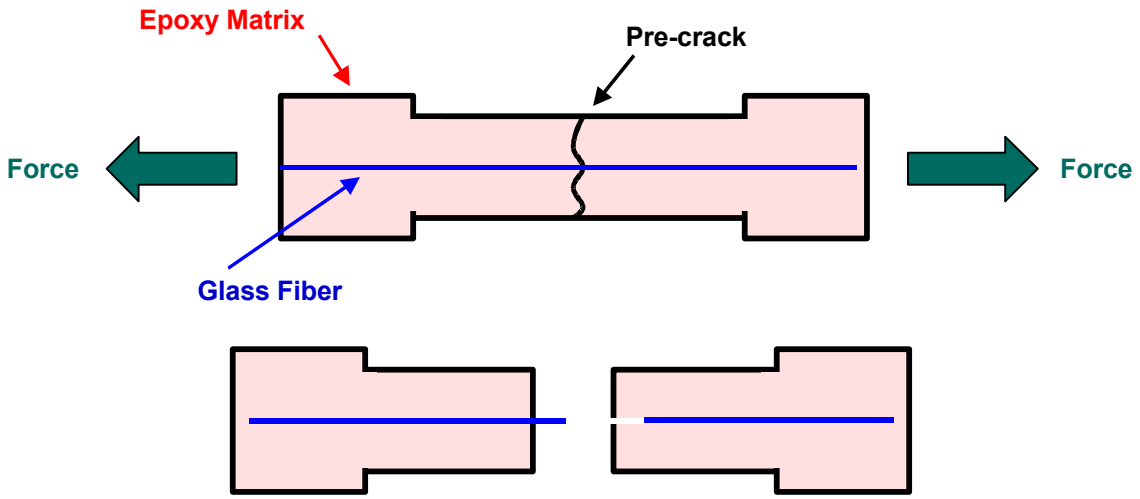


Figure 2-14. Schematic of fiber pull-out test as performed by DiFrancia.[67,68]

DiFrancia was able to observe the entire load versus extension data range generated during the fiber pull-out test rather than simply reporting the maximum load required for fiber debonding. DiFrancia was able to identify specific zones correlating to crack initiation, frictional debonding, crack completion, the steady frictional sliding pull-out of the fiber, followed by the removal of the frictional zone. These zones are represented graphically in Figure 2-15. From these zones DiFrancia was able to calculate the critical strain energy release rate for crack initiation and propagation, interfacial debond shear stress, as well as the stress during frictional sliding. The primary advantage of using this type of experimental set up is that the embedded length of fiber does not have to be less than or equal to the critical strain length of the fiber. In other words, this method accounts for the fiber breaking prior to pull-out.

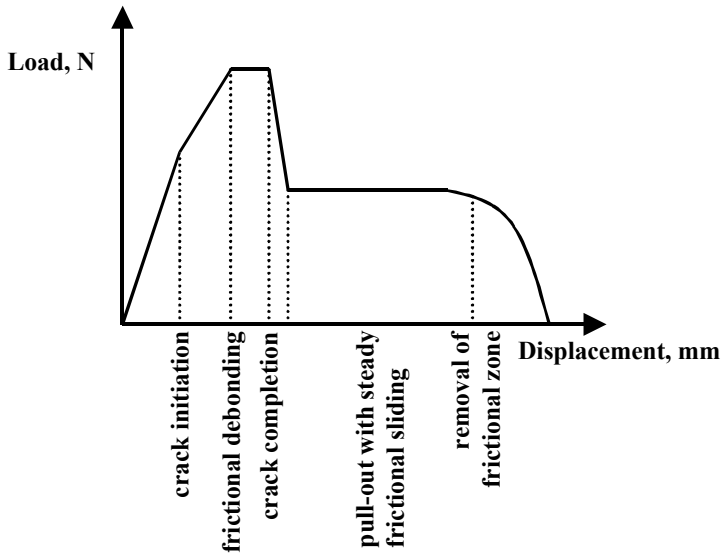


Figure 2-15. Load versus extension trace for single fiber pull-out proposed by DiFrancia[67]

The most recent research performed at Virginia Tech involving single fiber composites was conducted by Clark.[63] Clark used the single fiber pull-out test to characterize the mechanical properties of nylon 6,6/E-glass composites. This test is very similar to the microbond pull-out test except that one end of the fiber is embedded into a pot of resin rather than bonding a single drop of matrix polymer to the center of the fiber. Equation 5 is used to approximate $\tau_{avg}$ for the fiber debond test.

$$\tau_{avg} = \frac{F_d}{\pi d l_e} \tag{5}$$

d = fiber diameter

$l_e$ = fiber embedded length

#### 2.7.1.2 Limitations

Single fiber composite testing has limitations. In the fiber fragmentation test the dogbone matrix polymer must be transparent and have high yield strength. The microbond pull-out test and fiber debond tests are both fairly simple to describe mathematically, but generate data with a large amount of scatter. This scatter in the

experimental data is believed to be caused by irregularities on the surface of the fiber. But, the microbond pull-out technique also has the potential of generating noisy data depending on the applied load's point of contact on the drop.[69] Sample preparation for each of these tests is also extremely difficult. In the fiber debond test the embedded length must be less than 150μm if small fiber diameters are used (d < 100μm) in order to avoid breaking the fiber before debonding.

In addition to the experimental difficulties associated with single fiber pull-out characterization techniques Piggott[70] has identified some more specific theoretical inconsistencies with this type of testing. The large amount of scatter generated with these tests is the result of brittle fracture, but starter cracks are seldom observed. The debonding stage is a function of Poisson's contraction in the fiber, matrix pressure due to cure shrinkage, and the surface roughness of the fiber. Each of these factors are irrelevant to the adhesion between the matrix and fiber, but are measured. The fiber-matrix entrance point has a much higher stress level than the embedded end point of the fiber. This uneven distribution of stresses results in calculated values of interfacial shear strength that are much greater than the strength of the matrix. There is also a mixing of failure modes between shear and tension during the pull-out process. Piggott states that the polymer chains can only slide over each other to a small extent before breaking in a tensile mode.[70] This is why the fibers always appear clean after pull-out and the interfacial shear strengths can be high. This interpretation needs substantial qualification.

### 2.7.2 Short Beam Shear Test

#### 2.7.2.1 Theory

The short beam shear test is a common method for determining the apparent interlaminar shear strength in composite materials. The composite sample is loaded in a three-point bending fixture as shown in Figure 2-16. The primary advantage of using the short beam shear test is that the testing samples are relatively easy to produce and the testing fixtures are simple to operate.[71]

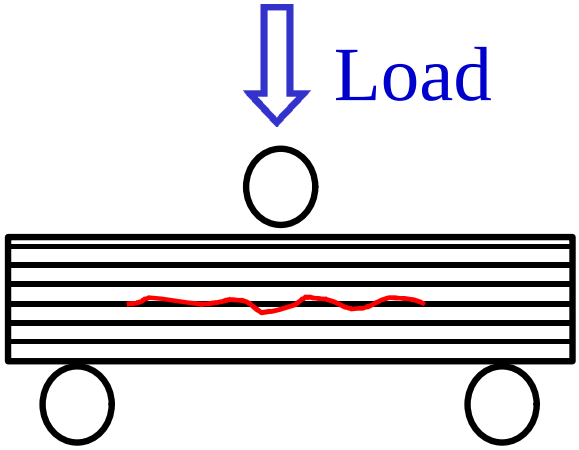


Figure 2-16. Three-point bending configuration used for the short beam shear test.

The interlaminar shear strength for the short beam shear test is derived from an elementary beam theory analysis.[72,73] The maximum flexural stress for a rectangular cross sectioned beam in a three-point bending fixture is given by the following equation.[72]

$$\sigma_{max} = \frac{3}{2}\frac{P}{bt}\frac{l}{t} \tag{6}$$

In this equation $\sigma_{max}$ is the maximum flexural stress, P is the applied load at failure, l is the support span length, t is the composite thickness, and b is the composite width. The maximum interlaminar shear stress for the beam is given in the following expression.

$$\tau_{max} = \frac{3}{4}\frac{P}{bt} \tag{7}$$

The maximum shear stress and flexural stress can be related by dividing Equation 7 by Equation 6.[72]

$$\tau_{max} = \frac{\sigma_{max}}{2(l/t)} \tag{8}$$

The American Society of Testing and Materials (ASTM) recommends using a span to thickness ratio (l/t) of 5 for glass fiber composites in ASTM D 2344.[74] Equation 7 is then used to solve for $\tau$.

#### 2.7.2.2 Limitations

Madhukar and Drzal[75] have cited several potential drawbacks of the short beam shear test. The composite sample for this test will fail if either the interfacial shear stress or matrix shear stress exceeds the stress applied to the center of the beam. Therefore, failures in the matrix phase could be mistaken for interfacial failure. There are also non-uniform stress states due to mixing of failure modes. Herrera-Franco and Drzal[69] also states that the shear stress may not always occur in the center of the beam. These researchers believe that the short beam shear test should only be used for estimating interfacial shear strengths and as a preliminary test for evaluating mechanical properties.

Adams and Lewis[72] also performed an in depth study with respect to the influence of sample variation during the short beam shear test. These researchers found that the largest variation in experimental data will result when the length span to thickness ratio of the test is changed. If elementary beam theory is correct then the measured interlaminar shear strength should remain constant below a length span to thickness ratio of 7.5. The shear strength of a composite will increase to a large extent as the length span to thickness ratio is decreased, which cannot be adequately described by the simple beam theory. The sample thickness will also change the experimental results of this test. The shear strength will increase as the sample thickness decreases due to a lower number of defects contained within the sample. Adams and Lewis suggest that due to the actual complex stress states generated by this testing configuration that numerical finite element analysis is required for analysis.

#### 2.7.2.3 Short Beam Shear Test Literature Results

Hoecker and Karger-Kocsis[76] investigated the micro and macro-mechanical properties of an epoxy-carbon fiber composite via the fiber fragmentation test, microdroplet debond test, and short beam shear test. Fiber volume fraction, fiber aspect ratio, fiber orientation, and fiber and matrix moduli influence the ultimate properties of composite materials. The advantage of performing macro-mechanical testing, such as the short beam shear test, on actual composite samples is that all of these factors can be incorporated into the test. However, the stress states in a large composite sample are difficult to describe and model mathematically. Micro-mechanical testing offers the potential of a more direct

quantification of the interfacial properties of the composite. But, these micro-mechanical methods cannot duplicate actual manufacturing methods.

Hoecker and Karger-Kocsis[76] carried out a comparative study of these micro and macro-mechanical techniques using carbon fiber that had been pretreated with sizings which were intended to yield good or poor interfacial adhesion between the epoxy matrix and carbon fibers. The fiber fragmentation technique yielded interfacial shear strength of 95.2 MPa for good adhesion and 63.2 MPa for poor adhesion. The microdroplet debond method provided $\tau$ values of 41.1 MPa and 28.4 MPa for good and poor interfacial adhesion, respectively. The two micro-mechanical technique values differ, but the reported values followed the expected trends. An interlaminar shear strength of 51 MPa for both the good and poor sizing agent was determined using the short beam shear test. The inability of the short beam shear test to differentiate the fiber sizings was attributed to a more cohesive matrix type failure using this method.

Larson and Drzal[77] compared the micro-indentation technique and short beam shear test for characterizing the fiber-matrix adhesion of vinyl ester/E-glass composites. The microindentation technique uses a small probe to debond the fiber from the matrix by indentation. The theoretical considerations for the micro-indentation technique are similar to fiber pull-out methods. In this study Larson and Drzal correlated the surface free energy of the fiber as well as the miscibility between the fiber sizing and matrix phase to the overall interlaminar shear strength of the composite. This study concluded that a high fiber surface free energy ($\gamma_f$) and degree of interaction between the fiber sizing and matrix phase are essential for good interfacial mechanical properties. An interesting find of this study was that a bare E-glass fiber ($\gamma_f$ = 59 mJ/m$^2$) showed higher interfacial shear strengths than non-interacting insoluble polyurethane fiber sizings ($\gamma_f$ = 35 mJ/m$^2$). The only fiber sizings that improved the mechanical properties of the composite were the sizings that interacted chemically with the matrix, such as soluble polyester or epoxy sizings. The insoluble polyurethane sized fiber composites short beam shear strength was 30 MPa in comparison to the strength of 50 MPa when bare E-glass fibers were used. The soluble polyester and epoxy sizings only increased the short beam shear strength to 60 MPa. The fiber-matrix adhesion strength measured using the microindentation technique were approximately 50 percent greater than the short beam shear

determinations. Larson and Drzal attributed these results to the greater number of flaws present in the composite samples.

Drown *et al.*[78] also used the microindentation technique and short beam shear tests to compare the mechanical properties of epoxy/E-glass composites. Using the microindentation technique the interfacial shear strength of an epoxy compatible sized fiber composite was 35 percent greater than when unsized fibers were used. The short beam shear strength test was not as sensitive and only recorded a 12.4 percent difference in interfacial shear strengths. These researchers observed a change in the interfacial failure mode mechanism during the short beam shear test. This test produced large matrix cracks that propagated rapidly as the load was increased. This is believed to be a limiting factor in the load that can be applied to the composite during the short beam shear test. If the matrix of the composite were failing inopportunely then the interfacial sensitivity of this test would become limited.

## 2.8 Viscoelasticity

### 2.8.1 Dynamic Mechanical Analysis

Dynamic mechanical analysis is a very common and convenient method for characterizing the linear viscoelastic properties of polymers. In this type of experiment a small oscillating stress or strain, at some angular frequency $\omega$, is applied to the material.[83] The strain level is low to insure linear response (stress is proportional to strain). The typical range of $\omega$ for a dynamic mechanical analysis experiment lies in the 0.001 to 100 Hz range. If a sinusoidal stress ($\sigma$) is applied to a perfectly elastic material then the resulting strain ($\varepsilon$) will be in-phase. If a sinusoidal stress is applied to a perfectly viscous fluid the resulting strain will be 90° out-of-phase with the applied stress. Polymers have a combination of viscous and elastic properties (viscoelastic), so the strain will be at some intermediate phase angle ($0° < \delta < 90°$) behind the applied stress. This is shown in the vector diagram of Figure 2-17.

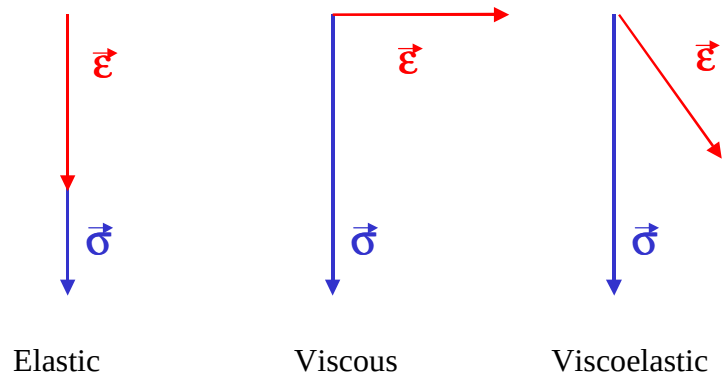


Figure 2-17. Dynamic stress and strain vectors for A) an elastic material B) a viscous material C) a viscoelastic material.[83]

The in-phase tensile modulus (E ) and out-of-phase tensile modulus (E ) from dynamic mechanical analysis are derived through the following equations.[83] The stress σ(t) is related to the strain ε(t), as a function of time t, of a material that has undergone some continuous strain history through the following expression:

$$s(t) = \int_{-\infty}^{t} \frac{de(u)}{du} E(t-u)du \tag{9}$$

By substituting t-u with the variable s Equation 9 becomes the following:

$$s(t) = -\int_{0}^{\infty} \frac{de(s)}{ds} E(s)ds \tag{10}$$

An applied sinusoidal strain can then be separated into real and imaginary components:

$$e(t) = e_o e^{iwt} = e_o(\cos wt + i\sin wt) \tag{11}$$

Equation 11 can then be substituted back into Equation 10 to give the following expression:

$$\frac{s(t)}{e(t)} = E^*(t) = \int_{0}^{\infty} iwe^{-iwt} E(s)ds = \int_{0}^{\infty} w(\sin ws)E(s)ds + i\int_{0}^{\infty} w(\cos ws)E(s)ds \tag{12}$$

The real component (E ) of the complex modulus ($E^*$) is referred to as the storage modulus. Therefore, this is the elastic contribution. Hooke's law states that a spring stores energy. Hence the name storage modulus. The imaginary component is named the loss modulus (E ). The loss modulus represents the out-of-phase, or viscous, component

of the complex modulus. A perfectly viscous liquid dissipates, or "loses", the deformation energy as heat. Therefore, the out-of-phase component is referred to as the loss modulus. Models that incorporate springs and dashpots are often used to represent these concepts. The loss tangent (tan δ) is proportional to the phase angle between the applied stress and the resultant strain.

$$\tan\delta = \frac{E''}{E'} = \frac{\omega\int_0^\infty \cos\omega s E(s)ds}{\omega\int_0^\infty \sin\omega s E(s)ds} \tag{13}$$

### 2.8.2 Distribution of Relaxation Times

As mentioned in the previous section, springs and dashpots are often used to represent the viscoelastic behavior of a polymer. One such model is the Maxwell element shown in Figure 2-18. The spring has a modulus, or stiffness, of E and the dashpot, or damper, is filled with a liquid of viscosity η.

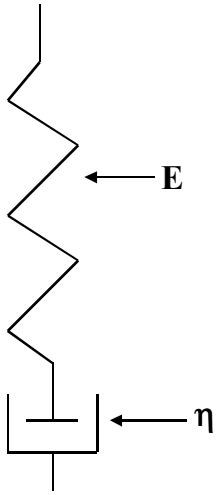


Figure 2-18. Schematic diagram of the Maxwell element.[83]

The tensile stress relaxation modulus of the Maxwell model is given in the following equation.

$$E(t) = Ee^{\frac{-t}{\tau}} \tag{14}$$

In Equation 14, t is the time of the experiment and τ is the characteristic relaxation time of the Maxwell element. The stress relaxation modulus of a real polymeric material

would be impossible to describe with a single Maxwell element. Many elements are required to describe a distribution of relaxation times for the polymer. A continuous integral function is often used to model the distribution of relaxation times.[83]

$$E(t) = \int_0^{\infty} E(\tau) e^{\frac{-t}{\tau}} d\tau \tag{15}$$

This distribution of relaxation times is accounted for in dynamic mechanical experiments via the following set of equations.[83]

$$H(\tau) = \tau E(\tau) \tag{16}$$

$$E'(\omega) = \int_{\ln\tau=-\infty}^{\ln\tau=\infty} H(\tau) \frac{\omega^2\tau^2}{1+\omega^2\tau^2} d\ln\tau \tag{17}$$

The equations used to derive the distribution of relaxation times are complex. Fortunately, key assumptions pertaining to the distribution of relaxation times can be used to predict key mechanical and viscoelastic properties without ever directly determining the distribution. This is taken advantage of in the time-temperature superposition principle. Temperature will have a dramatic effect on the relaxation times of a polymer. However, the key assumption is that even though the relaxation times are changing with temperature the shape of the relaxation time distribution is not. For this assumption to be valid the molecular relaxation mechanism must also not change with temperature.

Time-temperature superposition is used to construct master curves. If the isothermal response of a polymer is known as a function of time or frequency then the isotherms can be shifted to predict long time or high frequency behavior. A master curve for stress relaxation is illustrated in Figure 2-19.

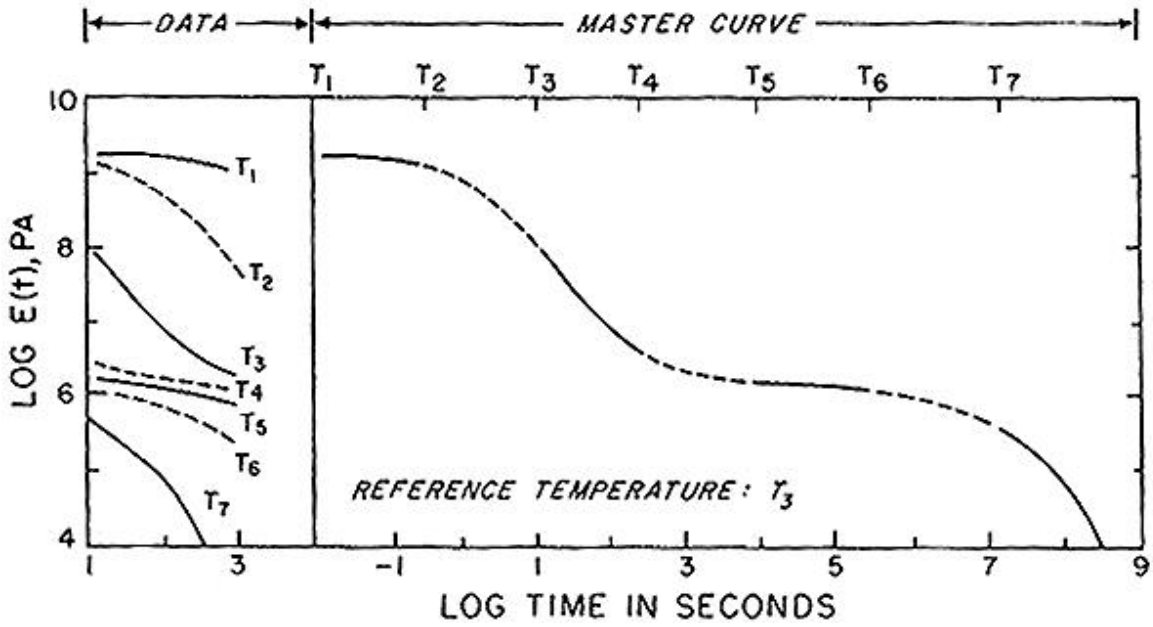


Figure 2-19. Stress relaxation master curve.[83]

The isotherms of the master curve are shifted horizontally on the log time or frequency axis relative to some reference temperature ($T_R$). The amount of horizontal shift is called a shift factor ($\log a_T$). The shift factor simply represents the ratio of the apparent relaxation times ($\tau^*$) at the new temperature in comparison with the apparent relaxation times at the reference temperature. The shift factors are often plotted versus T-$T_R$. The empirical Williams-Landel-Ferry (WLF) equation (Equation 18) is often fitted to the shift factor plots.[83] A typical shift factor plot is portrayed in Figure 2-20.

$$\log(a_T) = \log\frac{t^*(T)}{t^*(T_R)} = \frac{-C_1(T - T_R)}{C_2 + T - T_R} \tag{18}$$

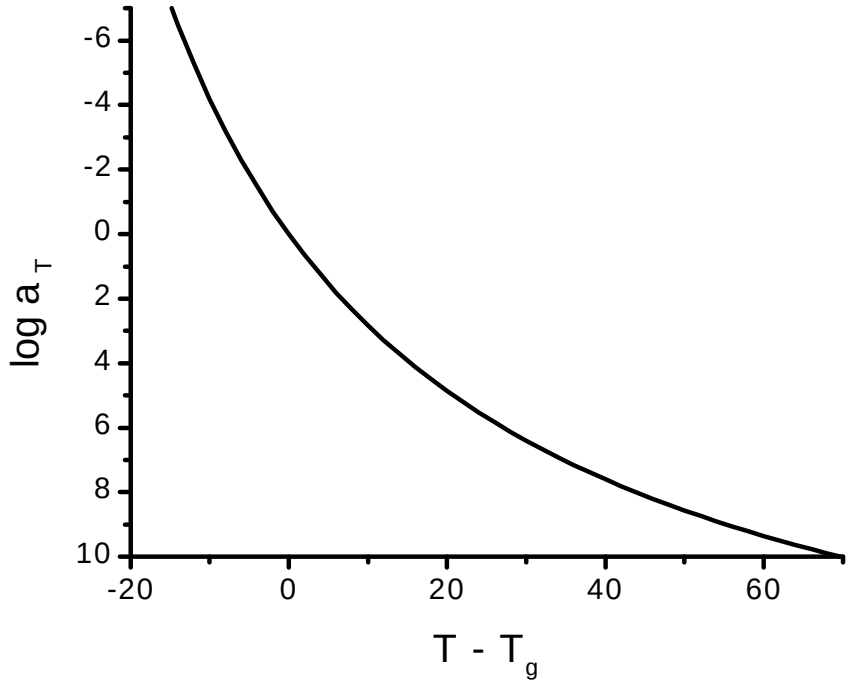


Figure 2-20. WLF equation shift factor plot.

By collecting dynamic mechanical data at multiple frequencies and using time-temperature superpositioning to construct master curves, one can determine the $C_1$ and $C_2$ constants of the sample in question for the WLF equation. This is done by plotting $1/\log(a_T)$ versus $1/\log(T-T_R)$ and linearizing Equation 19. The shift factors will be known for each temperature once the master curve is made. The activation energy of the α-transition ($E_\alpha$) can then be found through the following equation:

$$E_a = R\frac{d[\ln(a_T)]}{d(1/T)}\bigg|_{T=T_R} = 2.303R\frac{C_1 T_R^2}{C_2} \tag{19}$$

where R is the molar gas constant.

### 2.8.3 Cooperative Motion

Angell[79] first proposed the concept of fragility in examining the temperature dependence of relaxation times for glass forming liquids. Angell's goal was to describe the time scales in which stressed liquids return to their equilibrium states at temperatures above and below $T_g$. "Fragile" glasses were described as having a relatively large

increase in entropy at the glass transition. This large increase in entropy will result in a substantial change in the heat capacity and there will be a substantial change in relaxation time of the liquid. "Strong" glasses do not exhibit as large a change in entropy, heat capacity, and in relaxation times at the glass transition. In other words, the structure of a "strong" glass is only changed by a very small degree at the glass transition. Angell found that it was convenient to classify strong and fragile liquids by plotting the viscosity in Arrhenius form versus a normalized temperature scale. Selecting a reference temperature where the viscosity is equal to some fixed arbitrary value enabled one to establish this normalization scheme to quantify intermolecular forces.

Angell[79] derived a theory for the classification of "strong" and "fragile" liquids which is based on a two-dimensional plot of chemical potential ($\mu$) versus a collective coordinate (Z) for an *n* potential energy surface. These plots are illustrated in Figure 2-21. Assuming that kinetics is not an issue, the liquid can gain access to the minima that correspond to a lower energy than *k*T, where *k* is the Boltzmann constant. It becomes increasingly difficult for the liquid to locate a lower potential energy level as the number of minima decreases. This decrease in potential energy is accompanied by a decrease in the configurational entropy ($S_c$) of the liquid.[80] If a liquid finds a large number of these potential energy minima then there will be a large change in the configurational entropy and relaxation time ($\tau$) as the temperature is increased past $T_g$. These liquids lose their short range order at $T_g$ and are therefore "fragile". A "strong" liquid will only gain access to relatively few potential energy minima in the glassy state.

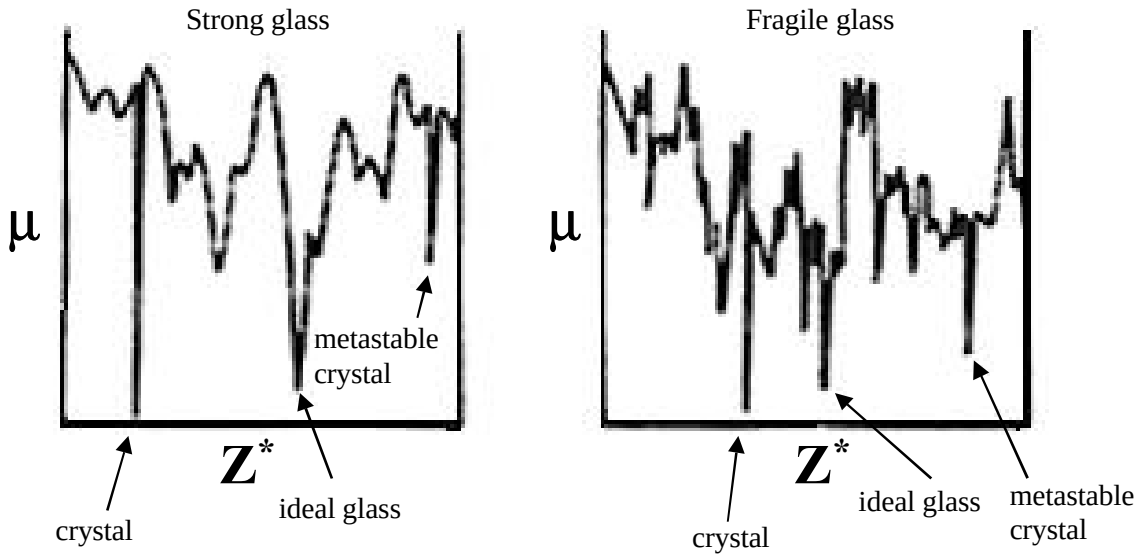


Figure 2-21. "Strong" and "fragile" potential energy surfaces proposed by Angell.[79]

This recent concept of fragility, or cooperativity, is not a new idea. Cooperativity is just a means of classifying viscoelastic behavior in a simplified fashion. Angell[79] bases the concept of fragility on the theory of Adam and Gibbs, which was published in 1965.[81] Adam and Gibbs used the idea that the transition from the glassy to the liquid state was more complicated than single molecules overcoming an energy barrier. These researchers proposed that relaxation phenomena in liquids occur in cooperatively rearranging regions. The Adam and Gibbs relaxation time for a cooperatively rearranging region is given in Equation 20.

$$t = t_0 \exp(C / TS_c) \tag{20}$$

In Equation 20, C is equal to $\Delta\mu/k$, where $\Delta\mu$ is equal to the height of the free energy barrier which must be overcome for the relaxation of the cooperatively rearranging region. The constant $\tau_o$ is equal to an arbitrary reference relaxation time. Angell used the Adam and Gibbs model, stating that because the configurational entropy is a function of temperature that the Kauzmann paradox should be included. Kauzmann was the first to realize that if the entropy of a polymeric glass was extrapolated to low temperatures that the entropy would achieve a value of zero before absolute zero was reached.[82] Kauzmann publications indicated that this paradox violates the third law of thermodynamics. The problem arises because a glass cannot reach a low configurational

entropy when cooling through the glass transition due to mobility and kinetic considerations. Kauzmann proposed that if a glass could be cooled infinitely slowly enough, then there would be some temperature ($T_k$) where the glass will have the same configurational entropy as a crystal. Angell then expresses the configurational entropy as a function of the change in heat capacity between the liquid and the glass ($\Delta C_p$).

$$S_c = \int_{T_K}^{T} \frac{\Delta C_P}{T} dT \tag{21}$$

Angell concluded that if the heat capacity is hyperbolic function of temperature ($\Delta C_p$=K/T) then the solution to the integral of Equation 21 is equal to the following.[79,80]

$$S_c = \mathrm{a}\left(\frac{T - T_k}{T_k T}\right) \tag{22}$$

Angell substitutes Equation 22 back into the Adam and Gibbs equation to give the following:

$$\mathrm{t} = \mathrm{t}_o \exp\left[\mathrm{a}\left(\frac{\Delta \mathrm{m}}{K}\right)\frac{T_o}{T - T_o}\right] = \mathrm{t}_o \exp\left[D\frac{T_o}{T - T_o}\right] \tag{23}$$

Equation 23 is equivalent to the Vogel-Tammann-Fulcher equation.[80] In the form chosen by Angell, $T_o$ is an arbitrary reference temperature and is therefore a constant value. Angell proposed that the $\Delta\mu$ and K terms, which are included in the D constant of Equation 23, are related to the two dimensional potential energy surface. The constant K is related to the number or density of energy minima while $\Delta\mu$ is related to the depths of the energy minima.

The analysis of Angell[79] represented a new view, or interpretation, of viscoelastic concepts that had been theorized for some years. It is interesting that Angell can correlate the constants of the empirical Vogel-Tammann-Fulcher equation to physical parameters. The Vogel-Tammann-Fulcher equation describes the temperature dependence of relaxation times. Equation 23 can be written in the following form.[83]

$$\log a_T = \frac{1}{\mathrm{a}(T - T_o)} - \mathrm{b} \tag{24}$$

Equation 24 is equivalent to the Williams Landel-Ferry equation (Equation 18) where $\beta$ is equal to $C_1$, $\alpha$ is equal to $1/C_1C_2$, and $T_0$ is equivalent to $T_g - C_2$.

Angell[79] was interested in studying the relaxation times of inorganic glasses, and did not apply temperature scale normalization to polymeric relaxation times. Therefore, Angell's paper does not provide a great deal of molecular interpretation from a polymer point of view. But, the equations and theory Angell used are also very common to polymer science. A polymer perspective would follow shortly after Angell's first paper with the work of Ngai, Plazek, and Roland.

Ngai and Plazek[84] applied this concept to amorphous polymers and coined the term "cooperativity" for describing the changes in the relaxation time of amorphous polymers at the glass transition via a normalized temperature scheme. In this case the temperature scale of the time-temperature shift factors is normalized by a fractional deviation from the glass transition temperature $(T-T_g)/T_g$. It has been shown that the temperature sensitivity of the logarithmic time-temperature shift factors can be related to the coupling constant ($n$) of the Kohlrausch-Williams-Watts (KWW) equation through a coupling model of relaxation.[84,85,86]

$$E(t) = E(0)\exp\left[-\left(\frac{t}{\tau^*}\right)^{(1-n)}\right] \tag{25}$$

In Equation 40, $\tau^*$ is the measured relaxation time and $n$ ranges from 0 to 1. The coupling constant parameter provides a measure of the width of the distribution of relaxation times.[84] When $n$ is equal to 0 then the KWW equation describes the single relaxation time of a simple Debye oscillator, or the Maxwell element described above.[87] But, the molecular environment of a polymer is much more complicated than either of these simpler approaches. Polymers display a broad distribution of relaxation times reflecting the heterogeneous broadening of the spectrum due to many statistical factors. As the $n$ increases the distribution of relaxation times also increases.

Ngai and Roland[85] proposed that a high degree of intermolecular interactions increase the breadth of the distribution of relaxation times in a polymer. If a polymer segment could be isolated as a single unit then at $T_g$ this segment would have a unique relaxation time. Under the dense conditions of the solid state the polymer is in close contact with neighboring chains. As segmental motion begins to occur at $T_g$ some of the segments cannot relax as simply as reflected by the isolated relaxation times. The constraining effect on neighboring chains slows down the overall relaxation time. The coupled

segmental relaxations of the polymer chains do not occur at the same time or rate throughout the sample. This leads to an increase in the broadness of the distribution of relaxation times. A higher degree of intermolecular coupling and constraints from neighboring segments will increase the amount of cooperative segmental motion required to pass through the glass to rubber transition.[88] In other words, the segmental motion of neighboring segments is correlated to a greater degree. Polymers with a high amount of cooperativity have viscoelastic properties that exhibit more rapidly changing temperature dependence of the time-temperature shift factors in the glass transition region. This is referred to as "steeper" dependence.

Ngai and Plazek[84] were able to determine values for the coupling constant (*n*) by quantifying cooperativity. This was done through a derivation beginning with Ngai's coupling model, which relates the measured relaxation time to relaxation times due to intramolecular interactions ($\tau_o$).

$$t^* = \left[(1-n)w_c^n t_o\right]^{\frac{1}{(1-n)}} \tag{26}$$

A ratio is then taken at a measured temperature (T) and a reference temperature ($T_R$). This is the exact definition of $a_T$, which is defined as a ratio of relaxation times at a measured and reference temperature. The coupling crossover frequency ($\omega_c$) cancels out when taking the ratio resulting in the following expression.

$$(1-n)\log a_T = (1-n)\log\frac{t^*(T)}{t^*(T_R)} = \log\frac{t_o(T)}{t_o(T_R)} \tag{27}$$

Ngai and Plazek then plotted shift factor data from the literature, with and without carrying the term (1-*n*) in front of $\log a_T$ (Figure 2-22 and Figure 2-23 respectively), for a wide variety of polymers versus $(T-T_g)/T_g$.[84] Their results indicated that the temperature dependencies of the underlying segmental motions were identical for the polymers that were studied. A Williams, Landel, and Ferry (WLF) type of equation accurately fit the available data.

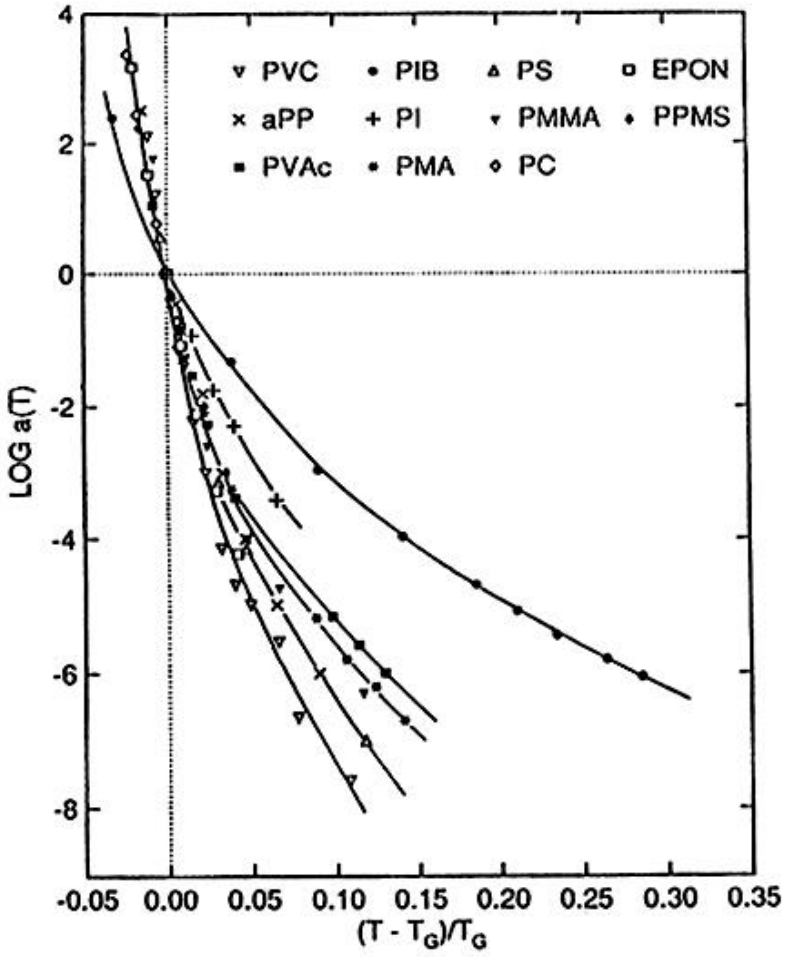


Figure 2-22. Temperature dependence of log $a_T$ for varying polymers.[84]

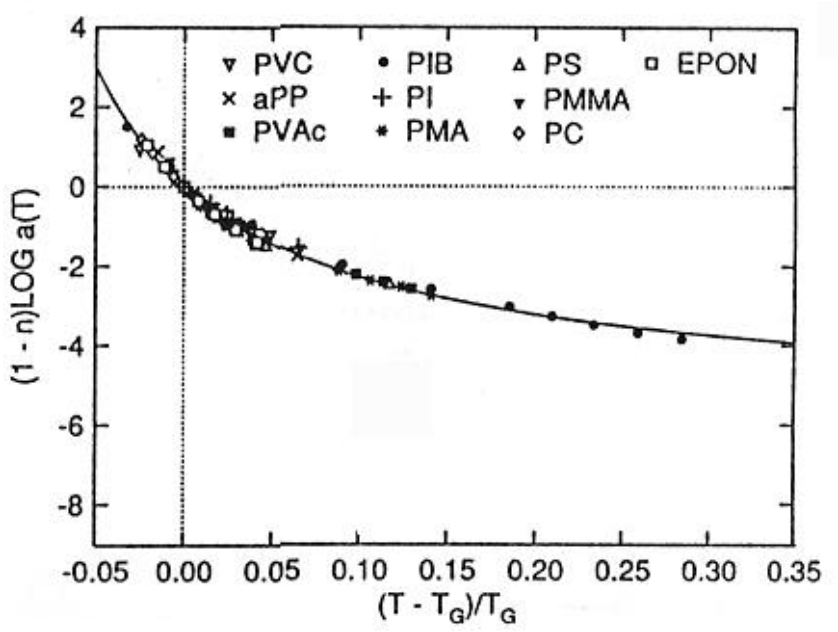


Figure 2-23. Shift factor data from Figure 2-22 plotted in the form of Equation 27.[84]

$$(1-n)\log a_T = \frac{-C_1(T-T_g)/T_g}{C_2+(T-T_g)/T_g} \tag{28}$$

Ngai and Plazek determined the statistical solutions to $C_1$ and $C_2$ to be equal to 5.49 and 0.141, respectively, when all of their data was included. It is important to keep in mind that the $C_1$ and $C_2$ constants of Equation 28 were empirically derived and have no bearing on the actual cooperativity ranking of actual experimental results.

The steepness index (S), which is the slope at $T=T_g$, of the cooperativity plot can be used to calculate the activation energy ($E_a$) of the glass transition using an Arrhenius relationship through Equation 29, Equation 30, and Equation 31.[83]

$$S = -T_g\left[\frac{d\log a_T}{dT}\right]_{T_g} = \left[\frac{d\log a_T}{d(T/T_g}\right]_{T_g} \tag{29}$$

$$\log a_T \propto -\frac{E_a}{2.303RT} \tag{30}$$

$$E_a = 2.303RT_gS \tag{31}$$

### 2.8.4 Dynamic Mechanical Analysis of Filled Polymers and Composites

There are many articles in the literature that indicate that it is possible to derive information pertaining to the nature of the interphase between a polymer and a substrate via dynamic mechanical analysis of polymers containing an inorganic filler.[89-102] The primary advantage of studying a filled polymer for adhesive research is that each component of an adhesive system is incorporated. Changes in the interphase properties between the filler (substrate) and the polymer (adhesive) should be able to be detected by DMA. As will be discussed in greater detail in this section, any changes in the properties in the interphase region have traditionally been observed in the loss tangent curve (tan $\delta$).

Lewis and Nielsen[89] performed an early comprehensive study of glass bead filled epoxy composites, which is frequently cited in the literature. These authors studied the dynamic mechanical effects, via torsional braid analysis (TBA), of an epoxy that had been filled with spherical A-glass particles. The A-glass spherical beads had particle sizes ranging in diameter from 5-10, 10-20, 30-40, and 75-90μm. In addition to studying the effect of particle size to the dynamic mechanical properties of the composite, the volume fraction of the filler ($\phi_2$) was also varied from between 0 and 40 percent. The matrix material consisted of Epon 828, 5% phenyl glycidyl ether, and triethylene tetramine as the curing agent. Lewis and Nielsen were mainly interested in determining the relative shear modulus ($G'_r$) of filled composites in comparison to an unfilled epoxy control sample. They observed that $G'_r$ increased with increasing volume fraction of filler and decreasing particle size. The effect of increasing shear modulus was more pronounced in the rubbery region above $T_g$. A slight temperature dependence of $G'_r$ was also observed in the glassy region, but this was believed to have been caused by residual curing stresses arising from a mismatch between the coefficients of thermal expansion between the glass filler and the epoxy matrix.

In this study Lewis and Nielsen[89] also examined the dynamic mechanical effects of pretreating the glass filler with different coupling agents. Methylchlorosilane and γ-glycidoxypropyltriethoxysilane were used to promote poor and good adhesion respectively between the filler and the matrix epoxy. Figure 2-24 shows the experimental

shear loss modulus ($G''_r$) and damping ($\Delta$) curves that were experimentally obtained for the various pretreatments, including untreated A-glass filler. No noticeable effects were evident in the shear storage modulus curves. However, the shear loss modulus and damping curves varied significantly depending on the coupling agent that was used. The damping of the methylchlorosilane treated composite was greater than that of γ-glycidoxypropyltriethoxysilane composite. The width of the γ-glycidoxypropyltriethoxysilane damping curve was also wider than the methylchlorosilane damping curve. Lewis and Nielsen attributed these changes in amplitude and width in the damping curves to the specific interfacial properties between the epoxy matrix and the glass filler. Above the glass transition no difference in the damping curves existed.

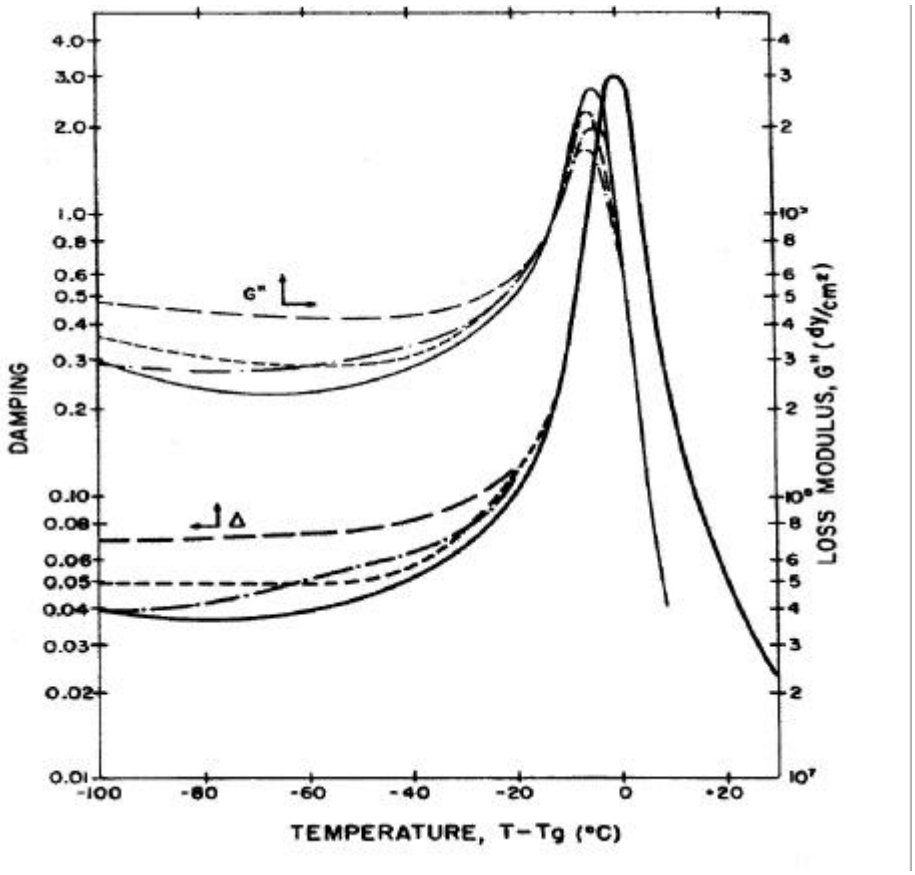


Figure 2-24. Damping and loss modulus curves versus T-$T_g$ for $\phi_2$ = 0.30, (-) γ-glycidoxypropyltriethoxysilane, (---) methylchlorosilane, (-·-·) untreated.[89]

Cousin and Smith[90] studied the dynamic mechanical behavior of a sulfonated polystyrene ionomer when filled with small diameter alumina particles. The alumina was either left untreated or was pretreated with 3-aminopropyltriethoxysilane. The alumina had an average particle diameter of 0.01μm and was added to the polymer at a volume fraction equal to 30 percent. Cousin and Smith varied the strength of the polymer-filler interactions by changing the number of styrene-sulfonic acid groups present in the polymer. Cousin and Smith found that the $T_g$ of the polymer increased with increasing the number of acid groups in the polymer. It was also noted that for a given number of styrene-sulfonic acid groups that the amine treated alumina filler composites always produced the highest glass transition temperatures. Both the untreated and pretreated alumina filled samples resulted in a broadening of the loss tangent peak, as well as a decrease in peak maximum amplitude, at the glass transition. Cousin and Smith believe that this can be attributed to the strength of the polymer-filler interactions occurring at the interface. A strong interaction between the polymer and filler will yield a broad loss tangent peak near the glass transition as well as a possible increase in $T_g$. Cousin and Smith also state that these strong polymer-filler interactions will decrease the mobility and the free volume of the polymer chains near the polymer-filler interface. It was also noted in this article that a filler will have a relatively small effect on the glassy storage modulus. But, the addition of a filler will significantly increase the storage modulus of the polymer in the rubbery region above $T_g$. This can be modeled by considering the filler acting as a physical crosslink.

Eisenberg and Tsagaropoulos[91,92] provide an excellent review of the effects of filler particles on the glass transition, as observed by DMA, and compare these effects to similar behavior that has been observed with ionomers. These authors adapted the Eisenberg, Hird, and Moore (EHM) model of ionomer cluster formation to describe the dynamic mechanical behavior of polymers that have been filled with very fine particles. The EHM model postulates that the ion pairs present in ionomers can aggregate together, due to electrostatic forces, and form multiplets. The polymer immediately surrounding the multiplet will be restricted in mobility when compared to the bulk polymer. If enough of these multiplets are present in the polymer then it is possible for these regions of restricted mobility of different multiplets to overlap each other. These aggregates of

multiplets then form what is referred to as a cluster. The polymer chains within and near the clusters are extremely restricted in mobility. Therefore, the polymer in these regions will have a much higher $T_g$ than the bulk polymer. Eisenberg and Tsagaropoulos proposed that very small filler particles can act in the same manner as a cluster and restrict the mobility of the polymer chains near the surface of the filler particle.

To test this theory Eisenberg and Tsagaropoulos[92] added silica particles to a wide variety of polymers including poly(vinyl acetate) (PVac), polystyrene (PS), poly(4-vinylpyridine) (P4VP), and poly(methyl methacrylate) (PMMA). The silica particles had an average particle diameter of 7nm and were added to the polymers in concentrations up to 50 weight percent. Dynamic mechanical analysis revealed the presence of a second loss tangent peak approximately 100°C above the $T_g$ of the polymer in question. This second loss tangent peak was assigned to the chains that are bound to the surface of the silica. Chains that are bound to the surface of the silica would be reduced in mobility.

As can be seen in Figure 2-25, a second glass transition is clearly evident at temperatures much greater that the $T_g$ of the bulk polymer. It is interesting to note that the magnitude of the second loss tangent peak actually decreases with increasing filler content. At first this would seem to contradict what has been proposed. One would expect there to be more restricted polymer chains with increased filler loading and hence a more noticeable second loss tangent peak. Eisenberg and Tsagaropoulos devised a schematic, Figure 2-26, of what was occurring as the filler content was increased to explain these results.

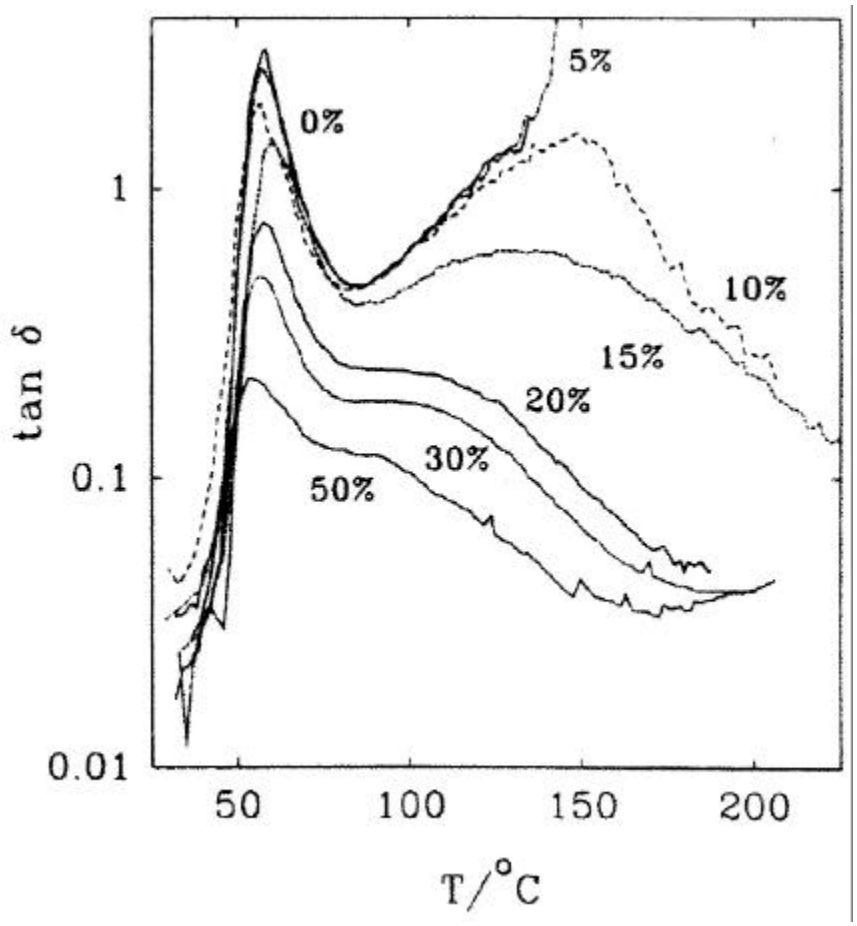


Figure 2-25. Tan δ versus temperature for PVAc with silica filler.[92]

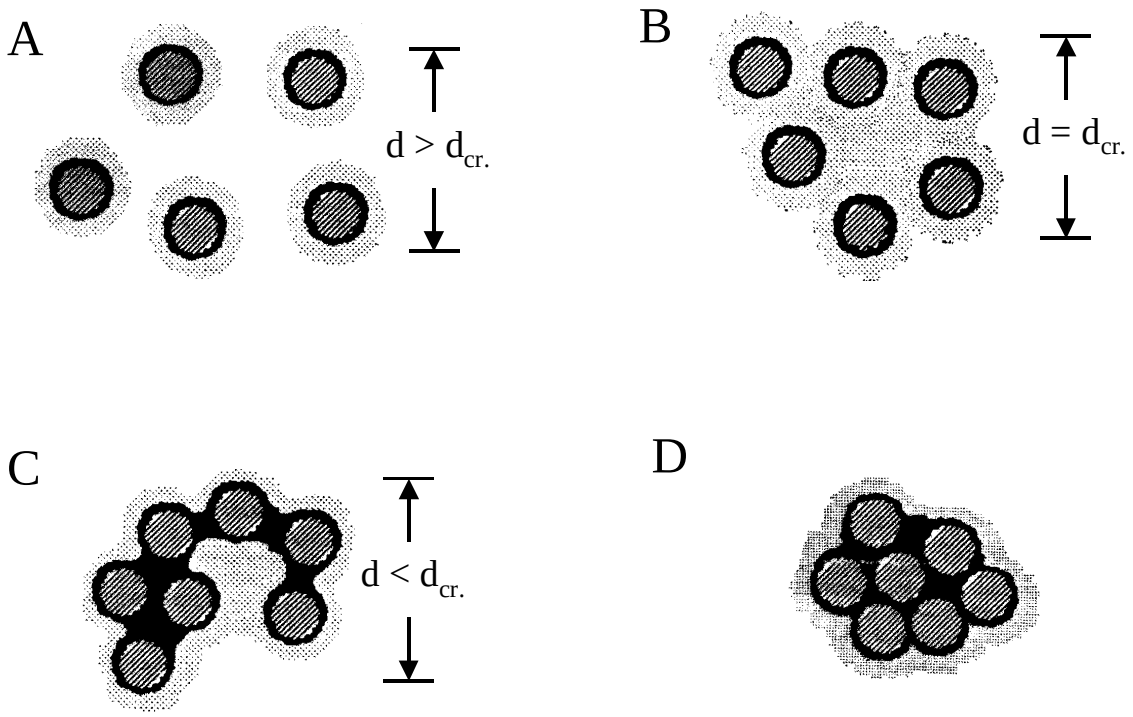


Figure 2-26. Schematic representation of the Eisnenberg and Tsagaropoulos model of polymer filler interactions.[92]

In this illustration there are two regions of polymer immediately surrounding the filler particle. The light gray areas are the regions where the polymer chains are slightly restricted in mobility. Eisenberg and Tsagaropoulos refer to these areas as regions of loosely bound polymer. It is the polymer chains in these loosely bound regions that are responsible for the second glass transition. The polymer chains in the black regions, which are directly attached to the surface of the filler particle, are highly restricted in mobility. Eisenberg and Tsagaropoulos refer to these areas as regions of tightly bound polymer. These researchers proposed that the polymer chains in these tightly bound regions are so highly restricted in mobility that they cannot participate in any transitions that are measurable by DMA.

The schematic presented by Eisenberg and Tsagaropoulos in Figure 2-26 adequately describes the experimental DMA results that these authors obtained. In slide A of Figure 2-26, low filler loadings, the interparticle distance (d) is too great for the loosely bound regions of polymer to over-lap. This means that the DMA will not detect a second glass transition. However, the magnitude of the loss tangent peak could be reduced due to a

lower volume fraction of bulk polymer chains participating in the glass transition. In the second slide, Figure 2-26B, enough filler has been added for the interparticle distance to be low enough for the loosely bound polymer regions to overlap ($d < d_{critical}$). Eisenberg and Tsagaropoulos estimated that the regions of restricted mobility surrounding the filler particle have a thickness on the order of the persistence length of the polymer. This is at the critical point where DMA will detect a second large loss tangent peak above the glass transition temperature of the bulk polymer. Then as more filler is added, Figure 2-26C and D, the mobility restrictions on the polymer are increased to such an extent that a significant volume fraction of tightly bound polymer is formed. This high volume fraction of tightly bound polymer does not participate in a glass transition. As a result the DMA can only detect the glass transition of the much lower volume fraction bulk and loosely bound polymer. This explains the decreasing magnitude of the second loss tangent peak as the volume fraction of filler is increased. Eisenberg and Tsagaropoulos did not observe a second glass transition when 44μm diameter size silica particles were used. The second glass transition can only be seen when extremely small filler particles are used at high volume fractions. The volume fraction of loosely bound polymer is just too low for the larger particle size composites to be measured by DMA. Eisenberg and Tsagaropoulos also noted that the characteristics of the second loss tangent peak depended on the molecular structure, molecular weight, and thermal history of the polymer.

Bernreitner *et al*.[93] studied the effects of spherical mineral talc fillers on the dynamic viscoelastic properties of polypropylene. Their study focused on the factors of filled composite materials that alter the linear viscoelastic response of the matrix polymer. Bernreitner's study revealed that the main factors that influence the rheological properties of a filled polymer are the filler concentration, particle size distribution of the filler, as well as the filler's degree of dispersion in the matrix polymer. Bernreitner's paper does not specifically investigate the polymer-filler interfacial interactions. However, it was stated in this paper that the volume fraction of filler is not the only contributing factor to the viscoelastic response of the matrix polymer. Bernreitner states that polymer-filler interactions also play an important role.

Gerard *et al*.[94] studied the dynamic mechanical behavior of a DGEBA/dicyandiamide

epoxy matrix that had been filled with spherical A-glass beads. The glass beads had an average particle diameter of 26μm and were added to the matrix epoxy at various volume fractions ranging up to 30 percent. The glass beads were treated with γ-aminopropyltriethoxysilane, a rubber elastomer, or no surface pretreatment at all. These authors state that DMA can be used to show that polymer composites possess a three phase structure. These phases are the matrix polymer, filler particles, and the interphase between the bulk polymer and the filler particles. Gerard also states that the interphase surrounding the filler particles will have very different properties from the bulk matrix polymer. When the loss tangent peaks for the various composites were compared at the glass transition it was noted that the silane pretreated filler caused the loss tangent peak to shift towards higher temperatures in comparison to the other surface pretreatments used. The elastomer coated filler caused a decrease in $T_g$ as well as a more noticeable broadening of the loss tangent peak. These changes in the loss tangent curves were related to the strength of the adhesive interactions between the glass filler and the epoxy matrix. Gerard believes that the silane treated filled composite will cause the polymer chains near the interface to be reduced in mobility. This is because the epoxy is capable of reacting with this coupling agent and forming a covalent bond, which chemically bonds the resin to the coupling agent. Therefore, the $T_g$ of the silane treated filled composite was the greatest. It was also determined that the elastomer coating pre-treatment used could plasticize the surrounding epoxy matrix. The plasticizing effect could lower the $T_g$ of the surrounding epoxy matrix as well as broaden the loss tangent peak near the glass transition.

Careful examination of the loss tangent curves obtained by Gerard raises some questions. For example, Figure 2-27 shows the loss tangent peaks at the glass transition for the silane pretreated, elastomer coated, and untreated glass filled composites.

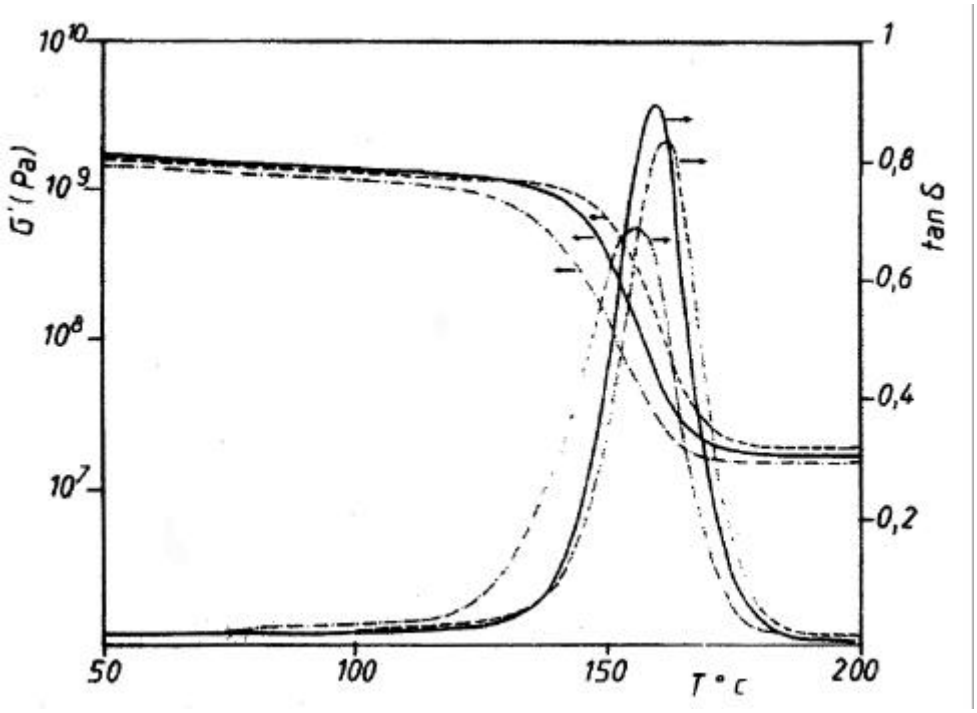


Figure 2-27. Loss tangent curves obtained by Gerard.[94] (-) untreated, (---)silane treated, (-.-.) elastomer coated (e/r = 4.2 %) glass beads (20% vol. fraction).

It can be seen in this figure that there is only a very slight difference in the loss tangent curves between the untreated and silane pretreated composites. There is however a much more noticeable difference in the loss tangent peak when an elastomer coating was applied to the glass beads. The reasoning provided by Gerard for the lowering of $T_g$, as well as the broadening of the loss tangent peak, seems to be acceptable. The width of the loss tangent peak is going to be determined by the distribution of relaxation times of the polymer at the glass transition. If the polymer is subjected to a wider range of environments, or configurations, then this peak, as measured by DMA, will become broader. In this paper Gerard states that the $T_g$ of the silane pretreated composite increased due to the restricted mobility of the polymer chains near the surface of the glass particles. This may be true, but if Gerard's experiments were detecting this mobility shift then the loss tangent peak should have also been broader. Gerard calculated an interparticle distance of approximately 70μm at 20 percent volume fraction filler. This is much larger than the distance needed for the loosely bound polymer regions to overlap as reported by Eisenberg and Tsagaropoulos.[91,92] The elastomer coatings used had a

thickness that was on the order of approximately 5 percent of the particle radius. This was probably large enough to be detected by DMA. This is also supported by the fact that the glass transition of the elastomer was observed as a shoulder on the β transition peak of the matrix epoxy. Gerard also failed to point out that dicyandiamide can potentially precipitate out of the epoxy resin onto the surface of the substrate, to which it is applied. The differences in the loss tangent peaks could have resulted from varying amounts of curing agent near the interface of the glass beads. Gerard's work presents the argument that DMA can detect the differences in the interfacial properties between composites. This may be true, but the differences probably have to be extreme and great care must be taken in interpretation.

Gerard[95] also used DMA to characterize interfacial effects between an epoxy matrix and an elastomeric coating that had been deposited on the surface of carbon fibers. Gerard was able to observe differences in the loss tangent curves at the glass transition of the epoxy matrix when the elastomer coated fiber composite was compared to an untreated fiber composite. Differences in impact resistance and three-point bending tests were also observed. The elastomer coated fiber composite had much better impact properties and failed by a different deformation mechanism in the three-point bending tests. Scanning electron microscopy (SEM) of the three point bending fracture surfaces revealed that material was left on the surface of the elastomer coated fibers. The non-coated fibers showed clean brittle fracture surfaces. This paper by Gerard illustrates the point that while DMA may be a useful method for determining the interfacial properties of composite materials, other methods are also needed to confirm any conclusions drawn by DMA.

Not all dynamic mechanical studies of spherical glass filler or fiber epoxy composites have concluded that interfacial properties can be determined by DMA. Harris *et al.*[96] studied a wide variety of carbon fiber pretreatments in a phenolic novolac epoxy matrix composite. These researchers examined carbon fibers that were pretreated by dip coating, oxidation, electro-polymerization, and plasma-polymerization. The DMA results that these researchers obtained were inconclusive. Thomason[97] published results, which indicate that, a second peak in the loss modulus or tan δ curves of a fiber-reinforced composite could be an artifact of the DMA. Thomason states that a second peak can

result due to thermal lag between the portion of the sample that is exposed between the clamps and the actual material that is held by the clamps. An artificial second peak can then originate because of a fast sample heating rate, poor thermal conductivity of the composite, and residual stresses in the composite. The glass transition for the clamped portion of the composite simply falls behind, giving a false second transition peak at higher temperatures. Obviously, caution must be used in drawing conclusions from DMA results on complex systems.

The conclusion drawn from this section of the literature review is that DMA could be a useful technique for examining interfacial behavior in glass-epoxy composites, but other characterization techniques should definitely be used to verify the results. Thomason[98] was able to use nuclear magnetic resonance spectroscopy, X-ray photoelectron spectroscopy, differential scanning calorimetry, and secondary ion mass spectroscopy in addition to DMA in characterizing the interface of glass fiber-epoxy composites. Water uptake experiments have also been performed in conjunction with DMA to study the adhesive properties between the epoxy-glass interface in composite materials.[99,100] These studies indicated that composites with strong epoxy-glass adhesion absorb lower amounts of water than those with weak interfacial adhesion. Other researchers have used mechanical tests, such as the short beam shear test and double cantilever beam test, to verify conclusions made by DMA.[101,102] Dynamic mechanical analysis of composite materials offers the advantage of measuring the properties of the entire adhesive system, but this method still needs to be supported by other techniques.

### 2.8.5 Cooperativity Analysis of Filled Polymers

Landel[103] completed a viscoelastic study in 1958, which examined the effects of fillers to the distribution of relaxation times in polymers. Landel examined the viscoelastic properties of non-crosslinked polyisobutylene (PIB) which was filled with non-interacting glass beads. Landel concluded that a filler will increase the modulus and broaden the distribution of relaxation times of a polymer. Landel did not observe significant changes to the short relaxation times at temperatures close to $T_g$. Landel noted that the long relaxation times of the polymer were shifted the most by the filler particles. Landel attributed this to the adsorption of polymer chain segments to the filler

particles. Landel proposed that this segment-filler adsorption will mainly influence the relaxation times of the longer chain segments, which is why this portion of the relaxation spectra was broadened the most at higher temperatures. Landel also stated that the filler should not change the temperature dependence of the relaxation times for the polymer unless the interactions are strong.

Gambogi and Blum[104] used solid state NMR to study the molecular mobility of the interphase in a bismaleimide-silica composite. The silica was pretreated with deuterated aminobutyltriethoxysilane. These researchers compared the molecular motions of the silane when reacted with the bismaleimide as a bulk system and as the coupling agent of the composite. These authors concluded that the relaxation mechanism of the surface bonded silane changed in comparison to the bulk relaxation mechanism.

Wang and Blum[105,106,107] concluded that the mobility of the coupling agent in composite intefaces is an important aspect of mechanical properties. Wang and Blum studied the mode 1 fracture toughness of epoxy/glass composite using double cantilever beam and compact tension tests. The glass fibers were pretreated with either γ-aminopropyltriethoxysilane (APS) or γ-aminobutyltriethoxysilane (ABS). Composites with untreated glass fibers were tested as well. The APS pretreated glass fiber composite had a higher critical energy release rate than the ABS pretreated composites. Both silane pretreatments yielded increased critical energy release rates over the untreated glass composites. Wang and Blum believe that the shorter alkyl chain length of APS results in a lower interfacial mobility and a greater mechanical strength than ABS. This work implies that the epoxy-glass interphase region of untreated glass fibers has a greater molecular mobility than silane pretreated glass fibers. In these studies Wang and Blum also state that the interfacial mobility of a composite material should be an important consideration when selecting a coupling agent for a composite application.

Lacrampe *et al*.[108] also concluded that the interfacial mobilities of composite materials are also important with respect to mechanical properties. These researchers used dynamic mechanical analysis to examine the viscoelastic responses of epoxy/E-glass fiber composites. Based on the shapes of the tan δ signals it was concluded that the interfacial mobility of the composite is restricted when γ-aminopropyltriethoxysilane is used as a fiber pretreatment. Lacrampe did not study the dynamic mechanical properties

of composites with untreated glass; therefore no ranking was assigned to the interfacial mobility when untreated E-glass is used.

Fitzgerald *et al.*[109] performed an extensive study of the viscoelastic properties of poly(vinylacetate)/silicon dioxide filled composites. These researchers used dielectric spectroscopy to construct master curves of the dielectric loss in the frequency domain. The dielectric loss curves were then fitted to the KWW equation to determine the coupling parameters. Fitzgerald concluded that the incorporation of filler broadened the distribution of relaxation times. This was credited to the strong interactions, via hydrogen bonding, between the poly(vinylacetate) and silicon dioxide filler particles. These polymer-filler interactions then restrict the mobilty of the polymer chains in the interphase region. Fitzgerald also noted that time-temperature superposition principle did not work when high concentrations of filler were added to the polymer. The activation energies for the glass transition of the polymer remained essentially unchanged when the filler was added. This paper is essentially a cooperativity study. Fitzgerald obtained the coupling parameters for the KWW equation by directly fitting the dielectric loss master curves instead of via cooperativity plots.

Other research groups have also concluded that the interphase region of composite materials differs in molecular mobility when compared to the bulk phase. Koenig *et al.*[110] reached this conclusion from solid state NMR studies. Dufresne and Lacabanne[111,112] determined that the interphase is restricted in mobility based on creep studies. However, Sullivan *et al.*[113] state that the glass fibers in a composite will impart no changes in the relaxation times of the matrix polymer. But, Sullivan only considered the glassy region and did not examine the long time region above the glass to rubber transition region. If the interphase is restricted in mobility in comparison to the bulk matrix phase, then changes in the relaxation spectra should only become apparent at temperatures greater than $T_g$.

## 2.9 Moisture Uptake

There are many examples of moisture uptake experiments with respect to epoxy-glass composites in the literature. These studies have been completed by exposing the composite material to humid atmospheres as well as total immersion in water. In

addition to plasticizing the matrix epoxy, water can degrade the matrix-fiber interface. Both of these conditions will independently deteriorate the mechanical properties of the composite, which will result in unacceptable bond performance and durability. Water uptake experiments should be of particular interest for composites prepared with waterborne epoxies. Because of the addition of an added hydrophilic surfactant to the matrix resin, one would expect the absorption of moisture to be a problem with these materials.

Dewimille and Bunsell[114] studied the diffusion of water in a unidirectional E-glass fiber reinforced epoxy resin. Dewimille and Bunsell do not cite which coupling agent or specific surface chemistry was used for the research in the article. The matrix resin was a DGEBA epoxy that was cured with an anhydride hardener. Samples of the composite were cut both perpendicular and parallel to the direction of the fibers prior to water immersion. The objective of Dewimille and Bunsell's research was to determine if water diffusion into the composites followed Fickian behavior at temperatures ranging from 22°C to 100°C. The diffusion constant (D) for Fickian moisture absorption is given below in Equation 32:[115]

$$D = \pi\left(\frac{h}{4M_\infty}\right)^2\left(\frac{M_2 - M_1}{\sqrt{t_2} - \sqrt{t_1}}\right)^2 \tag{32}$$

$M_t$ = moisture mass uptake at time = t

$M_\infty$ = equilibrium moisture mass uptake at time = ∞

t = time

h = specimen thickness

Equation 32 basically states that moisture uptake is directly proportional to the square root of time. Shen and Springer[115] derived Equation 32 from a simple one-dimensional diffusion model. In this model the driving forces for moisture uptake are the temperature and concentration gradients described by Fourier's and Fick's equations, respectively. A typical moisture uptake plot that follows Fickian behavior is shown in Figure 2-28, where moisture mass uptake is plotted versus the square root of time. It can be seen that the moisture mass uptake curves are initially linear with respect to the square root of time and then level off once equilibrium is reached between the sample and the water.

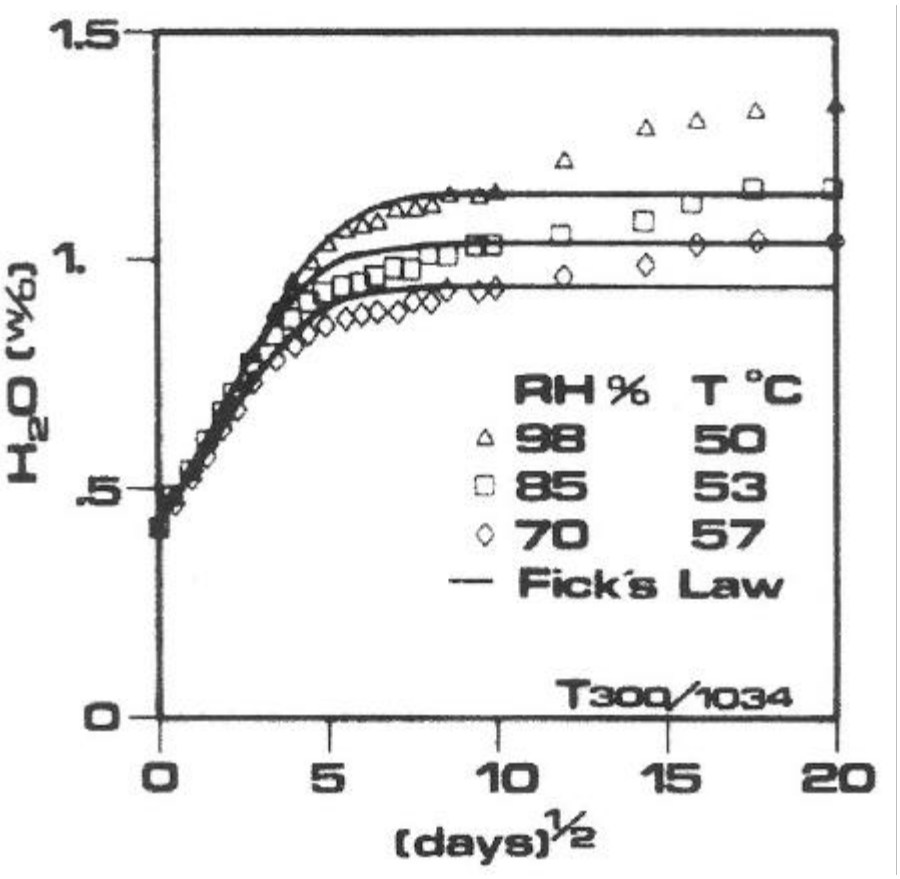


Figure 2-28. Typical Fickian diffusion plot.[114]

Dewimille and Bunsell[114] found that the rate of moisture diffusion was much faster at higher temperatures than simple Fickian diffusion could predict. These authors suggest that this was caused by matrix-fiber interfacial microdamage of the composite at elevated temperatures. This interfacial microdamage leads to an increased number of possible pathways available for moisture ingress. Dewimille and Bunsell also observed that the composite samples that were cut parallel to the fiber direction absorbed more water, and at a faster rate, than samples that were cut perpendicular to the direction of the fibers. This was also attributed to interfacial effects, which cause a positive deviation from Fickian behavior. Dewimille and Bunsell did not examine the effects of surface chemistry on the water uptake properties of the composite. Assuming that the glass fibers that Dewimille and Bunsell used were untreated, then perhaps the composite samples would have absorbed less moisture if an epoxy compatible coupling agent were used to pretreat the fiber surfaces.

Apicella *et al.*[116] studied the moisture absorption characteristics of epoxy thermosets that were filled at a concentration of 60 weight percent with quartz or alumina powder. A polyurethane/dolomia powder composite was also studied using an identical filler concentration. These researchers determined that the equilibrium mass uptake of water for the epoxy filled with alumina powder was four times greater than the equilibrium mass uptake of the epoxy-quartz composite. This was ascribed to weak adhesion between the epoxy and the alumina particles. Weak adhesion between the epoxy and alumina particles could cause debonding and the accumulation of water at the interface between the matrix epoxy and the filler. The equilibrium mass uptake of water for the polyurethane composite was significantly greater than the equilibrium moisture uptake levels achieved by either of the epoxy composites. Polyurethane possesses a larger number of hydrophilic sites to associate with the water than the epoxy resin that was used. Apicella *et al.* then concluded that there are two basic mechanisms for water absorption through a crosslinked polymeric network. One mode of moisture absorption is diffusion of water molecules through the free volume of the polymer while the other mode involves hydrogen bonding to hydrophilic groups that may be present in the polymer. These researchers postulated that weak adhesion between the matrix and filler particles will lead to greater moisture absorption than predicted by simple Fickian diffusion.

Diament *et al.*[117] examined the moisture absorption characteristics of a simple crosslinked epoxy thermoset that contained no filler or fiber reinforcing. These researchers believe that water absorption will be influenced mainly by the free volume of the network and the number of hydrophilic sites available for hydrogen bonding with water. As the crosslink density of the epoxy increases the free volume should decrease. This decreased free volume will result in a decreased number of holes being available for the water molecules to diffuse through. Adding more curing agent can sometimes elevate the crosslink density of an epoxy. If the curing agent used is hydrophilic then this will also increase moisture absorption, even though the free volume has decreased through additional crosslinking. Therefore, one of these two factors, the free volume or the number of hydrophilic sites in the polymer, could possibly dominate over the other.

Diamant *et al.*[117] tested this hypothesis by substituting stoichiometric amounts of a

diamine curing agent with a monoamine curing agent. These researchers crosslinked DGEBA epoxy resin with *m*-phenylenediamine as the curing agent. To decrease the crosslink density of the cured epoxy, stoichiometric amounts of the *m*-phenylendiamine were replaced with aniline. A schematic representation of these reactions is shown in Figure 2-29.

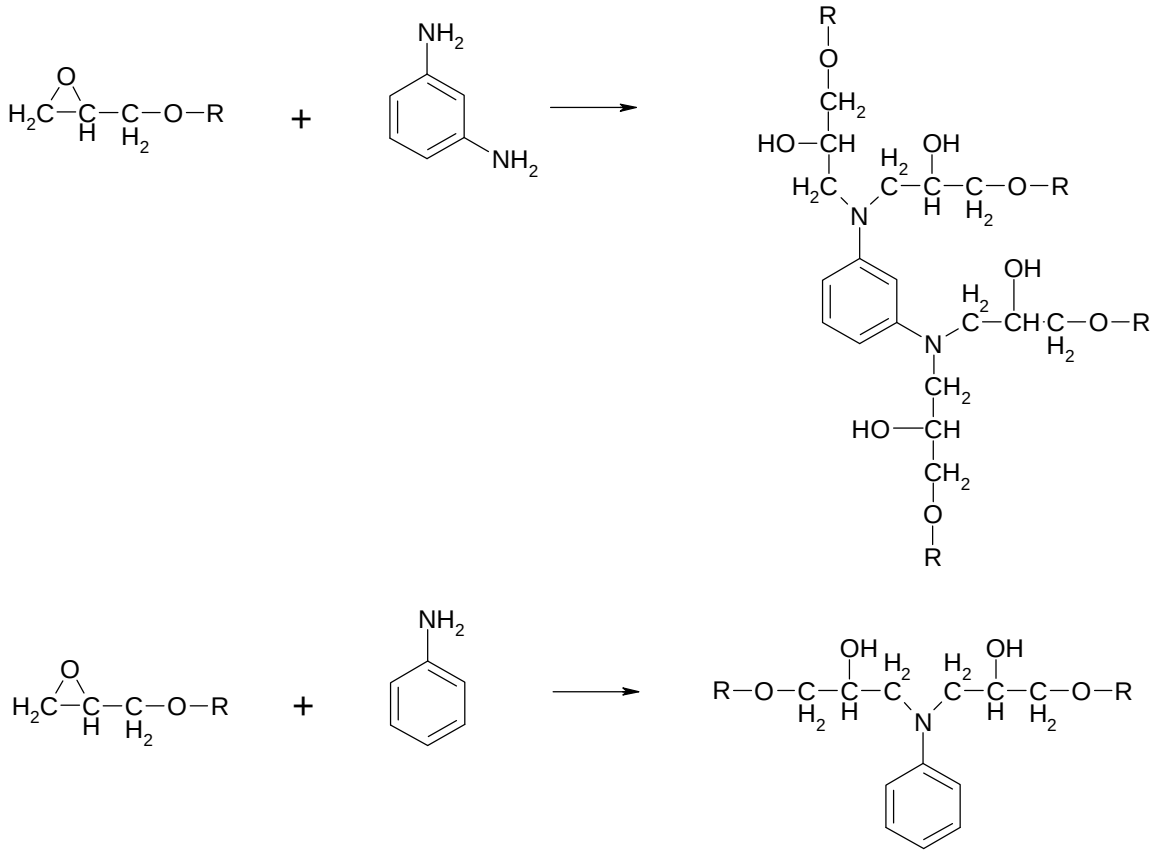

Figure 2-29. Epoxy functional molecule reacting with m-phenylenediamene to form a crosslink point of aniline to form a junction point.[117]

Density measurements of the epoxies that were partially reacted with aniline confirmed that the crosslink density was decreasing as more aniline was added. These samples contained a higher free volume than the epoxy cured entirely with *m*-phenylenediamine and yet absorbed less water. Aniline is not as polar as *m*-phenylenediamine. This is because there are more resonant states available to the benzene ring on the *m*-phenylenediamine. This increased number of resonant states facilitates a higher negative charge on the benzene ring of *m*-phenylenediamine, which

makes this molecule water soluble. Aniline is not water soluble. This was given as a possible explanation by Diamant *et al.*[117] as to why the epoxy that was cured only using *m*-phenylenediamine absorbed more water than those epoxies reacted partially with aniline. This again illustrates how important hydrophilic interactions are to the uptake of moisture in a crosslinked epoxy. This could be an important factor governing the moisture uptake properties of a waterborne epoxy.

Lekatou *et al.*[118] summarized the absorption mechanisms of water into a bulk polymer and a polymer matrix composite. These researchers also state that the two basic modes of water diffusion through bulk polymer are absorption by the free volume and the absorption caused by the hydrogen bonding of the water molecules to any hydrophilic groups present in the polymer. Water diffusion in a composite material can also involve direct moisture absorption along the filler-matrix interface, cracks, and small pores. Lekatou *et al.* also state that if water is being absorbed along the fiber-matrix interface then the water mass gain will deviate from the Fickian model. The presence of microdamage in the composite will sometimes result in a decrease in mass gain after extended periods of time due to the water leaching away portions of the composite.

Experimentally, Lekitou *et al.*[118] were able to show that an epoxy-glass composite filled with uncoated A-glass microspheres absorbed more water than an identical system filled with A-glass microspheres that were untreated. These researchers believed that the coupling agent provided a stable barrier against glass-epoxy bond degradation in the presence of water. The research of Lekatou *et al.* also emphasizes the importance of matrix-filler adhesion with respect to moisture absorption.

Wang and Ploehn[99] were able to characterize the matrix-filler interfacial adhesive properties of a glass filled epoxy composite by correlating dynamic mechanical analysis experiments to moisture uptake experiments. These researchers studied a DGEBA epoxy that was cured with triethylene tetramine (TETA). The epoxy was filled 40% by volume with glass beads that averaged 40μm in diameter. Comparisons were then made between composites filled with untreated beads, beads that were pretreated with 3-glycidoxypropyltrimethoxysilane, and the plain matrix epoxy that contained no filler.

Water uptake experiments performed on the samples revealed that all three systems followed Fickian behavior until a saturation level was reached. The silane pretreated

composite absorbed water at the slowest rate and achieved an equilibrium percent weight gain of 2.58%. The weight percent weight gain of the plain matrix was 3.32% and the untreated composite gained 5.68% in weight when exposed to water. The increased water gain of the untreated composite was attributed to poor adhesion between the glass filler and the epoxy matrix. The lack of chemical bonding at the glass-epoxy interface could have exposed more hydrophilic sites on the surface of the glass to the absorbed water molecules. The silane coupling agent will bond to and remove these hydrophilic hydroxyl groups on the surface of the glass. The silane pretreated composite could have also absorbed less water than the plain matrix sample because the coupling agent could have increased the crosslink density at the matrix-filler interface. This increased crosslink density would result in a lower available free volume for moisture absorption. SEM images of the fracture surfaces of the composites supported this reasoning. The fracture surfaces of the untreated composite were clean in appearance where a noticeable amount of matrix material was left on the surfaces of the glass beads in the pretreated composite.

Wang and Ploehn[99] also studied these samples by dynamic mechanical analysis before and after exposing to water. Figure 2-30 is an illustration of the DMA spectra of each of the tested samples in both the dry and wet states.

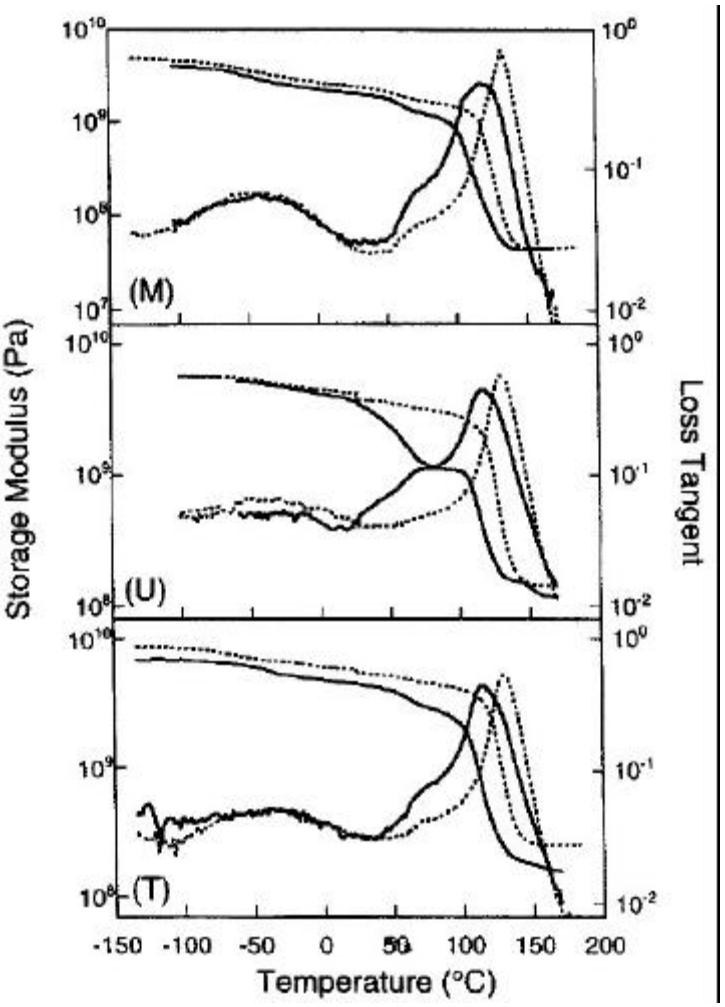


Figure 2-30. DMA of dry and wet composites.[99] M-plain matrix, U-untreated composite, T-treated composite, solid lines-wet, dashed lines-dry.

It can be seen from Figure 2-30 that only slight differences exist between the two composites and the plain matrix when the samples are dry. However, when DMA was used to characterize the wet samples the spectra for each of the samples differed significantly. There is an approximate 15°C depression in $T_g$ for each of the samples in addition to a broadening of the loss tangent peak at the glass or α transition. The water saturated samples also displayed a new transition at approximately 75°C. Wang and Ploehn[99] refer to this water induced transition as the ω-relaxation. These researchers believe that the ω-relaxation is the α-transition of that fraction of the matrix epoxy that has been extremely plasticized by the water. This may be the epoxy that is in the immediate vicinity of microcracks at the epoxy-glass interface. Figure 2-30 shows that

the water has the largest effect on the ω-relaxation of the untreated composite as visible by the loss tangent curve.

Wang and Ploehn[99] also calculated the apparent activation energies of the dry sample α-transitions using the empirical WLF in Equation 19. When the α-transition activation energies were determined Wang and Ploehn found that the activation energy of the untreated composite was lower than those of the silane pretreated composite or the plain matrix. Wang and Ploehn believe that the untreated composite had the lowest activation energy because of low interfacial crosslinking between the matrix epoxy and the glass filler. The plain matrix epoxy had the highest α-transition activation energy. This was presumably due to the low residual stresses and a greater number of crosslinks in the plain epoxy matrix.

Other researchers have also identified fiber-matrix degradation as an additional mechanism during moisture absorption in composite materials. [119,120,121] However, Thomason[122] has identified the void content of a composite as the dominant factor in moisture absorption. The primary concern with using a waterborne epoxy based printed circuit board is increased moisture absorption, so these types of experiments should be performed.

## 2.10 Literature Review Conclusions

Based upon the content of the literature review, the study of the matrix-fiber interfacial properties of composite materials is an extremely complex problem. The study presented for this thesis examines epoxy-surfactant, epoxy-surfactant-substrate, and epoxy-surfactant-substrate-aqueous phase interactions. This thesis research is further complicated by the similar chemical structures of the surfactant and the matrix epoxy phase, which will eliminate the possibility of most spectrosciopic studies. Therefore, this research will rely upon a combination of basic testing, such as the short beam shear test and moisture uptake studies, in conjunction with the novel idea of viscoelastic cooperativity studies.

# Chapter 3 Experimental

## 3.1 Materials

A model epoxy-surfactant system consisting of diglycidyl ether of bisphenol A (DGEBA) epoxy (Shell EPON® 828) and the nonionic surfactant Triton X-100 (Aldrich) was studied. The curing agent/catalyst used to crosslink the epoxy was 2-ethyl-4-methyl imidazole (EMI-24), which is available from Aldrich. These substituents are illustrated in Figure 1-2. The epoxy and surfactant were chosen because they are both very common in industry and have been highly studied in the literature. The imidazole curing agent/catalyst was used because it has the advantage of being water soluble and will therefore work in a waterborne system. For comparative purposes, the model system was compared to a commercially available waterborne epoxy produced by Shell (EPI-REZ® 3510-W-60). To model the epoxy-surfactant-glass interactions E-glass filler and E-glass cloth was used to construct glass filled and composite samples, respectively. The sample details for the E-glass used for this thesis research are described in the sample preparation section.

## 3.2 Sample Preparation

### 3.2.1 Model System

Epoxy resin was added to a 3-neck 500 mL round bottom flask and placed in a 50°C oil bath. After de-gassing the resin under vacuum, 2 parts per hundred resin (phr) by weight EMI-24 (3.4 moles of EMI-24 per 100 moles of epoxy groups) was added and mixed using a mechanical stirrer equipped with a glass stirring rod and PTFE mixing blade (see Figure 3-1). This amount of EMI-24 was decided upon after examining several concentrations of catalyst (see results section). The combined epoxy-catalyst system was then simultaneously mixed and de-gassed until no visible crystals of EMI-24 and air bubbles were observed. Bulk samples of neat resin were prepared by pouring the heated resin into silicone molds and casting into small bars (13mm x 1.5mm x 52mm).

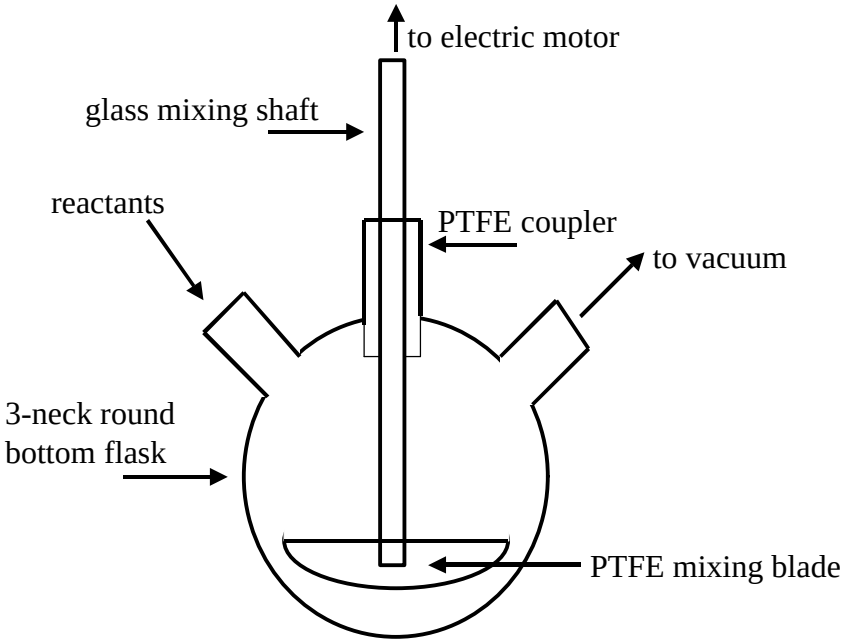


Figure 3-1. Schematic of bulk epoxy mixing set up.

The samples used for the cooperativity studies were prepared by casting the epoxy/imidazole resin as films on 10cm x 10cm sections of 1080 E-glass cloth (Figure 3-2). The 1080 E-glass cloth studied in these experiments had a specific surface area of $0.267 m^2/g$ and was pretreated with either 3-aminopropyltriethoxysilane (APS) or 3-glycidoxypropyltrimethoxysilane (GPS) silane coupling agents. Prior to surface pretreatment, the cut sheets of 1080 E-glass cloth were then etched in concentrated sulfuric acid (18M) for a period of 24 hours at room temperature. The glass cloth was then rinsed in acetone and distilled water. Once cleaned the glass cloth was dried in an oven at 100°C for 24 hours to remove any residual acetone or water. This cleaning and drying procedure constituted the untreated glass surface preparation.

The APS coupling agent was applied to glass by forming a 1% solution (by weight) in distilled water and then adding the glass cloth to the solution for a few seconds. The APS solution did not require any acid or base (for pH adjustment) since the amine catalyzes the hydrolysis of the ethoxy groups to react with the hydroxyl groups at glass surfaces. The GPS coupling agent was applied in the same fashion as the APS, however, the 1% GPS in $H_20$ solution was adjusted to a pH of ≈ 4.5 using acetic acid. The remaining steps

were identical as in the application of the APS. The 1080 E-glass cloth that was used is the actual material that IBM uses in constructing their printed circuit boards.

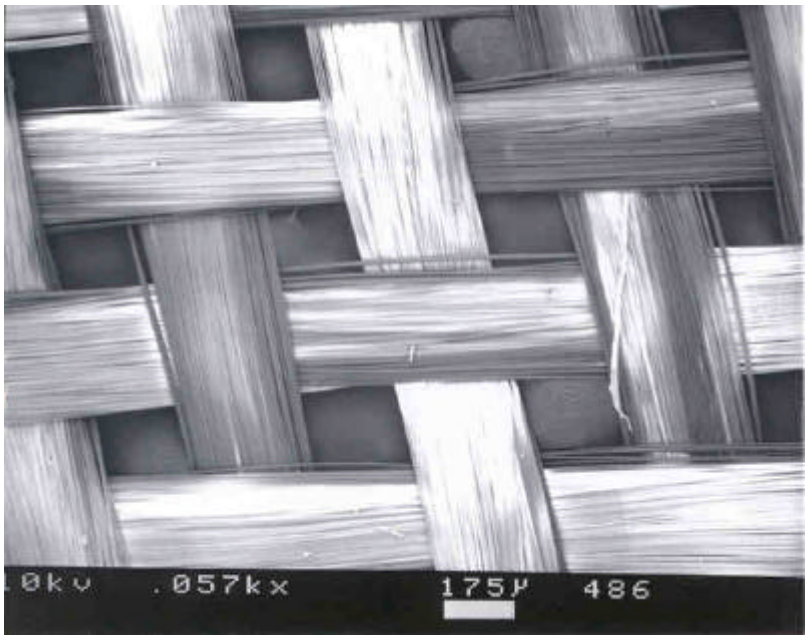


Figure 3-2. SEM image of 1080 E-glass cloth.

Resin was then poured into pre-weighed 250 mL round bottom flasks and a calculated amount of X-100 (w/w%) was added to each flask. After mixing and de-gassing the surfactant added samples, these samples were then also poured into silicon molds, cast into small bars, as well as thin films on the 1080 E-glass cloth. The molds were then placed in the center of a programmable oven equipped with a nitrogen purge. Thin PTFE sheets and aluminum blocks were then placed on top of the silicon molds. The 1080 E-glass cloth samples were also placed between PTFE sheets and aluminum blocks. The oven was then heated at approximately 5°C/min and held isothermally at 195°C for 2 hours. The oven was then allowed to slow cool back to room temperature before the samples were removed. The typical thickness of the thin films, including the glass cloth substrate, was approximately 0.080mm. The weight fraction of glass cloth in these samples was close to 40 percent glass by weight as determined by thermo-gravimetric analysis (TGA).

### 3.2.2 Commercial Waterborne Epoxy

The particle size distribution for the commercial waterborne epoxy (EPI-REZ 3510-W-60®) is illustrated in Figure 3-3. The commercial waterborne epoxy resin has an average particle size diameter of approximately 1.5μm (Shimadzu SA-CP3). Commercial resin, with no water present, was prepared by placing EPI-REZ 3510-W-60® in an oven at 105°C until the water of the emulsion had evaporated. The commercial resin was then cured with 2.0 phr EMI-24 and cast as small bars of bulk material and thin films on the glass substrate in the exact same manner as the model system. The only difference between the model system and the commercial system was that no surfactant was added to the commercial resin. In addition to preparing commercial epoxy samples without the water, commercial samples were also cast on the glass cloth from the intended aqueous emulsion. In this case 2.0 phr EMI-24 was simply added to the waterborne resin and mixed using a magnetic stirrer. Thin films of the waterborne epoxy with catalysts were then spread over the surface of the glass cloth using a small metal spatula. The films were allowed to air dry at ambient temperatures until complete visible coalescence had occurred. This usually required approximately 10 minutes. The waterborne films were then placed between PTFE sheets and aluminum weights and oven cured as previously mentioned. Once cured, the films were similar in appearance and thickness to the model and commercial system films that were prepared without any water.

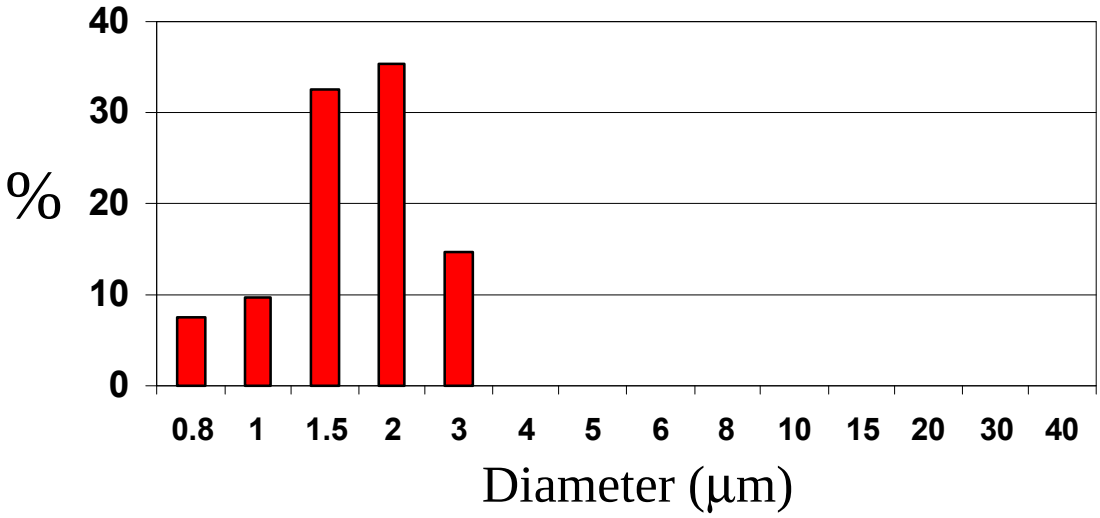


Figure 3-3. Particle sized distribution for commercial waterborne epoxy resin.

### 3.2.3 Model Waterborne Epoxy

Waterborne epoxy resins were prepared by reverse emulsification. The epoxy resin and surfactant were added to a 1000 mL glass reaction vessel. A high torque motor and metal bow-tie coil mixing paddle were used to stir the resin and surfactant (see Figure 3-4). De-ionized and distilled water was added drop wise until phase inversion occurred. Enough water was added to produce a waterborne epoxy resin that was 60 percent solids by volume. Particle size analysis (Shimadzu SA-CP3) determined an average particle diameter of 11.9 μm, with particles ranging from 1.5 μm to 30 μm (see Figure 3-5). The imidazole used as the catalyst/curing agent is completely water soluble. A magnetic stirrer was used to mix the waterborne epoxy resin with the EMI-24. The waterborne resin/EMI-24 mixture was then cast on the surface of the E-glass cloth using a metal spatula. The waterborne resin/EMI-24 mixture was allowed to coalesce prior to sandwiching between the PTFE sheets. These samples were then oven cured at 195°C for two hours.

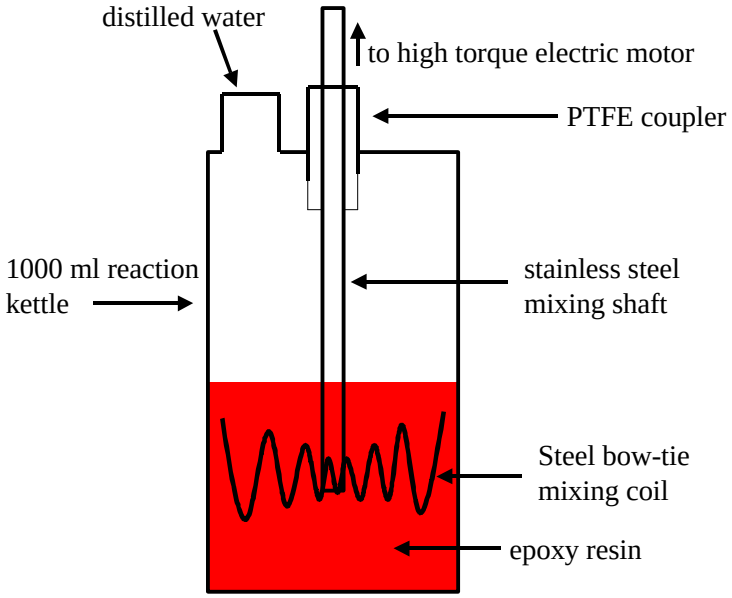


Figure 3-4. Schematic of waterborne epoxy emulsion set up.

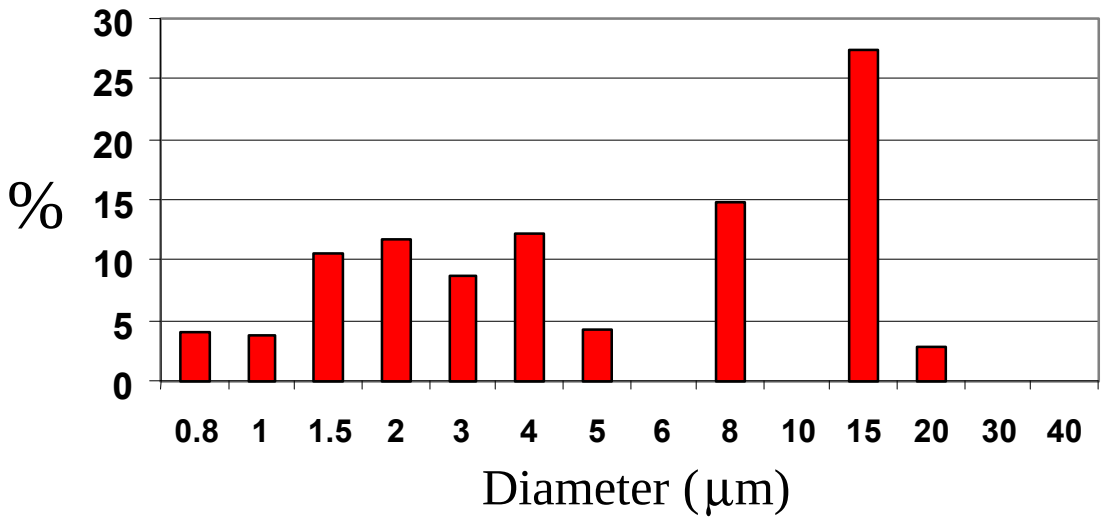


Figure 3-5. Particle sized distribution for model waterborne epoxy resin.

The solids content and surfactant concentration were decided upon to mimic the commercially available waterborne epoxy resin Shell EPI-REZ® 3510-W-60. This resin is also 60 percent solids by volume, but the average particle diameter lies in the 2.0 – 2.5 μm range. The dispersive properites of the Shell waterborne resin are very stable over long periods of time. The model waterborne resin is only stable for a few days before significant agglomeration begins to occur. Formulating stable waterborne resins involves

a high degree of “art” as well as “science”. The model resin contains no additional additives (co-surfactant, stabilizers, etc.) that could be present in a commercial formulation. This, coupled with the larger particle diameter, is most likely why the model waterborne is not as stable as the commercial resin. But, in the context of this study the stability of the model waterborne resin was not an issue.

### 3.2.4 E-Glass Bead Filled Samples

E-glass bead filled bulk epoxy samples (13 mm x 1.5 mm x 52 mm) were also prepared to study moisture uptake. The E-glass filler was obtained from Potters Industries (Cleveland, OH) and has an average particle diameter of 3.9 μm and specific surface area of 0.88 $m^2/g$, as determined by particle size analysis (Figure 3-6). The epoxy resin, EMI-24, and E-glass beads (30 percent by volume) were also mechanically stirred in a 2-neck 250 mL round bottom flask at 50°C under vacuum. The samples were poured into silicon molds and oven cured at 195°C for two hours. Samples were also made that contained surfactant. The moisture uptake experiments were performed by immersing the samples in water baths at 25°C and 65°C. Moisture uptake measurements were then made by periodically weighing the samples on an analytical balance (Mettler AE 200). Minimums of 5 individual specimens were tested for each glass filler/matrix epoxy combination.

Prior to the application of the coupling agents, the E-glass beads were etched in concentrated sulfuric acid and washed with distilled water. The E-glass beads were then also pretreated with either APS or GPS silane coupling agents. The GPS coupling agent was applied in the same fashion as the APS, however, the 1% GPS in $H_20$ solution was adjusted to a pH of ≈ 4.5 using acetic acid.

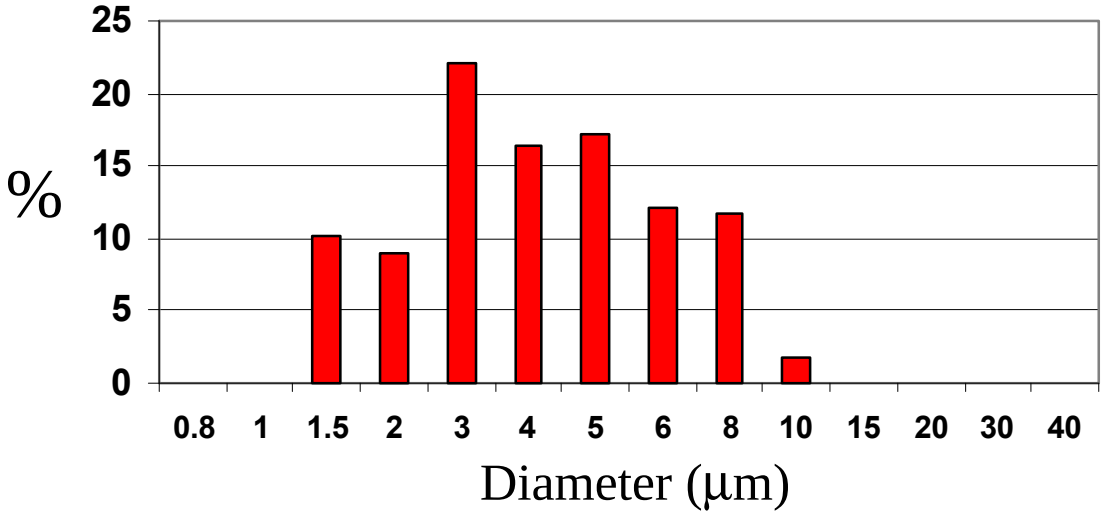


Figure 3-6. Particle sized distribution for E-glass bead filler.

### 3.3 Single Fiber Pull-Out Test

The modified single fiber pull-out test as reported by DiFrancia was performed.[67,68] Samples were prepared by placing a single fiber length wise in the center of a dog bone shaped silicon rubber mold. The molds were prepared by cutting silicone rubber sheets using a hydraulic press and a dog bone shaped cutter. A continuous single sheet of silicone rubber was then bonded to the back of the cut sheet to from the mold. The sample dimensions were 25.4 x 3.0 x 2.4mm for the gauge section and 8.2 x 15.3 x 2.4 mm for the grip tabs. The fibers were vertically centered by cutting small notches for the fiber ends at each inner end of the silicone molds. Fused silica glass on glass optical fibers from Polymicro Technologies Inc. (105/125/500μm) were used in the tests. Prior to use in the fiber pull-out test, the outer polymeric coating of the fibers was removed by soaking in 18M sulfuric acid over night. The etched fibers were then rinsed in acetone and distilled water. The epoxy was then de-gassed under vacuum at 50°C and carefully poured into the molds to avoid trapping air near the fibers. The samples were then oven cured at 195°C for two hours and allowed to slow cool in the oven to room temperature. The fiber embedded epoxy samples were then pre-cracked in the center of the dog bone using a razor blade. The samples were the loaded in tension using a Polymers Laboratories Miniature Materials Tester (Minimat) at a strain rate of 1 mm/min at room

temperature. In addition to testing dry samples, tests were also performed after exposing the samples to water for 1 hour and 24 hours. The relative interfacial shear strength was then determined from the maximum load at break ($P_{max}$).

### 3.4 Short Beam Shear Test

A hand lay-up procedure was used to construct epoxy/E-glass composite plaques. Sheets of 2116 plain weave E-Glass cloth (Clark-Schwabel) were cut in 152.4mm x 152.4mm squares. This type of E-glass was used for the composite samples because the weave density is higher than 1080 E-glass cloth (5.37 Oz./Yd.$^2$ versus 2.87 Oz./Yd.$^2$).[123] The higher weave density of the 2116 E-glass cloth eased the handling of the glass without causing any fraying. The 1080 E-glass cloth that IBM uses for printed circuit board construction is very difficult to handle without disrupting the cross hatched weave pattern. The 2116 E-glass was etched, cleaned, and pretreated with either APS or GPS following an identical procedure as with the 1080 E-glass cloth mentioned previously.

Three types of epoxy matrices were used for the short beam shear measurements. A neat epoxy matrix was used that consisted of only the DGEBA epoxy resin and 2 phr EMI-24. An epoxy matrix comprised of DGEBA epoxy resin, 2 phr EMI-24, and 5 phr Triton X-100 (no water) was also used to study the effects of the surfactant. The third matrix was cast from the waterborne emulsion of the epoxy/surfactant system. The glass sheets were then poured into a 152.4mm x 152.4mm aluminum mold. A schematic of the mold is illustrated in Figure 3-7. Prior to casting the epoxy/E-glass composites the mold was pretreated with mold release. A thin PTFE sheet was also placed on the bottom of the mold to prevent the epoxy from bonding to the aluminum. The E-glass sheets were added individually to the mold and de-gassed epoxy resin was poured into the mold. A total of 21 sheets of E-glass were used for each sample. Another sheet of thin PTFE film was then placed on top off the poured epoxy to prevent bonding to the top plate. 2.2mm aluminum spacers separated the top and bottom plates of the mold. This glass and spacing configuration was used to achieve a volume fraction of glass fibers ($V_f$) of 40 percent. The waterborne composites were prepared in a similar fashion, except that the emulsion was allowed to coalesce on the glass before adding the next sheet.

The uncured epoxy/E-glass composite was then degassed in a vacuum oven at 50°C for 4 hours to aid in the wetting of the fibers by the resin. The composites were then cured in Tetrahedron MTP model 14 press using a pressure of 500 pounds per square inch. The press was heated at a rate of 5°C/min to 195°C, held isothermal for 2 hours, and cooled at a rate of 5°C/min. Rectangular short beam shear test samples (38.1mm x 12.7mm) were then cut from the composite plaques using a band saw.

An Instron tensile testing instrument with a 5000N load cell was used to measure the short beam shear strength of the samples. A three-point bending test fixture was used with a span length of 11.00mm (see Figure 2-16). A crosshead rate of 1.3mm/min as per ASTM D 2344 was used. The load versus displacement curves were recorded on a computer. The peak of the curve was taken as the load to failure (P) of the sample. The average interlaminar shear strengths, taken from 8 to 13 samples, were calculated using Equation 7.

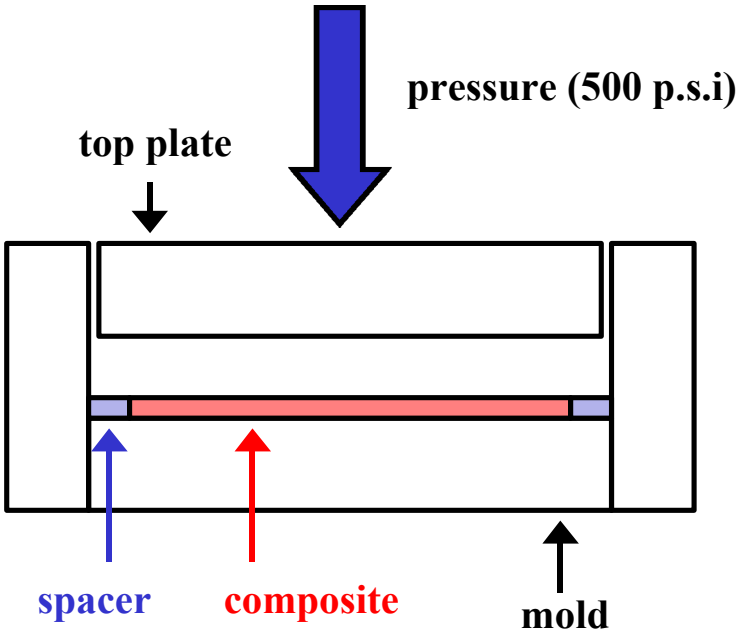


Figure 3-7. Schematic of mold used for casting composite samples.

## 3.5 Equipment

### 3.5.1 Dynamic Mechanical Analysis

The research presented in this paper was performed at two facilities, the IBM Thomas J. Watson Research Center and Virginia Tech. Subsequently, several dynamic mechanical analyzers (DMA) were used in characterizing the samples. A Rheometrics DMTA Mk III was used at IBM's facility while a Polymer Laboratories DMTA Mk II and a Netzsch DMA 242 were used at Virginia Tech. The Rheometrics and Polymer Laboratories DMTA use an identical head set-up, but slight variation in the experimental results may have occurred due to small differences in calibration between the two instruments. Samples were analyzed using the single cantilever beam mode. The medium frame, "C" clamps, and a displacement of 16μm were used for the bulk samples. The small frame, wide faced knife edged clamps, and a displacement of 40μm were used for the glass cloth samples. The Netzsch DMA 242 was run the in double cantilever beam mode for the bulk samples and in the tension mode for the glass cloth samples. These modes are illustrated in Figure 3-8. Despite these differences, all three instruments produced results in excellent agreement with one another. Single frequency sweeps were scanned at 1 Hz from 50 to 225°C at a rate of 2.5°C/min under a nitrogen atmosphere. Sub-ambient runs, when required, were initiated at a temperature of -135°C. Multiple frequency sweeps were measured at 0.1 Hz, 0.33 Hz, 1.00 Hz, 3.33 Hz, 10.00 Hz, and 33.33 Hz in the temperature range of 75°C to 225°C in 3°C isothermal steps. In an effort to minimize experimental error caused by using more than one instrument, groups of experiments were performed on a single DMA when possible.

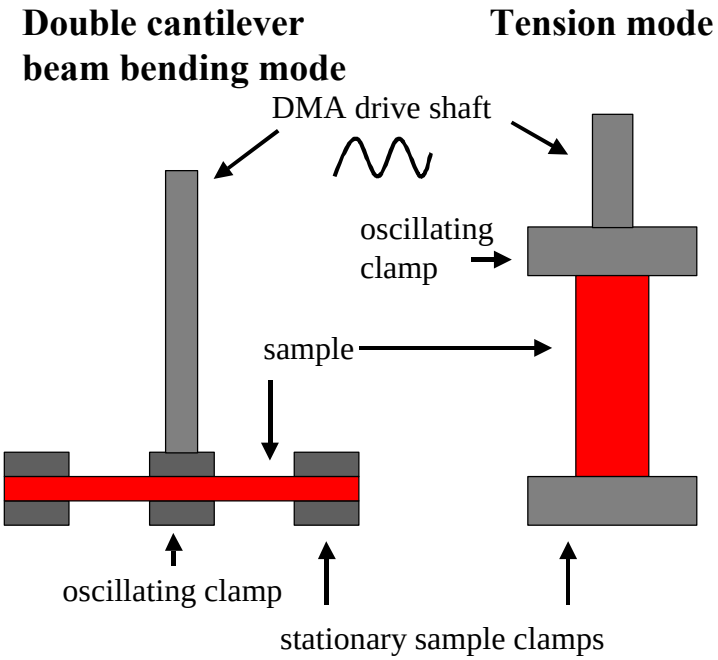


Figure 3-8. DMA configurations.

### 3.5.2 Other Characterization Instrumentation

Differential scanning calorimetry measurements of the Triton X-100 were made on a Perkin-Elmer Pyris DSC equipped with a liquid nitrogen cooling accessory. The samples were rapidly quenched at -140°C and heated to room temperature at a rate of 10°C/min. The $T_g$ was then taken as the half extrapolated change in heat capacity ($C_p$).

Atomic force microscopy was performed using a Digital Instruments Dimension 3000 equipped with a Nanoscope IIIa controller. The images were taken on microtomed surfaces using a tapping mode and phase imaging.

A Philips 420T TEM operated at 100kV was used to obtain transmission electron micrographs. An International Scientific Instruments scanning electron microscope (SEM) was used to acquire images of brittle fracture surfaces. A tungsten filament with a beam voltage of 20 KeV was used. The samples were sputter coated with gold prior to imaging.

Surface analysis was performed using X-ray photoelectron spectroscopy (XPS) with a Perkin Elmer model 5400. A Mg source operated at 14 KV (300 Watts) of power was used. A spot size of 1 mm x 3 mm was analyzed from the surfaces of the samples.

FTIR was performed using a Nicolet 510 spectrophotometer (4 $cm^{-1}$ resolution). Spectra were collected using the transmission mode (average of 120 scans) of samples sandwiched between KBr salt plates.

Gel Permeation Chromatography (GPC) was performed using a Waters 2690 Separations Module equipped with a Viscotek laser refractometer and Viscotek T60A dual detector.

High Performance Liquid Chromatography (HPLC) was executed using a Hewlett Packard HP Series 1050. The solvent was 100 percent acetonitrile at a flow rate of 1 mL/min. The column temperature was maintained at 50°C. A Phenomex C18 column was used in the instrument.

# Chapter 4 Results

## 4.1 Catalyst Concentration

Before examining the effects of the added X-100 surfactant to the epoxy system, knowledge of the amount of EMI-24 to properly catalyze and crosslink the network was important. It was desirable to use a concentration of catalyst that would produce a relatively high $T_g$ and at the same time yield a reasonably narrow tan δ curve peak width at the glass transition. Such a result was needed to highlight any plasticization effects, such as $T_g$ depression, due to the surfactant. Figure 4-1 is a plot of the DMA result on the cured network $T_g$ showing the effect of catalyst concentration. Table 1 contains the corresponding tabulation of catalyst concentration used in phr and moles of EMI-24 per 100 moles of epoxide groups (mol %), $T_g$, and the resulting tan δ peak width at half height. The glass transition temperature was taken as the temperature of the peak maximum in the tan δ curve for the α-transition. $T_g$ measurements were made at a heating rate of 2.0°C/min at a frequency of 1 Hz.

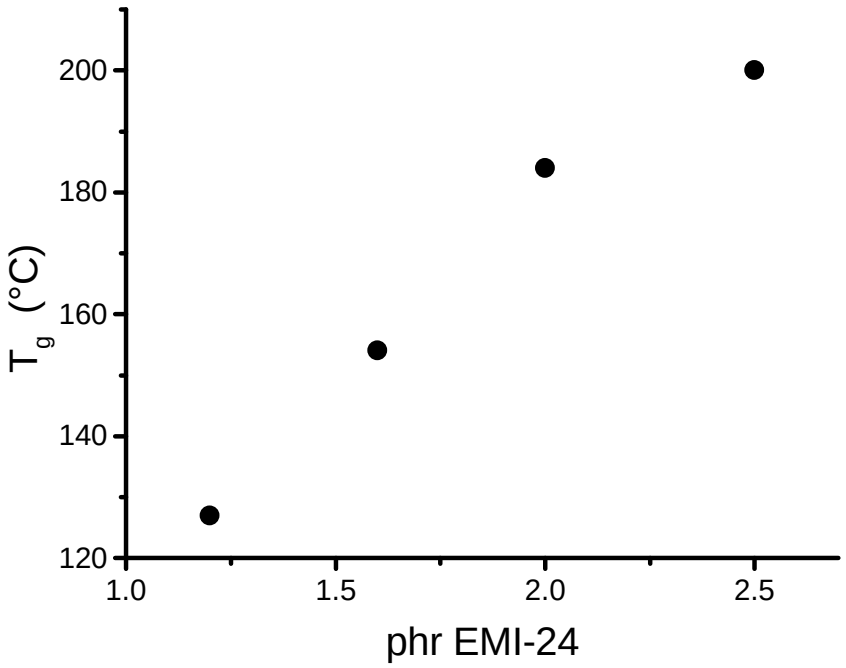


Figure 4-1. $T_g$ of fully cured epoxy versus phr EMI-24.

| phr EMI-24 | moles EMI-24 / 100 moles epoxide groups | $T_g$ (°C) | tan δ width at half height (°C) |
|---|---|---|---|
| 1.2 | 2.1 | 127 | 29 |
| 1.6 | 2.8 | 154 | 37 |
| 2.0 | 3.5 | 184 | 35 |
| 2.5 | 4.3 | 200 | 41 |

Table 4-1. EMI-24 concentration summary.

Using this data an optimum catalyst concentration of 2.0 phr was used. This amount of EMI-24 agrees well with the results of Heise and Martin.[11,12,13] These authors have performed extensive studies in the crosslinking ability and concentration dependence of EMI-24 on DGEBA. Heise and Martin proposed that once the epoxy-imidazole adducts are formed that crosslinking occurs through an etherification mechanism. Therefore, a low concentration of imidazole will result in more epoxide groups being available to form crosslinking ether bonds. This explains why the $T_g$ of the epoxy was so high when only a very low concentration of EMI-24 was used as a crosslinking agent/catalyst. Heise and Martin's research indicates that 7 mol % EMI-24 provided the greatest $T_g$. The research presented in this thesis obtained a maximum $T_g$ using 4.3 mol % EMI-24. This slight difference is probably due to Heise and Martin's use of a highly monodispersed development resin in comparison to the commercially prepared resin of the present study. They also used a higher purity imidazole for their research.

Lower levels of catalyst (1.2 and 1.6 phr) result in a $T_g$ that may be too low for detecting small depressions in the glass transition temperature due to plasticizer effects from the surfactant. Higher concentrations of catalyst (2.5 phr) resulted in a $T_g$ that exceeded the cure temperature. This raises the question of whether or not a full cure can be obtained at high concentrations of catalyst when using a cure temperature of 195°C in such systems. An answer is important to prevent chemical changes in the DMA while a measurement is being made. Also, there is a risk of degradation if the cure temperature is increased much past 195°C. Also, the tan δ width at half height was the broadest for the

highest concentration of catalyst (41°C). The tan δ width at half height for the 2.0 phr catalyst sample was reasonable (35°C).

As mentioned previously, the sample needs to remain chemically stable while being analyzed in the DMA. Figure 4-2 is a plot of tan δ and log storage modulus (E') versus temperature for consecutive first and second runs of the 2.0 phr catalyst containing sample.

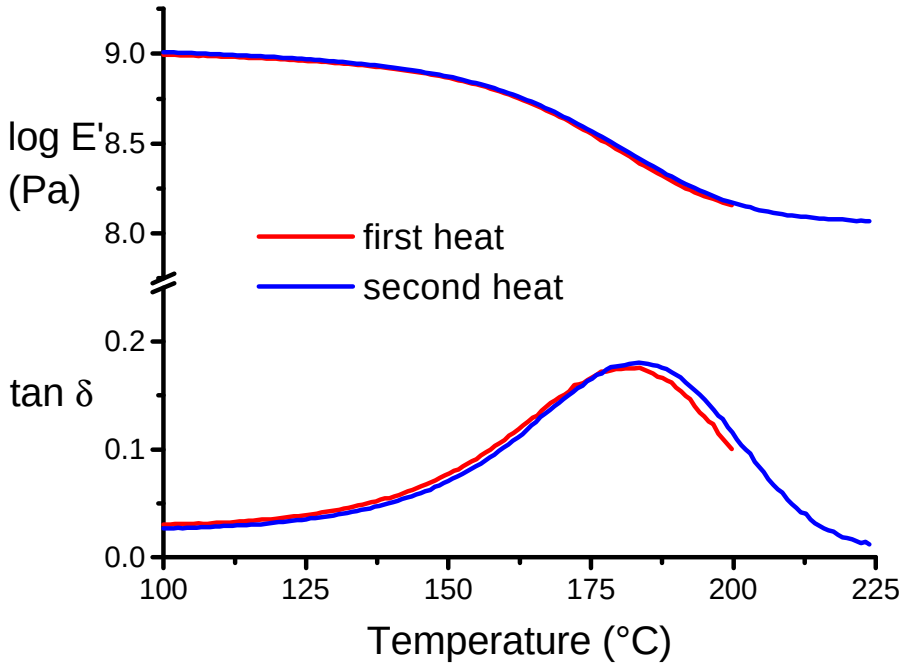


Figure 4-2. First and Second DMA experiments on 2 phr EMI-24 bulk sample.

As can be seen from Figure 4-2 there is very little difference in the loss tangent or storage modulus curves between the first and second experiments. The $T_g$ of the first run was approximately 183°C while the $T_g$ of the second heat was approximately 185°C. The symbols used in the plot overlap so well that it is difficult to distinguish between the first and second runs. After reviewing this information confidence could be placed in using a catalyst concentration of 2.0 phr and curing at a temperature of 195°C for 2 hours.

## 4.2 Model Surfactant Effects on Bulk Epoxy

Once a catalyst level of 2.0 phr EMI-24 had been selected the effects of adding X-100 surfactant to the bulk model epoxy could be studied. To minimize the error involved with adding catalyst to each sample separately, a large master batch of epoxy and catalyst was prepared. Material from the master batch was then partitioned out and placed in pre-weighed 250 mL flasks. Predetermined amounts of surfactant were then added, ranging in concentration from 1.2 to 14.6 phr. This ensures that no effects on $T_g$ due to varying catalyst levels were present when comparing neat and surfactant added samples. Figure 4-3 illustrates an overlay of the tan δ versus temperature plots obtained for each bulk sample. Table 2 lists the corresponding data for concentration, $T_g$, and tan δ peak width at half height.

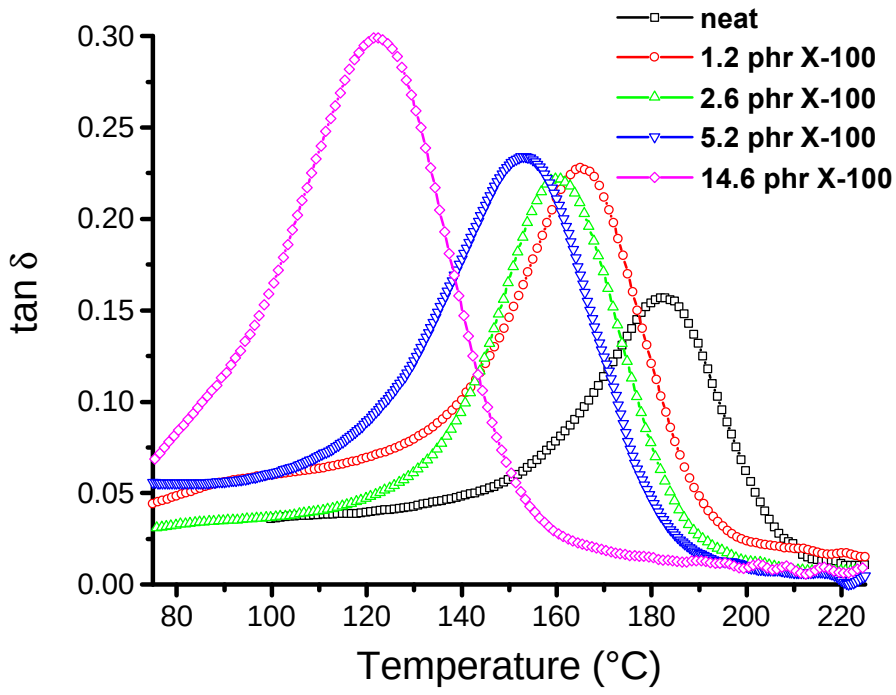


Figure 4-3. Tan δ versus temperature for various concentrations of X-100 surfactant in bulk samples.

| phr X-100 | moles X-100 / 100 moles DGEBA | $T_g$ (°C) | $T_g$ (K) | tan δ width at half height (°C) |
|---|---|---|---|---|
| neat | 0 | 182 | 455 | 33 |
| 1.2 | 0.6 | 165 | 438 | 32 |
| 2.6 | 1.4 | 160 | 433 | 31 |
| 5.2 | 3.0 | 153 | 426 | 36 |
| 14.6 | 8.6 | 122 | 395 | 39 |

Table 4-2. Summary of $T_g$ as a function of X-100 concentrations for bulk model samples.

The plots in Figure 4-3 show a trend of decreasing $T_g$ with increasing concentration of surfactant. The loss tangent peak widths at half height also increase slightly at higher levels of surfactant. The peak width at half height is widest for the 14.6 phr surfactant sample with a value of approximately 39°C.

### 4.2.1 Epoxy-Surfactant Miscibility

The large decrease in $T_g$ upon the addition of surfactant to the model epoxy indicated that the surfactant is acting like a plasticizer. If the assumption is made that the surfactant is completely miscible with the epoxy then the Fox equation can be applied to the system:

$$\frac{1}{T_g} = \frac{w_A}{T_{gA}} + \frac{w_B}{T_{gB}} \tag{33}$$

$\omega_A$ = weight fraction of epoxy

$\omega_B$ = weight fraction of surfactant

$T_{gA}$ = $T_g$ of epoxy in degrees Kelvin

$T_{gB}$ = $T_g$ of surfactant in degrees Kelvin

$T_g$ = $T_g$ of combined epoxy-surfactant system measured in degrees Kelvin.

Rearranging Equation 33 into linear form one obtains the following.

$$\frac{1}{T_g} = \left( \frac{T_{gA} - T_{gB}}{T_{gA} T_{gB}} \right) w_B + \frac{1}{T_{gA}} \tag{34}$$

Thus, plotting $1/T_g$ versus weight fraction of surfactant should yield a straight line if the surfactant is completely miscible with the epoxy. The regression data for the slope and intercept can then be used to calculate a theoretical glass transition temperature for the surfactant. Figure 4-4 is such a Fox equation plot using the $T_g$ values listed in Table 2. The phr concentration levels have been converted to weight fractions.

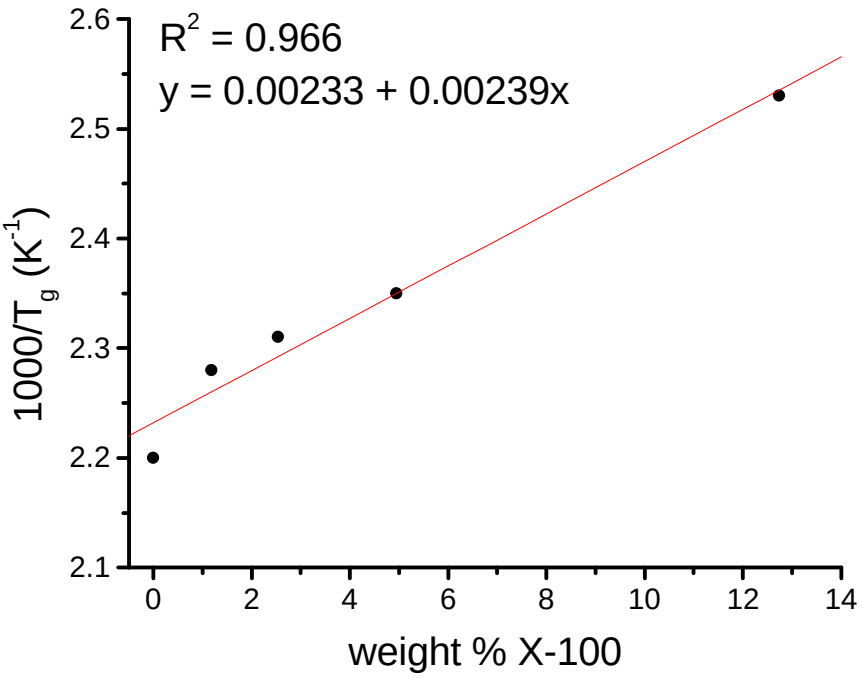


Figure 4-4. Fox equation plot for bulk model

The calculated theoretical $T_g$ values of the surfactant and neat epoxy are -57°C and 175°C, respectively, from the regression analysis. The theoretical and experimental glass transition temperatures of the neat epoxy are in good agreement (175°C versus 182°C). Experimental verification of the glass transition temperature of the surfactant can be used to support the assumption of the model. Figure 4-5 is a DSC thermogram obtained on Triton X-100, which reveals a $T_g$ of -59°C. Although DSC is traditionally a difficult technique for the direct determination of a glass transition temperature of a surfactant, this experiment was in excellent agreement with the predicted value estimated using the Fox equation. The excellent cooling and subambient temperature control of the DSC contribute to such a satisfactory outcome.

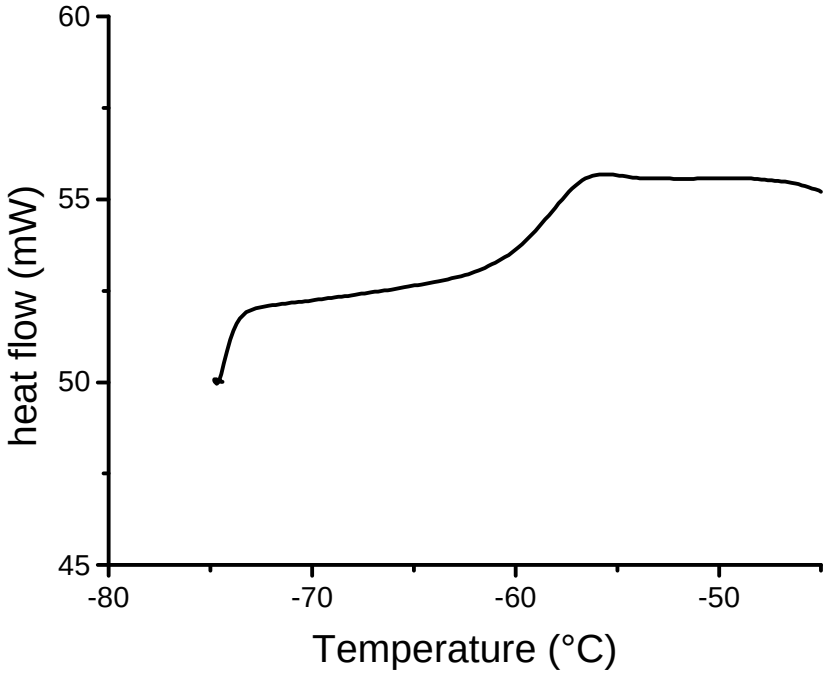


Figure 4-5. DSC thermogram of Triton X-100

Sub-ambient DMA of the bulk model epoxy samples that contained a high concentration of X-100 (14.6 phr) also indicated that the surfactant is highly miscible with the epoxy. Figure 4-6 shows that there are no significant changes in the β transition when high amounts of X-100 are added to the neat epoxy. If the surfactant were phase separating, then the DMA should have revealed a large difference in the loss tangent curves near -60°C.

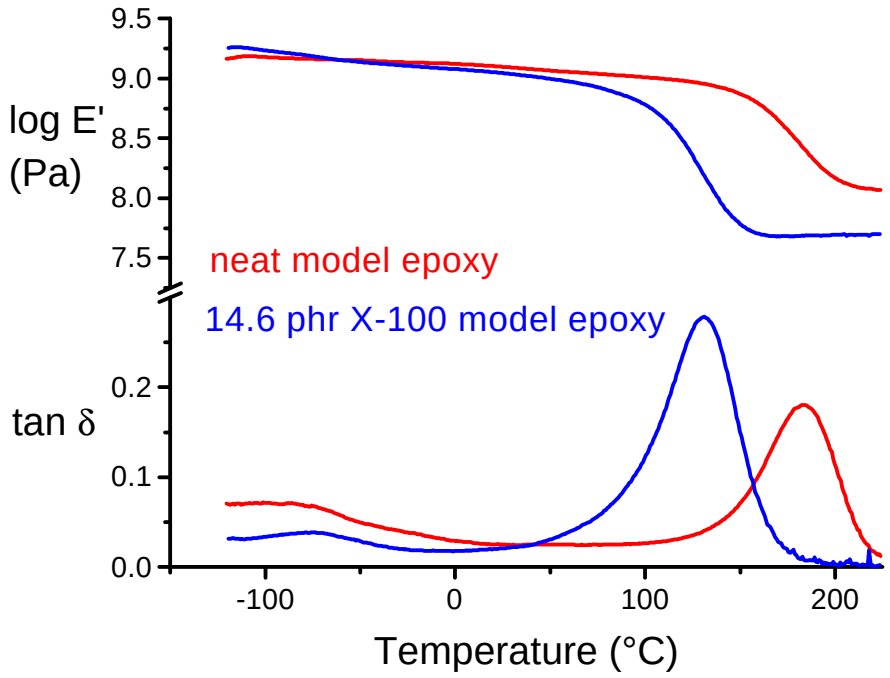


Figure 4-6. Neat versus 14.6 phr X-100 bulk model epoxy samples illustrating β transition.

Atomic force microscopy and transmission electron microscopy were used to examine thin microtomed sections of the bulk model and commercial samples. Figure 4-7 shows the micrographs for the 14.6 phr X-100 model epoxy. As can be seen in Figure 4-7, neither AFM nor TEM detected significant phase separation. Similar results were obtained for commercial epoxy as well. The miscibility between the surfactant and the epoxy system could be due to specific interactions between the hydroxyl and ether functional groups present in either molecules to a chemical reaction between the surfactant, imidazole, and epoxy. As previously mentioned, Heise and Martin[11,12,13] proposed an epoxy-imidazole adduct as the initial step of the curing reaction. Once this adduct is formed, these authors believe that the crosslinking of the epoxy will occur through the alkoxide anions and hydroxyl groups that are formed when the imidazole opens the epoxide rings of the DGEBA. If this were true then the terminal hydroxyl of the surfactant could also exchange a proton and become an alkoxide anion. This would lead to the surfactant becoming chemically reacted in with the epoxy network.

While concentrations of surfactant greater that 15 wt. % were not studied, this should not be important because it is likely that a concentration of surfactant not exceeding 5 wt. % would actually be used in a practical waterborne formulation. It is not known if the miscibility between the epoxy and surfactant is arising due to a chemical reaction or specific interactions. Despite this uncertainty, it appears as if the polymer-surfactant interactions are very favorable.

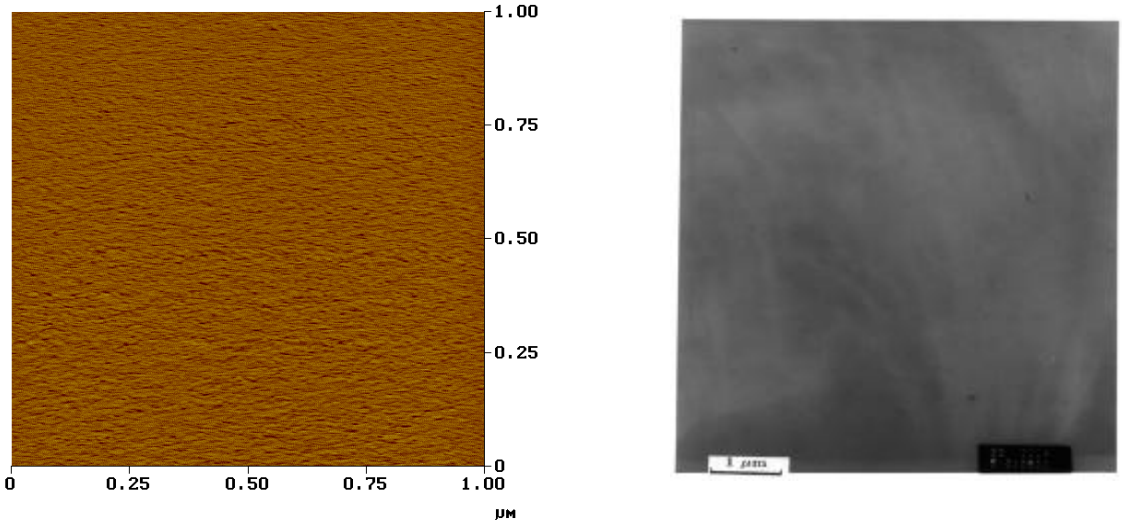


Figure 4-7. AFM (left) and TEM (right) micrographs of 14.6 phr X-100 bulk model epoxy.

The chemical nature of the polymer-surfactant interactions was probed more closely in the next set of experiments. The first clue that the surfactant has a negligible influence on the reaction mechanism between the epoxy and EMI-24 can be seen in the storage modulus curves for the bulk samples. Figure 4-8 shows the dynamic storage modulus curves for the neat model epoxy and 5.2 phr X-100 model epoxy. If the surfactant were reacting with the epoxy resin to a large extent, then the crosslink density ($\rho_c$) of the cured epoxy should decrease. The crosslink density, $\rho_c$ , is directly proportional to the rubbery modulus (E) and is defined in Equation 35.

$$\rho_c = \frac{E}{3RT} \tag{35}$$

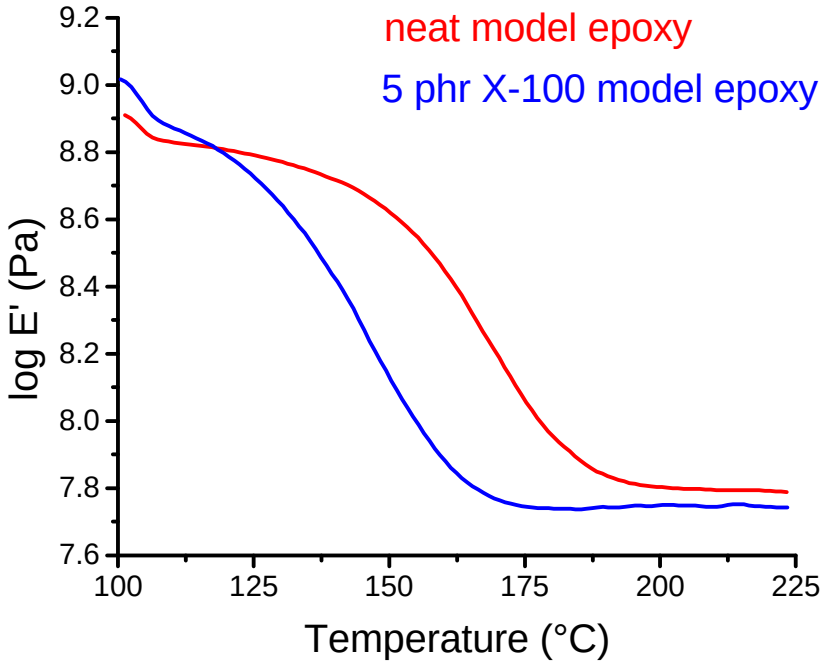


Figure 4-8. Storage modulus curves for neat model epoxy and 5 phr X-100 model epoxy.

As can be seen in Figure 4-8 the only surfactant effect is to decreases the $T_g$ of the epoxy. The rubbery modulus is only lowered a very small amount upon the addition of the surfactant.

### 4.2.2 Surfactant Migration

The ability of the surfactant to migrate to the epoxy-glass interface could be an important factor in the durability of a waterborne composite. Surfactant migration could certainly occur with greater ease if the surfactant does not chemically react with the epoxy during cure. But, due to the highly crosslinked network structure of the cured epoxy, extraction of any unreacted surfactant is difficult. To avoid this problem a model reaction using Phenyl glycidyl ether, PGE, (see Figure 2-1) was devised. PGE cannot crosslink with EMI-24 because it contains only a single epoxy functional group. Etherification through an alkoxide anion is the primary crosslinking reaction mechanism between DGEBA epoxy resin and EMI-24. When PGE is substituted for DGEBA then

the etherification mechanism should lead to some degree of polymerization of the PGE without crosslinks. Therefore, examination of the reaction products should be easier.

The model reaction was carried out by mixing PGE with EMI-24 with a ratio of 3.5 moles of EMI-24 per 100 moles of epoxy functional groups. This is completely equivalent to 2 phr EMI-24 in DGEBA epoxy resin. Surfactant was then added to the PGE-EMI-24 mixtures in concentrations of 1.5 and 3.5 moles of X-100 per 100 moles of PGE. These molar concentrations duplicate surfactant concentrations of 5 and 15 phr X-100 in DGEBA epoxy resin, respectively. The mixtures were then heated in an oven at 195°C for 2 hours to duplicate the curing conditions of the DGEBA epoxy resin.

Prior to curing, the PGE / EMI-24 / X-100 mixtures were clear (slight yellow tint) in appearance and had liquid-like viscosities. After curing all of the mixtures became very viscous and were dark brown in color. The fully cured DGEBA epoxy samples are also dark brown. The high viscosity of the cured PGE / EMI-24 / X-100 mixtures indicated that some degree of polymerization had occurred.

FTIR spectroscopy and GPC measurements were taken on the reacted specimens. Figure 4-9 shows the FTIR absorption spectra for the model PGE / EMI-24 reactions with and without surfactant. No changes can be detected due to the surfactant. Also, no changes in the molecular weight distribution of the products could be detected by GPC (Figure 4-10). Table 4-3 provides a summary of the number average molecular weight ($M_n$) and weight average molecular weight ($M_w$) for each of the samples. The molecular weights were lower than expected ($M_n \approx 600$ g/mol; $M_w \approx 1000$ g/mol), but are very similar.

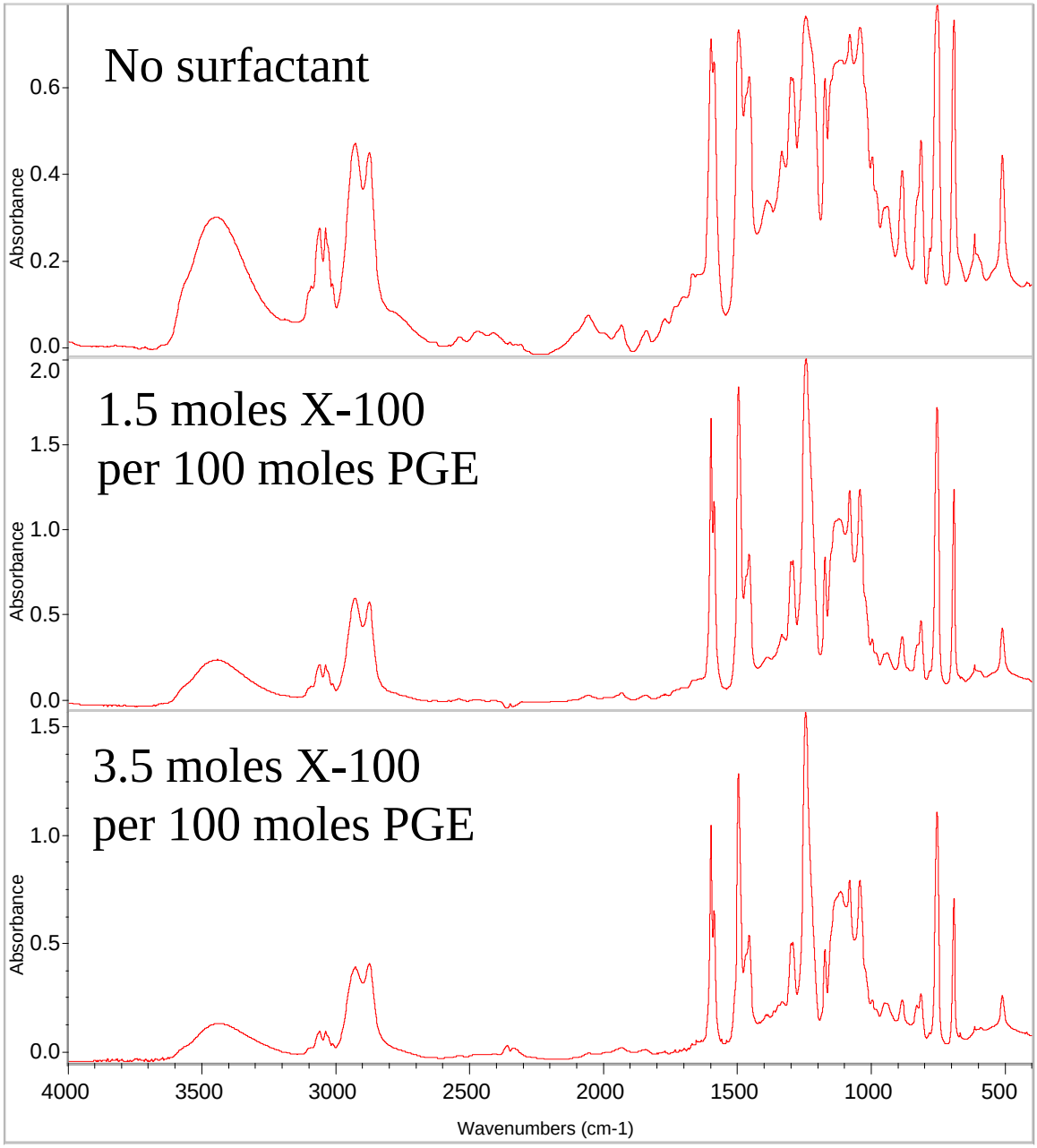


Figure 4-9. FTIR absorption curves for model PGE / EMI-24 reactions.

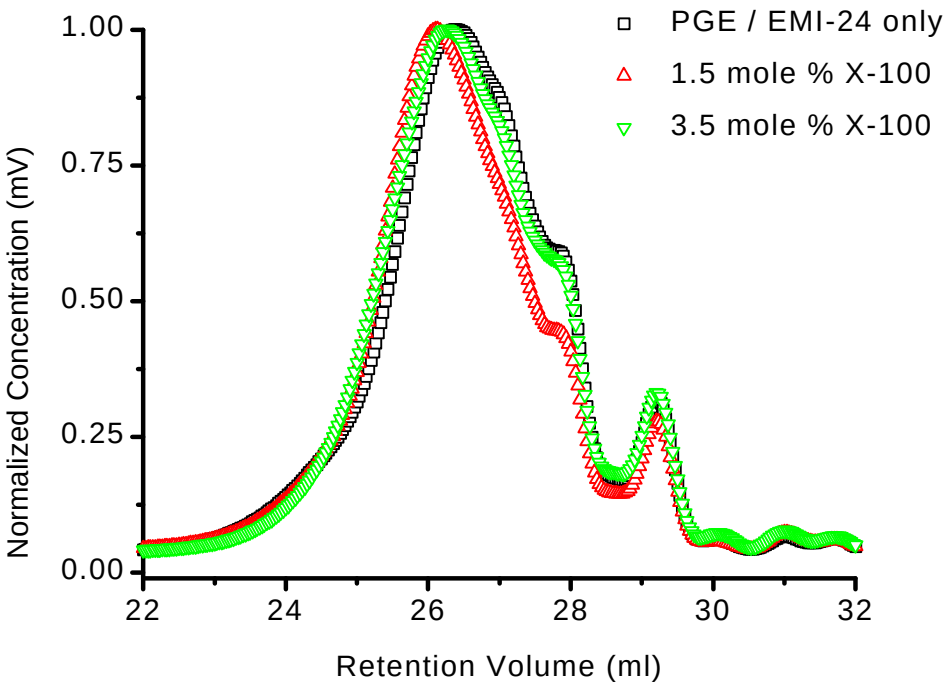


Figure 4-10. GPC traces for model PGE/EMI-24/ Triton X-100 reactions.

| sample | $M_n$ (g/mol) | $M_w$ (g/mol) |
|---|---|---|
| **PGE / EMI-24 only** | 580 | 1040 |
| **1.5 mole % X-100** | 660 | 1000 |
| **3.5 mole % X-100** | 620 | 830 |

Table 4-3. Summary of GPC measurements.

An exhaustive extraction of the unreacted surfactant was done with ordinary distilled water. After this set of experiments it was visibly apparent that some of the surfactant had not reacted with the PGE or EMI-24. For example, the aqueous extract became very soapy when agitated or stirred. Figure 4-11 shows the HPLC chromatographs for pure X-100 and the extract. Pure X-100 had an elution time of 4.01 minutes under the specific column conditions. The water extract chromatograph also shows a peak at 4.01 minutes. These chromatographs were not calibrated with a standard, so a concentration determination cannot be made with this data. The extract also had a slight yellow tint.

The imidazole catalyst is the only yellow reactant used. The peaks at 2.63 and 2.92 minutes with the high absorptions could be unreacted EMI-24. These experiments show that atleast some of the surfactant remains unreacted after the completion of the epoxy-imidazole cure cycle. But, it is not ruled out that the possibility exists that some of the surfactant is reacting with the epoxy.

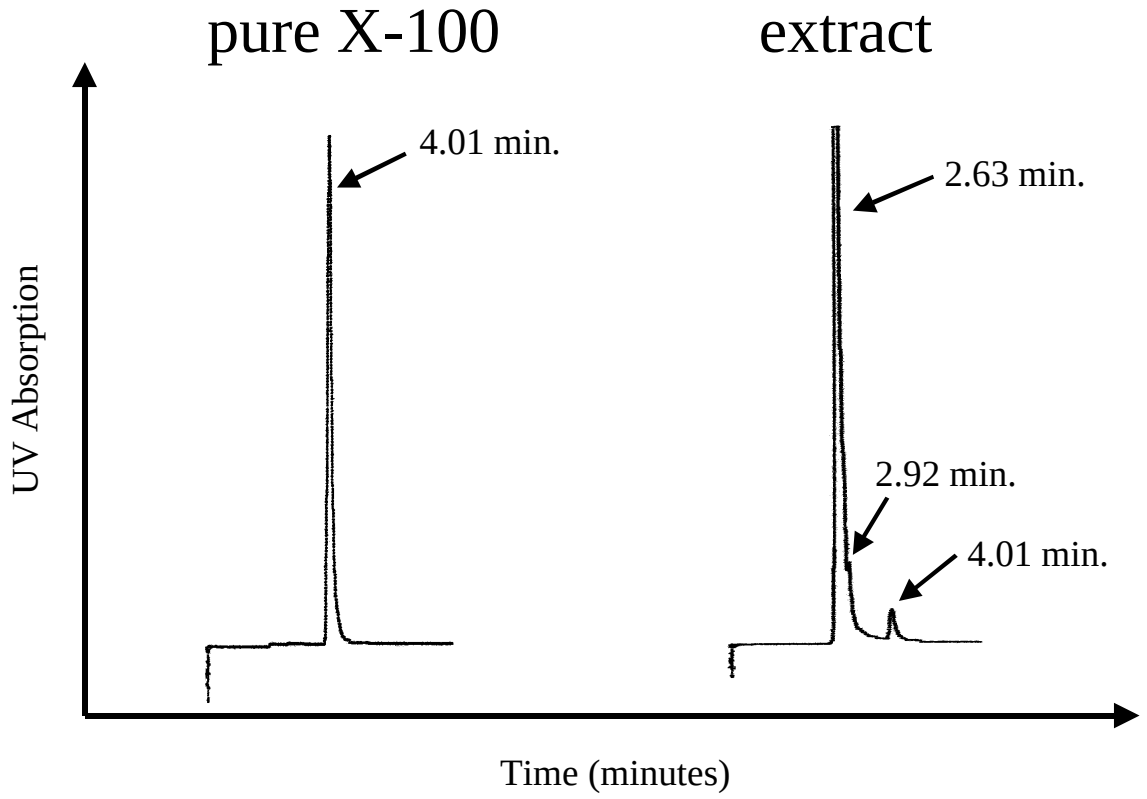


Figure 4-11. HPLC results from extraction experiments.

## 4.3 Moisture Uptake

### 4.3.1 Coupling Agents

Silane coupling agents are an integral component of a glass laminated circuit board. The coupling agents reduce moisture levels at the epoxy-glass interface by providing a chemical bond between the silanol groups of the glass and the matrix phase.[3] Prior to the addition of the E-glass beads to the epoxy matrix an amino or epoxy functional silane coupling agent was applied to the glass surface. Figure 4-12 shows the XPS survey scans of the untreated, APS pretreated, and GPS pretreated glass beads. The elemental survey

of the untreated glass reveals a large number of metal peaks, which is common to the surface composition of E-glass.[3] Ubiquitous carbon is also detected on the surface of the untreated E-glass. After the application of either the GPS of APS silane coupling agents these metal peaks decrease in intensity. Because of the epoxide functionality of GPS, the oxygen intensity is the greatest for this surface pretreatment. The amine functionality of APS is responsible for the small nitrogen peak detected in the APS pretreated glass XPS survey. Incomplete surface coverage of the glass surface by the silane coupling agents could be responsible for residual metal peaks in the XPS survey. The atomic concentrations are reported in Table 4-4. The samples were prepared in a consistent manner and the reported trends are qualitatively correct.

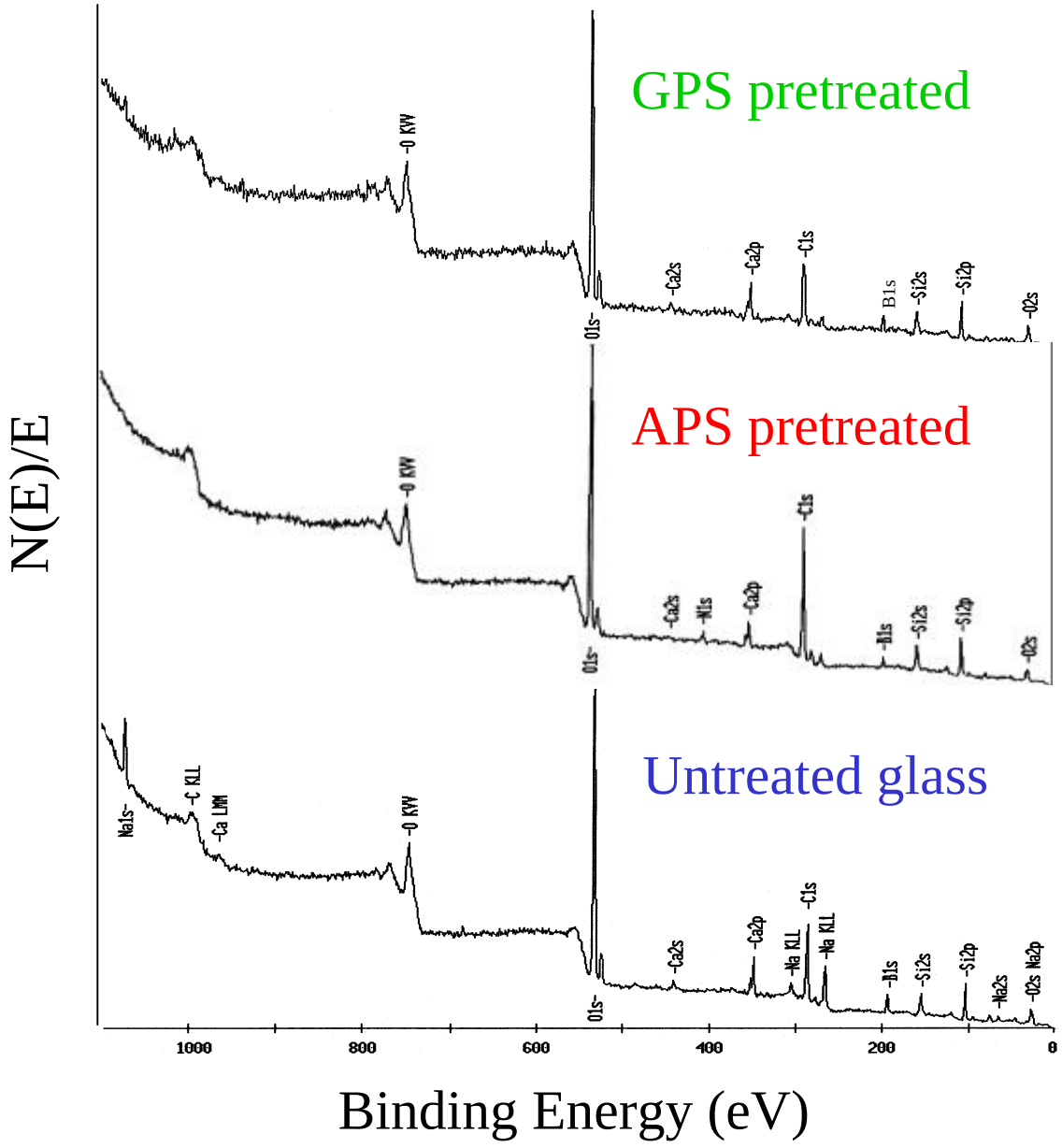


Figure 4-12. XPS survey scans of untreated, APS pretreated, and GPS pretreated E-glass.

| sample | C (%) | O (%) | Si (%) | N (%) |
|---|---|---|---|---|
| **untreated glass** | 32.8 | 43.0 | 9.2 | < 0.2 |
| **APS pretreated** | 45.6 | 34.8 | 9.7 | 3.0 |
| **GPS pretreated** | 31.2 | 52.2 | 13.0 | < 0.2 |

Table 4-4. Summary of atomic concentrations for glass surfaces.

Figure 4-13 shows the SEM brittle fracture surfaces of the untreated glass filled neat epoxy samples. No pictorial evidence of adhesion can be seen between the untreated glass beads and the matrix epoxy in comparison to the pretreated glass fracture surfaces of Figure 4-14 and 4-15. The untreated glass bead SEM images were identical in appearance for the neat and the surfactant additive epoxy samples. This was an expected result, as there was no silane coupling agent to bond the matrix epoxy to the surface of the glass beads. A surprising result was that the APS and GPS fracture surfaces for the neat and surfactant additive epoxy matrices (Figure 4-14 and Figure 4-15) also appeared to be identical. The APS pretreated glass samples are similar in appearance to the GPS pretreated glass samples. It can be concluded that once a coupling agent has been applied to the glass that the matrix material adheres to the glass. If the coupling agent is properly applied then filler particle-matrix adhesion should occur. If the surfactant were migrating to the surface of the glass and coating the beads then a dramatic decrease in the efficiency of the coupling agent could be expected. But, as the SEM images of Figure 4-14 indicate, the coupling agents still function even after surfactant has been added to the matrix phase. The XPS surveys of the glass and SEM images of the fracture surfaces indicate that the silane coupling agent application procedure produced the dominating features of interfacial adhesion, even in the presence of surfactant.

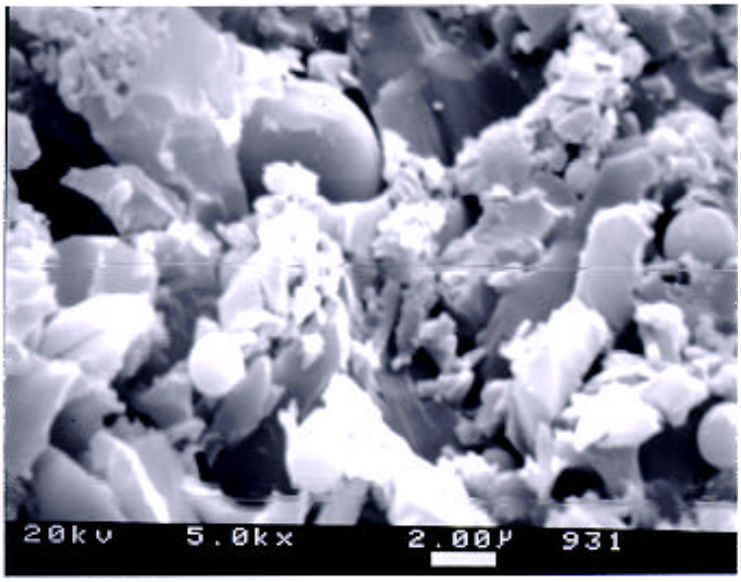


Figure 4-13. SEM image of untreated glass filled epoxy fracture surfaces (neat matrix).

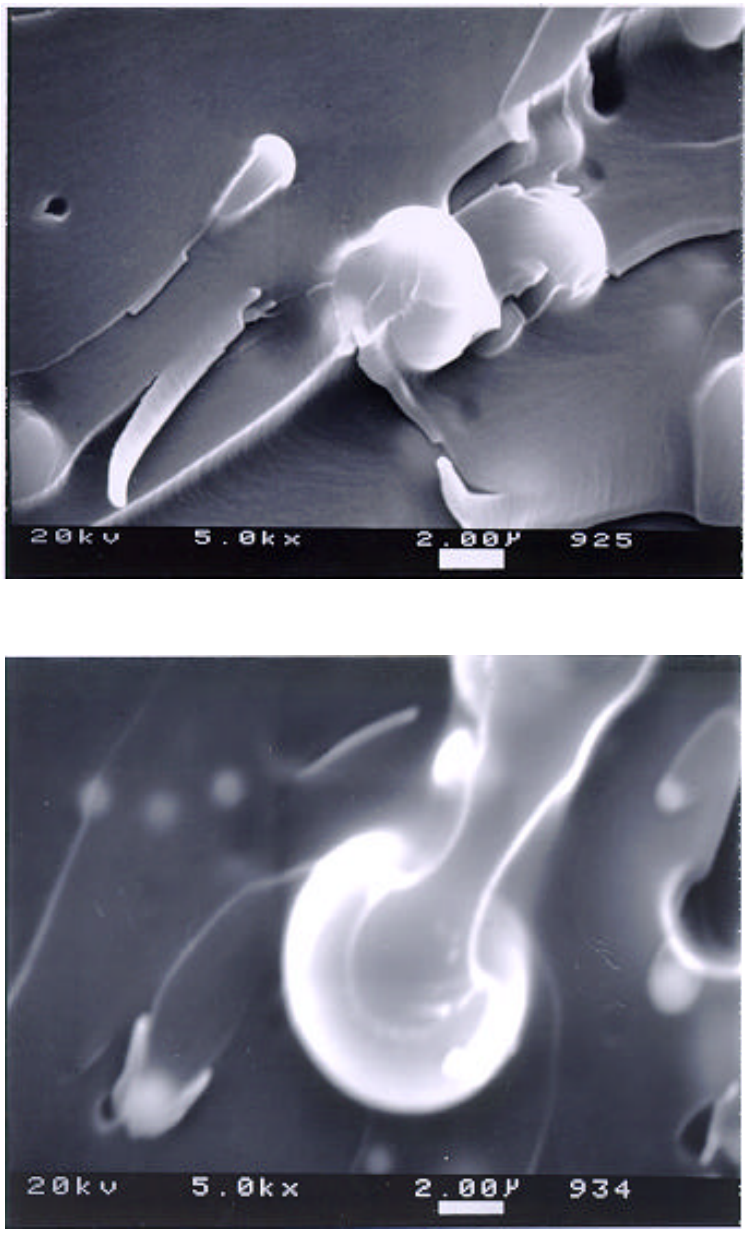


Figure 4-14. SEM image of APS pretreated glass filled epoxy fracture surfaces (surfactant on top, neat matrix image on bottom).

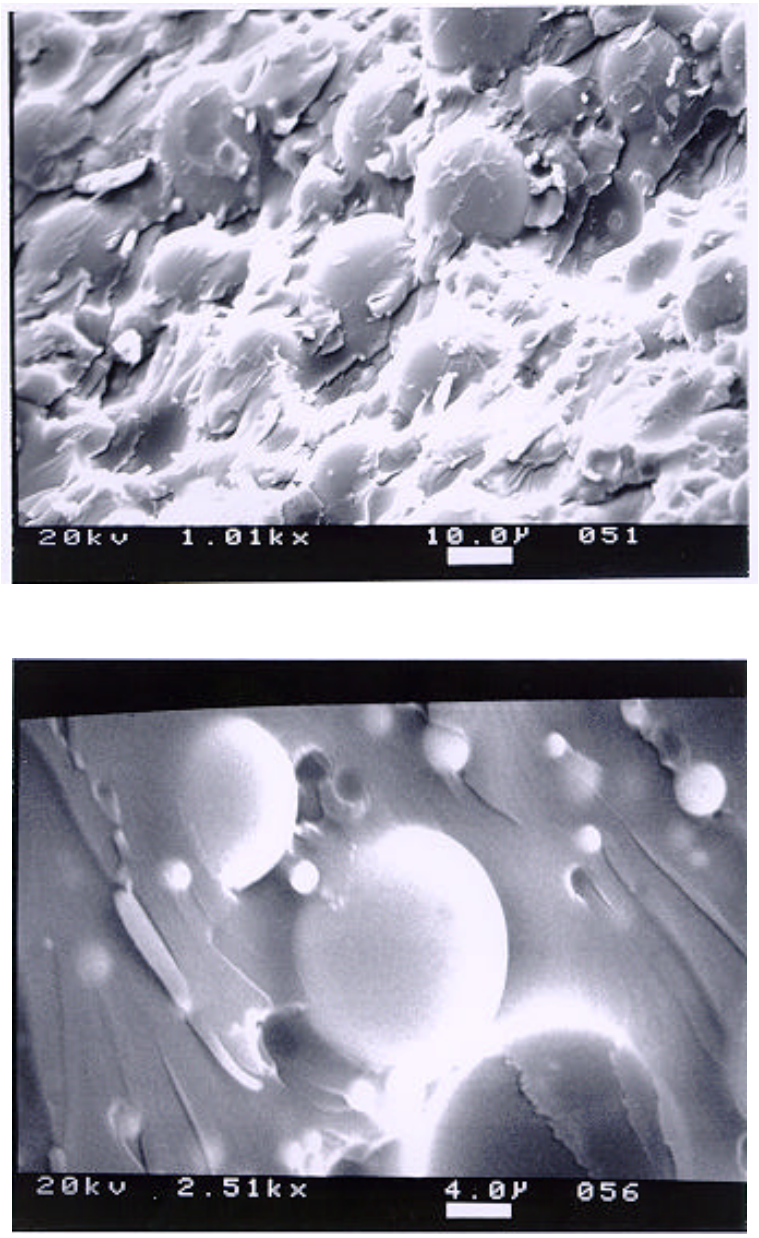


Figure 4-15. SEM image of GPS pretreated glass filled epoxy fracture surfaces (surfactant on top, neat matrix image on bottom).

### 4.3.2 Water Sorption Studies

The Fickian diffusion model developed by Shen and Springer[115] (Equation 32) was used to analyze the moisture uptake properties of the glass filled composites as well as the non-reinforced matrices. Figure 4-16 demonstrates the impact of surfactant on the moisture uptake properties of the non-reinforced matrix epoxy at 65°C. The epoxy adsorbs water at a rapid rate for approximately the first 25 hours of exposure. This plot indicates that the surfactant has a negligible impact on either the diffusion constant or the equilibrium moisture uptake levels of the non-reinforced epoxy. The adsorption experiments at 65°C were terminated after 800 hours because the samples were not gaining any additional mass due to moisture exposure. The initial diffusion constant is equal to approximately 1.2 (± 0.2) x$10^{-2}$ $mm^2$/hr in both cases.

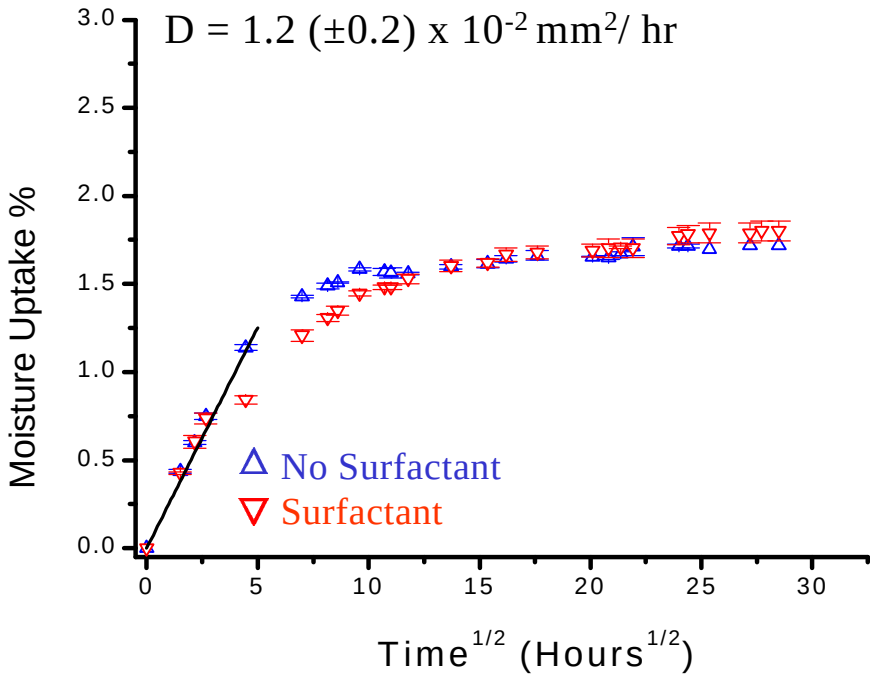


Figure 4-16. Moisture uptake data at 65°C for the non-reinforced matrices. Error bars represent the experimental standard deviation of 5 samples.

The addition of the E-glass beads to the epoxy matrix results in an increase in the equilibrium moisture uptake levels, $M_\infty$, over the moisture levels obtained for the non-

reinforced matrices. Figure 4-17 displays the moisture uptake curves for the E-glass filled/neat epoxy matrix samples. The moisture uptake percentage for this plot has been normalized to the mass of the epoxy matrix, since the E-glass does not adsorb any of the water. The initial diffusion constant remains the same as calculated for the non-filled matrices. The untreated and GPS pretreated E-glass filler produce the largest increases in $M_\infty$ over the non-filled matrix. The increase in $M_\infty$ by the glass filler particles could be the result of microcracking and voiding at the epoxy-glass interfaces.[99] These voids would then be capable of adsorbing a high concentration of water. The APS pretreated glass samples have a value of $M_\infty$ intermediate between the non-reinforced neat matrix and the untreated glass filled samples.

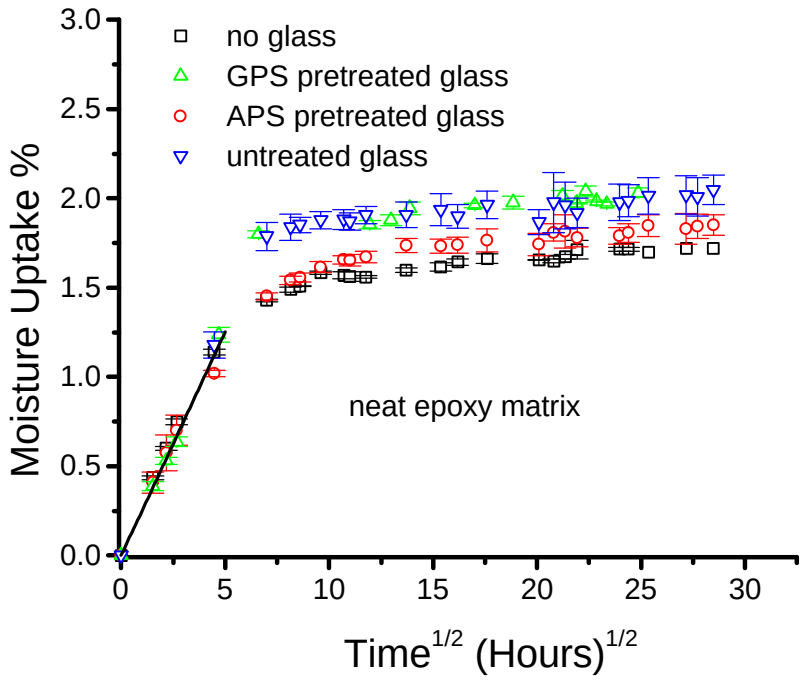


Figure 4-17. Moisture uptake data at 65°C for the E-glass filled epoxy with no surfactant. Uptake calculations are normalized to the mass of the epoxy in the composite. Error bars represent the experimental standard deviation of 5 samples.

The surfactant has little influence on the moisture uptake properties of the non-reinforced epoxy matrix, but this changes when the glass filler is also taken into

consideration. Figure 4-18 illustrates the enhancement in $M_\infty$ for the glass filled epoxy samples that contained surfactant in the epoxy matrix. The equilibrium moisture content for the untreated glass samples increases from 2.04 ($\pm$ 0.08) % for the neat epoxy matrix to 2.68 ($\pm$ 0.05) % when surfactant has been added to the epoxy. The surfactant also produced $M_\infty$ values that were slightly higher for the APS and GPS pretreated glass samples, but these values do not approach the $M_\infty$ level obtained for the untreated glass filled epoxy. It is interesting that the surfactant did not alter the moisture adsorption properties of the epoxy until an interface, in this case epoxy-glass, was present.

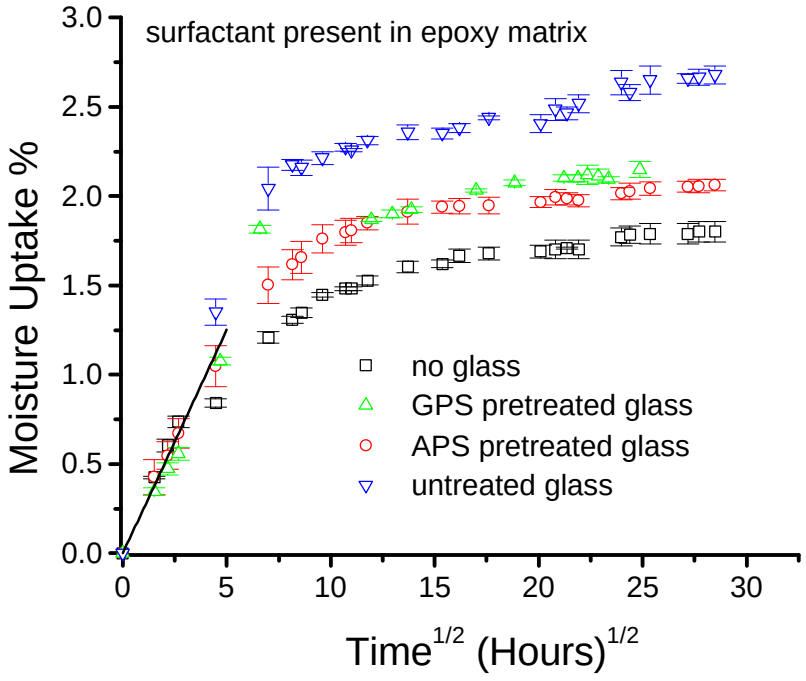


Figure 4-18. Moisture uptake data at 65°C for the E-glass filled epoxy with surfactant in the matrix. Uptake calculations are normalized to the mass of the epoxy in the composite. Error bars represent the experimental standard deviation of 5 samples.

Even though a portion of the surfactant seems to migrate to the glass surface, the silane coupling agents are still effective in reducing $M_\infty$ to below the untreated glass filled epoxy levels. The trends in moisture adsorption were similar, but not as pronounced, at 25°C (Figure 4-19, Figure 4-20, and Figure 4-21). The diffusion constant

at 25°C was reduced to 1.5 (± 0.2) x$10^{-3}$ $mm^2$/hr with equilibration times of approximately 2350 hours. The entire assortment of silane coupling agent pretreated glass filled epoxy samples showed a large amount of interfacial damage when examined by SEM after the completion of the moisture uptake experiments (Figure 4-22). The results of the moisture uptake experiments at 25°C and 65°C are summarized in Table 4-5.

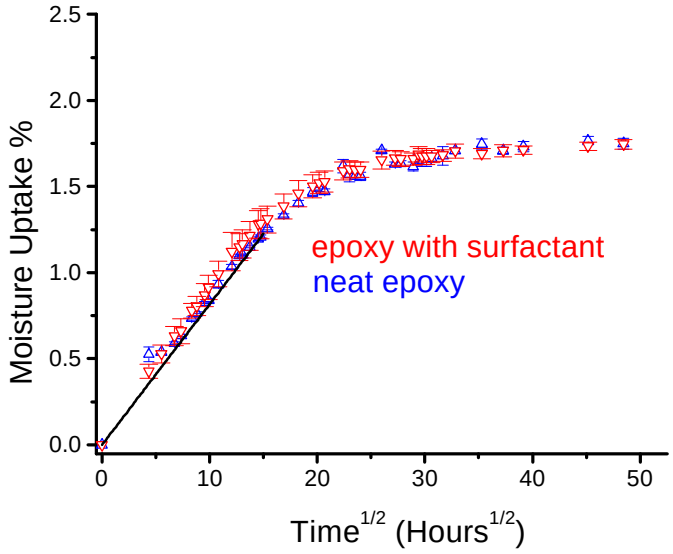


Figure 4-19. Moisture uptake data at 25°C for the non-reinforced matrices. Error bars represent the experimental standard deviation of 5 samples.

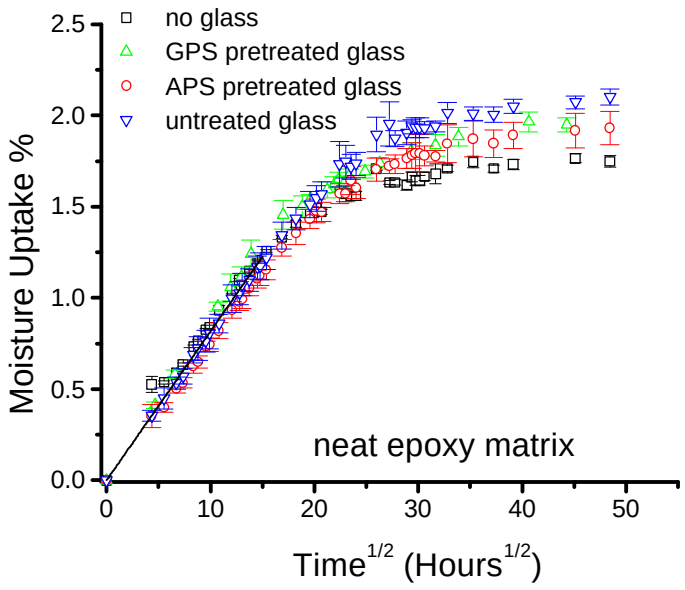


Figure 4-20. Moisture uptake data at 25°C for the E-glass filled epoxy with no surfactant. Uptake calculations are normalized to the mass of the epoxy in the composite. Error bars represent the experimental standard deviation of 5 samples.

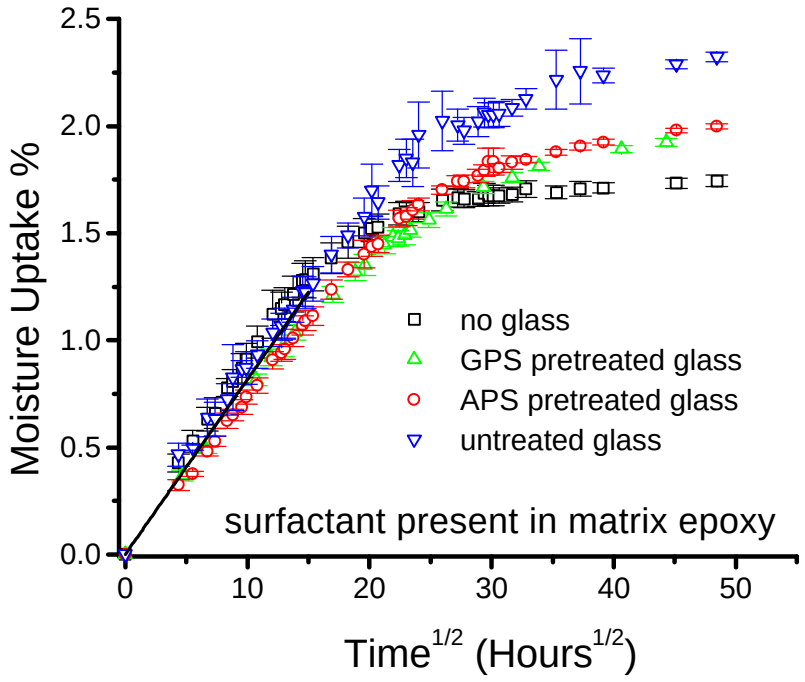


Figure 4-21. Moisture uptake data at 25°C for the E-glass filled epoxy with surfactant in the matrix. Uptake calculations are normalized to the mass of the epoxy in the composite. Error bars represent the experimental standard deviation of 5 samples.

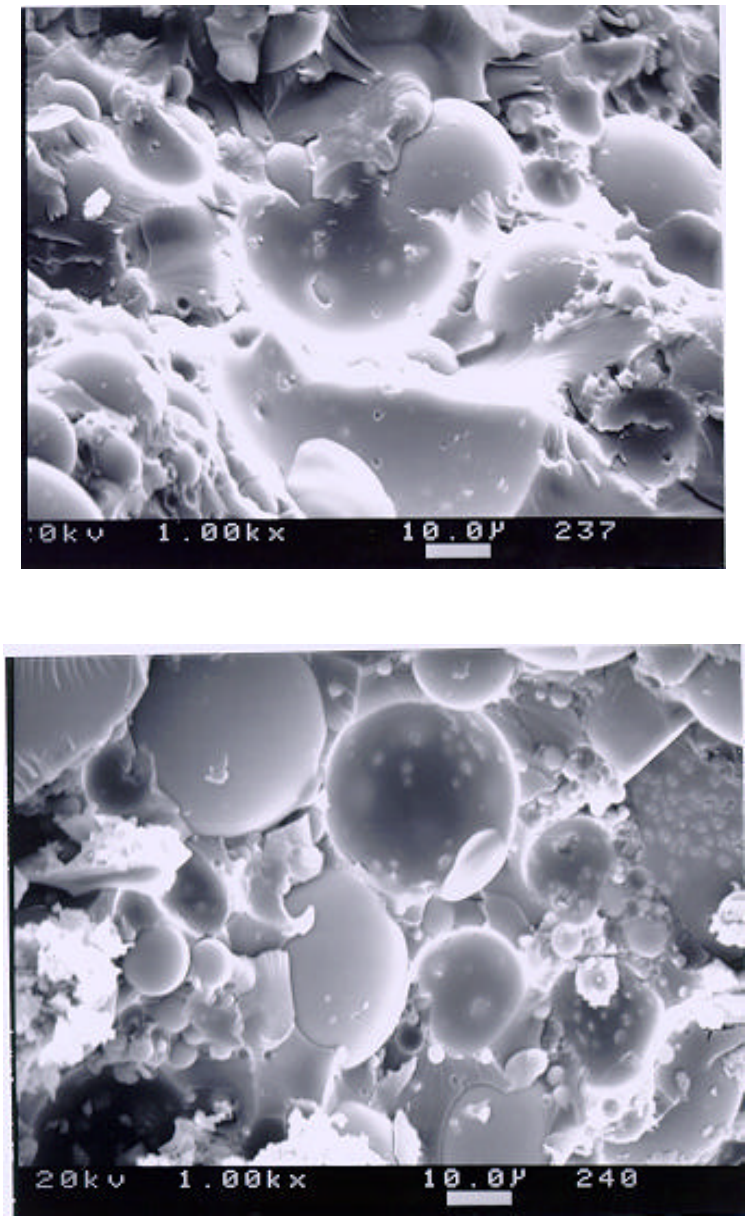


Figure 4-22. SEM images of brittle fracture surfaces after moisture exposure at 65°C for 800 hours. Top image matrix contains surfactant additive while bottom image matrix is neat. Glass beads were pretreated with GPS in both images.

| Epoxy Matrix | D ($mm^2$/hr) | $M_\infty$ (no filler) | $M_\infty$ (untreated glass) | $M_\infty$ (APS pretreated glass) | $M_\infty$ (GPS pretreated glass) |
|---|---|---|---|---|---|
| **Neat (25°C)** | $1.5 \pm 0.2 \times 10^{-3}$ | $1.74 \pm 0.03$ | $2.10 \pm 0.04$ | $1.93 \pm 0.09$ | $1.94 \pm 0.03$ |
| **Surf. (25°C)** | $1.5 \pm 0.2 \times 10^{-3}$ | $1.74 \pm 0.03$ | $2.32 \pm 0.02$ | $1.99 (\pm 0.01)$ | $1.92 (\pm 0.02)$ |
| **Neat (65°C)** | $1.2 \pm 0.2 \times 10^{-2}$ | $1.72 \pm 0.01$ | $2.04 \pm 0.08$ | $1.85 \pm 0.06$ | $2.03 \pm 0.03$ |
| **Surf. (65°C)** | $1.2 \pm 0.2 \times 10^{-2}$ | $1.80 \pm 0.06$ | $2.68 \pm 0.05$ | $2.06 \pm 0.03$ | $2.14 \pm 0.05$ |

Table 4-5. Summary of water uptake data. $M_\infty$ values taken at 800 hours for 65°C samples and 2350 hours for 25°C samples. Error values are the experimental standard deviations.

### 4.3.3 Waterborne Epoxy Composites

The moisture uptake experiments of the E-glass filled epoxies were attractive for several reasons. The volume fraction of filler was easily controlled and voiding could be held to a minimum. But, this technique cannot be applied to the waterborne resin due to the aqueous phase of the emulsion. Waterborne epoxy resins can only be cast as thin films to allow for proper coalescence and water evaporation. Therefore, actual multi-ply laminated E-glass composites were prepared to determine the moisture uptake properties when the fully dispersed waterborne epoxy resin was used as the matrix material.

The moisture uptake data for the composites are summarized in Figure 4-23 - Figure 4-32 and Table 4-6. The samples used for these experiments were cut from the same plaques that were used for the short beam shear test. There is much more scatter in the moisture uptake data for the composites than for the filled samples. From Table 4-6 it can be seen that the volume fraction of fibers was difficult to control. The moisture uptake levels for the fiber reinforced composites are greater than the uptake levels

reported for the samples containing the spherical glass filler. The specific surface area of the spherical glass filler is 0.88 $m^2/g$ versus 0.27 $m^2/g$ for the glass fibers. Based on the weight fractions of glass in both the filled and fiber reinforced composites, it is estimated that the total surface area of glass in the filled samples is 2.7 times greater than the total surface area of glass in the fiber reinforced composites. The increased level of moisture sorption in the fiber reinforced composites is probably due to more micro-cavities and voids than in the filled epoxy samples. Because the glass fibers of the composite are continuous, the moisture diffusion constant could be expected to increase in comparison to the value for the filled epoxy samples. The average diffusion constant is 0.86 ($\pm$ 0.5) x $10^{-2}$ $mm^2$/hour for the composite samples. This is quite close to the average diffusion constant of 1.2 ($\pm$ 0.2) x $10^{-2}$ $mm^2$/hour for the glass filled epoxy samples.

The equilibrium moisture uptake values for the composites are greater than those for the glass filled epoxy samples. The waterborne based composite fabricated with the untreated glass fibers exceeds an $M_\infty$ value of 3.8 percent. But, even with the increase in data scatter, the untreated glass composites always absorb the most water. The coupling agent is still at least partially effective even when a waterborne epoxy matrix is used. Adhesion is evident between the fibers and the matrix phase for the composites with silane pretreated fibers (Figure 4-26 - Figure 4-31). The GPS pretreated glass fiber composites also produced large $M_\infty$ values when the waterborne matrix was used. However, these two samples had the largest fiber volume fractions, which could lead to increased levels of interfacial voiding and defects. The waterborne epoxy matrix results in the greatest values of $M_\infty$ regardless of the fiber surface pretreatment. However, it should be noted that the waterborne composites were much more difficult to process than when water was absent from the epoxy resin. The waterborne composites had to be held under vacuum for longer periods of time to evacuate the air bubbles from the epoxy resin. The high levels of moisture absorption in the waterborne composites are probably due to voiding caused by the water boiling during processing.

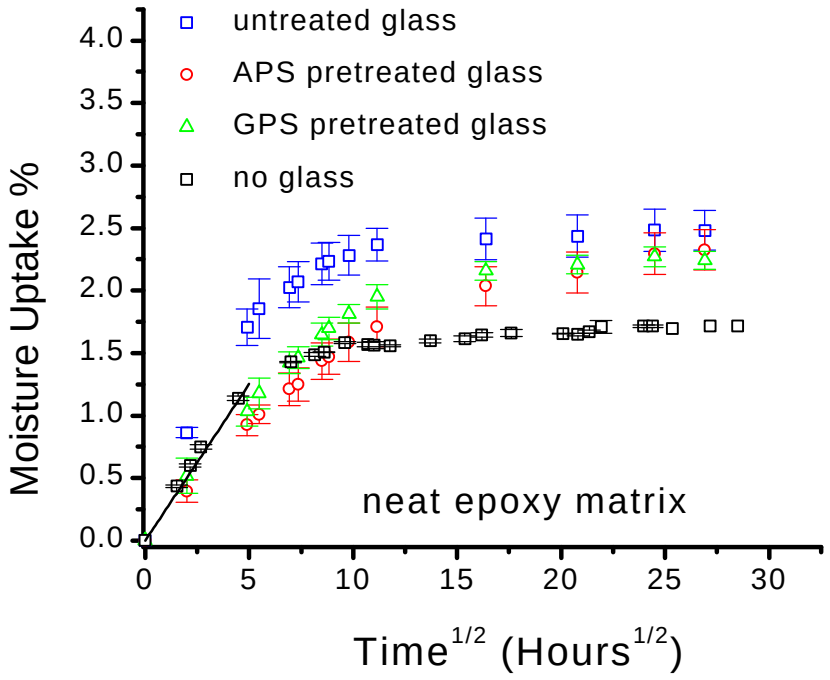


Figure 4-23. Moisture uptake data at 65°C for the E-glass fiber composites with neat epoxy matrix. Uptake calculations are normalized to the mass of the epoxy in the composite. Error bars represent the experimental standard deviation of 5 samples.

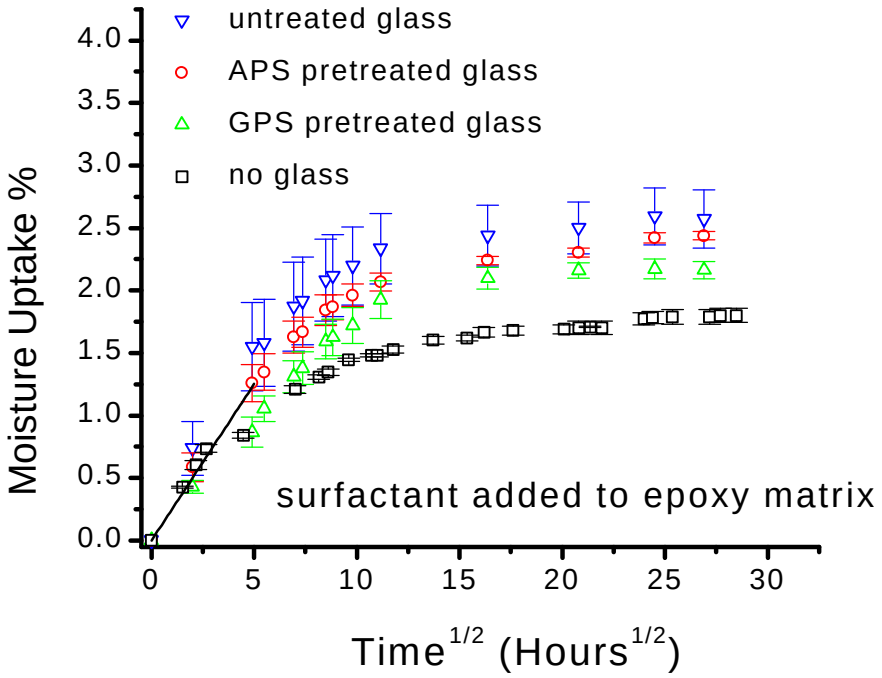


Figure 4-24. Moisture uptake data at 65°C for the E-glass fiber composites with surfactant present in the epoxy matrix. Uptake calculations are normalized to the mass of the epoxy in the composite.

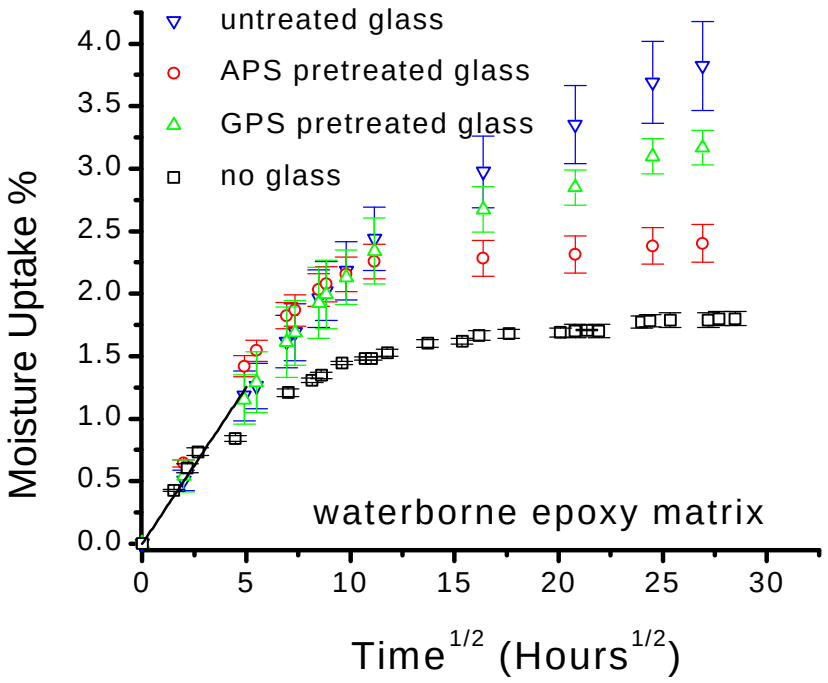


Figure 4-25. Moisture uptake data at 65°C for the E-glass fiber composites with waterborne epoxy matrix. Uptake calculations are normalized to the mass of the epoxy in the composite. Error bars represent the experimental standard deviation of 5 samples.

| sample | $V_f$ (%) | D (x$10^{-2}$ $mm^2$/hour) | $M_\infty$ |
|---|---|---|---|
| **neat/untreated** | 39.6 ± 0.3 | 1.9 | 2.48 ± 0.16 |
| **neat/APS** | 39.2 ± 0.9 | 0.69 | 2.33 ± 0.16 |
| **neat/GPS** | 44.4 ± 1.8 | 0.70 | 2.24 ± 0.07 |
| **surf/untreated** | 39.1 ± 0.7 | 1.3 | 2.57 ± 0.23 |
| **surf/APS** | 41.7 ± 0.4 | 1.0 | 2.44 ± 0.03 |
| **surf/GPS** | 45.1 ± 0.4 | 0.52 | 2.16 ± 0.07 |
| **waterborne/untr.** | 48.2 ± 1.1 | 0.30 | 3.82 ± 0.36 |
| **waterborne/APS** | 40.3 ± 6.4 | 0.92 | 2.40 ± 0.15 |
| **waterborne/GPS** | 50.9 ± 0.5 | 0.38 | 3.17 ± 0.14 |

Table 4-6. Summary of water uptake data taken at 65°C for the composite samples. $M_\infty$ values measured at 724 hours. Error values are the experimental standard deviations.

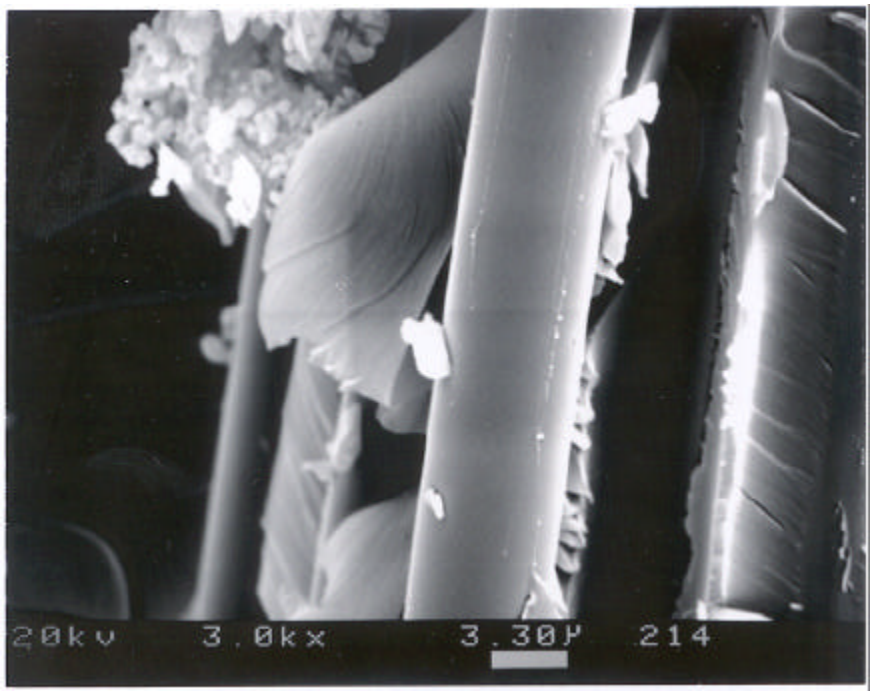


Figure 4-26. Fracture surface of untreated E-glass fiber composite with surfactant in the epoxy matrix.

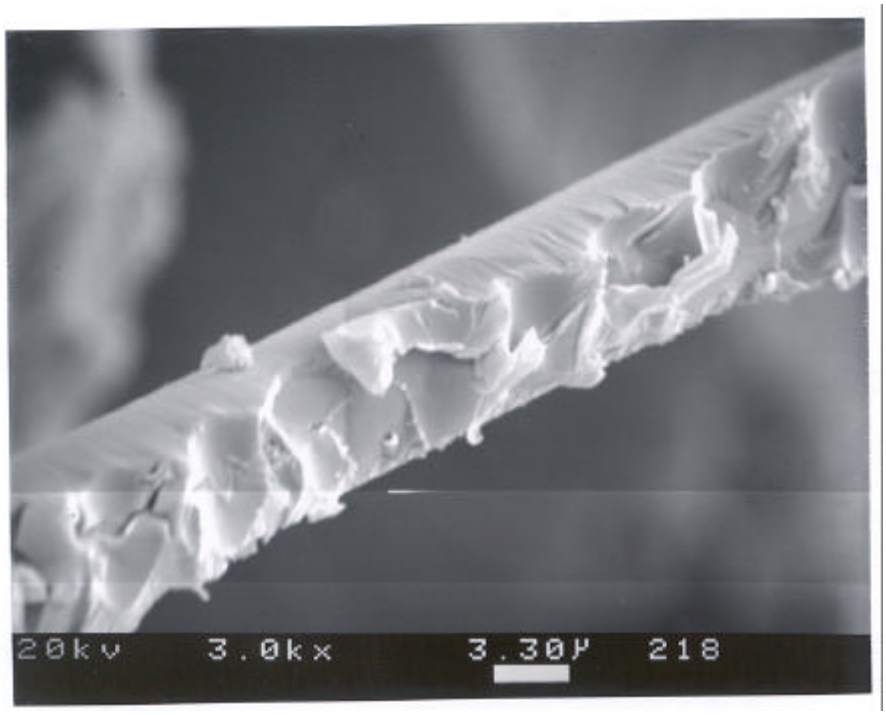


Figure 4-27. Fracture surface of APS pretreated E-glass fiber composite with surfactant in the epoxy matrix.

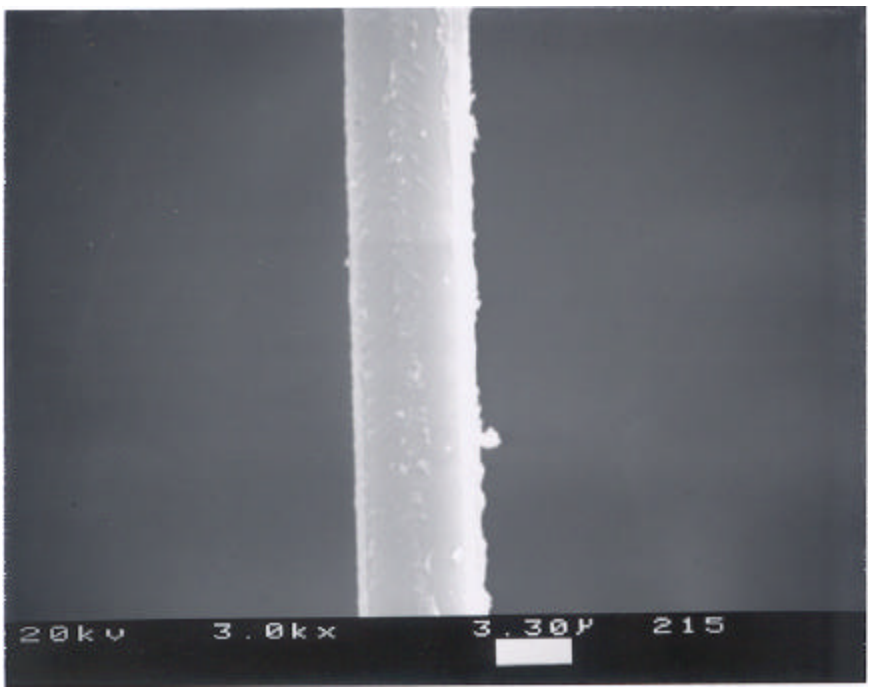


Figure 4-28. Fracture surface of GPS pretreated E-glass fiber composite with surfactant in the epoxy matrix.

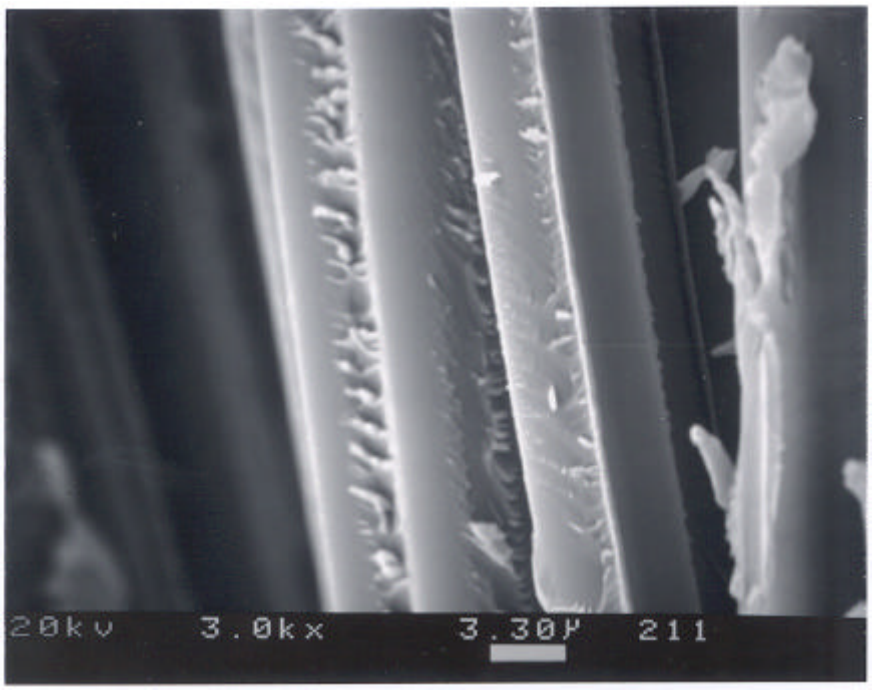


Figure 4-29. Fracture surface of untreated E-glass fiber composite with waterborne epoxy matrix.

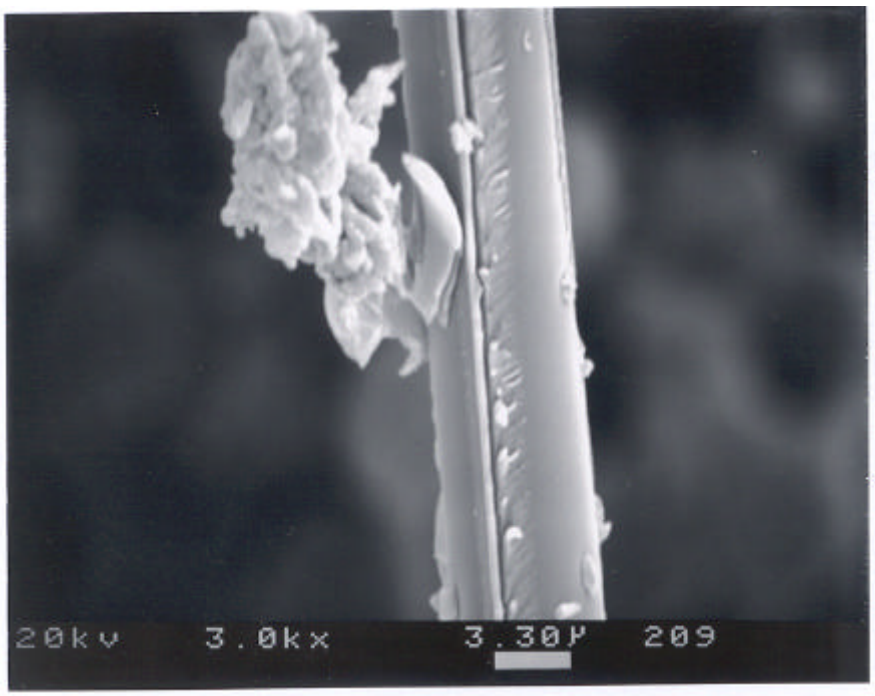


Figure 4-30. Fracture surface of APS pretreated E-glass fiber composite with waterborne epoxy matrix.

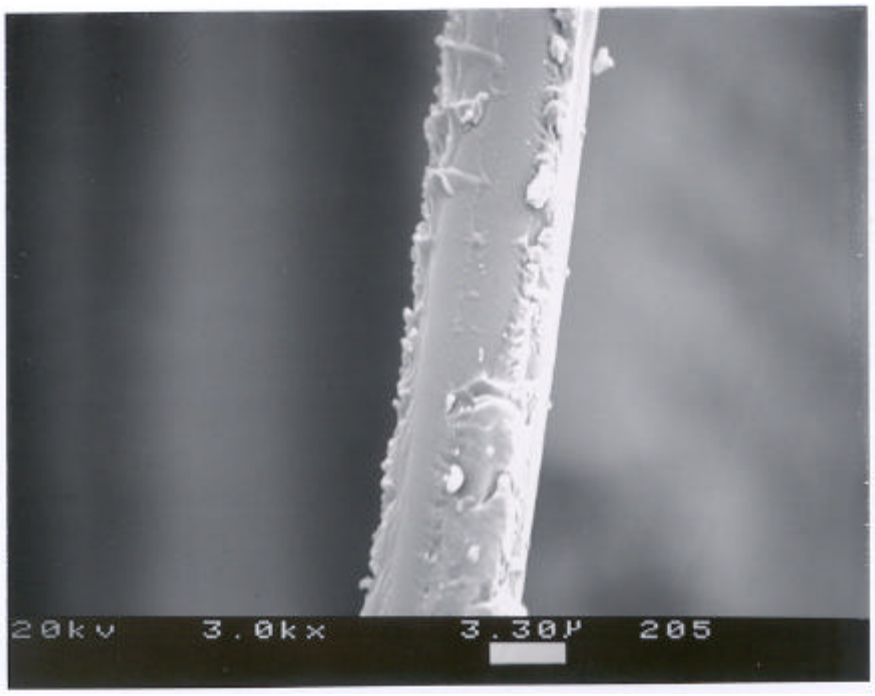


Figure 4-31. Fracture surface of GPS pretreated E-glass fiber composite with waterborne epoxy matrix.

## 4.4 Cooperativity Analysis

### 4.4.1 Bulk Samples

Cooperativity plots were constructed for the bulk model and commercial systems. The shift factors for each system were determined from master curves obtained from dynamic storage modulus curves in the frequency domain, as illustrated in Figure 4-32, and analyzed based on the fractional deviation from $T_g$. The experimental data ($T > T_g$) were then fitted to Equation 28 and the coupling constants were determined using a least squares fit (see Appendix A).

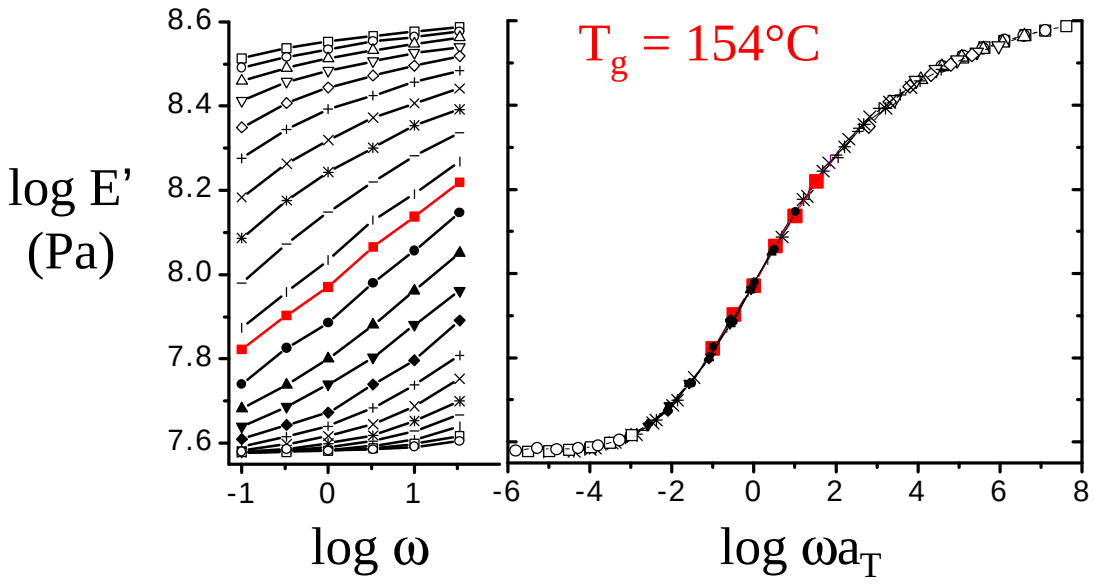


Figure 4-32. Isotherm data used for the master curve construction of the 2.6 phr X-100 bulk model epoxy sample. The isotherms were measured from 125°C to 187°C in 3°C increments.

The cooperativity plots provide insight as to the nature of the epoxy-surfactant interactions. As can be seen in Figure 4-33, the addition of surfactant to the bulk model epoxy decreases the intermolecular cooperativity of the network chains, as revealed by the decreased (negative) slopes of the lines. The plasticizer effects of the surfactant were well described by Equation 33. If the surfactant is acting as a plasticizer by increasing the free volume of the epoxy network, then the segmental motion at the glass transition would become less restricted by neighboring network chains. Another possible contribution to the decrease in the coupling parameter (cooperatvity) could be due to the large difference in $T_g$ between the surfactant and the epoxy. The segmental motions of the surfactant are fully activated when the segmental motion of the epoxy is beginning to occur on heating. Therefore, at the $T_g$ of the epoxy any intermolecular constraints due to the surfactant would be negated. Such molecular arguments have been applied in a cooperativity study of tetramethyl-Bisphenol A polycarbonate/polystyrene miscible blends.[124] Equation 28 provided a reasonable fit for the experimental points in Figure 4-33 at temperatures greater than $T_g$. The experimental data does not agree very well with Equation 28 at temperatures below $T_g$. Plazek and Ngai[84] determined the constants

of Equation 28 using experimental data collected from polymers cooled closer to thermodynamic equilibrium in the glassy state. The samples studied for this research were allowed to cool slowly in the oven after the completion of the cure cycle, but are probably restricted from rapidly approaching equilibrium in the glassy state due the high crosslink density of the fully cured epoxy. Once at temperatures $T > T_g$ the epoxy has sufficient molecular mobility to allow for equilibrium behavior. All of the samples examined displayed this non-equilibrium behavior in the glassy state; therefore, focus is placed on the viscoelastic properties at temperatures $T > T_g$. The coupling constant showed a decrease from 0.63 for the bulk neat model epoxy to 0.53 for the 14.6 phr X-100 bulk model epoxy. The differences in coupling parameters are significant. While the coupling parameter can theoretically vary from 0 to 1, most polymers have coupling parameters lying within a range of 0.45 (polyisobutylene) to 0.76 (polyvinylchloride).[84] These experimental results are summarized in Table 4-7, and they emphasize the role of the surfactant in lowering coupling behavior.

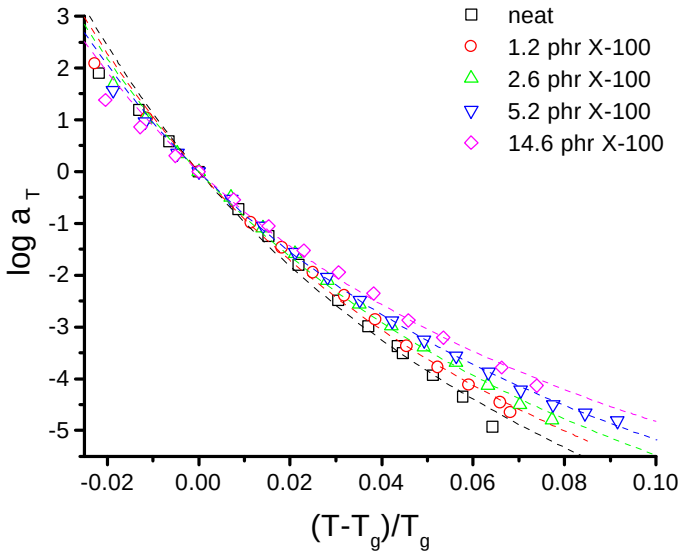


Figure 4-33. Cooperativity plot of bulk model epoxy as a function of surfactant concentration. (see Appendix A for fitting procedure)

| Sample | $T_g$ (K) | coupling constant *n* | estimated variance |
|---|---|---|---|
| **neat** | 459 | 0.627 | 0.023 |
| **1.2 phr X-100** | 440 | 0.603 | 0.010 |
| **2.6 phr X-100** | 427 | 0.583 | 0.009 |
| **5.2 phr X-100** | 426 | 0.560 | 0.003 |
| **14.6 phr X-100** | 392.4 | 0.528 | 0.008 |

Table 4-7. Summary of coupling constants for bulk model epoxy.

The viscoelastic properties of the commercial waterborne epoxy resin were then investigated. To eliminate water as a variable the water was evaporated at 100°C from the commercial waterborne epoxy prior to use. This bulk commercial epoxy was then mixed with EMI-24 and cured using an identical procedure as with the model epoxy system. Figure 4-34 shows the cooperatvity plots for the cured 5.2 phr X-100 model epoxy and cured bulk commercial epoxy. The bulk commercial epoxy has a $T_g$ of 165°C in comparison to the 5.2 phr X-100 model epoxy $T_g$ of 153°C. The coupling parameter of the bulk commercial epoxy is equal to approximately 0.570 (estimated variance = 0.009), which is in close agreement with the 5.2 phr X-100 model epoxy coupling parameter of 0.560. Based on these results, a concentration 5 phr X-100 surfactant was used as the model standard for all of the E-glass composite studies.

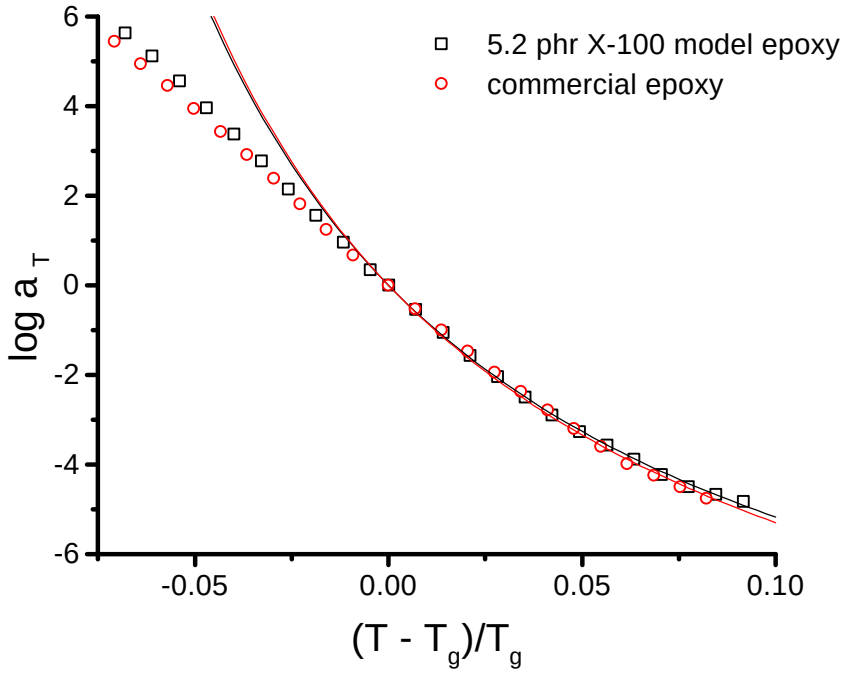


Figure 4-34. Cooperativity plots of bulk 5.2 phr X-100 model epoxy and commercial waterborne epoxy. The water was evaporated from the commercial resin prior to curing. (see Appendix A for fitting procedure)

### 4.4.2 Composite Samples

The next series of experiments examines the possible influence of the epoxy/E-glass interphase properties on the cooperative motions of the epoxy. These viscoelastic studies were performed using single-ply epoxy/E-glass laminates. Figure 4-35 shows the normalized 1 Hz tan δ curves for the neat epoxy matrix glass laminates as well as for the neat bulk matrix with no glass. The temperature scale has been normalized to the glass transition temperatures of the individual samples. The presence of the glass substrate has no effect to the shapes or broadness of the normalized tan δ curves regardless of the surface pretreatment. The temperature scale normalization was used to offset small variations in $T_g$. The differences in the $T_g$ for the neat epoxy matrix laminates were small and were within the experimental error of the DMA. The heights of the tan δ curves were

normalized to correct for matrix volume fraction and sample geometry effects. The presence of the surfactant in the matrix epoxy also has no influence on the shapes of the tan δ curves, as seen in Figure 4-36. The $T_g$, taken as the peak temperature of the 1 Hz tan δ curves, of all of the samples studied are summarized in Table 4-8. The data emphasize the inadequacy of a partial DMA study in differentiating material viscoelastic response. Below, it will be explained that a cooperativity analysis yields much further information.

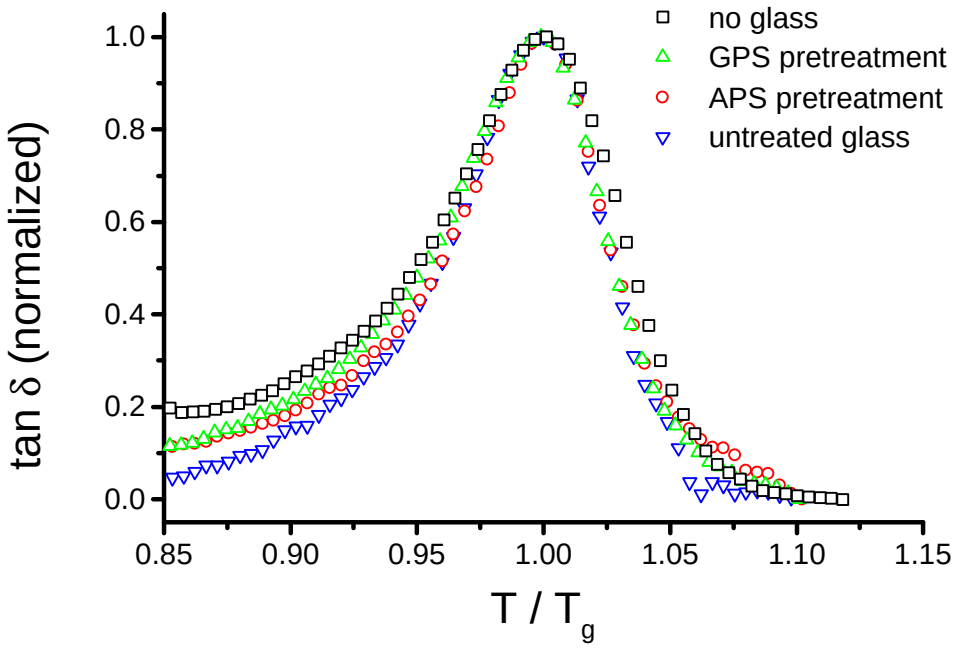


Figure 4-35. Normalized tan δ curves for neat epoxy matrix single-ply E-glass laminates.

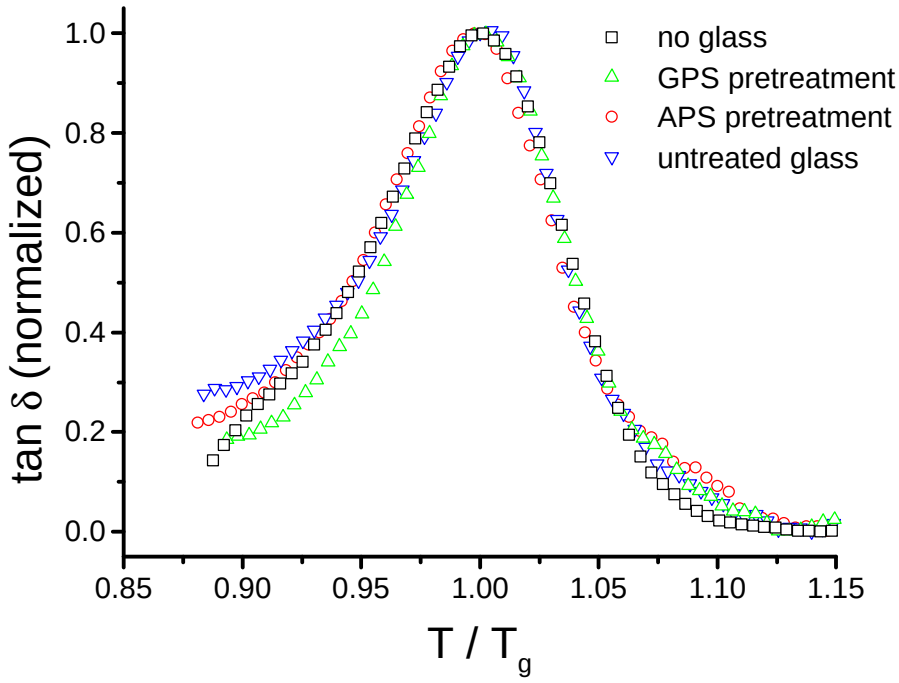


Figure 4-36. Normalized tan δ curves for epoxy/surfactant matrix single-ply E-glass laminates.

| Sample | $T_g$ (K) |
|---|---|
| **neat (untreated)** | 450.3 ± 2.0 |
| **neat (APS)** | 449.0 ± 1.0 |
| **neat (GPS)** | 443.7 ± 3.0 |
| **neat (bulk)** | 445.7 ± 2.7 |
| **surf (untreated)** | 429.6 ± 1.6 |
| **surf (APS)** | 434.7 ± 9.6 |
| **surf (GPS)** | 423.4 ± 0.8 |
| **surf (bulk)** | 424.6 ± 2.4 |
| **waterborne (untreated)** | 406.5 ± 2.8 |
| **waterborne (APS)** | 408.6 ± 2.1 |
| **waterborne (GPS)** | 419.7 ± 3.6 |

Table 4-8. Summary of glass transition temperatures for single-ply composites.

While the E-glass cloth substrate causes no appreciable changes in the normalized tan δ curves, clear differences arise due to surface pretreatment of the glass once master curves of the storage modulus (E ) are created. The normalized master curves for the neat epoxy matrix laminates are represented in Figure 4-37. The master curves were generated by collecting dynamic mechanical data in the step-isothermal mode at multiple frequencies. The $T_g$ of the samples were used as the reference temperatures. Figure 4-32 illustrates typical raw data that is used in preparing a master curve. From Figure 4-37 it can be seen that the laminate with untreated glass has a glass to rubber transition region that can be shifted towards the lowest frequencies (or longest times). At low frequencies the shift in the modulus master curve of the untreated glass laminate is followed in order by the APS treated glass laminate, the GPS treated glass laminate, and finally the bulk neat matrix with no glass reinforcement as frequency increases. The master curves of the APS and GPS treated glass laminates are similar to the bulk matrix in the glassy region at higher frequencies. The untreated glass laminate shifts towards higher frequencies in the

glassy state. But, it may be more difficult to qualify any differences in the glassy modulus due to the non-equilibrium state of polymeric glasses.

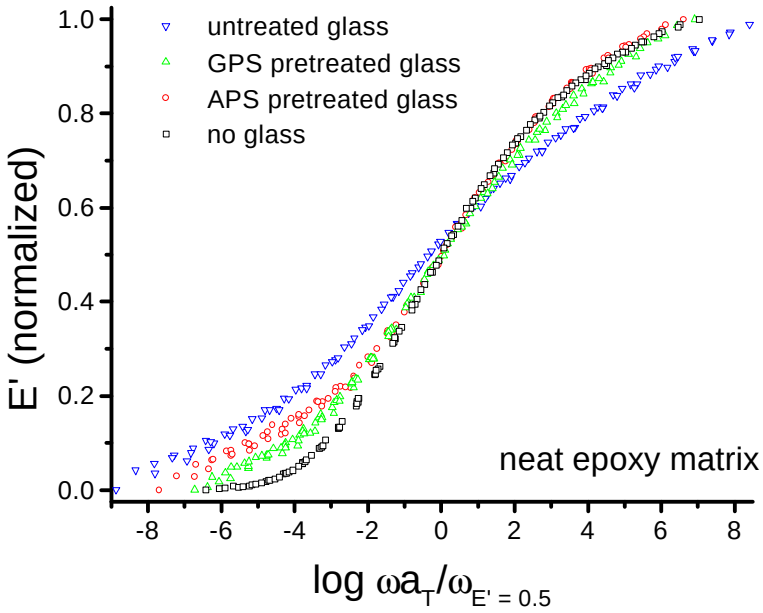


Figure 4-37. Normalized master curves for the neat epoxy matrix laminates (no surfactant).

Figure 4-38 shows the master curves of E for the epoxy-glass laminates with surfactant present in the epoxy matrix phase. A similar trend is observed in the glass to rubber transition region in that the untreated glass results in the greatest shifts towards lower frequencies. The shift in the master curves are again followed in order by that for the APS treated glass laminate, the GPS treated glass laminate, and the epoxy-surfactant bulk matrix as frequency goes up. The grouping of the master curves is tighter in the rubbery region when surfactant has been added to the matrix phase, but the trends in the shifting of the modulus are identical to those observed with the neat epoxy matrix samples. The glassy modulus responses of the laminate samples with surfactant added to the matrix phases are similar in all cases.

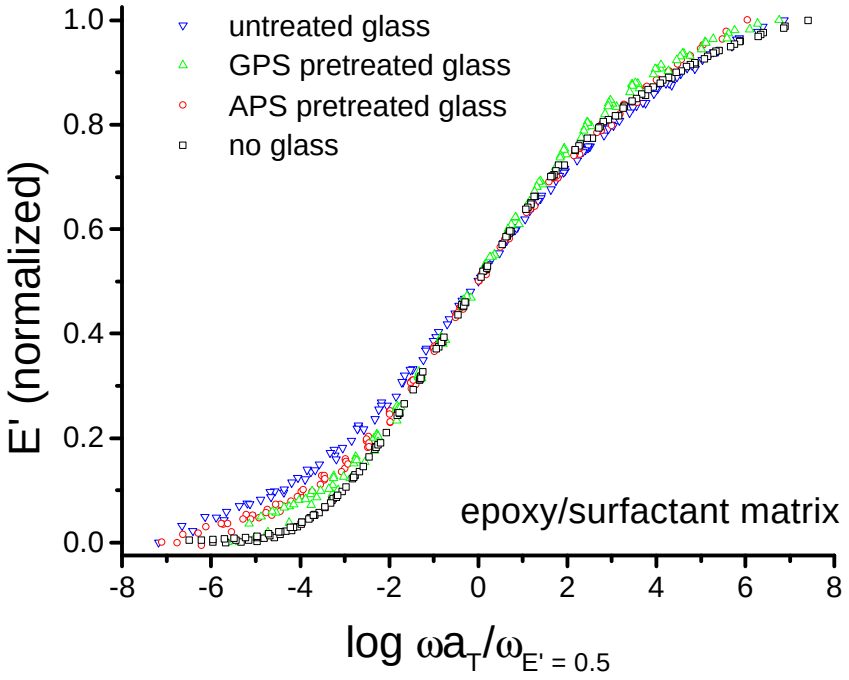


Figure 4-38. Normalized master curves for the epoxy/surfactant matrix laminates.

Figure 4-39 summarizes the cooperativity plots for the neat epoxy matrix laminates in comparison to the neat bulk epoxy. The cooperativity of the laminates is a function of the surface pretreatment of the glass at temperatures $T > T_g$. The untreated glass causes the largest increase in cooperativity followed by the cooperativity value for the APS and GPS treated glass respectively. The GPS treated glass laminate cooperativity is nearly identical to the neat bulk epoxy cooperativity. The activation energies at $T = T_g$ were calculated using Equation 31. The activation energy and calculated coupling parameter values also increase as the cooperativity of the neat epoxy laminates increases. But, the untreated and APS treated glass laminates deviate significantly from Equation 28 at temperatures $T > T_g$. But, the trends in cooperativity do not depend on the fit of the experimental data to Equation 28. The calculated values obtained for S (steepness index as defined by Plazek and Ngai[84]), $E_a$, and *n* for the neat epoxy-glass laminates are listed in Table 4-9, but the values obtained for the untreated and APS treated glass should be considered with caution. The error analysis of the cooperativity plots is outlined in Appendix A.

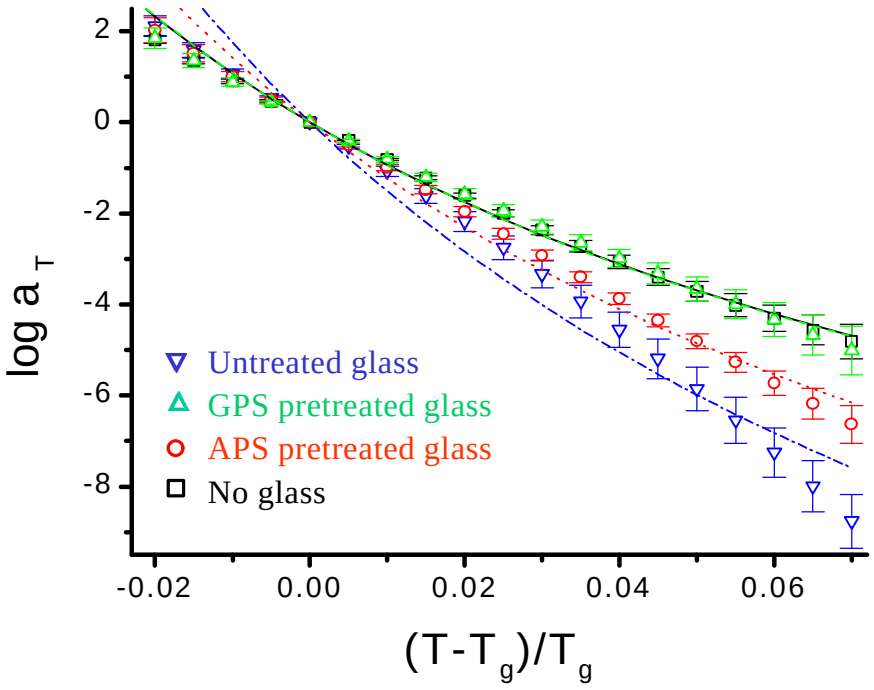


Figure 4-39. Cooperativity plots for the neat epoxy matrices showing the effects of glass reinforcement. (see Appendix A for fitting procedure)

Once the surfactant had been added to the matrix epoxy phase of the laminates the trends in cooperativity remain the same as were observed with the neat epoxy matrices (Figure 4-40). The magnitude of the increase in cooperativity of the untreated and APS pretreated epoxy-glass laminates are not as great when surfactant has been added to the matrix phase, but the differences due to the surface pretreatments of the glass are still evident. The calculated values of S, $E_a$, and *n* are also summarized in Table 4-9.

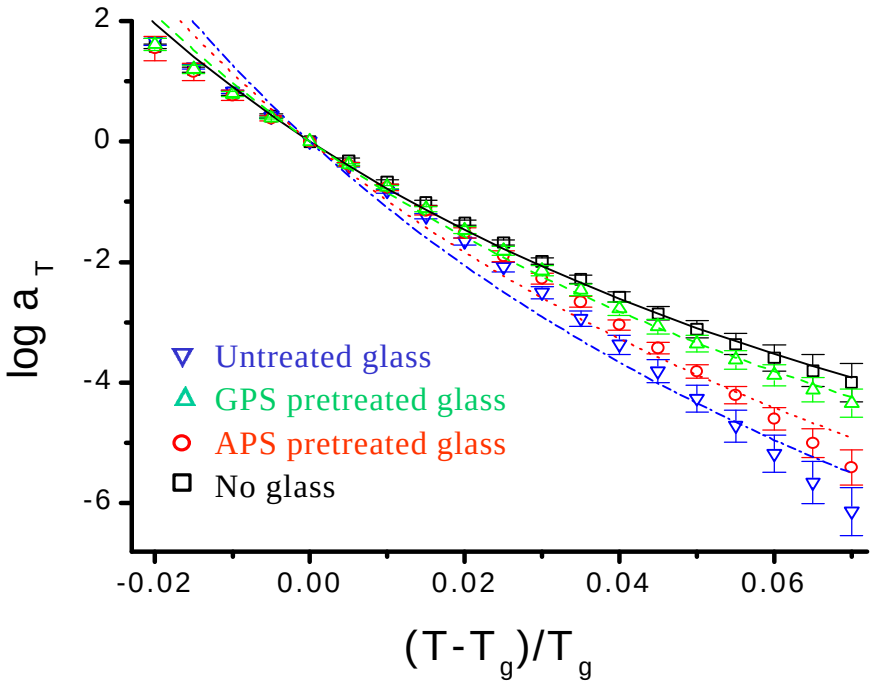


Figure 4-40. Cooperativity plots for the epoxy matrices with surfactant showing the effects of glass reinforcement.

The next sequences of experiments were aimed at determining the influence of the water interactions on the viscoelastic properties of the epoxy-glass laminates. Rather than simply mixing surfactant with epoxy and casting on the surface of the glass cloth, the epoxy and surfactant were actually emulsified in these laboratories to form a true waterborne. An identical casting procedure was then used to produce these laminates, except that the waterborne epoxy was allowed to coalesce prior to oven curing. As can be seen in Figure 4-41, the normalized loss tangent curves differ very little as the surface pretreatment of the glass is changed. The E modulus master curves for these fully cured waterborne epoxy-glass laminates are illustrated in Figure 4-42. Again, master curve of the untreated glass laminate is shifted towards the lowest frequencies in the glass to rubber transition region. The laminates containing glass that was pretreated with the coupling agents can no longer be distinguished from each other at temperatures $T > T_g$. The APS and GPS pretreated glass laminate master curves overlap the bulk epoxy-surfactant matrix curve at temperatures above $T_g$. The glassy moduli of all of the

waterborne laminates differ, but the data were not as reproducible at temperatures below $T_g$.

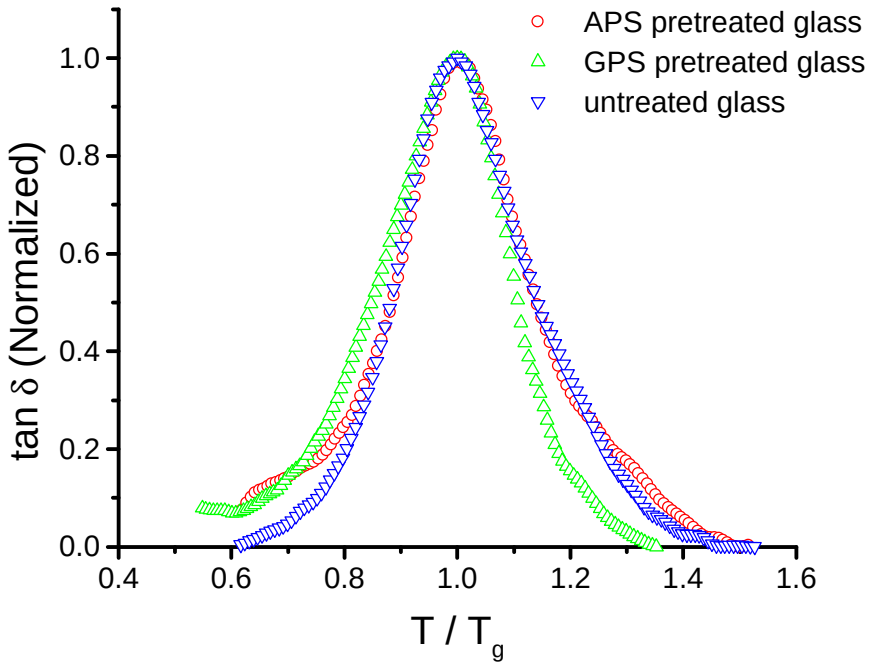


Figure 4-41. Normalized tan δ curves for waterborne epoxy matrix single-ply E-glass laminates.

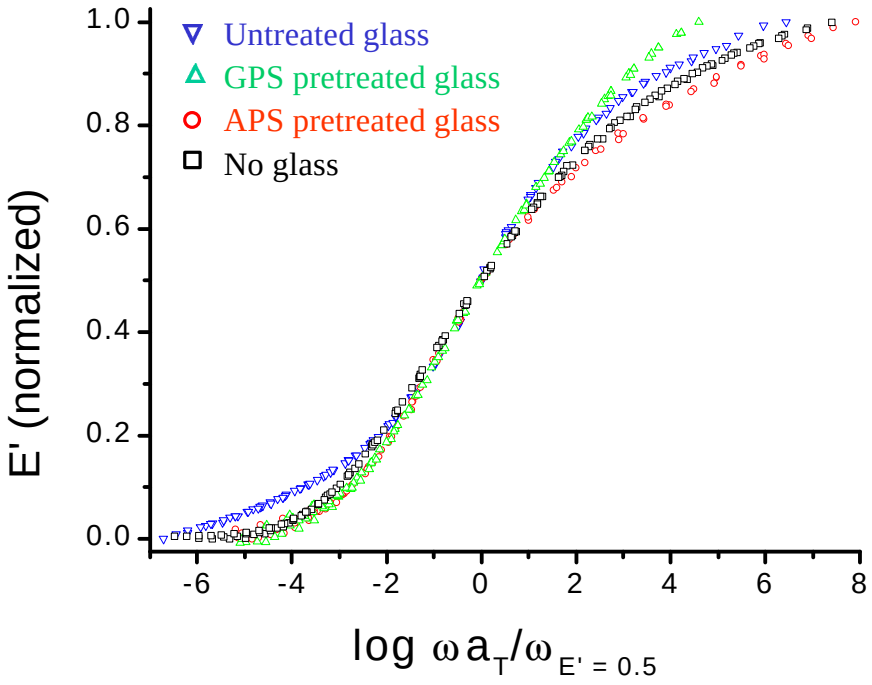


Figure 4-42. Normalized master curves for the waterborne epoxy matrices showing the effects of glass reinforcement.

Figure 4-43 shows the cooperativity plots for the waterborne laminates in comparison with the bulk epoxy-surfactant matrix. There is really no statistically different value for the cooperativity curves between the APS and GPS pretreated waterborne glass laminates and the bulk epoxy-surfactant matrix. The untreated glass waterborne laminate still has higher cooperativity, but is slightly closer to the bulk epoxy-surfactant matrix than when no water was present. The aqueous phase of the waterborne has a definite influence on the viscoelastic properties of the epoxy-glass laminates. The calculated values of S, $E_a$, and *n* for the waterborne epoxy-glass laminates are also summarized in Table 4-9.

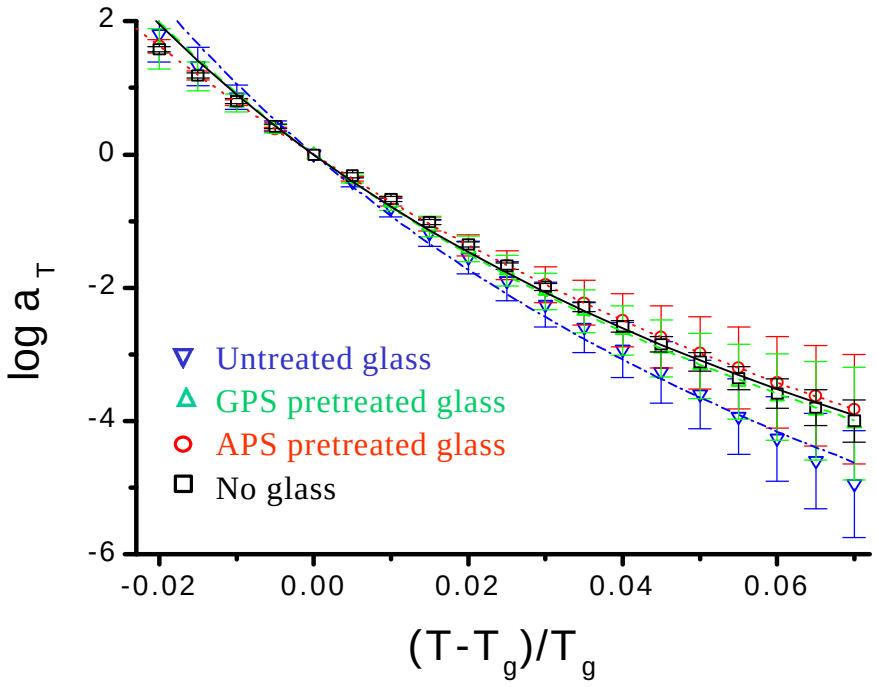


Figure 4-43. Cooperativity plots for the waterborne epoxy matrices showing the effects of glass reinforcement. (see Appendix A for fitting procedure)

| Sample | $T_g$ (K) | S | $E_a$ (KJ/mol) | *n* | Estimated Variance in *n* |
|---|---|---|---|---|---|
| **neat (untreated)** | 450.3 ± 2.0 | 107 ± 10.9 | 923 ± 98 | 0.761 | 0.350 |
| **neat (APS)** | 449.0 ± 1.0 | 99.9 ± 10.0 | 857 ± 84 | 0.704 | 0.074 |
| **neat (GPS)** | 443.7 ± 3.0 | 84.8 ± 9.6 | 721 ± 87 | 0.612 | 0.026 |
| **neat (bulk)** | 445.7 ± 2.7 | 85.6 ± 3.7 | 730 ± 31 | 0.612 | 0.010 |
| **surf (untreated)** | 429.6 ± 1.6 | 82.1 ± 3.5 | 675 ± 31 | 0.669 | 0.116 |
| **surf (APS)** | 434.7 ± 9.6 | 76.5 ± 7.6 | 638 ± 78 | 0.629 | 0.072 |
| **surf (GPS)** | 423.4 ± 0.8 | 77.2 ± 4.1 | 626 ± 34 | 0.570 | 0.006 |
| **surf (bulk)** | 424.6 ± 2.4 | 73.3 ± 1.1 | 596 ± 12 | 0.535 | 0.006 |
| **waterborne (untreated)** | 406.5 ± 2.8 | 83.2 ± 15.9 | 648 ± 128 | 0.606 | 0.027 |
| **waterborne (APS)** | 408.6 ± 2.1 | 72.2 ± 9.0 | 565 ± 67 | 0.517 | 0.001 |
| **waterborne (GPS)** | 419.7 ± 3.6 | 75.1 ± 13.3 | 603 ± 103 | 0.544 | 0.003 |

Table 4-9. Summary of steepness indexes, activation energies, and coupling parameters.

The cooperativity analysis of the composite samples provided a unique aspect for determining fiber-matrix interfacial properties. The cooperativity of a composite is definitely sensitive to the fiber surface pretreatment at temperatures $T > T_g$. These results indicate that the matrix epoxy is constrained to the greatest extent when untreated glass fibers are used. Also, the presence of the surfactant alone does not alter the observed trends in cooperativity. However, the aqueous phase of the waterborne epoxy results in a shift towards lower cooperativity for the composite samples. These results have important implications towards understanding interfacial viscoelastic properties and will be discussed in more detail in the following chapter.

## 4.5 Graphite Composites

### 4.5.1 Materials and Experimental

The use of cooperativity plots to characterize the viscoelastic response of a composite material has not been reported. During the course of this research an opportunity

appeared to evaluate this characterization technique with an entirely different composite system than presented above. This new composite was composed of graphite carbon fibers with a pultrudable vinyl-ester matrix.[125] This research and the results are presented at this point since they help illuminate the interpretation of the cooperativity arguments above.

The vinyl-ester resin is illustrated in Figure 4-44. This vinyl-ester cures via a free radical mechanism to form a crosslinked network structure. The graphite fibers were sized with either poly(vinylpyrrolidone) (PVP), polyhydroxyether (phenoxy), or a proprietory industrial G sizing. The molecular structures of the PVP and phenoxy sizings are shown in Figure 4-45.

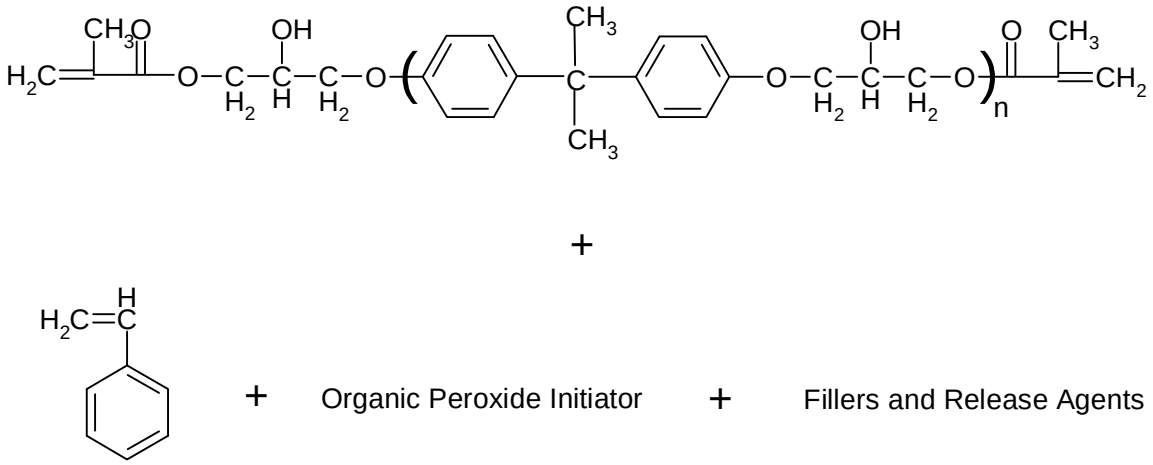


Figure 4-44. Pultrudable vinyl-ester resin matrix used in graphite composites.

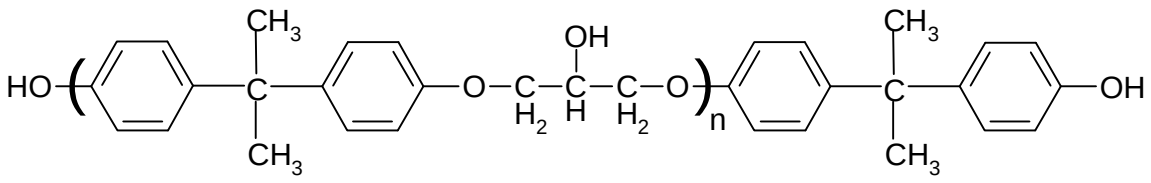


polyhydroxyether

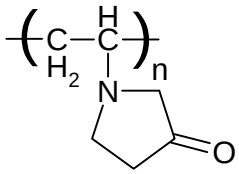


poly(vinylpyrrolidone)

Figure 4-45. Sizings used to pretreat the graphite fibers.

Dynamic mechanical analysis was performed using a DuPont instruments DMA 983 in flexural bending mode with an amplitude displacement of 0.20 mm peak to peak. Typical clamped sample dimensions were 30.0 x 12.8 x 1.9 mm. The primary advantage of using the DuPont DMA is that the clamp width can be set wide for very stiff composites. The clamp width of 30.0 mm yielded excellent results. The temperature was ramped from 80°C to 220°C in 3°C increments under a nitrogen atmosphere. At each temperature step, the viscoelastic response of the composite was measured at frequencies of 0.03, 0.1, 0.3, 1, 3, and 10 Hz. Upon completion of the measurements at 220°C the composite specimen was allowed to slowly cool to room temperature in the instrument and the measurement procedure was repeated. This cooling usually required two hours. All of the data used for this paper were taken from the second run measurements in the DMA. This insures that each sample has the same thermal history. A minimum of four individual samples was measured for each group of composite specimens.

### 4.5.2 Results

The dynamic storage modulus curves (E ) obtained at 1 Hz for the composite samples and for the non-reinforced matrix are illustrated in Figure 4-46. From this data it is readily apparent that the addition of the graphite fibers significantly increases the

modulus of the matrix polymer. The glassy modulus is elevated from approximately $10^{9.5}$ Pa for the matrix to about $10^{10.8}$ Pa for the composites. All of the composite samples have similar glassy modulus values. The rubbery modulus is also much higher in the composites than in the non-reinforced matrix. The G sizing yielded the largest rubbery modulus, while the phenoxy and PVP sized fiber samples have similar values of rubbery modulus. The increased value of rubbery modulus for the G sized fiber samples could be due to a slightly higher volume fraction of fibers. The glass-to-rubber transition regions of the composite samples are also much broader than those for the non-reinforced matrix.

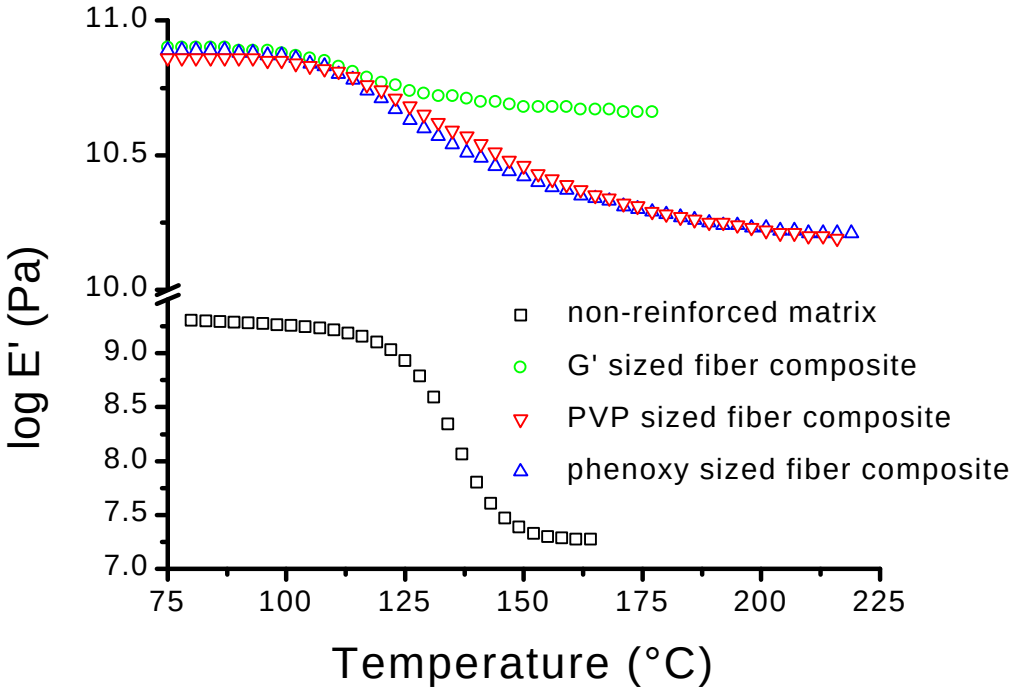


Figure 4-46. Storage modulus curves for graphite composite samples as well as non-reinforced matrix versus temperature obtained from DMA (1 Hz).

A closer examination of the glass-to-rubber transition of the composites and the non-reinforced matrix can be seen in the normalized tan δ curves (1 Hz) shown in Figure 4-47. The matrix material has the highest $T_g$ (138°C), as defined by the peak maximum of the α-transition. This was probably due to the absence of processing aids in this sample, which could act as plasticizers in depressing the glass transition temperature.

There could have also been some small variation in the stoichiometry of the reactants in the non-reinforced matrix in comparison to the composite samples. The $T_g$ of the composite samples range from 116°C for the G sized fiber sample to 122°C and 125°C for the phenoxy and PVP sized fiber samples respectively. The α-transition of the PVP and phenoxy sized composite samples was taken as the first shoulder in the tan δ curves. Both the PVP and phenoxy sized fiber composites exhibit a distinct second transition peak above 150°C. The first shoulders on the phenoxy and PVP curves both occur near the same temperature as the α-transition peak of the G curve. The second transitions in the phenoxy and PVP sized fiber composites could be due to the glass transitions of the sizings themselves or a highly restricted interphase region near the fiber surface. The second transitions in the tan δ curves were very consistent and reproducible.

Thomason[97] published results which indicate that a second peak in the loss modulus or tan δ curves of a fiber-reinforced composite could be an artifact of the DMA. Thomason states that a second peak can result due to thermal lag between the portion of the sample that is exposed between the clamps and the actual material that if held by the clamps. An artificial second peak can then originate because of a fast sample heating rate, poor thermal conductivity of the composite, and/or residual stresses in the composite. His proposal is that the glass transition for the clamped portion of the composite sample simply lags the oven temperature, giving a second transition peak at a higher temperature. This hypothesis is rejected for the current results as explained in the following.

The measurement technique used for these experiments was the step-isothermal mode. The DMA increments in a 3°C step, equilibrates at the designated temperature, and then sweeps the assigned frequencies. The low frequency measurement (0.03 Hz) requires this sequence, making this procedure much slower than the common constant heating rate experiment at a frequency of 1 Hz. Total measurements (from 80°C to 220°C) were typically completed overnight with 25 - 30 minutes required at each individual temperature step. Due to the lengthy step times that the composites experienced in the DMA, confidence can be placed in the judgement that the second tan δ peaks in the phenoxy and PVP samples are not artifacts.

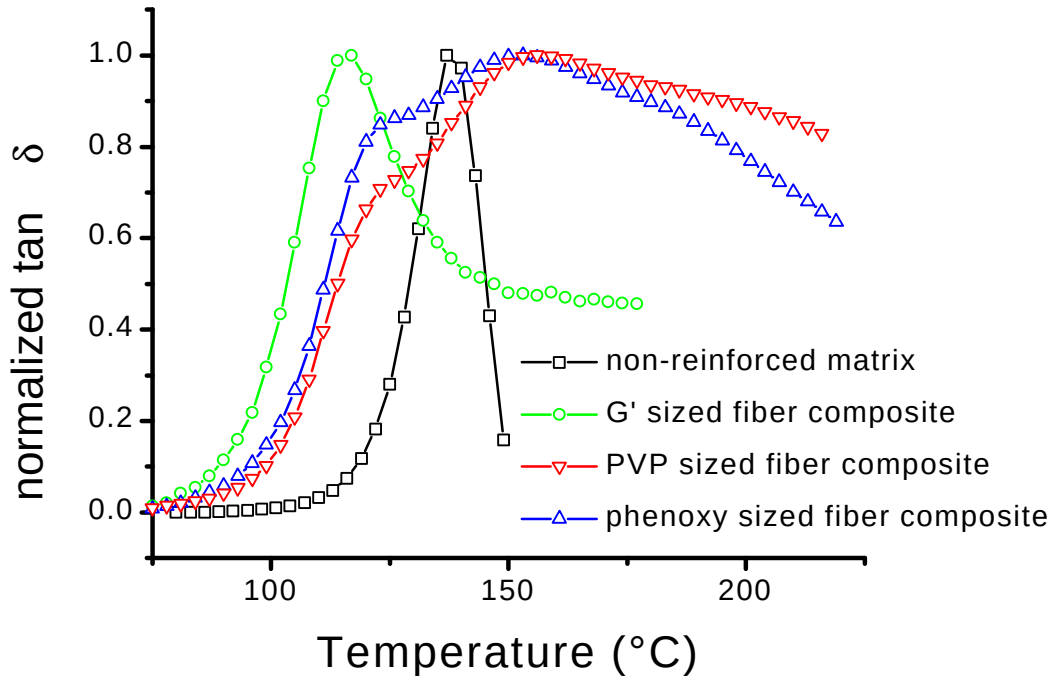


Figure 4-47. Normalized tan δ curves obtained from DMA measurements (1 Hz).

The composite samples also have tan δ curves that are much broader than those of the non-reinforced matrix. This increased peak broadness and absence of the second transition in the storage modulus curves are consistent with the findings of Lewis and Nielsen.[89] The transition temperatures obtained from the tan δ curves are summarized in Table 4-10.

| sample | $T_g$ (α-transition) | $T_{second\ transition}$ |
|---|---|---|
| **non-reinforced matrix** | 138°C | not present |
| **G sized fiber composite** | 116°C | not present |
| **PVP sized fiber composite** | 125°C | 159°C |
| **phenoxy sized fiber composite** | 122°C | 152°C |

Table 4-10. Summary of transition temperatures in non-reinforced matrix and fiber composite samples.

Figure 4-48 depicts the normalized dynamic loss modulus curves (E ) curves for the various samples. The same trends are evident in the loss modulus as were seen in the tan δ data previously discussed.

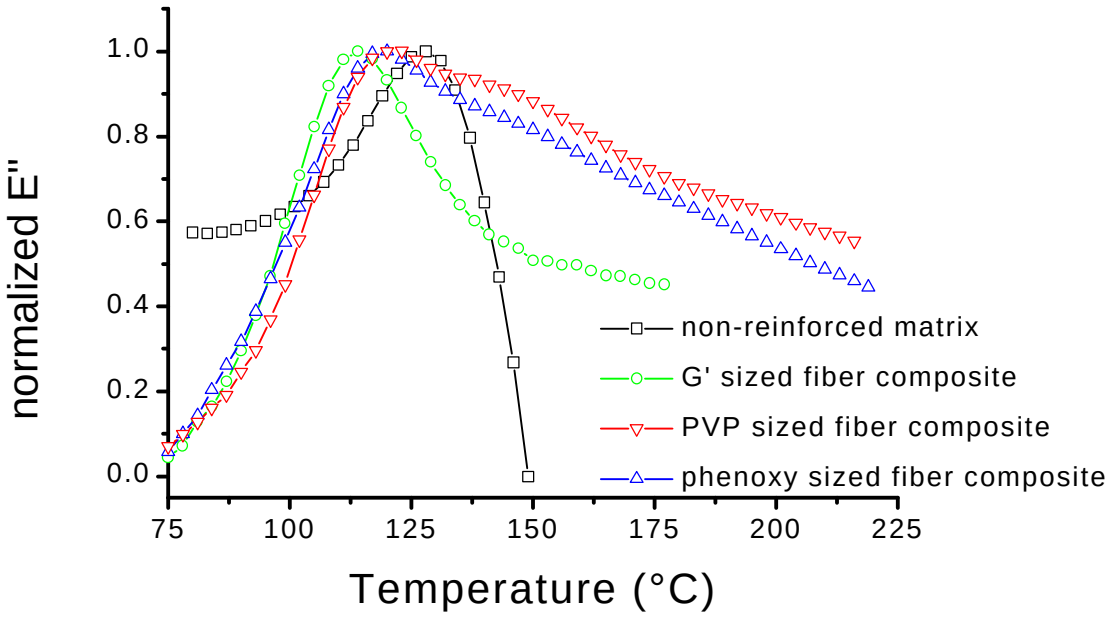


Figure 4-48. Normalized loss modulus curves obtained from DMA measurements (1 Hz).

The time-temperature superposition (tTSP) procedure was used to construct master curves of the storage modulus in the frequency domain for each sample. The glass transition temperatures, measured at 1 Hz from the tan δ peaks, were used as the reference isotherm. Master curves were successfully constructed without any vertical shifting from the storage modulus data. However, this was not the case for the loss modulus data. Vertical shifting of the loss modulus curves is required for the composite samples. This could be due to multiple relaxation mechanisms occurring simultaneously within the matrix, sizing, and/or interphase region. Or, additional temperature dependence may arise from the strong probability of residual stresses in this type of specimen. No trends were apparent with respect to the vertical shifting of the loss modulus curves. Sullivan *et al.*[113] also observed that vertical shifting was required for tTSP in vinyl ester/E-glass composites. These researchers also found no clear trends with regard to the vertical shift factors.

Figure 4-49 shows the normalized storage modulus curves for the composite and non-reinforced matrix samples. The composite sample master curve data were slightly noisier, but highly reproducible. The fiber reinforcement extents the glass-to-rubber transition zone to much lower frequencies, or longer times, than the non-reinforced matrix. The phenoxy sample extends to the lowest frequencies, followed by the PVP and G samples, respectively.

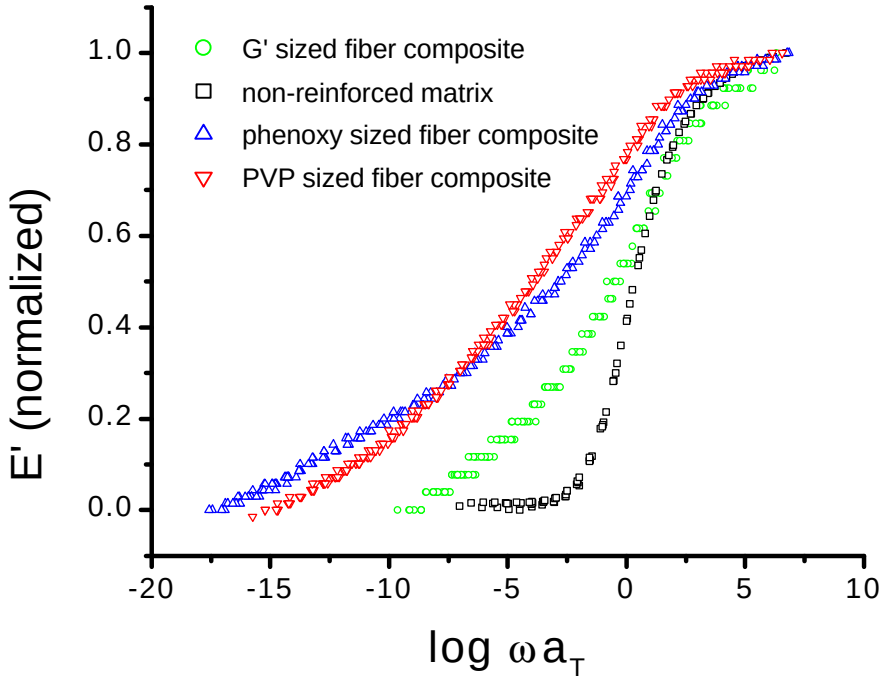


Figure 4-49. Normalized storage modulus master curves.

Horizontal shift factor values were obtained from the generation of the master curves. Cooperativity plots were then produced following the analysis of Plazek and Ngai.[84] The cooperativity plots are illustrated in Figure 4-50.

The cooperativity of the composite samples shown in Figure 4-50 clearly varies depending on the sizing that is used to treat the fibers. Keeping in mind that these sizings are "thick" layers compared to those found in coupling agents, this conclusion has implications for the research reported above on glass fillers, as will be discussed later. Again, these plots were very reproducible. Minimums of four samples were run for each sizing and the standard deviation is negligible. Error analysis followed the same method

as outlined in Appendix A. The log $a_T$ values for the composite samples have greater temperature sensitivity than the non-reinforced matrix (higher slopes in the plots). The phenoxy sized fiber composite shows the greatest temperature dependence, followed closely by the PVP sample. The G sample has an intermediate steepness between the matrix and the PVP sample. All of the composite samples exhibit similar behavior in the glassy state, which differs from the matrix sample. Sullivan *et al.*[113] determined that the viscoelastic relaxation times of E-glass composites seem to be universal in the glassy and short time regions near $T_g$. The cooperativity plots of the composites can also be extended to much higher temperatures above $T_g$ than for the non-reinforced matrix cases. As can be seen from the master curves, the rubbery modulus of the composites does not level off with increased temperature and obtain a plateau value. This is why tTSP of the E data can be extended to temperatures greater than $T_g$ in the composite samples. The fiber reinforcement must have a key influence on the relaxation of the matrix phase at temperatures greater than $T_g$.

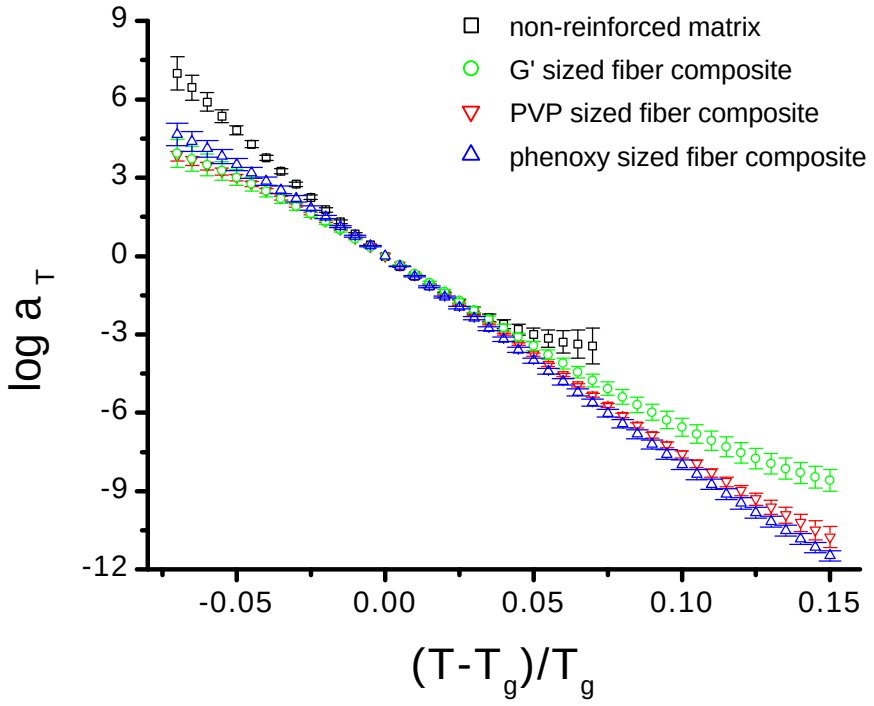


Figure 4-50. Cooperativity plots at temperatures above and below $T_g$.

Figure 4-51 shows an expanded view of the cooperativity plots in the temperature region near $T_g$ for all of the samples. The curves have also been best fit to Equation 28 using a non-linear regression. The analysis of Plazek and Ngai provides a reasonable description of the viscoelastic behavior of the non-reinforced matrix using the literature values for the constants $C_1$ and $C_2$. Equation 28 does not accurately fit the cooperativity data of the composite materials. Equation 28 predicts a curve that is concave up and that gradually levels off in such plots at $T >> T_g$. While the log $a_T$ values for the non-reinforced matrix begin to plateau at temperatures approximately 30°C greater than $T_g$ ($(T-T_g)/T_g \approx 0.05$), the log $a_T$ values for the fiber reinforced composites continue to climb steadily. Therefore, the cooperativity plots of the composites are much more linear and cannot be reasonably fit to Equation 28, but the cooperativity of the composites is increased regardless of the quality of the fit to Equation 28. In the small temperature range above $T_g$ all of the samples display nearly identical cooperativity. The curves begin to fan out near $T_g$ + 20°C ($(T-T_g)/T_g \approx 0.04$), and can be distinguished at this point. The effect of the fiber sizing becomes more pronounced at $T > T_g$ + 30°C. This indicates that the viscoelastic behavior of the polymeric component of a composite material is more complicated and is altered by the presence of the fibers.

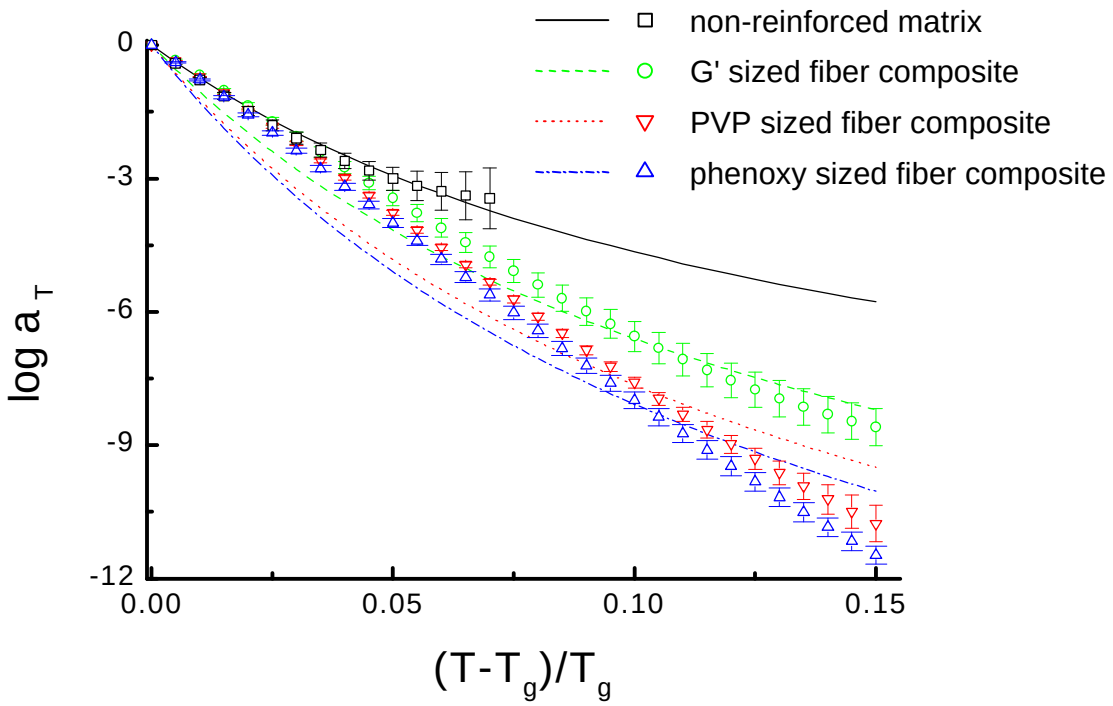


Figure 4-51. Cooperativity plots at $T > T_g$ with best fit approximations of *n* using Equation 28. (see Appendix A for fitting procedure)

The activation energies, $E_a$ , associated with these graphite composite experiments have also been summarized in Table 4-11. The calculated activation energy at $T_g$ is the greatest for the non-reinforced matrix as evidenced by the steepness of the shift factors in the glassy region. This $E_a$ method was used to quantify the slopes of the cooperativity plots due to the doubts about using Equation 28 for the composite samples. It is important to note that based strictly on the $E_a$ values for the composites at $T = T_g$ that the differences in the viscoelastic properties are not as pronounced as at temperatures $T > T_g$.

| sample | $T_g$ (K) | S | $E_a$ (KJ/mol) | *n* | Estimated variance in *n* |
|---|---|---|---|---|---|
| **non-reinforced matrix** | 411 | 82.2 ± 5.3 | 647 ± 42 | 0.510 | 0.014 |
| **G sized fiber composite** | 389 | 66.0 ± 3.9 | 492 ± 28 | 0.649 | 0.219 |
| **PVP sized fiber composite** | 398 | 69.8 ± 2.9 | 531 ± 22 | 0.701 | 0.624 |
| **phenoxy sized fiber composite** | 395 | 75.9 ± 3.3 | 574 ± 27 | 0.717 | 0.705 |

Table 4-11. Summary of coupling parameters, steepness indexes, and activation energies.

One goal of this composite research was to attempt to connect the viscoelastic and mechanical properties of the composite. Thus a collaborative effort with Nikhil Verghese and Dr. Jack Lesko in the Engineering Science and Mechanics Department at Virginia Tech was undertaken. The cooperativity analysis of the graphite composites showed a definite dependence on the particular sizing that was used to pretreat the fibers. The phenoxy sized fibers showed the largest shift towards increased cooperativity, followed by the PVP and G sized fibers respectively. These results are very interesting when compared to the short beam shear strength measurements of the same composite samples determined jointly with the engineers as illustrated in Figure 4-52. The phenoxy sized fibers have the greatest interfacial shear strength, followed by the PVP and G sized fibers respectively. The trends in cooperativity qualitatively match the mechanical properties performance as illustrated in Figure 4-53.

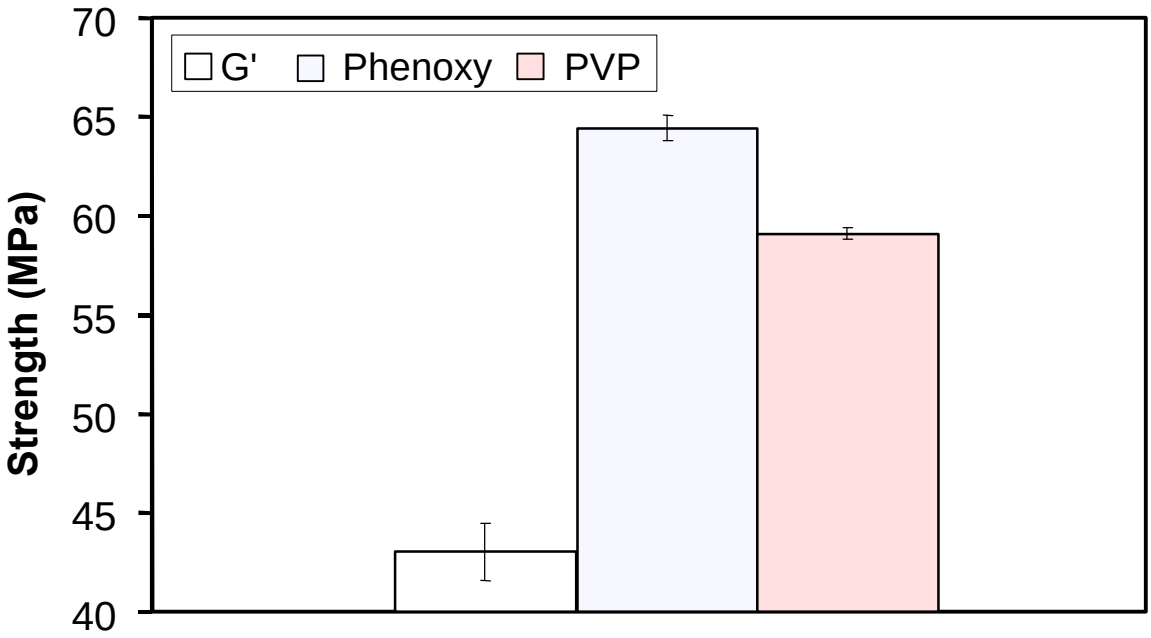


Figure 4-52. Short beam shear strength test results for graphite composites.[125]

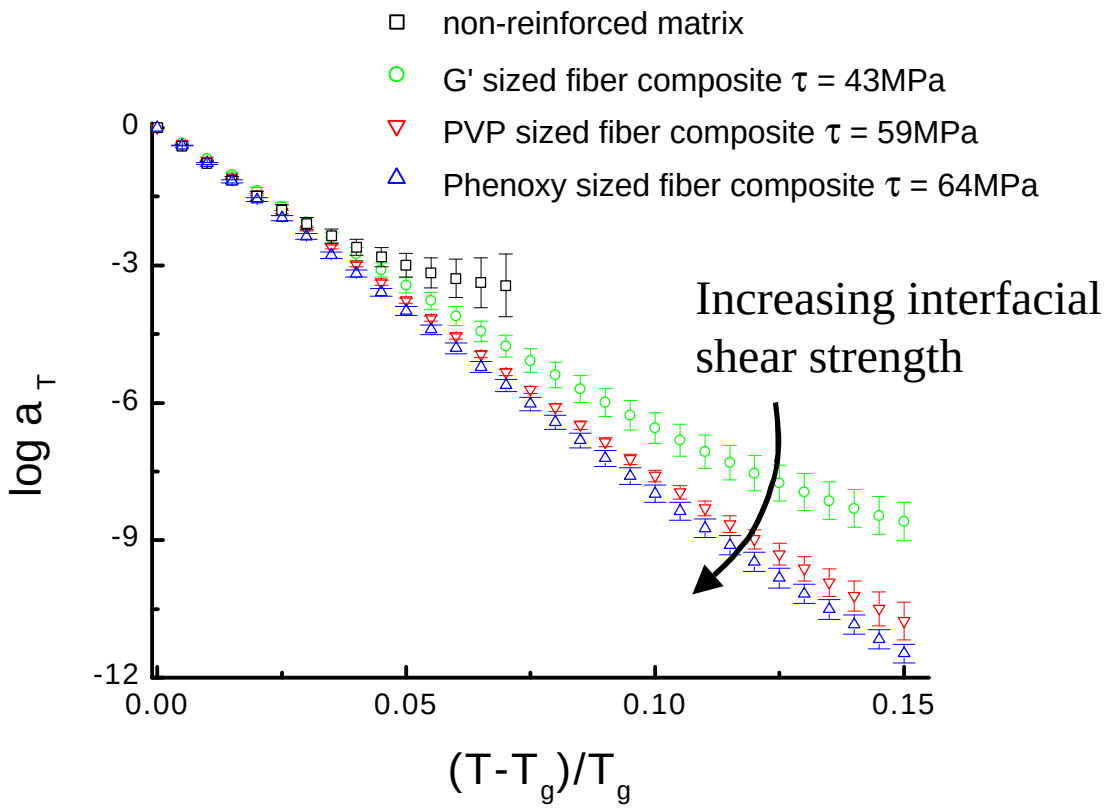


Figure 4-53. Qualitative correlation between viscoelastic and mechanical properties.

## 4.6 Single Fiber Pull-Out Test

The fiber pull-out test proved to be extremely difficult to execute. Each stage of the test presents a unique set of experimental hurdles that must be overcome. The first stage of the test involves pre-cracking the matrix near the center of the dog bone specimen with a razor blade. The pre-crack size and angle varied significantly from sample to sample, which altered $P_{max}$ to a large extent. A large pre-crack resulted in decreasing $P_{max}$ while a small pre-crack increased $P_{max}$. In many samples the embedded glass fiber was broken during the pre-cracking stage. Once a successful pre-crack is initiated the dog bone sample must be aligned and clamped perfectly parallel to the loading direction in the Minimat. If the fiber is not set properly in the Minimat then additional shear forces will be applied to the fiber in addition to the desired tensile forces. For this test to be consistent it is important that the load applied to the fiber be purely tensile. Because of the variation in pre-crack size and the alignment of the fiber along the load bearing axis there was considerable deviation in $P_{max}$ within each particular sample set. Most trials had to be discarded either due to a low $P_{max}$ or to irregular load versus extension curves. The actual standard deviations reported in Figure 4-56 would be much higher if these irregular runs had been included.

Experimental loads versus extension traces for the dry and wet samples are illustrated in Figure 4-54 and Figure 4-55. In the dry curves for both the neat epoxy matrix and epoxy/surf matrix the regions of interfacial failure identified by DiFrancia[67,68] are present. These curves show the initial crack initiation, frictional debonding along the fiber-matrix interface, crack completion, and steady frictional pull-out of the fiber from the matrix phase. The curve shape was variable from sample to sample. In many cases the frictional debonding was not observed at all. None of the samples exposed to moisture displayed the frictional debonding in the load versus extension curves. $P_{max}$ was the only common feature to all sample load versus extension curves.

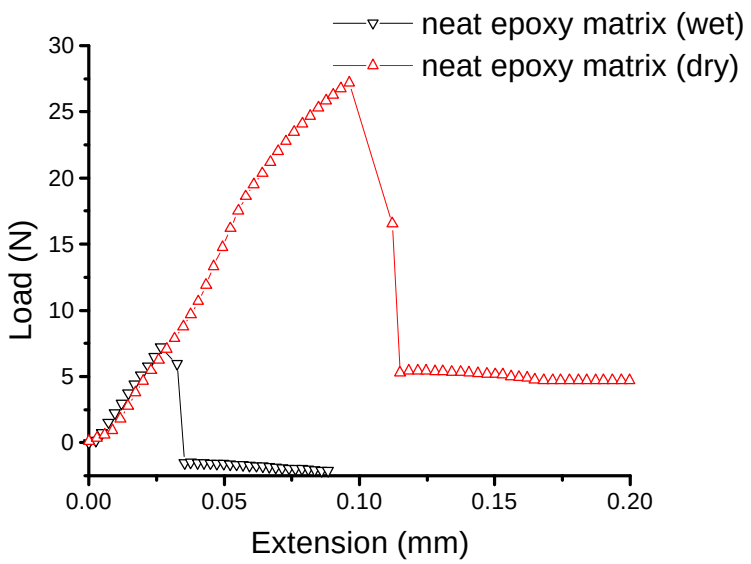


Figure 4-54. Tensile testing for fiber pull-out from neat epoxy matrix (dry and wet).

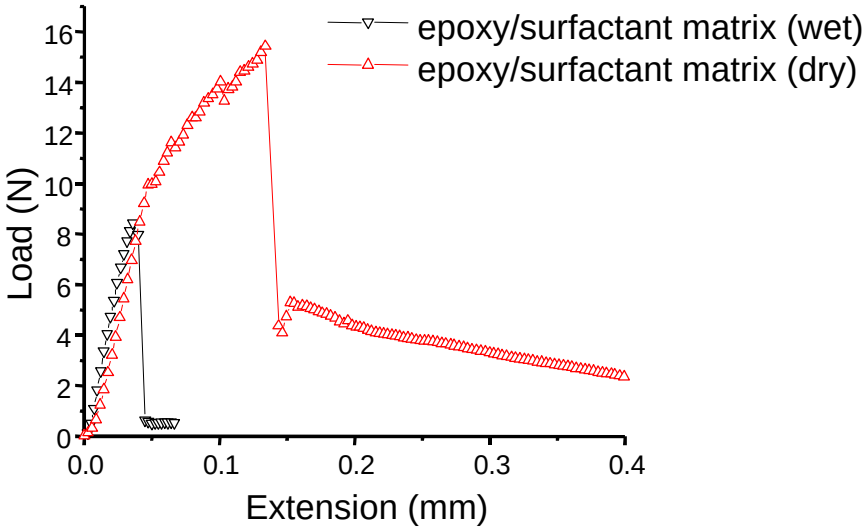


Figure 4-55. Tensile testing trace for fiber pull-out from epoxy/surf matrix (dry and wet).

Figure 4-56 provides a summary of the differences between the average $P_{max}$ of all of the epoxy matrix systems. Most of the $P_{max}$ values range within one standard deviation, although $P_{max}$ does appear to decrease after moisture exposure. The only exception to this is the neat epoxy exposed to water for 24 hours. This suggests two possibilities as an explanation to these results. One explanation is that the presence of the surfactant does

not affect the interfacial shear strength between the glass fiber and the epoxy matrix. The second possibility is that the fiber pull-out test is inadequate for testing the interfacial shear strength of this particular epoxy-fiber system. Again, the difficulties in performing this test cannot be over-emphasized. The samples are troublesome and very time consuming to prepare. Close to 25 samples for each data set were initially poured into the silicon molds. A few of these dog bone samples will break when removing from the molds or will contain trapped air. Out of the remaining potential samples roughly one half will break in half while pre-cracking the dog bone. The remaining samples yielded high scatter in $P_{max}$ and curve shape. This particular epoxy-imidazole system has a very high $T_g$ (195°C) and is very brittle. The compressive matrix pressure surrounding the embedded fiber must certainly be very excessive. Only untreated glass fibers were studied because it was concluded that the fiber pull-out test is inappropriate for interfacial adhesion testing for this epoxy-fiber system.

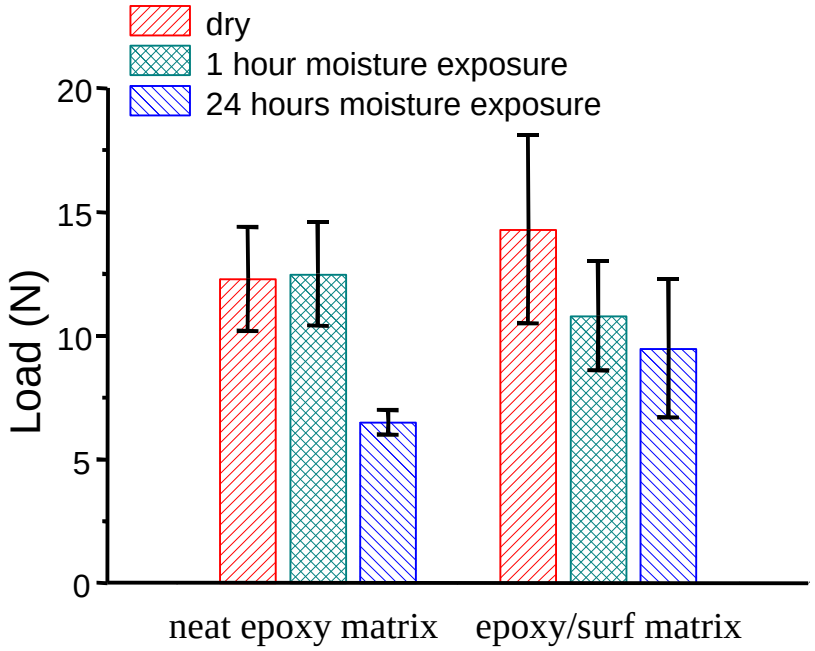


Figure 4-56. Summary of $P_{max}$ for dry and wet pull-out samples. Error bars represent the experimental standard deviations.

## 4.7 Short Beam Shear Test

Figure 4-57 shows a typical load versus displacement curve obtained from the short beam shear test measurements. No load recorded for the first 0.2mm of displacement as the test fixture has not made contact with the sample at this initial stage. The load then steadily increases until approximately 850N where the sample fails. A sharp cracking sound was always heard at the failure point of the composite. Inspection of the composite samples after failure revealed what appeared to be a slight level of interfacial debonding near the center loading point.

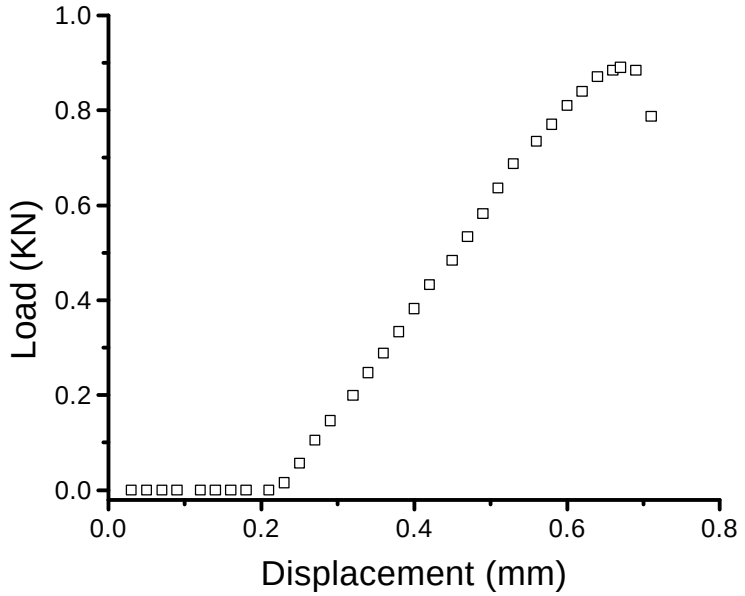


Figure 4-57. Typical load versus displacement curve for short beam shear tests.

Figure 4-58 summarizes the results of the short beam shear test for all of the composite samples studied. From this plot it can be seen that there are no clear-cut trends in the data. The composite with an epoxy/surfactant matrix with GPS pretreated fibers had the lowest interlaminar shear strength, $\tau$ , ($13.9 \pm 2.8$MPa). But, the corresponding waterborne version of this composite yielded the greatest value of $\tau$ ($28.1 \pm 2.3$MPa). The values of $\tau$, fiber volume fraction, and sample thickness are summarized in Table 4-12. The density measurements were performed according to ASTM C-373-88, which involves calculating the buoyancy of the sample in ethanol.[126] The density of the bulk

cured epoxy with no surfactant was determined to be 1.176g/cm$^3$ (± 0.001g/cm$^3$). A density of 1.174 g/cm$^3$ (± 0.004g/cm$^3$) was measured when the surfactant was added to the epoxy. These bulk densities were assumed as the matrix densities ($\rho_m$) of the composites. Once the density of the composite ($\rho_c$) is known, $V_f$ can be found using the rule of mixtures model.[127]

$$r_c = r_m + (r_f - r_m)V_f \tag{36}$$

A value of 2.54g/cm$^3$ was assumed as the density of the E-glass fibers.[128] The void content of the composites was assumed to equal zero. No visible voiding could be seen in the samples that were tested.

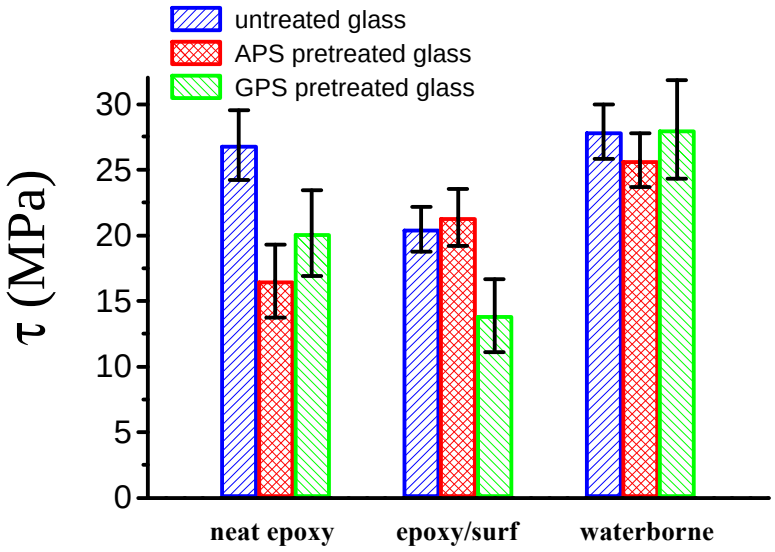


Figure 4-58. Summary of interlaminar shear strengths. Error bars represent the experimental standard deviations.

| sample | τ (MPa) | $V_f$ (%) | thickness (mm) |
|---|---|---|---|
| **neat/untreated** | 26.9 ± 2.7 | 39.6 ± 0.3 | 2.18 ± 0.03 |
| **neat/APS** | 16.5 ± 2.8 | 39.2 ± 0.9 | 2.14 ± 0.04 |
| **neat/GPS** | 20.2 ± 3.3 | 44.4 ± 1.8 | 1.93 ± 0.06 |
| **surf/untreated** | 20.5 ± 1.7 | 39.1 ± 0.7 | 2.14 ± 0.04 |
| **surf/APS** | 21.4 ± 2.2 | 41.7 ± 0.4 | 2.02 ± 0.04 |
| **surf/GPS** | 13.9 ± 2.8 | 45.1 ± 0.4 | 1.87 ± 0.04 |
| **waterborne/untr.** | 27.9 ± 2.1 | 48.2 ± 1.1 | 1.75 ± 0.04 |
| **waterborne/APS** | 25.7 ± 2.0 | 40.3 ± 6.4 | 1.74 ± 0.05 |
| **waterborne/GPS** | 28.1 ± 2.3 | 50.9 ± 0.5 | 1.67 ± 0.02 |

Table 4-12. Summary of interlaminar shear strengths, fiber volume fractions, and composite thickness. Error ranges show the experimental standard deviations.

The absence of any trends in τ for these specimens could be due to two possibilities. The samples could have been failing primarily in tension in the matrix phase. This could have resulted if the matrix shear stress exceeded the stress applied to the center of the beam. The epoxy matrix used for these composites is extremely brittle and could have been the limiting factor. Evidence of a tensile failure mechanism can be seen in the SEM image of a brittle fracture surface in Figure 4-59. The interlaminar shear strengths of the waterborne composites are the greatest, but these samples were also the thinnest. The interlaminar shear strength of the waterbornes would then be slightly increased in comparison to the thicker samples due to a lower number of flaws. The literature values for τ for epoxy glass composites found in the literature review are greater than the values reported in this research. Most of the literature values were obtained from unidirectional fiber composites, which probably contained a low number of defects.[75,76,77,78]

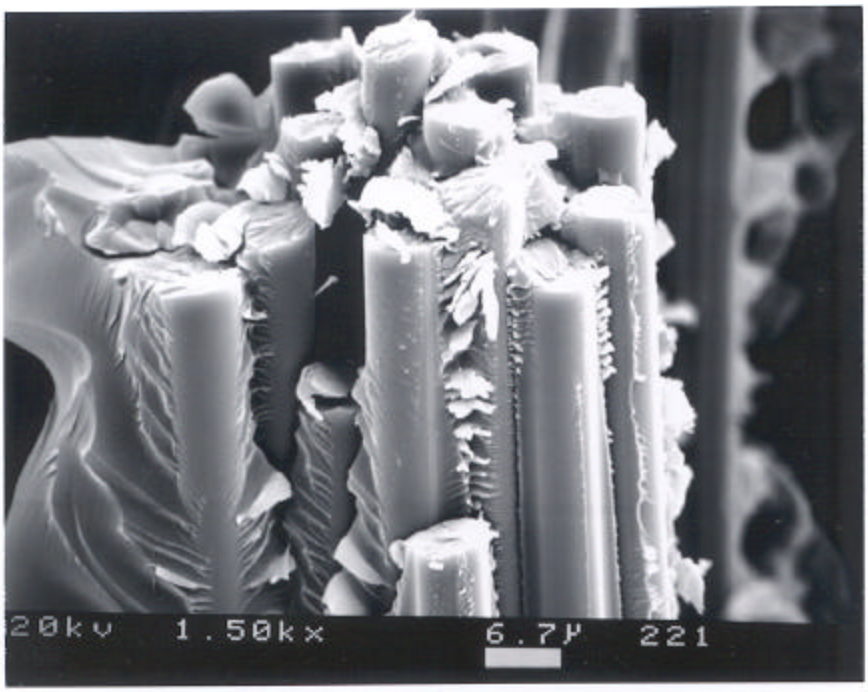


Figure 4-59. Fracture surface of APS pretreated E-glass fiber composite with neat epoxy matrix.

Another possible explanation for the absence of trends in the interlaminar shear strength data is simply that the surfactant or the silane coupling agents do not have any significant effects on the mechanical properties of the dry composites. The results of the single fiber pull-out tests seem to corroborate this point of view. Wu *et al.*[129] have suggested that silane coupling agents are not an important factor in the dry strength of polymeric E-glass composites. These researchers concluded that the matrix interactions with the tail group of the silane coupling agent are important for the mechanical properties of the dry composite. Therefore, a silane coupling agent may or may not improve the dry interlaminar shear strength of an E-glass composite. However, the presence of a silane on the surface of the glass fibers was only found to be critical in preserving mechanical properties when the composite were exposed to a moist environment.

Chua *et al.*[49] also reached this conclusion while studying the interfacial shear strength of vinyl ester/E-glass composites. These researchers observed the greatest value of $\tau$ after all of the silane coupling agent had been removed from the fiber via pyrolysis. The

lowest values of $\tau$ were observed when the fiber was coated with a thick layer of silane coupling agent. This suggests that the shear strength between the matrix phase and the outer physically adsorbed layers of coupling agent was quite low. These results have also been verified by Ahlstrom and Gerard[130] as well as Wang and Jones.[47,48] Untreated E-glass fibers either provided similar levels or actually had elevated values of $\tau$ in comparison to silane treated fibers. Again, the use of a silane coupling agent is probably most beneficial when the composite is exposed to a moist or humid environment.

# Chapter 5 Discussion

Good interfacial adhesion between the matrix phase and glass fiber reinforcement in a composite material for any application is essential for maintaining mechanical integrity under wet conditions.[52,131,132] Printed circuit boards (PCB) must also be resistant to electrical short-circuiting in addition to the stresses induced by the heating and cooling cycles of normal computer operation. If a hydrophilic surfactant is present at the epoxy-glass interface or interphase region, then the mechanical and moisture uptake properties of the PCB could certainly be altered. Water uptake experiments and cooperativity plot analysis may provide a reasonably straight forward means of probing the glass-matrix interphase of composite materials.

It was found that the surfactant has a negligible influence on the moisture uptake properties of a non-reinforced epoxy matrix (Figure 4-16). The moisture uptake diffusion constant and equilibrium uptake values of the epoxy were not enhanced by the surfactant. Perhaps the surfactant could have increased D or $M_\infty$ of the epoxy if some phase separation were occurring or if the epoxy itself did not contain polar groups. A surfactant that phase separates could potentially retain small micro-pockets of water in the bulk epoxy. The fully cured neat epoxy already contains hydroxyl groups, which can interact specifically with the diffusing water molecules. Therefore, it is a realistic expectation that a miscible surfactant present in low molar concentrations will have nearly no observable influence on the moisture uptake properties of the epoxy.

Once the E-glass beads have been added to the epoxy (Figure 4-17) changes in $M_\infty$ can be detected. The surfactant enhanced $M_\infty$ for the filled epoxy samples (Figure 4-18). The inclusion of unmodified glass beads in the epoxy results in the greatest increase in $M_\infty$, regardless of whether or not surfactant has been added to the matrix. The untreated glass surface will contain hydrophilic silanol (Si-OH) groups. Water then interacts with the surface silanols resulting in microcavities and voiding at the fiber-matrix interface.[131] These voids can then adsorb more water, giving the high $M_\infty$ values for the untreated glass filled epoxy composites. Surfactant at this interface would promote increased

moisture adsorption, which explains the very high level of $M_\infty$ found for the sample with surfactant in the matrix.

Once the silane coupling agents have been applied to the glass surface a covalent link between the epoxy matrix and glass surface is formed. The hydrolyzed silane coupling agent reacts with the surface silanols of the glass to form the less hydrophilic siloxane bond (Si-O-Si).[133] The SEM images of the filled composite fracture surfaces taken prior to moisture exposure (Figure 4-13, Figure 4-14, Figure 4-15) indicate that covalent bonding between the glass and the epoxy is occurring. The surfactant does not appear to completely negate bond formation between the glass and the epoxy matrix. Koenig has suggested that only a small number of covalent bonds are needed between the glass and the matrix phase to provide good mechanical properties.[134] But, the molecular model of the epoxy-glass interface is much more complicated than one of simple monolayer coverage of the glass surface by the silane coupling agent. Rather, a gradient of properties exists in an interphase region near the fiber surface due to the adsorption of multiple layers of silane coupling agent to the glass surface.[52] This model proposes a gradual layering of the silane coupling agent on the glass surface from chemisorbed to physisorbed.[135] In addition to the differences in adsorption, some of the silanes react with each other to form crosslinked structures.[134] The properties of this interphase region could be responsible for the differences observed in $M_\infty$ and also in the cooperativity plots between the APS and GPS pretreated epoxy-glass composites.

The physical properties (thickness, mobility, water permeability, etc.) of the glass fiber-matrix interphase region should be a function of the solubility and reactivity of the silane coupling agent with the epoxy matrix phase. For example, the outer physisorbed layers of silane are capable of mixing with and plasticizing the matrix epoxy network.[49] The fuctionality of the silane coupling agent must also be considered. The epoxide group of GPS can only react with the matrix phase to form a single covalent bond. But, APS can react with the matrix phase through a primary and secondary amine hydrogen. Therefore, APS should react with the matrix epoxy resin to form a more highly crosslinked interphase network structure than if GPS is used as the glass fiber surface pretreatment.

As a first estimate of the miscibility between two components the solubility parameters (δ) can be calculated using the following equations.

$$\Delta G^M = \Delta H^M - T\Delta S^M \tag{37}$$

$$\Delta H^M = V_M(\delta_1 - \delta_2)^2 f_1 f_2 \tag{38}$$

$$\delta = \frac{\left(\sum F\right)\rho}{M_0} \tag{39}$$

The change in the enthalpy of mixing ($\Delta H^M$), and hence the change in the Gibb's free energy of mixing ($\Delta G^M$), is then proportional to the square of the difference between the two solubility parameters of the mixture $(\delta_1-\delta_2)^2$. This expression always predicts a positive $\Delta H^M$. Therefore, favorable mixing is predicted when this term is minimized. The group contribution method of Equation 39 was used to calculate the solubility parameters of the matrix epoxy resin, GPS, and APS by summing the individual Hoy functional group contributions (F).[136,137] These calculated values are 21.1, 17.2, and 16.1 $(J/cm^3)^{1/2}$ respectively. The solubility parameters predict that GPS is more soluble in the epoxy resin than APS. This method does not account for specific interactions or chemical bonding, but it seems reasonable that GPS would have a higher solubility in the epoxy resin due to the similarities in molecular structure.

To model the chemical properties of the glass fiber-matrix interphase, 1:1 molar ratio mixtures of epoxy resin to silane coupling agent were cured with the imidazole catalyst. Using this reaction scheme the APS-epoxy resin mixture will contain twice as many equivalents of reactive sites as the GPS-epoxy resin mixture. The concentration of imidazole was kept at 3.4 moles of EMI-24 per 100 moles of epoxy groups. This is a simplified approximation of the glass fiber-matrix interphase, but has been used previously to model epoxy-silane coupling agent interfacial properties.[51] The mixtures were then oven cured in silicone rubber molds at 195°C for two hours.

Figure 5-1 shows the tan δ curves obtained from the dynamic mechanical analysis of the epoxy-silane coupling agent mixtures in a comparison with the neat epoxy results. GPS decreases the $T_g$ of the cured epoxy from 186°C to 72°C. APS decreases the $T_g$ to 144°C. The crosslink density, and therefore $T_g$, of the cured APS-epoxy resin mixture should be greater than the cured GPS-epoxy resin mixture due to a higher number of

reactive sites. The shapes of the tan δ also curves differ significantly between the GPS and APS epoxy mixtures. The GPS-epoxy mixture produces a symmetric tan δ peak at the glass transition of the cured epoxy. However, the tan δ curve of the APS-epoxy mixture contains a broad shoulder after the peak at 144°C. This shoulder indicates that some degree of phase separation is occurring. The cured APS-epoxy samples were optically clear, which means that the domain size of phase separation must be smaller than the wavelength of visible light. The incorporation of the surfactant (1.5 moles of X-100 per 100 moles of epoxy groups) did not alter the observed trends in the tan δ curves.

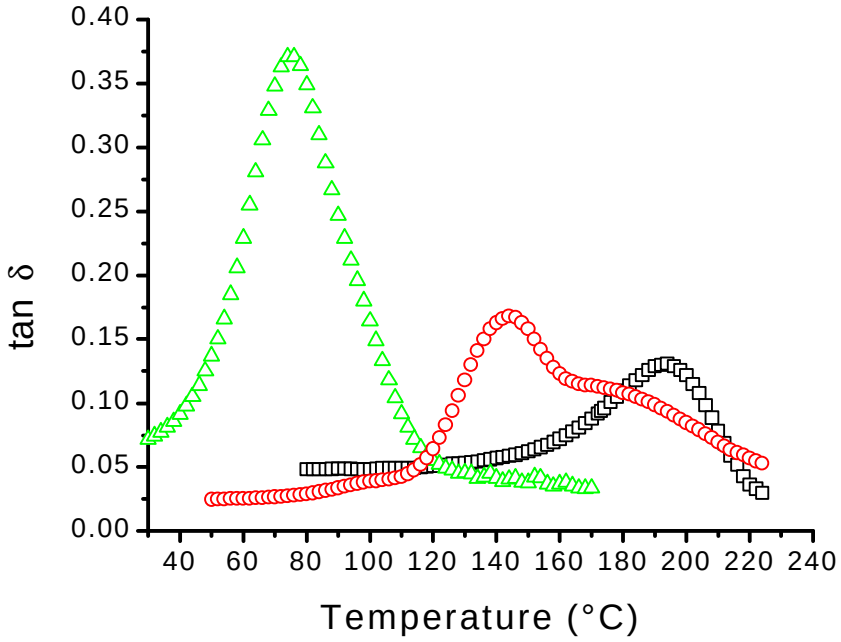


Figure 5-1. Tan δ curves for neat epoxy/EMI-24, epoxy/EMI-24/APS, and epoxy/EMI-24/GPS. The coupling agent samples were mixed at a ratio of 1 mole of coupling agent per 1 mole of DGEBA epoxy.

The solubility and reactivity of the silane coupling agent in the matrix epoxy resins could explain the higher concentrations of moisture found in the GPS pretreated glass bead filled composites after moisture exposure. If the glass fiber-matrix interphase were plasticized to a greater degree using GPS than APS then increased amounts of moisture adsorption would be expected. In addition, the crosslink density of the glass fiber-matrix

interphase could be lower when using GPS as the fiber pretreatment in comparison to APS. The moisture adsorption for the silane pretreated glass composites is only marginally elevated when surfactant is present in the matrix epoxy. If some of the surfactant were incorporated into the interphase then further plasticization would result. This would again increase the moisture adsorption levels of the composite. The moisture uptake experiments indicate that either APS or GPS is still effective in reducing the adsorption levels of the composite if a surfactant has been added to the matrix epoxy, even when a waterborne epoxy resin is used as the matrix phase.

The glass-epoxy interphase constitutes a very small volume fraction of the total matrix phase. The thickness of the interphase region has been estimated to measure between 0.02 μm and 2.0 μm.[134] In the experimental studies for this research only the epoxy-glass laminates showed changes in viscoelastic properties due to the glass. The glass bead filled samples could not be distinguished from each other based on a cooperativity analysis. The reason for this is probably related to the volume fraction of glass contained in the filled samples. The inter-particle spacing may have been too large for the interphase regions surrounding the filler particles to overlap and influence cooperativity.

The trends in the cooperativity plots (Figure 4-39 and Figure 4-40) of the epoxy-glass laminates correlate with the conclusions pertaining to the miscibility and chemical reactivity of the silanes with the matrix epoxy phase. The untreated glass produces the largest increase in cooperativity, followed by the APS and GPS pretreated glass, respectively. The silane coupling agent pretreated glass would intuitively be expected to show greater magnitudes of interfacial "constraining" due to the covalent linking between the epoxy and the glass. But, Arvanitopoulos and Koenig have used FT-IR spectroscopy to show that the aromatic rings of the gem-dimethyl groups of the epoxy resin are preferentially adsorbed and oriented on the surface of untreated E-glass.[133] Based upon the proposed molecular models of the silane adsorption to the surface of the glass and the miscibility and chemical reactivity of the silanes with the epoxy resin , the cooperativity plot analysis of the laminates is probably ranking the relative mobility and cooperative domain size at the fiber glass-matrix interphase of the laminates.

This ranking in interphase cooperative domain size of the laminates is qualitatively informative when comparing the differences between the epoxy matrices that were used.

The trends in the cooperativity plots remain the same when surfactant (without water) has been added to the epoxy matrix. The activation energies at the glass transitions (Table 4-9) for the laminates provide a more useful quantitative measure of the shifts in cooperativity than the coupling parameters or steepness indexes. The neat epoxy matrix $E_a$ values increase by 300 KJ/mol from the laminates with GPS pretreated glass to the untreated glass. When surfactant has been added to the matrix phase, the $E_a$ values for the respective laminates only increases by 33 KJ/mol. If some of the surfactant is acting as an additional plasticizer at the fiber glass-matrix interphase then the volume of the cooperative domains at the interphase should decrease.

The results presented just above contradict the research of Dufresne and Lacabanne.[111] These researchers used a thermo-stimulated creep analysis to determine that APS pretreated glass restricts the molecular mobility of a cured epoxy resin to a larger extent than untreated glass. The epoxy resin used in their study was cured with a combination of dicyandiamide and benzl dimethyl amine, which gives a fully cure $T_g$ of approximately 135°C. This epoxy system could interact differently with APS than an epoxy-imidazole matrix. It is difficult to compare epoxies that have not been crosslinked with the same curing agent or catalyst. Spectroscopic studies, such as FT-IR, could possibly be used to determine if curing agent migrates to the glass-epoxy interphase during cure. But, such FT-IR spectroscopic studies are difficult when the surfactant and matrix epoxy share common adsorption peaks.

When the epoxy matrix of the glass laminates has been cast from a waterborne resin the aqueous based phase interactions with the silane coupling agent become an important factor in governing the viscoelastic properties. Figure 16 indicates that there are no longer any differences in the cooperativity between the APS and GPS pretreated glass laminates when a waterborne epoxy has been used as the matrix. The aqueous phase could aid in dispersing the physisorbed layers of silane into the epoxy matrix. Solvents have been shown to increase the penetration of the epoxy resin into the glass-epoxy interphase in traditional solvent cast epoxy laminates.[138] An increased level of mixing between the physisorbed APS and the epoxy in the interphase region would lower the measured cooperativity. The activation energies at the glass transition for the untreated fiber laminates are 668 KJ/mol without water and 656 KJ/mol for the waterborne matrix.

Therefore, the water interactions with the physisorbed layers of silane are probably more important than the water-surfactant interactions at the interphase region. However, it is unlikely that the aqueous phase of the waterborne is washing away the silane coupling agent that has chemisorbed to the glass surface.[52] This was verified by the moisture uptake experiments performed on the multi-ply composites. The results of this research indicate that increased moisture uptake in a waterborne epoxy / E-glass composite is more likely to be caused by the presence of voids during than the initial processing than by the presence of the surfactant.

This present study has also pointed out the difficulties involving complex materials that reflect realistic commercial systems. High amounts of trial and error in solving these types of problems were encountered. Many adhesive studies in the literature are performed using highly idealized model systems. For example, the objectives and purpose of this research immediately eliminated the use of an ionic surfactant. An ionic surfactant would have made spectroscopic studies, such as XPS, FTIR, and SIMS, more informative since the epoxy resin and surfactant used for this project are very chemically similar. FTIR cannot detect the presence of the surfactant in the epoxy even at concentrations as high as 18 weight percent. The glass and silane coupling agents also yield complex substrate-adhesive interactions.

The cooperativity plot analysis of the composites is a new and unique characterization method. This technique has the advantage of analyzing a complete composite adhseive system. The cooperativity experiments provide meaningful interphase characterizations for both silane coupling agent pretreated E-glass composites as well as thermoplastic sized graphite fiber composites. The interfacial shear strength data for the graphite composites followed the same trends as observed with the correspoinding cooperativity plots. The interfacial shear strength data for the E-glass composites did not follow any apparent trends. This is probably due to the fact that a thermoplastic fiber sizing is much thicker than a silane coupling agent pretreatment. The silane coupling agent pretreatment has the primary task of protecting against moisture damage. The thicker thermoplastic sizing seems to have a larger role in the mechanical properties of a composite. But, a printed circuit board is not subjected to the same levels of loading as a composite airplane wing. For circuit board applications the presence of a surfactant seems to have little

effect on the viscoelastic and moisture durability properties provided the fiber receives some type of silane surface pretreatment.

# Chapter 6 Conclusions

This research has provided much insight as to the role of the surfactant and aqueous phase of waterborne epoxy on the viscoelastic and moisture uptake properties of glass composites. Many small steps were taken and much knowledge was gained during the course of this research. In the end this research can be summarized by a few basic, yet important conclusions.

1) Moisture uptake in the epoxy/E-glass composites is always reduced when the glass fibers are pretreated with a silane coupling agent. This was found to be true even when a surfactant has been added to the matrix epoxy or a complete waterborne epoxy system is used as the matrix phase.

2) Cooperativity analysis of composite materials is sensitive to the surface pretreatment of the reinforcing fibers. This was demonstrated experimentally with epoxy/E-glass and vinyl-ester/graphite carbon fiber composites.

3) The influence of the aqueous phase on the viscoelastic properties of the fiber-matrix interphase is as important a consideration as simply just the surfactant.

# Appendix A

The following procedure was used to analyze the cooperativity plot data. The examples outlined in this section are for the bulk neat epoxy samples. Master curves of the storage modulus are constructed using a graphing program. The shift factor data are then plotted using a spreadsheet as illustrated in Figure A-1.

**bulk neat epoxy**

| T (°C) | T (K) | (T-Tg)/Tg | log aT |
|---|---|---|---|
| 140.3 | 413.45 | -0.06765 | 6.17375 |
| 143.3 | 416.45 | -0.06089 | 5.60064 |
| 146.3 | 419.45 | -0.05412 | 4.94798 |
| 149.3 | 422.45 | -0.04736 | 4.33557 |
| 152.3 | 425.45 | -0.04059 | 3.6984 |
| 155.3 | 428.45 | -0.03383 | 3.09368 |
| 158.3 | 431.45 | -0.02706 | 2.46776 |
| 161.3 | 434.45 | -0.0203 | 1.83494 |
| 164.3 | 437.45 | -0.01353 | 1.21745 |
| 167.3 | 440.45 | -0.00677 | 0.59221 |
| 170.3 | 443.45 | 0 | 0 |
| 173.3 | 446.45 | 0.006765 | -0.5819 |
| 176.3 | 449.45 | 0.01353 | -1.14592 |
| 179.3 | 452.45 | 0.020295 | -1.6605 |
| 182.3 | 455.45 | 0.027061 | -2.12567 |
| 185.3 | 458.45 | 0.033826 | -2.6435 |
| 188.3 | 461.45 | 0.040591 | -3.11662 |
| 191.3 | 464.45 | 0.047356 | -3.56622 |
| 194.3 | 467.45 | 0.054121 | -4.01052 |
| 197.3 | 470.45 | 0.060886 | -4.39043 |
| 200.3 | 473.45 | 0.067651 | -4.75084 |

Figure A-1. Shift factor data spreadsheet.

Once the shift factor data for the individual sample are known, log $a_T$ is then plotted versus $(T-T_g)/T_g$. This plot is then fit to a third order polynomial as portrayed in Figure .

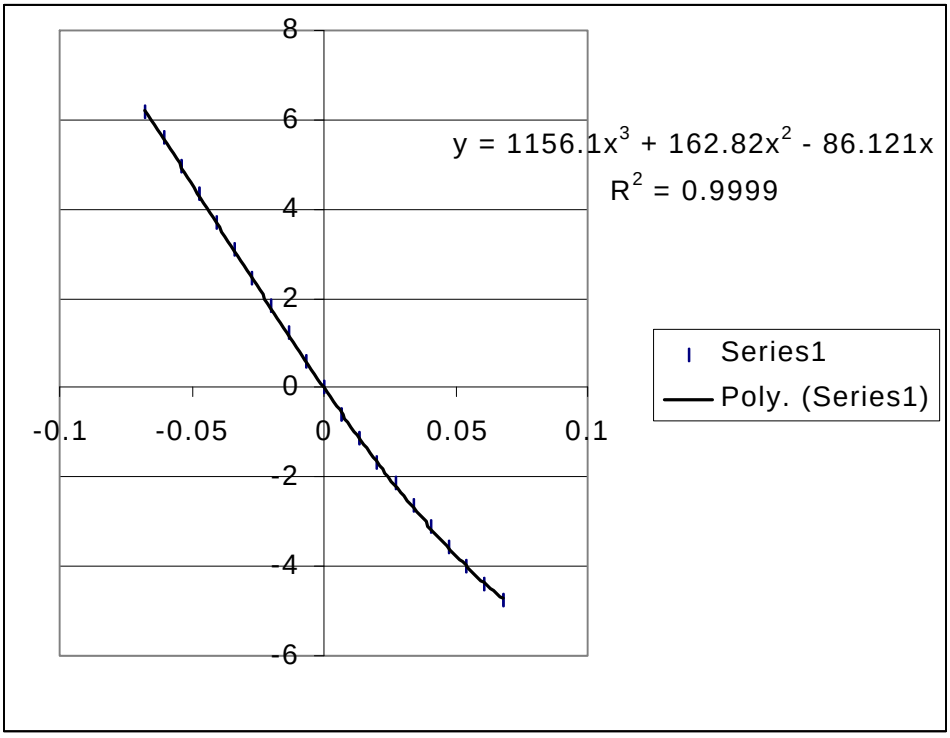


Figure A-2. Cooperativity plot for a single sample that has been fitted to a third order polynomial expression.

The polynomial expression is the key to averaging the cooperativity data for several samples of the same data set. Each individual sample within a sample set has a slightly different $T_g$. The data are averaged by re-calculating the shift factors at specific values of $(T-T_g)/T_g$. This is shown in the spreadsheet of Figure A-2.

| (T-Tg)/Tg | sample1 | sample2 | sample3 | sample4 | avg | std dev |
|---|---|---|---|---|---|---|
| -0.07 | 6.414081 | 6.201061 | 6.92085 | 6.79524 | 6.582808 | 0.333466 |
| -0.065 | 5.958224 | 5.748383 | 6.370499 | 6.322524 | 6.099907 | 0.298005 |
| -0.06 | 5.49882 | 5.296313 | 5.826693 | 5.843929 | 5.616439 | 0.266003 |
| -0.055 | 5.036736 | 4.84518 | 5.289965 | 5.360587 | 5.133117 | 0.237024 |
| -0.05 | 4.572841 | 4.395313 | 4.760845 | 4.873633 | 4.650658 | 0.210646 |
| -0.045 | 4.108001 | 3.947039 | 4.239867 | 4.384199 | 4.169777 | 0.186474 |
| -0.04 | 3.643083 | 3.50069 | 3.727561 | 3.893421 | 3.691189 | 0.164139 |
| -0.035 | 3.178955 | 3.056592 | 3.224459 | 3.402431 | 3.215609 | 0.143307 |
| -0.03 | 2.716482 | 2.615075 | 2.731094 | 2.912363 | 2.743754 | 0.123681 |
| -0.025 | 2.256534 | 2.176468 | 2.247998 | 2.424351 | 2.276338 | 0.105003 |
| -0.02 | 1.799976 | 1.7411 | 1.775701 | 1.939529 | 1.814076 | 0.087054 |
| -0.015 | 1.347675 | 1.309299 | 1.314736 | 1.45903 | 1.357685 | 0.069658 |
| -0.01 | 0.900499 | 0.881395 | 0.865634 | 0.983988 | 0.907879 | 0.052704 |
| -0.005 | 0.459315 | 0.457715 | 0.428929 | 0.515537 | 0.465374 | 0.03624 |
| 0 | 0 | 0 | 0 | 0 | 0 | 0 |
| 0.005 | -0.40161 | -0.37565 | -0.40517 | -0.39706 | -0.39487 | 0.013236 |
| 0.01 | -0.81962 | -0.78468 | -0.8015 | -0.83893 | -0.81118 | 0.023362 |
| 0.015 | -1.22816 | -1.18817 | -1.1833 | -1.26969 | -1.21733 | 0.040275 |
| 0.02 | -1.62638 | -1.5858 | -1.55005 | -1.68818 | -1.6126 | 0.059252 |
| 0.025 | -2.0134 | -1.97722 | -1.90122 | -2.09328 | -1.99628 | 0.079794 |
| 0.03 | -2.38837 | -2.36211 | -2.23627 | -2.48385 | -2.36765 | 0.102019 |
| 0.035 | -2.7504 | -2.74015 | -2.55466 | -2.85876 | -2.72599 | 0.126198 |
| 0.04 | -3.09864 | -3.11101 | -2.85588 | -3.21688 | -3.0706 | 0.152668 |
| 0.045 | -3.43221 | -3.47435 | -3.13938 | -3.55706 | -3.40075 | 0.181804 |
| 0.05 | -3.75026 | -3.82985 | -3.40463 | -3.87819 | -3.71573 | 0.214004 |
| 0.055 | -4.05191 | -4.17718 | -3.65111 | -4.17912 | -4.01483 | 0.249679 |
| 0.06 | -4.33629 | -4.51601 | -3.87828 | -4.45873 | -4.29733 | 0.289248 |
| 0.065 | -4.60255 | -4.84601 | -4.0856 | -4.71587 | -4.56251 | 0.333133 |
| 0.07 | -4.8498 | -5.16685 | -4.27256 | -4.94941 | -4.80966 | 0.381753 |

Figure A-2. Spreadsheet used to calculate the average cooperativity values for the bulk neat epoxy samples.

The average values and standard deviations reported in Figure A-2 are then used to plot the final cooperativity plot (Figure A-3).

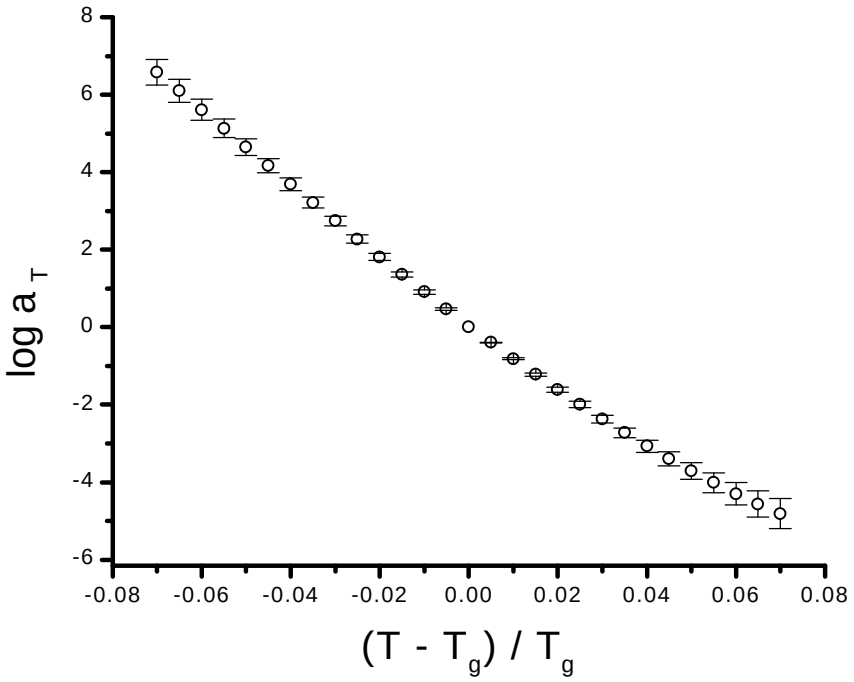


Figure A-3. Cooperativity plot for bulk neat samples. Average values and standard deviations reported in Figure A-2 are used for the data points.

The coupling parameter (*n*) is determined by fitting to Equation 28 using a non-linear analysis in Mathematica. Only the shift factor data above the glass transition temperature were used for the fit. The glass transition temperature was taken as the average of the individual samples within a data set. An example of this Mathematica program is illustrated in Figure A-4. The Mathematica program also provides an error analysis of the fit.

## neat / bulk

```
In[1]:= Clear@"`*"D

In[2]:= << Statistics`NonlinearFit`

In[3]:= data = 8{0, 0}, {.005,  0.39487}, {0.01,  0.81118}, {0.015,  1.21733}, {0.02,  1.6126}, {0.025,  1.99628},
          {0.03,  2.36765}, {0.035,  2.72599}, {0.04,  3.0706}, {0.045,  3.40075}, {0.05,  3.71573}, {0.055,  4.01483},
          {0.06,  4.29733}, {0.065,  4.56251}, {0.07,  4.80966<<;

In[4]:= c1 = 5.49
Out[4]= 5.49

In[5]:= c2 = 0.141
Out[5]= 0.141

In[6]:= Tg = 445.9
Out[6]= 445.9

In[7]:= f@T_D = -1/(1 - n) c1 T/(c2 + T)
Out[7]= -5.49 T/(H1 - nL H0.141 + TL)

In[8]:= z@T_D = NonlinearRegress@data, f@TD, T, 8n, .1, .9<D
Out[8]= :BestFitParameters → 8n → 0.6115<,
         ParameterCITable →
                    Estimate      Asymptotic SE      CI
           n        0.6115        0.00332257         80.604374, 0.618627<',
         EstimatedVariance → 0.0098826282204774,
                                    DF      SumOfSq               MeanSq
                    Model           1       135.115               135.115
         ANOVATable → Error         14      0.138356795086683     0.0098826282204774,
                    Uncorrected Total  15    135.254
                    Corrected Total    14    33.8678
         AsymptoticCorrelationMatrix → H1. L, FitCurvatureTable → $Failed>
```

Figure A-4. Mathematica program used to determine the coupling parameters.

Once the coupling parameter is known, Equation 28 can then be used to overlay a plot of the best fit with the experimental data points as in Figure A-5.

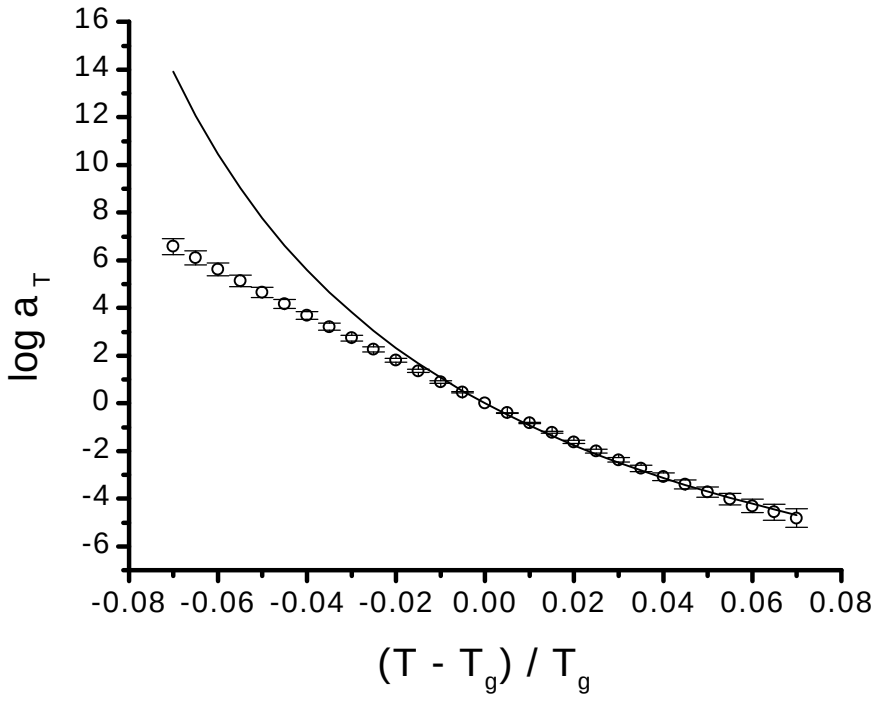


Figure A-5. Experimental cooperativity data points and theoretical fit to Equation 28 for the bulk neat epoxy samples.

To determine the activation energy of the glass transition the average shift factors listed in the spreadsheet of Figure A-2 must be re-calculated to correspond to temperature. This is shown in the spreadsheet of Figure A-6. These data are then plotted as log $a_T$ versus temperature (Figure A-7) and fit to a third order polynomial. The regression data are then used to calculate the slope of the plot at $T = T_g$. The slope at $T = T_g$ is the steepness (S) of the plot as defined in Equation 29. The activation energy is then calculated using Equation 30.

| bulk neat epoxy | | |
|---|---|---|
| (T-Tg)/Tg | T | log aT |
| -0.07 | 414.687 | 6.58281 |
| -0.065 | 416.9165 | 6.09991 |
| -0.06 | 419.146 | 5.61644 |
| -0.055 | 421.3755 | 5.13312 |
| -0.05 | 423.605 | 4.65066 |
| -0.045 | 425.8345 | 4.16978 |
| -0.04 | 428.064 | 3.69119 |
| -0.035 | 430.2935 | 3.21561 |
| -0.03 | 432.523 | 2.74375 |
| -0.025 | 434.7525 | 2.27634 |
| -0.02 | 436.982 | 1.81408 |
| -0.015 | 439.2115 | 1.35768 |
| -0.01 | 441.441 | 0.90788 |
| -0.005 | 443.6705 | 0.46537 |
| 0 | 445.9 | 0 |
| 0.005 | 448.1295 | -0.39487 |
| 0.01 | 450.359 | -0.81118 |
| 0.015 | 452.5885 | -1.21733 |
| 0.02 | 454.818 | -1.6126 |
| 0.025 | 457.0475 | -1.99628 |
| 0.03 | 459.277 | -2.36765 |
| 0.035 | 461.5065 | -2.72599 |
| 0.04 | 463.736 | -3.0706 |
| 0.045 | 465.9655 | -3.40075 |
| 0.05 | 468.195 | -3.71573 |
| 0.055 | 470.4245 | -4.01483 |
| 0.06 | 472.654 | -4.29733 |
| 0.065 | 474.8835 | -4.56251 |
| 0.07 | 477.113 | -4.80966 |

Figure A-6. Shift factors.

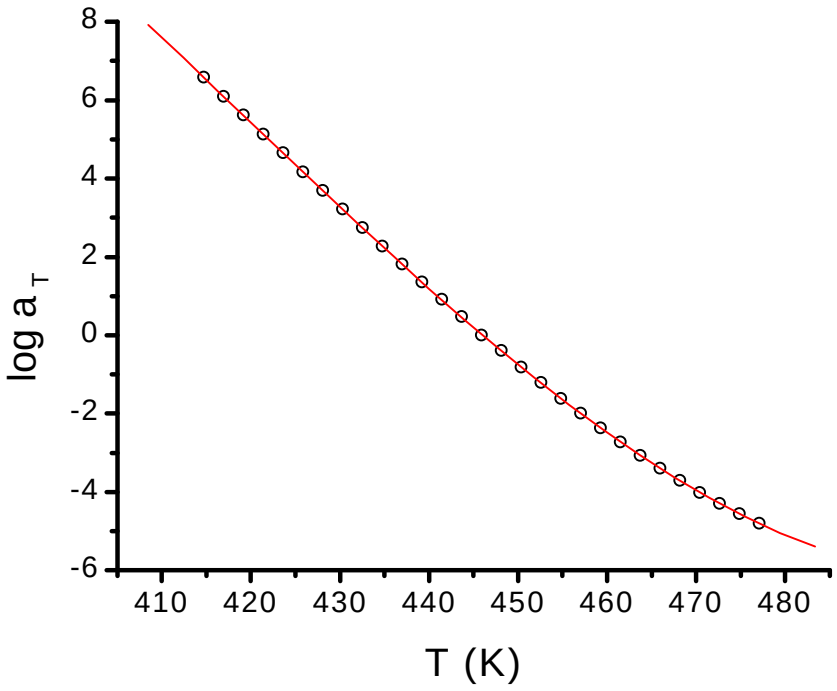


Figure A-7. Shift factor plot used to calculate an activation energy.

Polynomial Regression for bulk neat epoxy:
Y = A + B1*X + B2*X^2 + B3*X^3

| Parameter | Value | Error |
|---|---|---|
| A | -692.33466 | 19.23285 |
| B1 | 5.4375 | 0.12962 |
| B2 | -0.01351 | 2.90937E-4 |
| B3 | 1.07584E-5 | 2.17474E-7 |

| R-Square(COD) | SD | N | P |
|---|---|---|---|
| 1 | 0.00593 | 29 | <0.0001 |

## References


1. Lin, P. C.; Wang, D. W.; Fuerniss, S. J.; Poliks, M. D.; Obrzut, J.; Siperko, L. M.; Chen, W. T.; Havens, R. D.; Marcko, R. M. *Mat. Res. Soc. Symp. Proc.*, **323**, 309, (1994).
2. Schutte, C. L. *Mat. Sci. Eng.*, **R13**, 265, (1994).
3. Plueddemann, E. P. *Silane Coupling Agents*, Plenum Press, New York, 1982.
4. *Engineered Materials Hanbook; Vol. 3; Adhesives and Sealants*, ASM International, 1990.
5. Tai, R. C. L.; Szklarska-Smialowska, Z. *J. Mater. Sci.*, **1996**, 31, 1925.
6. Farkas, A.; Strohm, P. F. *J. Apply. Polym. Sci.*, **1968**, 12, 159.
7. Barton, J. M.; Shepherd, P. M. *Makromol. Chem.*, **1975**, 176, 919.
8. Ricciardi, F.; Romanchick, W. A.; Joullie, M. M. *J. Polym. Sci., Polym. Chem. Ed.*, **1983**, 21, 1475.
9. Jisova, V. *J. Apply. Polym. Sci.*, **1987**, 34, 2546.
10. Chang, S. *Polymer*, **1992**, 33, 4768.
11. Heise, M. S.; Martin, G. C. *J. Polym. Sci., Polym. Letters*, **1988**, 26, 153.
12. Heise, M. S.; Martin, G. C. *Macromolecules*, **1989**, 22, 99.
13. Heise, M. S.; Martin, G. C. *J. Apply. Polym. Sci.*, **1990**, 39, 721.
14. Shaw, D. J. *Introduction to Colloid and Surface Chemistry,* Butterworth-Heinemann Ltd, Boston, **1992**.
15. Hahn, D. W.; McGuire, J. L. *Ullman s Encyclopedia of Industrial Chemistry; 5th Edition*, A7, 462.
16. Sisley, J. P. *Encyclopedia of Surface-Active Agents*, Chemical Publishing, New York, **1952**.
17. Schick, M. J. editor *Nonionic Surfactants*, Marcel Dekker, New York, **1967**.
18. Schonfeldt, N. *Surface Active Ethylene Oxide Adducts*, Pergamon Press, New York, **1969**.
19. Mittal, K. L. editor *Solution Chemistry of Surfactants*, Plenum Press, New York, **1978**, vol. 1.
20. Keddie, J. L.; Meredith P.; Jones, R. A. L.; Donald, A. M. *Macromolecules*, **1995**, 28, 2673.
21. Charmeau, J. Y.; Kientz, E.; Holl, Y. *Proc. 19th Annual Meeting of the Adhesion Society*, The Adhesion Society, Myrtle Beach, SC, Feb. 1996, pp. 98-101.
22. Vanderhoff, J. W. *Br. Polym. J.*, **1970**, 2, 161.
23. Kientz, E.; Holl, Y. *Colloid Surface*, **1993**, 78, 255.
24. Charmeau, J. Y.; Gerin, P. A.; Vovelle, L.; Schirrer, R.; Holl, Y. *J. Adhesion Sci. Tech.*, **1999**, 13, 203.
25. Gerin, P. A.; Grohens, Y.; Schirrer, R.; Holl, Y. *J. Adhesion Sci. Tech.*, **1999**, 13, 217.
26. Niu, B. J.; Urban, M. W. *J. Appl. Polym. Sci.*, **1995**, 56, 377.
27. Tebelius, L.K.; Urban, M. W. *J. Appl. Polym. Sci.*, **1995**, 56, 387.
28. Huang, L.; Maltesh, C.; Somasundaran, P. *J. Colloid Interface Sci.*, **1996,** 177, 222.
29. Somasundaran, P.; Krishnakumar, S. *Colloids and Surfaces*, **1994**, 93, 79.
30. Veggeland, K.; Nilsson, S. *Langmuir,* **1995**, 11, 1885.
31. Rutland, M. W.; Senden, T. J. *Langmuir*, **1993**, 9, 412.

32. Gentle, I. R.; Saville, P. M.; White, J. W. *Langmuir*, **1993,** 9, 646.
33. Drzal, L. T. *Adv. Pol. Sci., Epoxy Resins and Composites*, Springer-Verlag, New York, **1986**, vol. 75
34. Reifsnider, K. L. *Composites*, **1994**, 25, 461.
35. Williams, J. G.; James, M. R.; Morris, W. L. *Composites*, **1994**, 25, 757.
36. Mahy, J.; Jenneskens, L. W.; Grabandt, O. *Composites*, **1994**, 25, 653.
37. DeLong, J. D.; Hook, K. J.; Rich, M. J.; Kalantar, J.; Drzal, L. T. *Controlled Interfaces in Composite Materials*, Elesevier Science Publishing Co., **1990**, 87.
38. Marshall, P. I.; Attwood, D.; Healey, M. J. *Composites*, **1994**, 25, 752.
39. Dirand, X.; Hilaire, B.; Lafontaine, E.; Mortaigne, B.; Nardin, M. *Composites*, **1994**, 25, 645.
40. Palmese, G. R.; McCullough, R. L. *J. Adhesion*, **1994**, 44, 29.
41. Larson, B. K.; Drzal, L. T. *Composites*, **1994**, 25, 711.
42. Shaw, D. J. *Introduction to Colloid and Surface Chemistry; 4th Ed.*, Butterworth-Heinemann Ltd, Boston, **1992**.
43. Shaw, D. J. *Introduction to Colloid and Surface Chemistry; 3rd Ed*, Van Nostrand Reinhold, New York, **1990**.
44. Niu, B. J.; Urban, M. W. *J. Appl. Polym. Sci.*, **1995**, 56, 377.
45. Tebelius, L. K.; Urban, M. W. *J. Appl. Polym. Sci.*, **1995**, 56, 387.
46. Arkles, B. Ed. *Metal-Organics Including Silanes and Silicones*, Gelest, Inc., **1995**.
47. Wang, D.; Jones, F. R. *Comp. Sci. Tech.*, **1993**, 48, 215.
48. Wang, D.; Jones, F. R. *J. Mater. Sci.*, **1993**, 28, 1396.
49. Chua, P. S.; Dai, S. R.; Piggott, M. R. *J. Mater. Sci.*, **1992**, 27, 913.
50. Mader, E. *Comp. Sci. Tech.*, **1997**, 57, 1077.
51. Al-Moussawi, H.; Drown, E. K.; Drzal, L. T.; *Polym. Comp.*, **1993**, 14, 195.
52. Chiang, C. H.; Koenig, J. L. *J. Polym. Sci.; Polym. Phys.*, **1982**, 20, 2135.
53. Cossins, S.; Connell, M.; Cross, B.; Winter, R.; Kellar, J. *Appl. Spectr.*, **1996**, 50, 900.
54. Yumitori, S.; Wang, D.; Jones, F. R. C*omposites*, **1994**, 25, 698.
55. Sottos, N. R.; Li, L. *J. Adhesion*, **1994**, 45, 105.
56. Cheng, T. H.; Zhang, J.; Yumitori, S; Jones, F. R.; Anderson, C. W. *Composites*, **1994**, 25, 661.
57. Piggott, M. R. *Mat. Res. Soc. Symp. Proc.*, **1990**, 170, 265.
58. Piggott, M. R. *Carbon*, **1989**, 27, 657.
59. Palmese, G. R.; McCullough, R. L. *J. Adhesion*, **1995**, 52, 101.
60. Tryson, L. D.; Kardos, J. L. *36th Annual Conf. Reinforced Plastics/Composites Inst.; Soc. Plast. Ind.*, **1981**, 1.
61. Madhukar, M. S.; Drzal, L. T. *J. Comp. Mat.*, **1992**, 26, 936.
62. Madhukar, M. S.; Drzal, L. T. *J. Comp. Mat.*, **1991**, 25, 932.
63. Clark, R. L. *Ph.D. Dissertation*, Virginia Polytechnic Institute and State University, VA, **1996**.
64. Wang, J. Y.; Ploehn, H. J. *J. Appl. Pol. Sci.*, **1996**, 26, 477.
65. Folkes, M. J. *Short Fiber Reinforced Composites*, Research Studies Press, New York, **1982.**
66. Commercon, P; Wightman, J. P. *J. Adhesion*, **1994**, 47, 257.

67. DiFrancia, C.; Ward, T. C.; Claus, R. O. *Composites*, **1996**, 27A, 597.
68. DiFrancia, C.; Ward, T. C.; Claus, R. O. *Composites*, **1996**, 27A, 613.
69. Herrera-Franco, P. J.; Drzal, L. T. *Composites*, **1992**, 23, 2.
70. Piggott, M. R. *Comp. Sci. Tech.*, **1997**, 57, 965.
71. Bai, S. L.; Djafari, V.; Andreani, M.; Francois, D. *Comp. Sci. Tech.*, **1995**, 55, 343.
72. Adams, D. F.; Lewis, E. Q. *J. Comp. Tech. Res.*, **1995**, 17, 341.
73. Beer, F. P.; Johnson, E. R. *Mechanics of Materials*, Second Edition, McGraw-Hill Book Co., New York, **1992**, 285.
74. *Annual Book of ASTM Standards*, **1998**, v15.03
75. Madhukar, M. S.; Drzal, L. T. *J. Comp. Mat.*, **1991**, 25, 932.
76. Hoecker, F,; Karger-Kocsis, J. *Composites*, **1994**, 25, 729.
77. Larson, B. K.; Drzal, L. T. *Composites*, **1994**, 25, 711.
78. Drown, E. K.; Al-Moussawi, H.; Drzal, L. T. *J. Adhesion Sci. Tech.*, **1991**, 5, 865.
79. Angell, C. A. *J. Non-Crystalline Solids*, **1991**, 131, 13.
80. Roland, C. M.; Ngai K. L. *Macromolecules*, **1992**, 25, 5765.
81. Adam, G.; Gibbs, J. H. *J. Chem. Phys.*, **1965**, 43, 139.
82. Kauzmann, W. *Chem. Rev.*, **1948**, 43, 219.
83. Aklonis, J. J.; MacKnight, W. J. *Introduction to Polymer Viscoelasticity*, Second Edition, John Wiley and Sons, New York, **1983**.
84. Plazek, D. J.; Ngai, K. L. *Macromolecules*, **1991** 24, 1222.
85. Roland, C. M.; Ngai K. L. *Macromolecules*, **1991**, 24, 5315.
86. Ngai, K. L.; Plazek, D. J. *J. Polym. Sci.; Polym. Phys.*, **1986**, 24, 619.
87. McCrum, N. G.; Read, B. E.; Williams, G. *Anelastic and Dielectric Effects in Polymeric Solids,* Dover Publications, New York, **1991**.
88. Roland C. M.; Ngai K. L.; O'Reilly J. M.; Sedita J. S., *Macromolecules*, **1992**, 25, 3904.
89. Lewis, T. B.; Nielsen, L. E. *J. Appl. Polym. Sci.*, **1970**, 14, 1449.
90. Cousin, P.; Smith, P. *J. Polym. Sci., Polym. Phys.*, **1994**, 32, 459.
91. Tsagaropoulos, G.; Eisenberg, A. *Macromolecules*, **1995**, 28, 396.
92. Tsagaropoulos, G.; Eisenberg, A. *Macromolecules*, **1995**, 28, 6067.
93. Gahleitner, M.; Bernreitner, K.; Neibl, W. *J. Appl. Polym. Sci.*, **1994**, 53, 283.
94. Amdouni, N.; Sautereau, H.; Gerard, J. F. *J. Appl. Polym. Sci.*, **1992**, 45, 1799.
95. Gerard, J. F. *Polym. Eng. Sci.*, **1988**, 28, 568.
96. Harris, B.; Braddell, O. G.; Almond, D. P; Lefebvre, C.; Verbist, J. *J. Mater. Sci.*, **1993**, 28, 3353.
97. Thomason, J. L. *Polym. Comp.*, **1990**, 11, 105.
98. Thomason, J. L. *Composites*, **1995**, 26, 487.
99. Wang, J. Y.; Ploehn, H. J. *J. Appl. Polym. Sci.*, **1996**, 59, 345.
100. Thomason, J. L. *Composites*, **1995**, 26, 477.
101. Kennedy, J. M.; Edie, D. D.; Banerjee, A.; Cano, R. J. *J. Comp. Mater.*, **1992**, 26, 869.
102. Chua, P. S. *Polym. Comp.*, **1987**, 8, 308.
103. Landel, R. F. *Trans. Soc. Rheo.*, **1958**, 2, 53.
104. Gambogi, J. E.; Blum, F. D. *Macromolecules*, **1992**, 25, 4526.
105. Wang, T. W. H.; Blum, F. D. *J. Mater. Sci.*, **1996**, 31, 5331.

106. Wang, T. W. H.; Blum, F. D. *Polym. Preprint*, **1994**, 35, 755.
107. Wang, T. W. H.; Blum, F. D. *Polym. Preprint*, **1995**, 36, 756.
108. Lacrampe, V.; Pascault, J. P.; Gerard, J. F. *Polym. Preprint*, **1995**, 36, 813.
109. Fitzgerald, J. J.; Landry, C. J. T.; Pochan, J. M. *Macromolecules*, **1992**, 25, 3715.
110. Hoh, K. A.; Ishida, H.; Koenig, J. L. *Polym. Comp.*, **1990**, 11, 121.
111. Dufresne, A.; Lacabanne, C. *Polym. Comp.*, **1993**, 14, 238.
112. Dufresne, A.; Lacabanne, C. *Polymer*, **1993**, 34, 3173.
113. Sullivan, J. L.; Wen, Y. F.; Gibson, R. F. *Polym. Comp.*, **1995**, 16, 3.
114. Dewimille, B.; Bunsell, A. R. *Composites*, **1983**, 14, 244.
115. Shen, C. H.; Springer, G. S. *J. Comp. Mater.*, **1976**, 10, 2.
116. Apicella, A.; Egiziano, L.; Nicolais, L.; Tucci, V. *J. Mater. Sci.*, **1988**, 23, 729.
117. Diamant, Y.; Marom, G.; Brontman, L. J. *J. Appl. Polym. Sci.*, **1981**, 26, 3015.
118. Lekatou, A; Faidi, S. E.; Lyon, S. B.; Newman, R. C. *J. Mater. Res.*, **1996**, 11, 1293.
119. Chateauminois, A.; Vincent, L.; Chabert, B.; Soulier, J. P. *Polymer*, **1994**, 35, 4766.
120. Jones, F. R.; Rock, J. W.; Wheatley, A. R. *Composites*, **1983**, 14, 262.
121. Bradley, W. L.; Grant, T. S. *J. Mater. Sci.*, **1995**, 30, 5537.
122. Thomason, J. L. *Composites*, **1995**, 26, 477.
123. Sober, D. *Printed Circuit Fabrication*, **1996**, 19, 22.
124. Roland, C. M.; Ngai, K. L.; O'Reilly, J. M.; Sedita, J. S. *Macromolecules*, **1992**, **25**, 3904.
125. Verghese, K. N. E.; Jensen, R. E.; Lesko, J. J.; Ward, T. C. *personal communications*
126. *Annual Book of ASTM Standards*, **1998**, v15.02
127. Loos, A. C. *ESM 5204 Composites Manufacturing Class Notes*, **1997**, 51.
128. *Potters Industries Inc. Spheriglass Bulletin SG304/496*
129. Wu, H. F.; Dwight, D. W.; Huff, N. T. *Comp. Sci. Tech.*, **1997**, 57, 975.
130. Ahlstrom, C.; Gerard, J. F.; *Polym. Comp.*, **1995**, 16, 305.
131. Dufresne, A.; Lacabanna, C. *Polymer*, **1995**, 36, 4417.
132. Gassan, J. ; Bledzki, A. K. *Polym. Comp.*, **1997**, 18, 179.
133. Arvanitopoulos, C. D.; Koenig, J. L. *Appl. Spect.*, **1996**, 50, 11.
134. Ishida, H.; Koenig, J. L. *Polym. Sci. Eng.*, **1978**, 18, 128.
135. Graf, R. T.; Koenig J. L.; Ishida, H. *J. Adhesion*, **1983**, 16, 97.
136. Cowie, J. M. G. *Polymers: Chemistry & Physics of Modern Materials; 2nd Ed.*, Blackie Academic & Professional, New York, **1994**.
137. Brandrup, J.; Immergut, E. H. (eds.) *Polymer Handbook; 3rd Ed.*, John Wiley & Sons, New York, **1989**.
138. Hoh, K. P.; Ishida, H.; Koenig, J. L. *Polym. Comp.*, **1988**, 9, 151.

# Vita

Robert Eric Jensen was born September 16, 1967 to the parents Robert and Sharon Jensen in Meridian, Mississippi. After graduating from Hatboro-Horsham High School in Horsham, Pennsylvania in 1985, Robert began his collegiate career at a local community college. The author had little patience in his younger days and dropped out of school to enlist in the United States Navy. Upon the completion of his enlistment in 1991 the author had gained some of the wisdom missing from his youth and enrolled in school at Francis Marion University in Florence, South Carolina. The author earned a B.S. degree in chemistry in 1994. The author then continued his education as a graduate student at Virginia Polytechnic Institute and State University as a chemistry major. The author worked under the guidance of Dr. Thomas C. Ward. While studying at Virginia Tech, Robert met his future wife Michelle Lian.